VYSOKÉ UČENÍ TECHNICKÉ V BRNĚ
BRNO UNIVERSITY OF TECHNOLOGY

FAKULTA CHEMICKÁ
ÚSTAV CHEMIE MATERIÁLŮ

FACULTY OF CHEMISTRY
INSTITUTE OF MATERIALS SCIENCE

STRUCTURE AND PROPERTIES OF COLLAGEN/HAP NANOCOMPOSITE NETWORKS

STRUKTURA A VLASTNOSTI NANOKOMPOZITNÍCH SÍTÍ KOLAGEN/HAP

DOKTORSKÁ PRÁCE
DOCTORAL THESIS

AUTOR PRÁCE
AUTHOR
Mgr. EMA JANČÁŘOVÁ

VEDOUCÍ PRÁCE
SUPERVISOR
prof. RNDr. JOSEF JANČÁŘ, CSc.

BRNO 2014

PROHLÁŠENÍ

Prohlašuji, že tato práce byla vypracována samostatně, a že všechny použité zdroje jsou správně citovány.

.....

Ema Jančářová

PODĚKOVÁNÍ

Tímto bych chtěla vyjádřit své poděkování všem, kteří mi byli nápomocni při vypracování dizertační práce a s ní souvisejících experimentů, zejména pak školiteli prof. RNDr. Josefu Jančářovi, CSc. za podnětné připomínky a konzultace. Dále bych pak ráda poděkovala Martinovi Kopuletému za podporu a zázemí, které bylo při práci tolik cenné, v neposlední řadě pak Michaele Voldánové za její pomoc v laboratoři.

Abstract

Polymer-based materials are some of the most promising materials for tissue engineering and controlled drug delivery. Collagen, as one of the most abundant proteins to be found in mammals, is especially interesting due to its tunable properties and excellent host reactions. This thesis is focused on the self-assembly and the mechanical properties of collagen in solution, its kinetics and general principles controlling the process. The effect of hydroxyapatite nanoparticles on the collagen self-assembly and mechanical properties is also investigated. Possible mechanisms of collagen/hydroxyapatite interactions are elucidated along with the description of structure evolution and properties at various structural levels. The shear rate dependences and viscoelastic behavior of collagen I and its nanocomposites with hydroxyapatite (HAP) were measured and interpreted molecularly. The structure of collagen I scaffolds was studied and the effect of HAP and cross-linking was determined. Finally, the results were discussed in terms of the applicability of collagen/hydroxyapatite nanocomposites in scaffolds for bone tissue regeneration.

Abstrakt

Polymerní biomateriály jsou jedním ze současných populárních témat vzhledem k možnosti potenciální aplikace v tkáňovém inženýrství a řízeného dávkování léčiv v organismech. Kolagen je jako jeden z nejčastěji se vyskytujících proteinů zvláště zajímavý díky svým rozmanitým vlastnostem bez imunoreakce organismu příjemce. Tato práce je zaměřena na samouspořádávací procesy, kinetiku, obecné zákonitosti řídící proces samouspořádání a mechanické vlastnosti kolagenních roztoků. Dále je zkoumán efekt hydroxyapatitových nanočástic na samouspořádávání kolagenu a mechanické vlastnosti výsledných nanokompozitních hydrogelů. Jsou objasněny možné mechanismy interakcí mezi kolagenem I a hydroxyapatitem spolu s popisem vývoje struktury a vlastností na různých úrovních struktury. Byly měřeny a molekulárně interpretovány závislosti viskoelastických veličin na smykové rychlosti spolu s viskoelastickým chováním. Dále byla studována struktura kolagenních scaffoldů a určen vliv HAP a síťování. Závěrem byly diskutovány výsledky v souvislosti s jejich aplikovatelností v tkáňovém inženýrství chrupavek tvrdých tkání a v regenerativní medicíně.

Key words

Collagen self-assembly, mechanical properties of protein materials, tissue engineering, bone, fibrillogenesis, rheology, hydroxyapatite, nanocomposites

Klíčová slova

Samouspořádávání kolagenu, mechanické vlastnosti proteinových materiálů, tkáňové inženýrství, kosti, fibrilogeneze, reologie, hydroxyapatit, nanokompozity

Table of Contents

1 Introduction

Damaged or diseased skeletal tissue frequently leads to progressive debilitation resulting in a marked decrease in the quality of life. Current approaches in bone engineering are mainly focused on the restoration of pathologically altered tissue structure based on the transplantation of mesenchymal stem cells in combination with supportive scaffolds. Although ceramics and metallic materials have been widely accepted for the development of implants, their non-resorbability and necessity of second surgical operation limit their applications in tissue engineering.

Bone represents a complex multi-scale hierarchical composite structure with large variation in local composition and spatial arrangement of collagen fibrils mineralized with hydroxyapatite. It has been shown that in addition to the content of hydroxyapatite (HAP) nanocrystals, properties of the collagen (coll) matrix as well as the relative spatial arrangement of coll and HAP play a significant role in determining the deformation behavior of bone tissue.

Tailored biomaterials with tunable functional properties have become increasingly important in medical applications due to their desired balance of properties and excellent host response in the field of regenerative medicine, tissue engineering and controlled drug delivery. To improve the predictability of biopolymer materials functionality, multiple design parameters need to be considered, along with appropriate models.

Self-organization is a fundamental process in which many biological structures are assembled from cell produced building blocks. (1) The understanding of natural materials design principles can be used in the synthesis of engineered materials. Most biological materials are produced under moderate conditions, in neutral aqueous solution and at ambient temperature, without high energy input. Additionally, the raw material is often abundantly available and the resulting product easily biodegradable. Therefore, a translation of natural processes to synthetic materials engineering would yield highly sustainable and functional materials. (2)

Many issues, however, remain unresolved, specifically the understanding of the biological material supramolecular structure evolution, interactions with cells and other substances. While the mechanical behavior of individual proteins and tissues is reasonably well understood, the discovery of the structure – function relationships of assemblies of proteins remains in its infancy. The focus of this Thesis is to contribute to the fundamental understanding of hierarchical self-assembly of collagen I, the most frequent structural protein in mammals.

Collagen is the primary structural material in vertebrate biology, determining the mechanical behavior of musculoskeletal and connective tissues such as tendon, bone, tooth and skin. Collagen constitutes one-third of the human proteome, providing mechanical stability, elasticity, and strength

to hard and soft tissues. Collagen is also the dominating material in the extracellular matrix and its stiffness controls cell differentiation, growth and pathology.

Despite extensive efforts in the investigation of the origin of collagen‘s unique mechanical properties, a full understanding of the relationship between its molecular structure and mechanical properties remains elusive, hindered by the complex hierarchical structure of collagen-based tissues. In particular, although extensive studies of viscoelastic properties have been pursued at the macroscopic (fiber/tissue) level, fewer investigations have been performed at the smaller scales, including, in particular, collagen molecules and fibrils. These scales are, however, important for a complete understanding of the role of collagen as an important constituent in the extracellular matrix. (3)

Fratzl et al. have summarized hierarchical structures of natural materials and basic principles involved in designing hierarchical biological materials. (4) Meyers et al. (1) and Espinosa et al. (5) have thoroughly investigated and reviewed the micro-/nano-scale mechanics of rigid biological materials and their relationships with hierarchical structures. The origin of the unique mechanical properties of collagenous tissues, and in particular its stiffness, extensibility, and nonlinear mechanical response at large deformation, remains to be discovered. (6)

The transfer of concepts observed in biology into engineering applications and novel material design paradigm– a field referred to as biomateriomics – remains a significant challenge for the scientific community with, however, a potentially enormous scientific and technological payoff. In particular, the combination of nanostructural and hierarchical features into material development could lead to discoveries of de novo functional materials. (7)

Biological protein materials (BPMs) such as skin, bone or cytoskeletons feature complex, hierarchical structures. Their macroscopic mechanical behavior is controlled by the interplay between various properties throughout multiple length and time scales. In order to understand their deformation and fracture mechanisms, it is crucial to elucidate relevant molecular mechanisms decisive for response at each individual length scale. BPMs have a significantly different molecular structure than crystalline materials, which induces a variety of novel deformation mechanisms. Whereas crystalline materials show mechanisms such as movement of dislocations or crack extension and bridging, hierarchical BPMs feature molecular unfolding or sliding, where hydrogen bond rupture is of particular importance. (7)

Understanding these mechanisms poses a great challenge for the scientific community. Furthermore, the application of the insight from such studies to address significant biological and biomedical questions or to suggest new biomimetic material designs are exciting intellectual and interdisciplinary opportunities. (7)

Although the mechanical properties of collagen itself have been broadly studied experimentally, its self-assembly in the presence of hydroxyapatite nanoparticles (nHAP) has not been investigated to date. The effect of nHAP on collagen self-assembly in solution and on the mechanical properties of coll/nHAP nanocomposite solutions/hydrogels has to be determined in order to enable new bone tissue engineering strategies to be developed.

Most of the existing mechanical models describing the effects of local nano-structure on the mechanical response of bone consider regular distribution of simple shaped rigid inclusions in a polymer continuum. Despite the fact that the discrete nature of the structure at the nano-scale is acknowledged in these models, the fundamental effects related to the molecular nature of the proteins forming the matrix are neglected and the fact that due to the highly non-local response of polymers, the classical continuum mechanics is of limited validity is not taken into consideration. It has been suggested that the validity of continuum elasticity models can be extended to account for the nano-scale non-locality of deformation response of polymeric component by using higher order elasticity combined with molecular dynamics.

2 Review of literature

Most natural (or biological) materials are complex composites whose mechanical properties are often outstanding, considering the weak constituents from which they are assembled. Their defining characteristics are hierarchy, multifunctionality and a self-healing capability. Self-organization is also a fundamental feature of many biological materials and the manner by which the structures are assembled from the molecular level up. Biological materials can be divided into polypeptides (proteins), polysaccharides and nucleic acids depending upon the building blocks they are composed of. (8) In the presented work, we focus on proteins, specifically collagen I.

Like every polymer, biopolymers are sequences of monomers that may be linear, circular, branched or cross-linked, thus forming a gel. Most of them are essentially heteropolymers, because they may contain a variety of monomeric units. The biological relevance of a biopolymer is ultimately based on its primary structure. (9) A fundamental characteristic of biopolymers is the bottom-up formation of their hierarchical superstructures at successive length scales and the abundance of weak inter- and intramolecular interactions, manifesting themselves into the material's properties. (7) With the recent development of experimental techniques, the research of biomaterials has expanded into the micro- and nano-scale which has allowed the design of novel advanced synthetic functional materials. (10)

Mechanical property maps, more commonly know as Ashby maps, have become a convenient manner of concentrating a large amount of information into one simple diagram. They have been extended from metals (11) to biological materials by Wegst and Ashby (12) as presented in Fig. 2.1.; they present the Young moduli and strength as a function of density. Biological materials have several striking features:

1. The density of biological systems is low, it rarely exceeds 3, whereas synthetic structural materials often have densities in the 4-10 range.
2. There is a broad range in Young moduli from 0,001 to 100 GPa, representing five orders of magnitude.
3. The range of strengths is almost as broad as the Young moduli, varying over four orders of magnitude: 0,1 – 1000 MPa.
4. There is an absence of metals, which require for the most part either high temperature or high electric current processing. Nature does not have these variables at its disposal. (1)

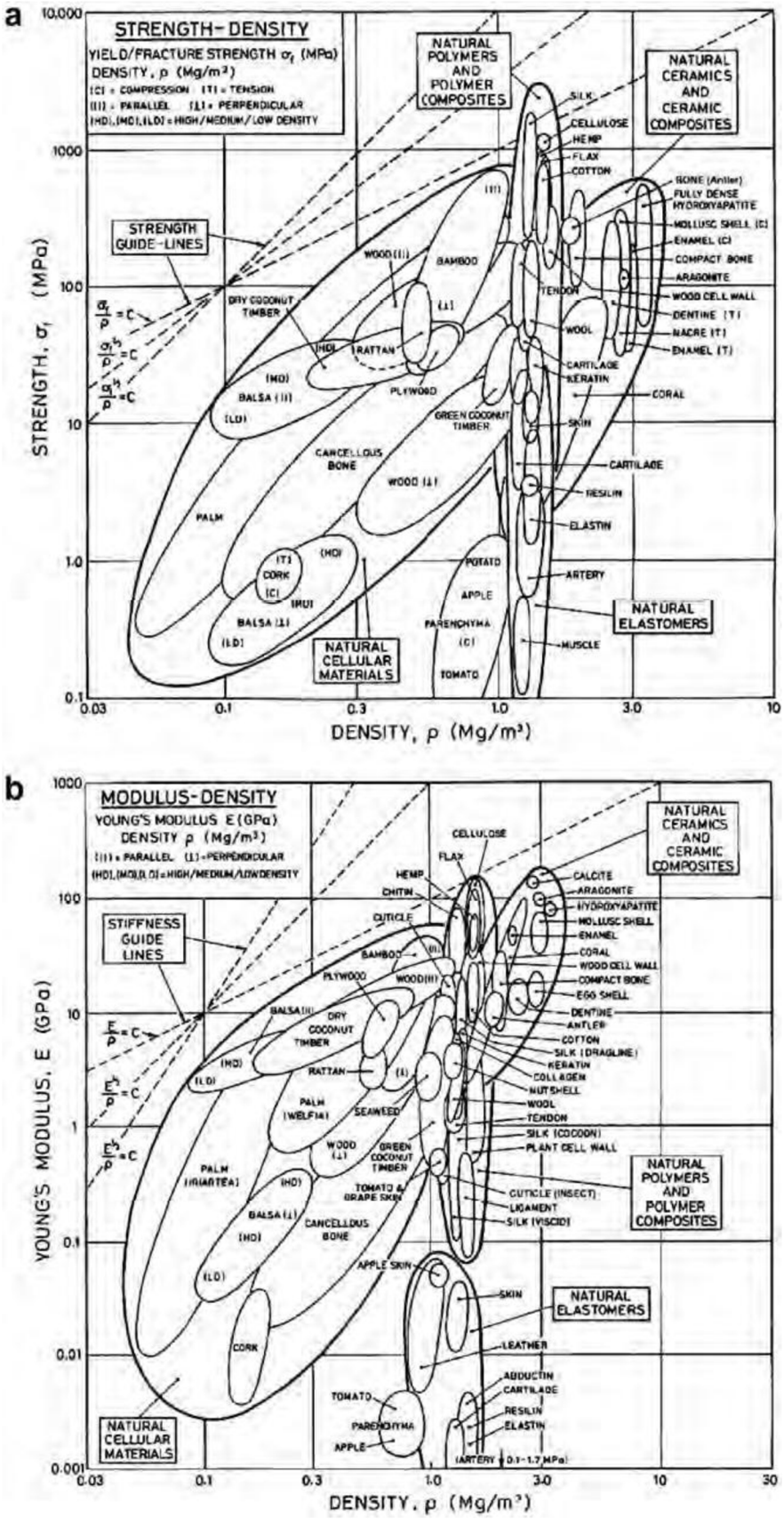

Fig. 2.1. Ashby plots for biological materials showing a) strength as a function of density and b) elastic modulus as a function of density. (12)

2.1 Tissue engineering

Biomaterials play a very important role in tissue engineering. Numerous scaffolds produced from a variety of biomaterials have been used in the biomedical field in attempts to regenerate different tissues and organs in the body. (13) Collagen, being the main protein of connective tissue and skin, as an extracellular matrix protein, is widely used as a biomaterial for tissue regeneration and implantation. The disadvantage of using collagen as a biomaterial for tissue repair is its high degradation rate, which leads to the rapid loss of mechanical properties. (14) (15)

Tissue engineering (TE) can be defined as an interdisciplinary field applying scientific and engineering principles to the design, construction, modification, growth, and maintenance of living tissues. Practically all tissues are capable of being repaired by tissue engineering principles, which usually include a scaffold conducive to cell attachment and maintenance of cell function. Recent advances in the fields of biomaterials, biomateriomics, and tissue engineering have focused attention on the potentials for clinical application. (16) (17) (18) (19) (20)

The goal of tissue engineering is to produce a scaffold material that will guide cells to differentiate and regenerate functional replacement tissue at the site of injury. (21) In recent years, functional biomaterial research has been directed towards the development of improved scaffolds and new drug delivery systems. Scaffolds are used to create the three-dimensional organization needed for appropriate cell interactions, to serve as vehicles to deliver and retain the cells at a specific site. (22) The extracellular matrix (ECM) is by definition nature's ideal biological scaffold material and its mechanical properties are largely a consequence of its collagen fiber architecture and kinematics. (23)

To repair a bone or cartilage defect, one of the ideal scenarios is presented in Fig. 2.2. and can be summarized as follows: the patient's own osteoblasts, chondrocytes, or mesenchymal stem cells are harvested, expanded (in vitro), and seeded onto and in a scaffold (in vitro). There has been considerable effort put into the design and fabrication of biocompatible and biodegradable porous scaffolds. The scaffold is then used to fill the defect cavity. In situ, the scaffold degrades slowly, as tissue growth proceeds towards complete filling of the defect. In an alternative scenario, a scaffold without cells is implanted directly into the defect cavity to serve as guidance for cell and tissue growth. (24)

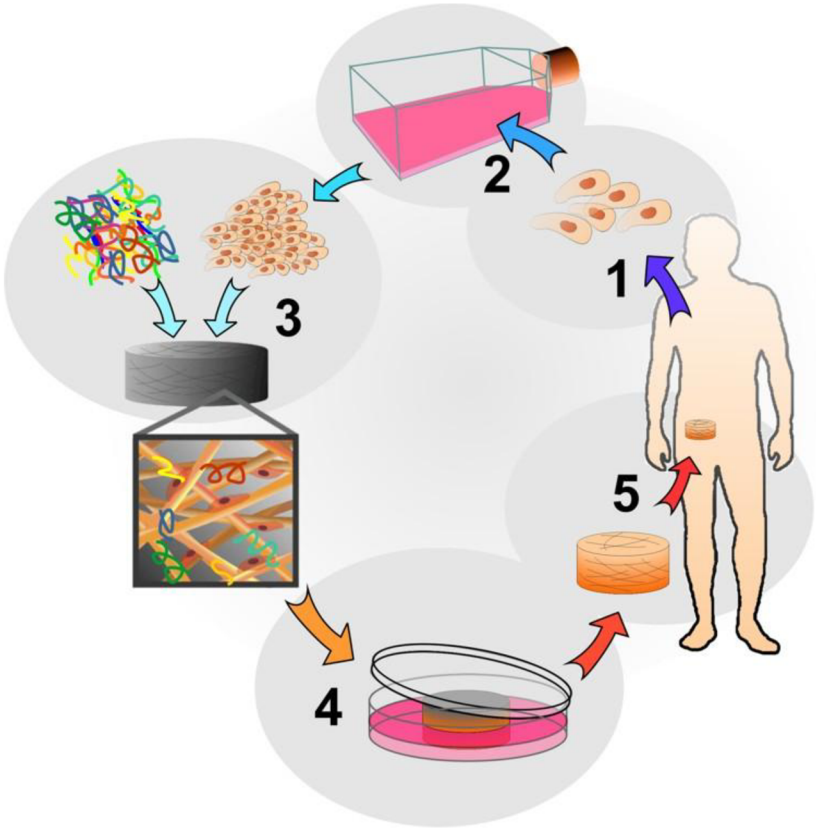

Fig. 2.2. Schematic representation of the tissue engineering process, specifically dealing with a hip implant. (25)

The last years have seen continuous refinement and improvement of tissue engineering strategies, but a number of tough practical problems persists. (26) (27) These are connected to the complex and truly multidisciplinary nature of this field, which integrates knowledge from polymer material properties, micro- and macro-structure of scaffolds, biomechanics, cell biology, etc. (24) (28) The tissue engineering field of interest in our case is bone TE.

Besides the TE approach to the preparation of artificial bone materials, biomimetic methods based on the biomineralization process and structural design on the nanoscale can be alternatively considered, in which three strategies are generally summarized. The first strategy is directly mixing nanoscale inorganic and organic components to form composites, which can easily result in the formation of nanocomposites. However, hierarchical structures inside composites are difficult to control through this approach. The second pathway is to use pre-formed polymer networks as biomineralization templates to prepare bone-like artificial materials. The third method involves the in situ formation of inorganic-organic nanocomposites during the self-assembly processes of organic molecules. Although these strategies have produced inorganic-organic nanocomposites that show some similarity to bone, up to now there are no structural bulk materials showing the outstanding mechanical properties of bone. (29), (30), (31) (32)

Bone is one of the few organs capable of self-regeneration following injury. However, when the injury is sufficiently severe to cause a loss of bone volume, a compromised vascular supply or infection of the wound site, bone may not heal correctly. In such instances, a fibrous non-union is formed which requires additional treatment to aid the healing process and restore mechanical function. (33) (34) In cartilage, the capacity for self-repair after trauma is limited. Superficial cartilage defects do not heal, which is mainly due to the intrinsic characteristics (aneural and avascular) of this tissue (35), and full thickness defects heal with a fibrocartilaginous tissue, which has poor biomechanical qualities. (36) (37)

The use of biomaterials to restore the function of traumatized or degenerated connective tissue has gained wide acceptance in dental and orthopedic surgery. However, the increased application and use of biomaterials in orthopedic procedures has led to the development of new problems, namely biomaterial failure and biological incompatibility. The potential causes for the failure of the biomaterial are usually fracture, wear, or corrosion. (17)The potential clinical efficiency of using tissue-engineereing constructs has been the subject of numerous studies, their use represents an enormous treatment potential for modern biomedicine. (38)

Properties that facilitate clinical use include the ability to inject the scaffold into a site of interest via minimally invasive procedures. Therefore, from a practical viewpoint the most important material properties would be the viscosity of the gel or particle size of a suspension to allow injection through a small bore needle. (23) An injectable treatment is more minimally invasive than implanting in-vitro engineered tissue, and is therefore more clinically appealing. Bio-derived materials such as fibrin glue and collagen natively contain peptide binding sequences that cells can adhere to via integrins. (39)

For complex tissue grafts that require stratified structural and mechanical properties, a new generation of biomaterials is helping to reconstruct the anisotropy, nonlinearity and local mechanical properties of the native tissue. (40) However, most implants in use today continue to suffer from problems of interfacial stability with host tissues, biomechanical mismatch of elastic moduli, production of wear debris and maintenance of a stable blood supply. In addition, all present day implants lack two of the most critical characteristics of living tissues: 1) the ability to self-repair and 2) the ability to modify their structure and properties in response to environmental factors such as mechanical load or blood flow. (41)

2.2 The structure and hierarchy of proteins

Protein materials are intriguing examples of materials that balance multiple tasks, representing some of the most sustainable material solutions that integrate structure and function. This is mainly attributed to their bottom-up structural formation with molecular precision. (7) (42) Proteins are the fundamental building blocks of a vast array of biological materials involved in critical functions of life. (7)

2.2.1 Structural levels of proteins

The basic building blocks of proteins are amino-acids, compounds containing both an amine and a carboxyl group, most of them have the structure depicted in Fig. 2.3.:

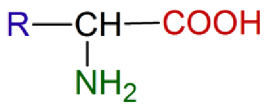

Fig. 2.3. The structure of the amino-acid: basic building block of proteins, containing an amine group (-NH_2) and a carboxyl group (-COOH), R stands for radical. (43)

The amino-acids are distinguished by their different side groups and can be classified according to the physical-chemical properties of these side-groups. It is clear that the higher order secondary and tertiary structures of proteins are intimately related to these properties, together with environmental factors such as the solvent quality.

All proteins are macromolecules with α-amino-acid monomeric units arranged according to genetic information stored in DNA. Proteins are therefore polypeptides of a defined sequence determined by the genetic code. The polypeptide backbone is not charged except the end groups, the charges on a protein chain are located in its side groups. Under physiological conditions, the protein is usually close to its isoelectric point, so that the positive and negative charges cancel out and the net charge is almost zero.

The primary structure of proteins is the sequence of amino-acids, these monomeric units in proteins are organized in a certain local molecular configuration, commonly referred to as the secondary structure and arising from the formation of bonds (hydrogen, van der Waals, and covalent bonds) between amino-acids on the same or different chains. (8) Proteins show a wide variety of secondary structures, which satisfy a number of criteria: the peptide bond is planar because little twisting is possible about the C-N bond, the steric interaction between the side groups of the amino-acids is minimal and the structure is stabilized by hydrogen bonding between the oxygen of the

carbonyl C=O groups and the hydrogen of the amide C-N groups. Major secondary structures include the α-helix and β-sheet, however these are by no means the only ones. (9)

At a larger length scale, a protein can adopt a defined 3-dimensional conformation, the so-called tertiary structure. This is particularly important for proteins, which largely relate their biological function to their function-specific 3-dimensional structure. Eventually, proteins can form even larger complexes among themselves or with smaller molecules in the cell and organism, forming the quaternary structure. The levels of protein structure along with a closer look at the alpha helix are presented in Fig. 2.4.

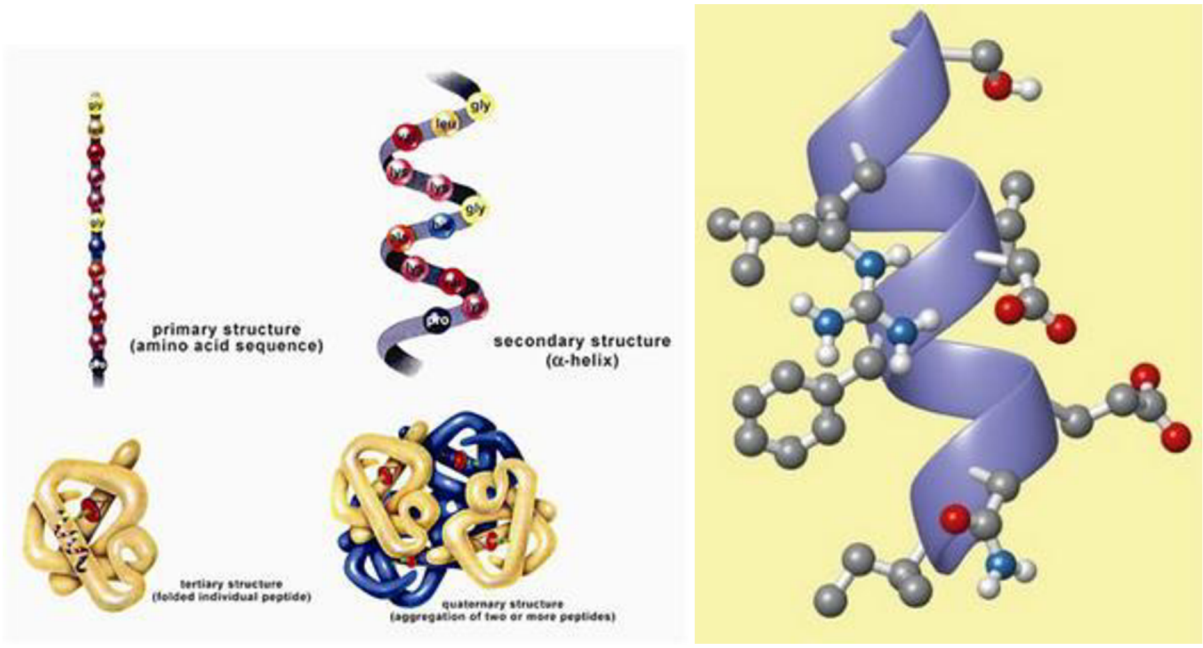

Fig. 2.4. a) The levels of protein structure; b) An example of protein secondary structure, the alpha helix (AH). (44)

2.2.2 Stabilizing interactions

As mentioned previously, proteins owe their biological function to their unique 3-dimensional tertiary structure. Yet, proteins are synthesized as linear chains of amino-acid monomers on ribosomes. Each newly synthetized protein chain has to adopt its native conformation, which also has to remain stable under working conditions. Both the kinetic folding pathway and the stability of the native state are determined by the amino-acid sequence. Relatively small proteins take their native structure spontaneously. For longer sequences, the folding process may be assisted by helper proteins (chaperones).

The 3-dimensional structure of a protein is determined by the interactions of the amino-acid residues among themselves and the surrounding medium. In particular, aqueous solvation properties are of paramount importance in stabilizing the native, folded state. The folding of the protein from a random coil state with an astronomical number of molecular conformations into its native state with a small number of possible conformations is accompanied by a tremendous loss of conformational entropy. In order to render the native state thermodynamically stable, this loss of entropy should be compensated by stabilizing interactions within the polypeptide sequence and/or an increase in another form of entropy. Both effects are involved in the folding process. (9)

Since proteins typically fold on a time scale of a minute or less, Levinthal recognized that a random search of all possible conformations is not feasible and should be biased. A bias can be introduced by imposing an energy cost for an incorrect link. Experimental evidence at the individual residue level has shown that there are often, if not always, multiple routes from the random coil to the native state. Accordingly, a multi-dimensional free energy landscape, which is a folding funnel, is thought to be a better description of the process. The selection of a specific pathway is often kinetically, rather than thermodynamically driven, because of the small differences in free energies between different states. (9) In the native (biologically active) folded state, the most important stabilizing interactions are summarized in the following and shown in Fig. 2.5:

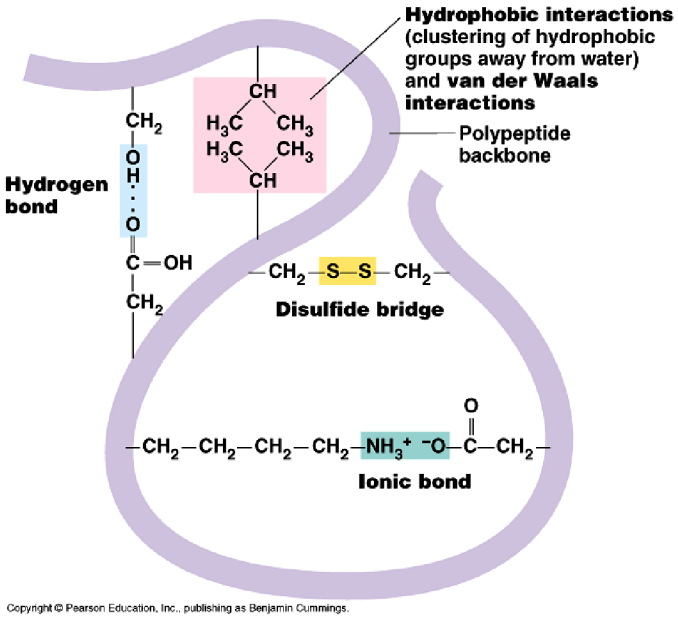

Fig. 2.5. An overview of stabilizing interactions participating in the folding of a protein. (44)

2.2.2.1 Electrostatic interactions

Many amino-acids contain side groups which are either positively or negatively charged, the electrostatic attractive forces stabilize the native state. (9)

2.2.2.2 Hydrogen bonding

Many side groups contain functional groups which can be involved in the formation of hydrogen bonds with other side groups and, if available, with the carbonyl oxygen and amide hydrogen on the polypeptide backbone. Although a single hydrogen bond is relatively weak, the sheer number of them can add a significant contribution to the stabilization of the folded state. (9) This is demonstrated in the following Fig. 2.6., showing a computational model of the hydrogen bonds stabilizing a beta sheet.

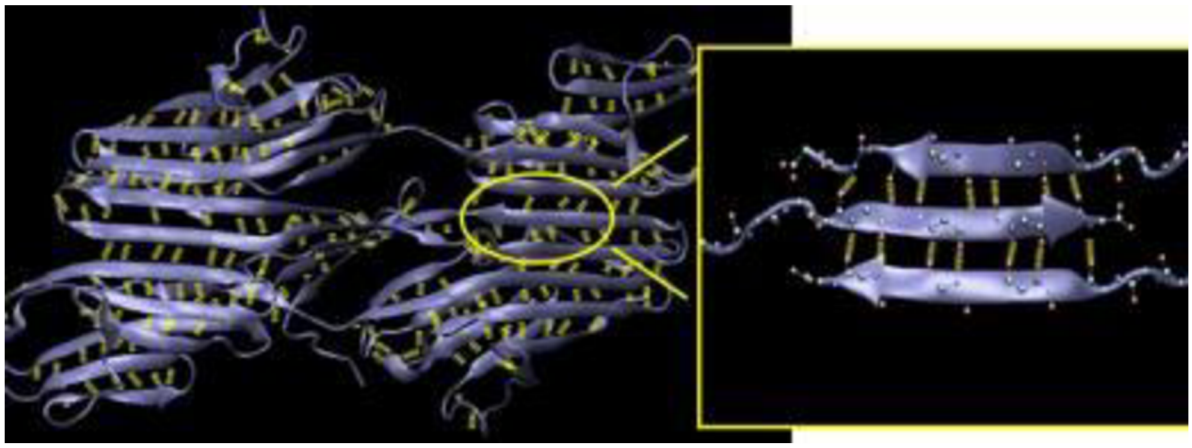

Fig. 2.6. The figure shows the structure of a beta-sheet protein. Hydrogen bonds are indicated as yellow lines. Buehler and Keten found that hydrogen bonds in beta sheet structures break in clusters of three or four, even in the presence of many more bonds. (45)

2.2.2.3 Van der Waals interactions

The interior of globular proteins is closely packed with many uncharged side groups. The weak interaction resulting from dipole and induced dipole interactions between these side groups adds up and results in a significant stabilizing force, which is shown for water molecules in Fig. 2.7. (9)

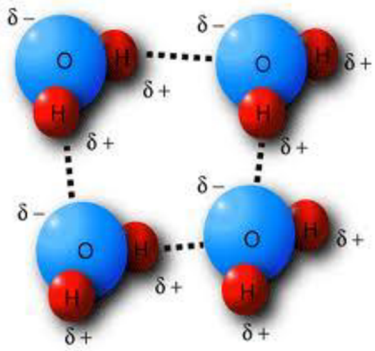

Fig. 2.7. Van der Waals interactions between water molecules. (46)

2.2.2.4 Disulfide bonding

If the protein is meant to function in an external oxidizing environment, as opposed to the reducing environment inside most cells, significant stabilization of the folded structure can come from the formation of disulfide bonds between cysteine residues. (9) The formation of a disulfidic bond between two polypeptide chains is shown in Fig. 2.8.

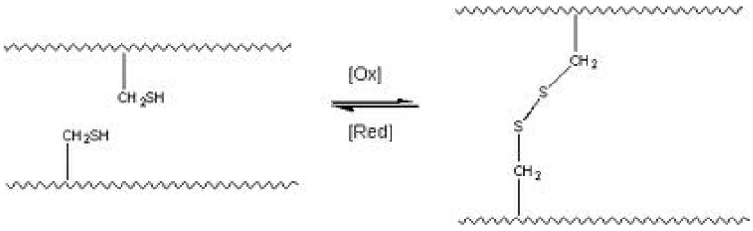

Fig. 2.8. If the thiol groups of the cysteine units on two different polypeptide chains are oxidized, the result is the formation of a disulfidic bond between the two chains. (47)

2.2.2.5 Hydrophobic interactions

Despite the fact that the aforementioned interactions stabilize the native state to a significant extent, the main contribution to the stability of the protein comes from the hydrophobic effect. If the hydrophobic side groups are buried in the interior of the globular protein, water molecules that were first restricted in their translational and rotational motions due to the interaction with the protein are released. This release of hydration results in an increase of the entropy of the whole system including protein and solvent, which partially offsets the tremendous loss in configurational entropy associated with the folding process. (9)

2.2.3 Protein classification

Depending on the tertiary structure, proteins can be divided into two main groups, globular and fibrous. Globular proteins are compact and more or less spherical enzymes, hormones, antibodies, etc., such as γ-globulin or fibrinogen. Fibrous (structural) proteins are elongated fibers with structural functions such as collagen, elastin, keratin, actin and myosin. (8) Structural proteins have mechanical properties associated with their hierarchical structure and the properties cannot be attributed to the individual building blocks. (9) Proteins are in most cases multi-unit assemblies that frequently form higher order complexes with other biopolymers.

2.3 Collagen

Collagen represents the most abundant structural protein in mammals, providing mechanical stability, elasticity, and strength to connective tissues such as tendons, ligaments, and bone, as well as the extracellular matrix (ECM). Yet, we understand relatively little about how collagen assembles to form larger-scale structures such as microfibrils and fibers and how they provide crucial mechanical properties to organisms. It is known that virtually all collagen-based tissues are organized into hierarchical structures, where the lowest hierarchical level consists of triple helical collagen molecules. (6)

2.3.1 Collagen structure and classification

Collagen consists of tropocollagen (TC) molecules that have a length $L \approx 280nm$ and diameter of $\approx 1{,}5nm$. Staggered arrays of TC molecules form microfibrils, which arrange to form collagen fibers. (48) It has been long known that the stability of the collagen triple helix is related to the total content of amino acids proline and hydroxyproline (shown in Fig. 2.9.),

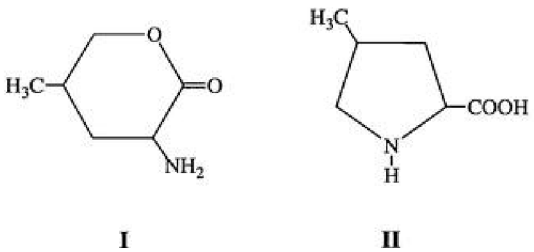

Fig. 2.9. I) Proline and II) hydroxyproline. (49)

which together make up about 20% of the total amino acids in human fibrous collagens. This is the result of the cyclic nature of the side chains that restricts flexibility about the peptide bond. (50) Fig. 2.10. shows the residue positions in greater detail, the proline and hydroxyproline residues connecting back to the chain backbone effectively stiffen the molecule.

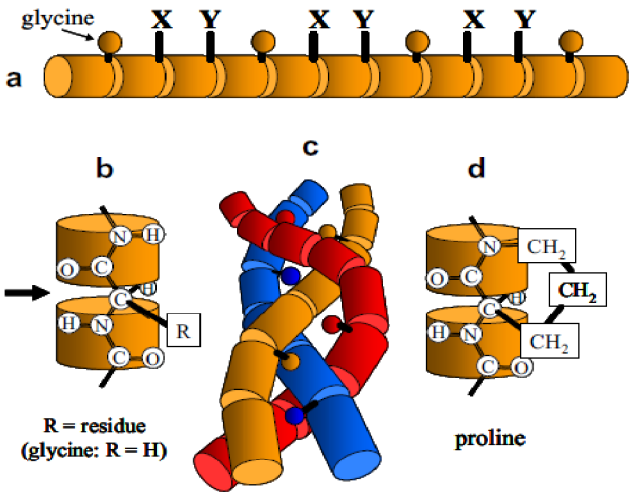

Fig. 2.10. Periodic repeat in the amino-acid sequence of a pro-collagen molecule. a) Every third residue is a glycine. The remaining residues, X and Y are frequently proline or hydroxyproline. b) Glycine is the smallest amino-acid where the residue is just a hydrogen atom. c) The triple-helical arrangement requires the glycine residues to point towards the inside of the helix. The other residues are on the surface of the helix. d) Proline and hydroxyproline have residues connecting back to the polypeptide chain, effectively stiffening the molecule. (4)

Collagen I is the most widely occurring collagen found in skin, tendon, bone, cornea, lung, and the vasculature; collagen II has a more specific tissue distribution being limited essentially to cartilage; collagen III is found in embryonic skin, lung and blood vessels; collagen V can be found in the cornea. (51) Altogether, more than 23 collagen types have been discovered to date. In the presented work, we will focus on collagen I only.

2.3.2 Collagen biosynthesis

The biological synthesis, secretion and assembly into definitive extracellular structures of collagen can be briefly described as follows. Firstly, the individual polypeptide chains, called pre-procollagen chains, are synthesized on membrane-bound ribosomes. These chains have three major domains: the α-chain, the amino-terminal peptide, and the carboxy-terminal peptide. In the cisternae of the rough endoplasmatic reticulum, three pro-α chains associate, and a procollagen molecule with a triple helix structure is formed. During this process, the propeptide sequences are removed, proline and lysine residues become hydroxylated, the propeptides are glycosylated and disulfide bonds are formed. After all these post-translational modifications take place, individual procollagen molecules are transported to the Golgi complex, packaged into secretory vesicles prior to export into the extracellular matrix. Procollagen processing occurs during or shortly after secretion followed by assembly of fibrils. (50) In the case of type I collagen, the extension peptides at both end

of the molecule must be cleaved before the fibers can be assembled. After removal of the extension propeptides, several collagen molecules associate in a process called fibrillogenesis (see Section 2.4). (52) (53) The whole process is summarized in Fig. 2.11.

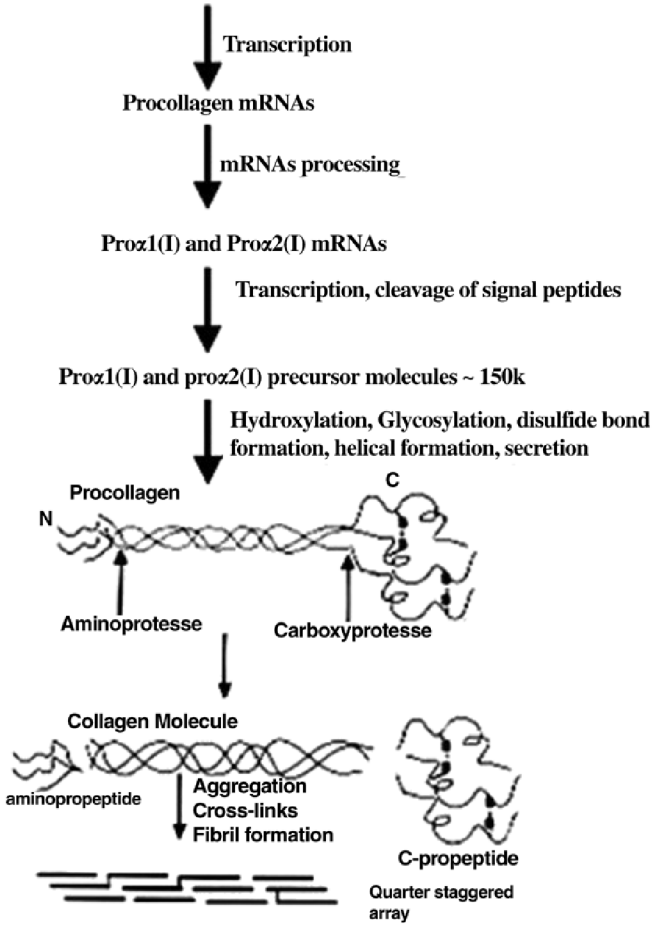

Fig.2.11. Schematic diagram showing steps in biosynthesis and assembly of type I collagen into fibrils. Type I collagen is composed of two polypeptide chains namely pro∝1(I) and pro∝ 2(I) (54)

2.4 Self-assembly processes, fibrillogenesis

Self-assembly in the classic sense can be defined as the spontaneous and reversible organization of molecular units into ordered structures by non-covalent interactions. (55) The first property of a self-assembled system this definition suggests is the spontaneity of the self-assembly process: the interactions responsible for the formation of the self-assembled system act on a strictly local level – in other words, the nanostructure builds itself. Three factors characterize a self-assembling process and the resulting structure, i.e. order, interactions and building blocks or constituents. (56)

Self-assembly is a promising technique for the construction of higher order structures by using a large number of individual particles as building blocks. The self-assembly process relies on various interparticle forces (van der Waals, electrostatic, magnetic, molecular and entropic). (57) (10)

Self-assembly is usually modelled employing equilibrium thermodynamics considering the system ergodic. The second law of thermodynamics states that in an isolated system, equilibrium is reached at maximum entropy, *S*. If *t* is defined as time, a system will approach equilibrium as

$$dS/dt > 0 \qquad (2.1.)$$

Using the Boltzmann equation, phenomenological entropy can be expressed as a function of the number of possible configurations, *W*, as:

$$S = k \ln W \qquad (2.2.)$$

Under isothermal and isobaric conditions, equilibrium is reached when the Gibbs free energy is minimized, i.e. $\Delta G \leq 0$. For systems with constant volume and temperature, the Helmholtz free energy, *F*, is used instead of *G*. Hence, the evolution of the structure of protein assemblies results in order enhancement and, thus, must be controlled by enthalpy, rather than entropy.

Prigogine's thermodynamics of irreversible systems provide a link between thermodynamics and evolution. Most complex systems are indeed open and non-equilibrium. Prigogine demonstrated that non-isolated systems can evolve by self-organization and self-assembly toward greater order, whereas this process is irreversible. (58) This distinguishes self-assembly from crystallization. Open systems exhibit fluxes of energy, matter, and exchanges in mechanical, electric and magnetic energy with the environment. The entropy variation can be expressed as having two components: one internal *i*, and one due to the exchanges, *e*:

$$dS/dt = dS_i/dt + dS_e/dt \qquad (2.3.)$$

For the isolated system, the $dS_e/dt = 0$. For the open system, this term is not necessarily zero. The second law, however, still applies to the internal components, *i*, thus $dS_i/dt > 0$. So it is possible to have a temporal decrease in *dS/dt*, if the flux component contributes with a sufficiently large negative term. The physical interpretation of Eq. 2.3. is that order can increase with time. This is a simple thermodynamic explanation for the origin of complex self-organization phenomena. (1)

2.4.1 Gelation

This connectivity transition from liquid to solid is caused by the formation of cross-links between polymer chains and can be described by a bond percolation model. Linking chains together leads to progressively larger branched polymers, at a certain extent of the reaction, a molecule spanning the whole system appears. Such a huge molecule will not dissolve in a solvent, but may only swell in it. This infinite polymer is called a gel or network, the critical point where gel first appears is called the gel point, the procedure is referred to as gelation. The fraction of all possible bonds that are formed at any point in the reaction is called the extent of reaction *p*, which increases from zero to unity as the reaction proceeds. At the percolation threshold or gel point p_c, the system undergoes a connectivity transition and one structure referred to as the incipient gel percolates through the entire system. (9) A rough estimate of the gel point for linking precursor molecules (or monomers) with functionality *f* is

$$p_c = \frac{1}{f-1} \qquad (2.4.)$$

Gelation is caused by the formation of crosslinks between polymer chains, the final state after crosslinking consists of linear polymer strands connected by crosslinks – a polymer network. Gelation can occur either by physical linking or chemical cross-linking, resulting in physical and chemical gels. (59) Strong physical gels have strong physical bonds between polymer chains that are effectively permanent at a given set of experimental conditions (such as glassy or microcrystalline nodules or double helices). These strong physical gels can only melt and flow when the external conditions such as the temperature change. Weak physical gels have reversible links formed from temporary associations between chains. These associations have finite lifetimes, weak physical bonds include hydrogen bonding, hydrophobic or ionic associations. Chemical gelation involves the formation of covalent bonds and always results in a strong gel.

Physical and chemical gelation have been studied in rheology experiments, where the experiment follows the network formation without disturbing the process. Under flow, competition arises between the formation of clusters by physical cross-linking and their disruption by the shear forces. de Carvalho (1997) proposed a microscopic model based on the analysis of flow curves and dynamic measurements, which describes the structure of the gelling solution: microgel particles grow to a maximum size which depends on the flow. When the volume fraction of these particles is high enough, percolation between them occurs suddenly and a yield stress fluid is formed (particulate gel). (60)

2.4.2 Crystallization

Crystallization is another example of a self-assembly process. (10) Polymer crystallization is kinetically controlled under conditions far from thermodynamic equilibrium involving molecular motions on various length and time scales. Nanocomposites with engineered surface chemistry represent novel means of both controlling the kinetics of morphogenesis in semicrystalline polymers and enhancing its long-term stability. However, the literature on crystallization kinetics of polymer nanocomposites with varying interfacial adhesion often provides contradictory conclusions. This is due to the experimental difficulty in achieving sufficient control over the interfacial energetics, inability to eliminate primary nucleation by adhering nanoparticles and by utilizing vastly different experimental protocols. With some exceptions, many of the studies vary multiple structural variables (particle size, shape, surface treatment, chain molecular weight, chain rigidity and polarity, nucleating agents, etc.) and test parameters (non-isothermal, specimen size, sample preparation, characterization technique, etc.) at the same time. This prevents separation of the various contributions to the overall crystal growth rate, often exhibiting opposite dependence on the given variable. (61)

The main shortcoming of the Avrami model, used to analyze experimental crystallization kinetics data in most of the non-isothermal investigations, consists of the fact that it averages the spherulite growth rate over the entire specimen rather than analyzing the growth rate of an individual spherulite. Hence, the Avrami model cannot capture the local nano-scale peculiarities of the crystallization process as affected by the presence of rigid heterogeneities with their length scale, D, similar to that for the chain radius of gyration, R_g.

Phenomenological description of the temperature dependence of the crystal growth rate, *G*, for the kinetically dominant growth front is described satisfactorily by the Lauritzen-Hofmann (LH) model:

$$G = G_0 \exp\left[-\frac{Q_D^{*0}}{R(T - T_V)}\right] \exp\left[-\frac{K}{T\Delta T}\right]. \qquad (2.5.)$$

The G_0 is an assumed temperature independent pre-exponential factor strongly dependent on the molecular characteristics, $\Delta T = (T_m^0 - T)$ is the under-cooling, T_m^0 is the equilibrium melting temperature, T is the crystallization temperature, Q_D^{*0} is the activation energy for the chain self-diffusion in the melt, T_V is the Vogel temperature.

During the crystal growth, the internal bond rotation is virtually the only way for a segment to move, hence, the chain motion is a consequence of the successive internal bond rotations of all the segments resulting in the chain reptation primarily in the lengthwise direction. Hoffman and

Miller rearranged Eq. (2.5) for the growth rate in neat PE, G_{II}^{0}, considering chain reptation as the mechanism for chain transport to the crystal growth front:

$$G_{II}^{0} \approx \frac{\kappa C_0^{\frac{1}{2}}}{N}\left\{\exp\left[-\frac{Q_D^{*0}}{R(T-T_V)}\right]\exp\left[-\frac{K}{T\Delta T}\right]\right\}. \qquad (2.6)$$

The C_0 is the configurational path degeneracy expressing the variation in the length of the attached stems and the growth rate reduction factor κ was expressed as:

$$\kappa \approx \frac{1}{\xi_0}\exp\left(\frac{Q_D^{*0}}{RT_0}\right). \qquad (2.7.)$$

Combining Eqs. (2.6.) and (2.7.) results in the G_{II}^{0} being inversely proportional to the chain friction coefficient ξ_c.

The term *dynamic fragility* is frequently used to express the strength of the temperature dependence of dynamical properties of glass forming liquids (the breadth of the glass transition region). Investigating crystallization kinetics of supercooled polymer melts, Sanz et al. (28) suggested that less fragile polymers exhibit far less strongly intermolecularly cooperative segmental dynamics compared to highly fragile stiff backbone polymers. Adding large specific surface area nanoparticles can substantially alter short distance coupling of motions of different parts of the polymer chain and its surrounding chains. Hence, segmental motions in the nanocomposite melt become increasingly decoupled both along the chain and in the neighbouring chains, thus, making formation of aggregates of chain segments (stems) exhibiting higher local orientation order in the melt less probable. Thus, one can predict that nanoparticles, greatly modifying both dynamics of individual chains and collective segmental motion in polymer melts, will slow down the crystal growth rate significantly under the condition of their negligible nucleation effect.

The effect of particle-chain interfacial interactions is accounted for by enhanced both chain friction coefficient, ξ_c, and the increased activation energy of chain self-diffusion, Q_D^{*}, compared to that in the neat polymer, Q_D^{*0}. The ξ_c for the neat PE chain with N monomer units, each exhibiting monomer friction coefficient ξ_0, equals to $N\xi_0$. By adding particles exhibiting attractive interfacial interaction with chain segments to the polymer melt, the ξ_c is enhanced substantially due to formation of trains on the particle surface. Considering N_a the average number of monomer units in the train, the ξ_c can be expressed as:

$$\xi_c = \left((N-N_a)\xi_0 + N_a\xi_a\right). \qquad (2.8)$$

The ξ_c is the friction coefficient of segments in the adsorbed trains (30). The only ξ_c data available in literature so far were measured for polystyrene (PS) containing weakly attractively interacting nanoparticles and $\xi_c \approx 5.6\text{x}10^3\xi_0$. One can assume that for the PE, the difference between ξ_0 and ξ_a may be of the same order. For weak and strong attraction, respectively, $N_a=N^{1/2}$ and $N_a=½N$, respectively, and, $N_a=0$ for non-interacting interface. For chains with $N < 10^6$, the $N^{1/2}\xi_0$ can be considered negligible compared to ξ_a, thus, the $\xi_c \approx N^{1/2}\xi_a$ and $\xi_c \approx ½N\xi_a$ for the weak and strong attraction, respectively. For the non-interacting interface, $\xi_c = N\xi_0$ similarly to the neat PE. Substituting for κ (Eq. (2.7)) in Eq. (2.6), the G_{II}^0 for the neat polymer can be expressed as:

$$G_{II}^0 \approx \left(\frac{C_0}{N}\right)^{\frac{1}{2}} \frac{1}{N^{\frac{1}{2}}\xi_0} \exp\left(\frac{Q_D^{*0}}{RT_0}\right)\left\{\exp\left[\frac{Q_D^{*0}}{R(T-T_V)}\right]\exp\left[-\frac{K}{T\Delta T}\right]\right\}. \qquad (2.9)$$

Similarly, the G_{II} for the nanocomposite with strong interafacial attraction can be expressed as:

$$G_{II} \approx \left(\frac{C_0}{N}\right)^{\frac{1}{2}} \frac{2}{N^{\frac{1}{2}}\xi_a} \exp\left(\frac{Q_D^{*}}{RT_0}\right)\left\{\exp\left[\frac{Q_D^{*}}{R(T-T_V)}\right]\exp\left[-\frac{K}{T\Delta T}\right]\right\}, \qquad (2.10)$$

for the weak interfacial attraction:

$$G_{II} \approx \left(\frac{C_0}{N}\right)^{\frac{1}{2}} \frac{1}{\xi_a} \exp\left(\frac{Q_D^{*}}{RT_0}\right)\left\{\exp\left[\frac{Q_D^{*}}{R(T-T_V)}\right]\exp\left[-\frac{K}{T\Delta T}\right]\right\}, \qquad (2.11)$$

and for the non-interacting interface :

$$G_{II} \approx \left(\frac{C_0}{N}\right)^{\frac{1}{2}} \frac{1}{N^{\frac{1}{2}}\xi_0} \exp\left(\frac{Q_D^{*}}{RT_0}\right)\left\{\exp\left[\frac{Q_D^{*}}{R(T-T_V)}\right]\exp\left[-\frac{K}{T\Delta T}\right]\right\}. \qquad (2.12)$$

Equations (2.10) and (2.11) suggest direct proportionality between G_{II} and ξ_a^{-1} in the nanocomposite melts and weakening of the M_n dependence of G_{II} in nanocomposite which is in agreement with experimental observations of M_n scaling of the G_{II} for monodisperse PE filled with fumed SiO_2. For the former prediction, reliable experimental data do not exist in the literature so far. Eq. (2.12) suggest the only effect of nanoparticles in non-interacting system is formation of additional topological constraints to the chain transport expressed in the enhanced Q_D^*. (61)

2.4.3 Liquid crystalline structure of collagen in solutions

Giraud-Guille and Besseau (61) (62) established that at high concentration in acidic solutions, type I collagen molecules spontaneously organize to form liquid crystalline phases, characterized in polarized light microscopy and X-Ray diffraction. (61) (63) These supramolecular arrangements appear in a viscous state with some fluidity, as molecules are free to move with respect to each

other. Collagen monomers assemble as a function of concentration in successive arrangements corresponding to defined geometries as alignments in nematics, undulations in precholesterics and continuous twist in cholesterics. (64)

The degree of order identified by optical microscopy increases with increasing collagen concentration, the liquid crystalline state was observed not just at an acidic pH, but also at neutral pH in a gel state. TEM observations validated these findings, the significant result being that the ultrastructure of stabilized liquid crystalline collagen faithfully mimics fibrillar patterns described in vivo in extracellular matrices. This strongly supports the hypothesis that liquid crystalline properties are involved in the morphogenesis of collagen matrices. (62)

2.4.4 Collagen fibrillogenesis

Collagen fibrils are formed by the self-assembly of individual collagen molecules in a process referred to as fibrillogenesis. It has been established that the formation of collagen fibrils is a spontaneous process initiated by the enzymatic cleavage of procollagen propeptides. (65) (66) (67) The fibrils vary in length and diameter depending on the conditions involved in growth. However, typically in vitro formed fibrils are up to 500nm in diameter, several tens of µm long and contain between 10^4 and 10^6 mature collagen molecules. (68)

Biomechanical functions of fibrillar collagens depend on their ability to assemble into fibrils. One of the major features of type I collagen is its ability to self-assemble into highly organized supramolecular structures, cross-striated fibrils, which in turn often form larger entities, namely, fibers and fascicles, which give living tissues their stability and their unique mechanical properties. Collagen is thus an ideal building block for tissue engineering, provided that a comprehensive understanding of its self-assembly properties can be reached so that the spatial packing of fibrils can be controlled. Fibrillogenesis is the key factor in connective tissue morphogenesis. (69) The individual stages of the fibril formation process are shown in Fig. 2.12.

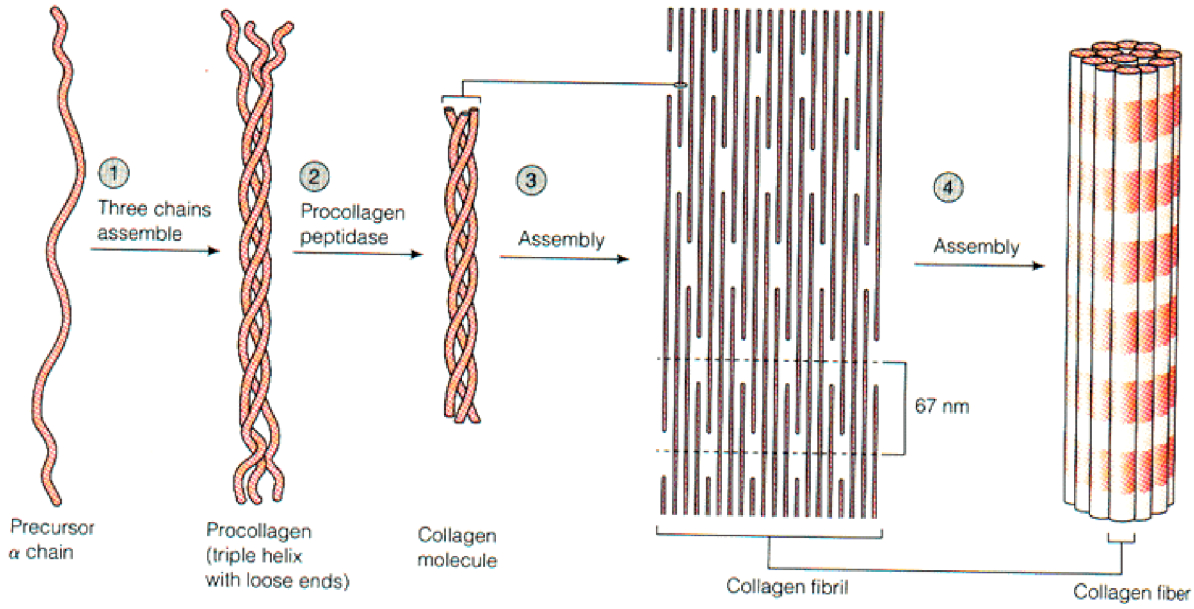

Fig. 2.12. Collagen fibril formation process.

The formation of collagen fibrils in vitro has been the subject of extensive research for over 50 years. Initial observations were focused on the reconstitution of fibrils from solutions of collagen in dilute weak acids. The major fibrillar collagens are water-soluble at low pH, for example in dilute acetic acid. When the pH is adjusted to around neutral and the temperature raised to around physiological, fibril formation occurs spontaneously resulting in banded fibrils. Fibrils are stabilized by the formation of covalent cross-links. (51) The structure of the resulting fibrils is influenced by several parameters including the presence of other types of collagen and substances other than collagen. (50)

Fibrils assemble spontaneously and are stable over a wide pH range of 6,2 – 12. The periodic stagger is constant at 66,5 nm and relates to the maximum interaction between oppositely charged side chains and large hydrophobic amino acids of adjacent triple helices. (70), (71)

Electrostatic forces, which may be responsible for the long range attraction and organization, might be negligible at close range, compared to other factors such as hydrophobic or van der Waals forces. These nonionic forces would be responsible for the subsequent stability of fibrils above the isoeletric point. This stability is probably reinforced by intermolecular cross-links that can occur when nonhelical ends, the telopeptides, are present. (69)

The influence of buffer composition on fibril formation has been studied by several authors, notably Williams et al. (1978), also the effect of temperature on fibril assembly was investigated by Holmes (1986), who arrived at the conclusion that fibrils formed at lower temperatures (20°C) have

larger diameters than those formed at higher temperatures (34°C). (72) Fibril width and organization depend strongly on the solution concentration, as shown by Gobeaux (2008), whose measurements were performed by two complementary techniques: transmission electron microscopy (TEM) and synchrotron X-ray scattering. TEM provided local structural information on length scales ranging from 15 nm to several micrometers, whereas X-ray scattering gave global structural information about the packing of collagen molecules within fibrils, on scales ranging from 1 to 50 nm. The non-monotonic change in fibril size with collagen concentration was explained as a result of competition between the availability of molecules and the viscoelasticity of dense solutions. (69)

The intactness of the N- and C- telopeptides also has a marked effect on fibril formation. Loss of diameter uniformity, induction of antiparallel packing and changes in the fibril assembly pathway have been observed depending on the extent of loss of N- and C- telopeptides. (73) Commercially available fibrous collagens are of two types, either acid soluble or pepsin soluble. In acid-soluble collagen, the telopeptides are usually intact, and these help both to initiate fibril formation and to produce long cylindrical fibrils. Pepsin-soluble collagen is produced by preparing tissue extracts with pepsin, which digests most protein structures except for the collagen triple helix. As a consequence, the non-helical telopeptides are mostly removed by this procedure, making self-assembly more difficult. (50)

While studies on collagen assembly have gradually switched from in vitro to in vivo, both approaches give complementary information on the molecular mechanisms involved. (50) The in vitro assembly of collagen into fibrils is described as follows: collagen monomers exist as triple helices that assemble into small aggregates of 5-17 molecules, and these aggregates further assemble into fibrils (30-300 nm wide), which may bundle into fibers (composed of two or more fibrils) that interconnect and interpenetrate to form a fiber network. (74), (75) Fibril formation is an entropy-driven process, in which self-assembly results in burying surface-exposed hydrophobic residues within the fibril, thereby increasing entropy in the solvent. Hydrophobic interactions can stabilize the monomer backbone, and in preparations in which the nonhelical ends of the collagen molecules are retained, covalent bonds form between the nonhelical monomer ends and helical crosslinking sites. Collagen fibrils and fibers may be stabilized with both noncovalent and covalent bonds. Interconnections between fibers formed in vitro are largely via entanglement, and thus, the fully developed collagen network is a complex physicochemical gel. (76)

Assembly proceeds by a nucleation and growth mechanism, as monitored typically by turbidimetry at a wavelength around 300 nm. The turbidity is proportional to both the concentration of collagen and the mass of the assembled structures. Turbidity curves classically show three phases: an initial lag phase with no change in turbidity, a rapid growth phase and finally a plateau region. (77)

During the lag phase, small numbers of collagen molecules associate to form metastable nuclei, upon which further molecules aggregate during the growth phase. The final step in the biosynthesis of collagen is the introduction of covalent cross-links to stabilize the different forms of supramolecular assembly. (50)

Collagen concentration is one of the most important factors affecting self-assembly, there have been several efforts to establish a critical concentration, below which self-assembly is not observed. Yan et al. found that the critical concentration lies in the interval 0,3-0,6 mg/ml. They have also established that the collagen concentration increases the rate constant in the growth kinetics, accelerating collagen self-assembly - the lag phase is shortened as collagen concentration is increased. (78)(69) It has been suggested that during the lag phase, triple helices form small multimeric intermediates that later aggregate into ordered structures. Fibril growth would then proceed by further addition of multimeric intermediates, the final size being governed by the number of collagen molecules available in solution. (69) Absorbance measurements have been employed as a direct method of self-assembly quantification. (78)

However, turbidity measurements cannot reveal details of fiber number and size, they also cannot reflect fibril or fiber connections (chemical or physical) that may develop late in the gelation process. Such connections have important consequences for the mechanical properties of the systems and are important considerations for bioengineering and biophysical applications of collagen-based gels.

The development of mechanical properties during collagen gelation has currently been studied by rheology rather than turbidity, as demonstrated by Yang and Kaufman (2009). (76) (79) The development of the gel viscoelasticity was monitored in time via oscillatory rheology, and the development of the collagen network was found to be consistent with the percolation theory of branched networks. To monitor mechanical properties during gelation, time-sweep rheology studies were performed, yielding new information on the structures that give rise to the mechanical properties of collagen gels during gelation as a function of collagen concentration and gelation temperature. (79)

The structural organization of collagen molecules within a fibril has long been the focus of attention, where the organization and topology of the collagen molecules are required to ensure strong intermolecular interactions. Although the axial intermolecular interactions seem to be well understood, the specificity of lateral interactions between collagen molecules appears to be far more variable. The lateral association of collagen molecules within a fibril requires to be understood in terms of fibrillogenesis, fracture properties, cross-linking, and molecular connectivity. (80)

The longitudinal orientation is the preferred collagen fiber orientation and hence is stiffer than the circumferential direction. (81) (82) The tendency of molecules and particles to form 1D

polymeric structures is a natural consequence of having directional intermolecular potentials. Dipolar interactions (or other highly directional interactions such as directional hydrogen bonding and π-π stacking interactions) are often involved, often in combination with van der Waals and many-body hydrophobic interactions, in the organization of supermolecular polymers and fiber structures. (83)

The mechanical properties of collagen fibers depend primarily on the formation of head to tail Schiff base cross-links between end-overlapped collagen molecules within the fiber induced by the enzyme lysyl oxidase. Inhibition of these cross-links results in the complete loss of mechanical strength of the fiber. During maturation these initial divalent cross-links react further with molecules in register from an adjacent fiber forming stable trivalent cross-links and further increasing its mechanical strength. (84) The collagen fibril provides the key to scaffolding structures in the body from the nanoscopic to the macroscopic length scales. The interaction with other materials such as proteoglycan, minerals, and elastic fibers can lead to the modulation of the overall structural and mechanical properties. (80) Molecular modeling suggests that this natural design of collagen fibrils maximizes the strength and provides large energy dissipation during deformation, thus creating a tough and robust structure. (48)

A number of models of collagen fibril formation have been proposed, some based on the assumption that fibrillogenesis is driven by the site-specific interactions between defined sites present within interacting collagen molecules. On the other hand, models exist where site-specific interactions are not required. One such model by Parkinson et al. (85) describes the growth of collagen fibrils from paraboloidal tips based on limited diffusion seen in electrochemical deposition. (72) In contrast, Silver et al. proposed a computer model of nucleation and propagation of a collagen fibril in which interactions between monomers depended on the site-specific binding. (75) . Steplewski et al. proposed another model, where the first stage of homotypic fibril formation depends on the interaction between C-terminal telopeptides and a specific site located in the region encompassed by α1-776 and α1-796 residues. (86)

Experimentally, Holmes et al. implemented quantitative scanning transmission electron microscopy (STEM) for the quantitative analysis of collagen fibril self-assembly in vivo and in vitro. and using this technique, obtained an axial mass distribution along a fibril. (73) Yan et al. studied the effect of concentration, pH and ionic strength on the kinetic self-assembly (78) and arrived at the conclusion that collagen self-assembly is a two-phase kinetic process: the formation of a nucleus center and nucleus growth, and it is controlled by the first phase. Collagen showed marked assembly behavior for concentration equal to or larger than 0,6 mg/ml. The optimum pH value was established to be 7,2. (78) Cisneros et al. observed the growth steps of collagen I self-assembly into fibrils directly by using time lapse atomic force microscopy (AFM). (87)

2.5 Biomineralization – formation of the mineralized fibril

2.5.1 Biomineralization

One of the defining features of the rigid biological systems that comprise a significant fraction of the structural biological materials is the existence of two components: a mineral and organic component. The intercalation of these components occurs at the nano, micro, or mesoscale and often takes place at a more than one-dimensional scale. The mineral component provides strength, whereas the organic component contributes to the ductility. This combination of strength and ductility leads to high energy absorption prior to failure. (88) Fig. 2.13. presents a nanocomposite of thin calcium-phosphate platelets intercalated between collagen molecules, thus forming a mineralized fibril.

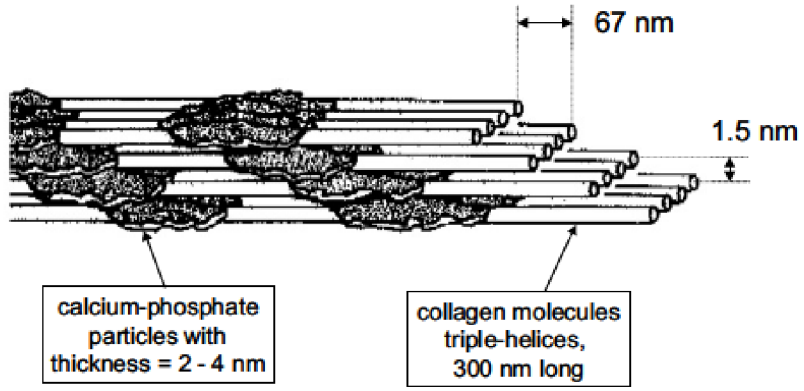

Fig. 2.13 The mineral crystals intercalated between collagen molecules are arranged parallel to the collagen fibrils in the bone composite in a regularly repeating staggered pattern. The staggering of the crystals is most likely due to the nucleation of mineral particles inside the gap zone of collagen fibrils. (4)

The most common mineral components are calcium carbonate, calcium phosphate (hydroxyapatite), and amorphous silica, although over 20 minerals have been identified. These minerals are embedded in complex assemblages of organic macromolecules which are hierarchically organized. (88) Understanding the molecular mechanisms underlying biomineralization is extremely important for the fundamental problem of novel biomaterial development for tissue engineering applications. (89)

2.5.2 Hydroxyapatite

Hydroxyapatite (HAP) is one of the frequently used bioceramics for bone and dental tissue reconstitution. It has excellent biocompatibility with hard tissues (90) (91), and high osteoconductivity and bioactivity despite its low degradation rate. (92) (93) It has neither antigenicity

nor cytotoxicity. (94) Specific characteristics of the HAP particles (size, shape, crystal structure and morphology) are among the important factors needed to control technological properties of the products. Micronisation increases the surface area with a consequent increase of dissolution rate and bioavailability of the HAP. (95) The crystalline structure is shown in Fig. 2.14.:

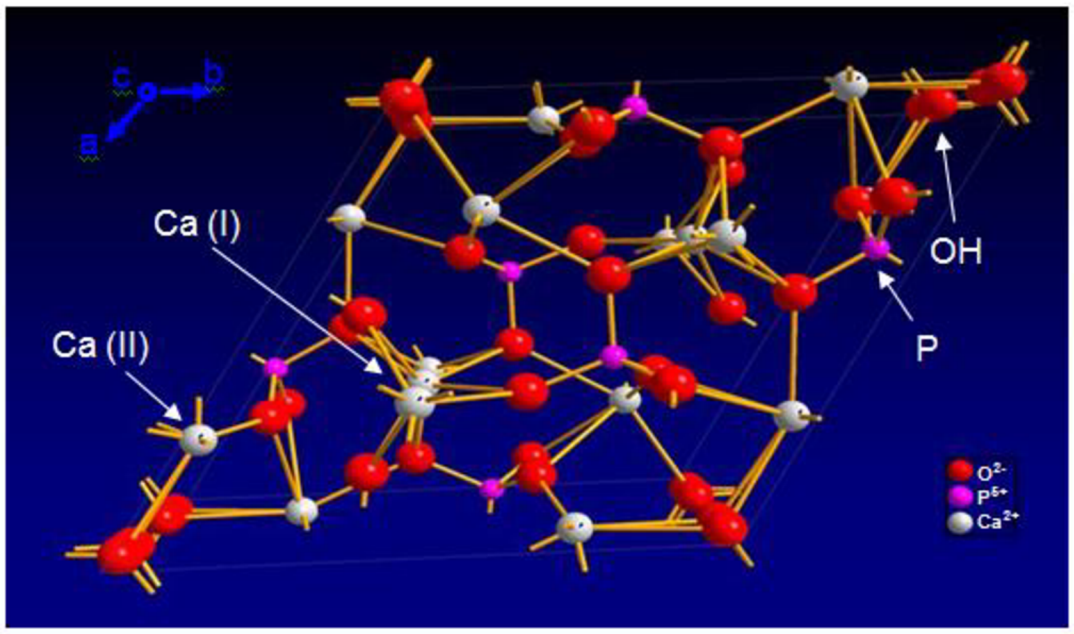

Fig. 2.14 The crystalline structure of hydroxyapatite.

The term "apatite" applies to a group of compounds (not only calcium phosphates) with a general formula in the form $M_{10}(XO_4)_6Z_2$, where M^{2+} is a metal and species XO_4^{3-} and Z^- are anions. The particular name of each apatite depends on the elements or radicals M, X and Z. In these terms, hydroxyapatite (HAP) has the molecular structure of apatite, where M is calcium (Ca^{2+}), X is phosphorus (P^{5+}) and Z is the hydroxyl radical (OH^-). This is known as stoichiometric hydroxyapatite and its atomic ratio Ca/P is 1.67. Its chemical formula is $Ca_{10}(PO_4)_6(OH)_2$, with 39% by weight of Ca, 18.5% P and 3.38% of OH.

Hydroxyapatite crystallizes in a hexagonal system, although with some exception in a monoclinic system. The HAP structure is formed by a tetrahedral arrangement of phosphates (PO_4^{3-}), which constitute the "skeleton" of the unit cell. Two of the oxygens are aligned with the c axis and the other two are in a horizontal plane. Within the unit cell, phosphates are positioned into two layers, with heights of 1/4 and 3/4, respectively, resulting in the formation of two types of channels along the c axis (see *a* and *b* in Fig. 2.14.).

Despite the fact that the usual stoichiometric hydroxyapatite is most frequently used as a model, it is noteworthy that hydroxyapatites produced biologically are much more complicated, they are not stoichiometric, have an atomic ratio Ca/P <1.67 and do not contain only ions and radicals of the HAP but also traces of CO_3, Mg, Na, F and Cl. These amounts vary according at the specific type of tissue, which is related to the properties and bioactivity of it.

One aspect that is important to note is that the closer the value of Ca/P to 1.67, the greater the stability of the material inside the human body as they tend to be inert, and on the other hand, if this value decreases (deficient HAP), the better the bioactivity. Another aspect we must consider is the degree of crystallinity. It has been observed that the crystallinity in the tissues for the tooth enamel is very high, while in the cases corresponding to dentin and bone, it is very poor. This means that the reactivity depends on the degree of crystallinity, since the reactivity in dentin and bone is higher than in tooth enamel. (96)

2.5.3 Interaction of collagen I with nHAP – collagen/nHAP nanocomposites

The mechanisms of interaction of collagen and hydroxyapatite are of scientific and practical interest, but are still not established clearly. Based on the results of experimental NMR investigations of Aminova et al. (2013) of collagen and water suspensions, it was shown that hydroxyapatite can form intermolecular complexes with collagen fragments by the interaction of calcium ions with a proline group, forming weak intermolecular bonds as modelled in Fig. 2.15.

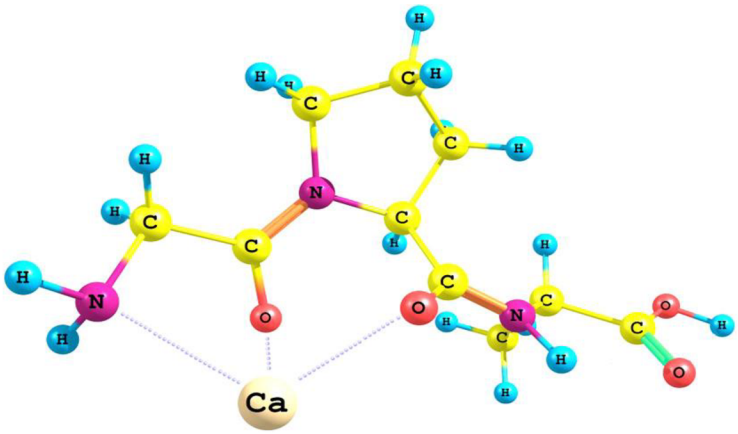

Fig. 2.15. Calcium ion forming a complex with a fragment of collagen by bonding calcium with oxygen atoms of proline and nitrogen atom of glycine.

In coll/HAP composites, the most important interactions involved are electrostatic interaction between opposite charged components or hydrogen bonding. These interactions occur between nHAP particles, between different collagen hierarchical structures and also between the organic and inorganic phases. The most important interactions are illustrated in Fig. 2.16.

Hydrogen bonding occurs inside the collagen molecule itself, between collagen molecules, fibrils and fibres; also in hydroxyapatite and between collagen and hydroxyapatite. Electrostatic interaction takes place especially between Ca^{2+} cations (from HAP) and carboxylate groups (from collagen) as well as between hydroxyapatite grains (especially between Ca^{2+} and the phosphate anions), inside collagen molecules and between collagen fibrils and fibers. (97)

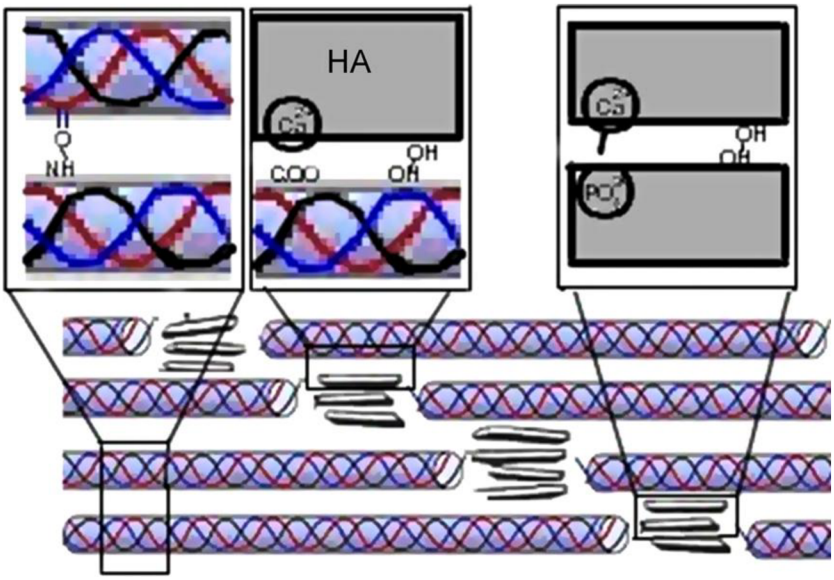

Fig. 2.16. Interaction types in collagen/HAP composites. (97)

Previous efforts on elucidating the mechanism of complex formation have been performed by Kikushi et al. (2004), whose model presents binding between collagen and hydroxyapatite as a consequence of the partial polarization of C=O bonds of the collagen fragments. This leads to the Coulomb interaction between the partial negative charge of the oxygen atoms of the collagen and positively charged calcium ions. Zhang et al. (2004) on the other hand proposes intermolecular bonds between the collagen and hydroxyapatite are formed due to the interaction of hydroxyapatite with partially negatively charged COO^- groups of some amino-acids on collagen (namely lysin, comprising about 2,6% of collagen). Currently, the opinion that the interaction with the carboxyl groups of hydroxyapatite is more probable prevails, but there is no definite agreement on the subject.

It is well recognized that nanocomposites formed by adding nanoparticles to polymers can have significantly enhanced properties relative to the native polymer. (98) The difference in the mechanical behavior between tendon and bone is not due to different fiber architecture, but due to the fact that bone is mineralized. The mechanical properties of bone and dentin depend to a large extent on the degree of mineralization, the organic matrix alone is not sufficient to provide the stiffness required for these tissues which have to carry considerable loads. The inclusion of tiny calcium-phosphate mineral particles leads to a considerable stiffening of the tissue. The mineral phase occupies about half the volume in compact bone. (51)

The outstanding mechanical properties of tissues that rely on fibrillar collagen are due to the optimization of their structure on many hierarchical levels. The interplay between structures is critical to the overall mechanical properties. (99) Although the principle that the addition of nanoparticles to a polymer can result in materials with significantly improved properties seems to be well established, several issues that determine a) the qualitative and quantitative description of the dispersion and organization of nanoparticles; b) polymer properties, including chain conformation, local motions, and nonlocal dynamics and c) how do these collectively affect the macroscale property improvements of the hybrids remain largely unresolved. (98)

Most of the resulting materials are not really nanocomposites, i.e. materials that are filled with individual nanometer-sized particles. Rather the materials contain relatively large particle aggregates that behave effectively like micron-sized fillers. Whereas the presence of such larger agglomerates can be beneficial to certain properties, nevertheless the dispersal of nanoparticles which have a very high specific surface area (and hence specific surface energy) into polymeric matrices remains an outstanding challenge. (98), (100)

Also further insight into mineralization requires understanding the influence of water molecules on collagen – HAP interactions. Employing piezogravimetry, IR and Raman spectroscopy, Sukhodub et al. (2004) showed that the level of sorption of water molecules for pure collagen is higher than for a collagen-HAP composite. It follows that the HAP molecules have a tendency to close some hydration sites within the collagen structure, as depicted in Fig. 2.17., so the mineralization of the collagen fibrils by HAP crystals located within the gap area dramatically decreases the number of water molecules present in the initial hydration shell. This process causes some structural changes within the structure of collagen, however without denaturation. (89)

The deformation response of collagen is substantially influenced by mineral proximity, as investigated by Katti et al. (2010), establishing that also the direction and orientation of the HAP-collagen interaction are also important considerations for proper collagen/HAP composite mechanical properties and their modeling. (101) (97) Ji et al. (2012) established through nanotensile tests on electrospun fibers that while pure collagen fibers exhibit tensile properties comparable to

the natural collagen fibril, Young's modulus of the HAP-filled nanocomposite fibers was found to be only slightly higher than that of pure collagen fibers, but significant improvements in strength, strain and toughness were obtained, the optimal mechanical properties arising at approx. 6-11 wt% HAP. (102)

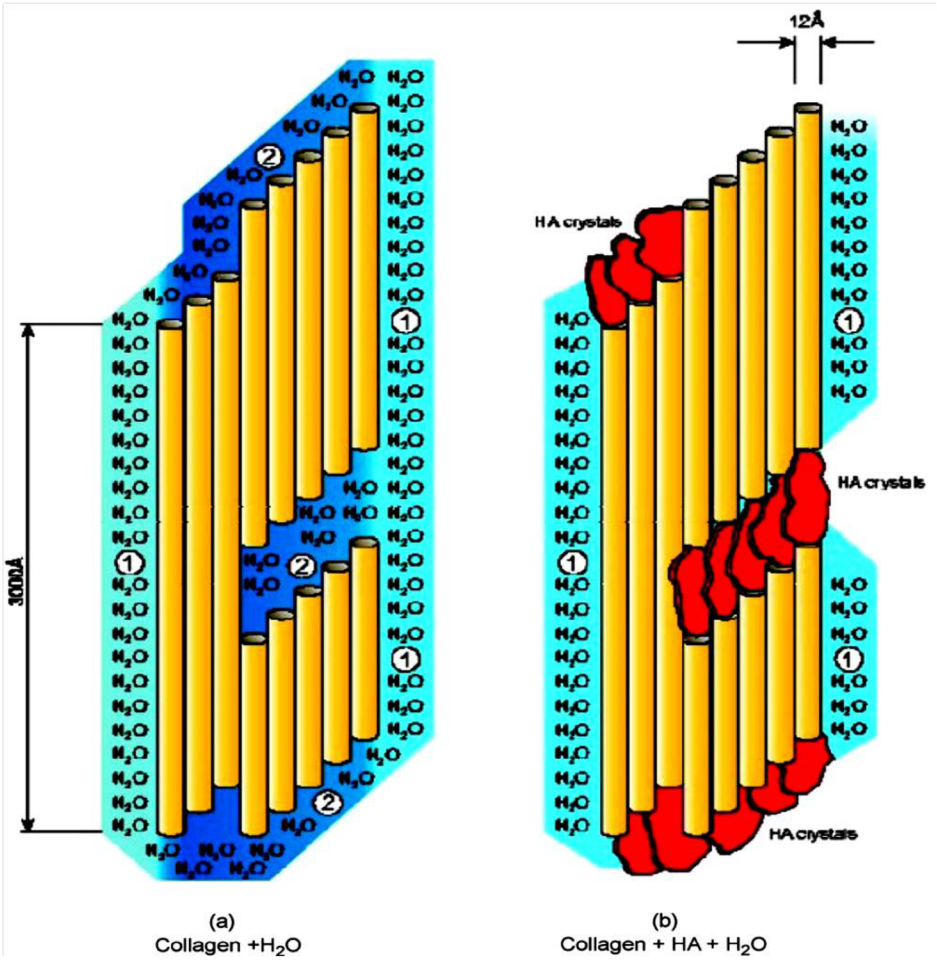

Fig. 2.17. A schematic diagram illustrating early mineralization of collagen in the water environment. (89)

Tien et al. (2012) also studied the problematic using FTIR spectrometry and XRD analysis to establish the effect of pH and came to the conclusion that higher pH (closer to the physiological pH of living organisms, approx. 8) favors composite formation, whereas lower pH leads to the dissolution of HAP. (103) Ficai et al. (2010) showed that the pH of mineralization affects the morphology of the resulting composites, increasing pH leads to the formation of elongated collagen molecules, whereas at lower pH, the collagen molecules adopt a crimpy shape. The self-assembling structure of collagen molecules with nanohydroxyapatite particles can be best shown by SEM (scanning electron microscopy), as presented in Fig. 2.18.

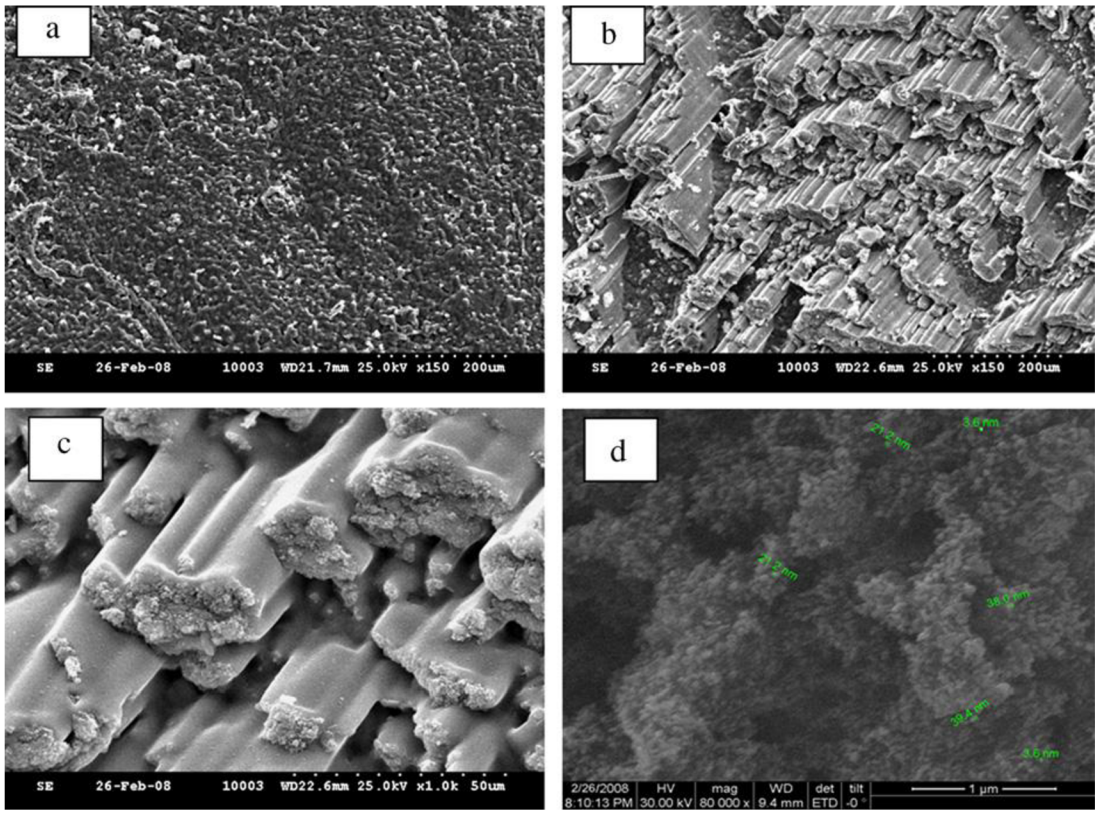

Fig. 2.18. The SEM images of collagen/hydroxyapatite composite materials, recorded at different magnification; (a) parallel view with the fibres, (b–c) perpendicular view with the fibres, (d) high resolution SEM at 80,000× magnification. (97)

2.6 Hierarchical collagen-based tissues – morphology and properties of bone, cartilage, tendons and dentin

Type I collagen molecules play a major role in tissue morphogenesis, since they form the greater part of the ECM proteins in dense connective tissues. (104) Tissue properties, as elasticity in the dermis, resistance to load in bone, resistance to shear or stretch in tendons all arise from specific matrix composition, fibril diameter or suprafibrillar organization. (63) Many biological tissues exhibit a hierarchical structure over several structural scales and their exceptional mechanical properties are believed to be due to a functional adaptation at all levels of hierarchy. (4)

2.6.1 Bone

Bone is a structural material that comprises the bulk of the vertebrate skeleton, its hierarchical structure has been described in a number of reviews. (29) (105) (31) Bone (or better: the ECM of bone) can be interpreted as a highly organized composite material. It is composed of assemblies of tropocollagen molecules and nanosized hydroxyapatite crystals, forming an extremely

tough yet lightweight material. (29), (30), (31) Several different types of bone are known which differ concerning their hierarchical organization, but all types consist of a nanocomposite made of collagen type I and a mineral phase, hydroxyapatite (HAP) at the nanometer scale. (106) The main roles of bone are: to provide the mechanical support for the body, to protect the vital inner organs and also act as a mineral reservoir for Ca^{2+} and PO_4^{3-}. (97) (107)

Fig. 2.19. shows the hierarchical architectures of bone, indicating its seven hierarchical levels. Level 1, the basic building blocks of bone, are collagen molecules and hydroxyapatite crystals. The next level is mineralized collagen fibrils in which plates of hydroxyapatite crystals are organized in layers that traverse across the fibril. At level 3, bone is an array of mineralized collagen fibrils, connected by a protein phase. Fibrils align and connect in random, parallel, tilted or woven orientations to form various fibre bundles as shown in level 4. The fibril bundles are organized into a lamellar structure with thickness of 3-7 µm. These lamellar structures are then stacked together to form cylindrical structures called osteons in level 5. The cylindrical structures are surrounded by circumferential lamellar rings with so-called “cement lines” at their outer boundaries. In the center of these cylindrical structures are large vascular channels (approx. 50-90 µm diameter). The cylindrical structures (osteons) further compose level 6 which contains spongy and compact microstructures depending on the positions of bone. The volume fraction distribution between the organic and mineral phase is approx. 60/40, making bone unquestionably a complex hierarchically structured biological composite. (1) (6) Finally the overall structural shape of bone in our body is constructed as shown in level 7. (10)

There are two fundamental types of bony tissue: trabecular and cortical. Although they are compositionally similar, due to the different hierarchical structuring, the properties are also different. Cortical bone is usually fairly dense with a porosity in the order of 6%, mainly due to the presence of blood vessels. Trabecular bone has a porosity in the order of 80% and can be considered as a foam-like network of bone trabeculae. (4)

The most important parameters which influence the properties of bone substitutes prepared in the collagen/HA system are: orientation of collagen molecules, fibrils and fibres that influence the hydroxyapatite structure and orientation; porosity; nature and quantity of cross-linking and processing methods. Among these, collagen orientation is the most important parameter which influences the properties without modifying composition. (97) From the microscale to the molecular scale, the structural levels of bone show sophisticated deformation and toughening mechanisms, which are also sources of inspiration for building advanced strong and tough materials based on the view of micro-/nanostructures. (10)

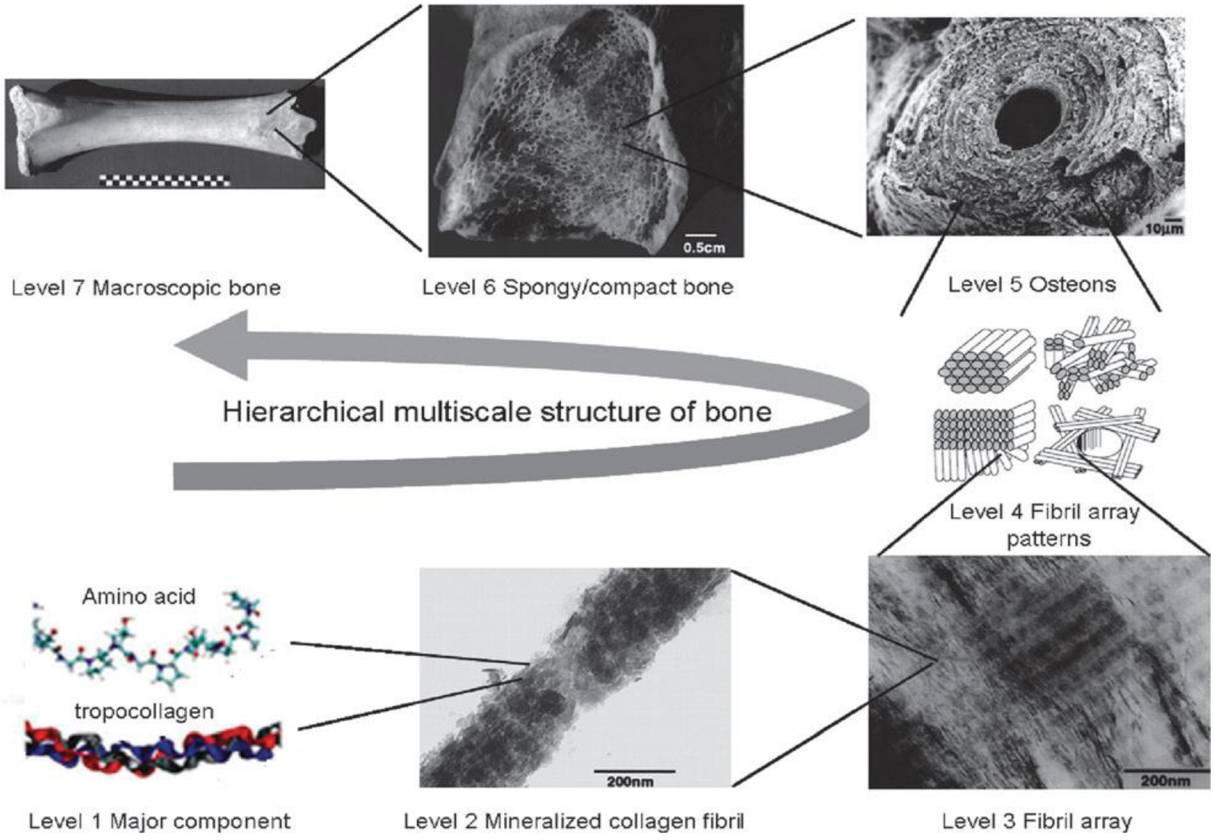

Fig. 2.19. The hierarchical organization of bone from the molecular to the macroscopic level. (10)

Deymier-Black et al. suggested that bone behaves like a traditional composite, shedding load from the more compliant, viscoelastic collagen matrix to the reinforcing elastic HAP platelets and also performed a finite element (FE) simulation of this at fibrillar level. (108) Fratzl et al. exemplified the hierarchical nature of bone deformation consistent with a staggered model of load transfer in the bone matrix (see Fig. 2.20.). (4)

In vivo, bone and tendon show a common feature of fibers joined by a thin glue layer which is loaded under shear. Plastic deformation in these systems is mediated mostly by the plastic flow of the glue layer. At small scales, the confined size of its building blocks has been shown to be an important element in reaching the characteristic mechanical properties of bone. (109) (110) Although bone has been quite widely studied in literature, the behavior of collagen-hydroxyapatite nanocomposites is relatively poorly understood, in particular from an atomistic perspective. The combination of full atomistic modeling techniques and coarse grain modeling can be successfully applied to describe collagenous tissues and bone from a fundamental point of view. (111) (112) (113)

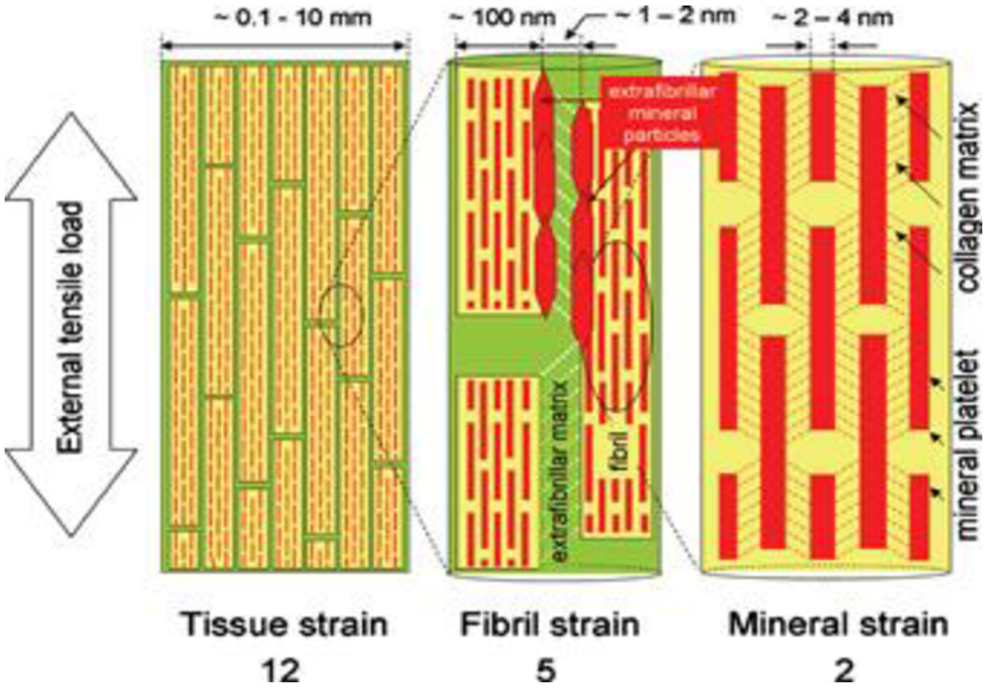

Fig. 2.20. Schematic model for bone deformation in response to external tensile load at three levels in the structural hierarchy from (114)*: at the tissue level (left), fibril array level (center), and mineralized collagen fibrils (right). The stiff mineralized fibrils deform in tension and transfer the stress between adjacent fibrils by shearing in the thin layers of extrafibrillar matrix. The fibrils are covered with extrafibrillar mineral particles shown only over a selected part of the fibrils (the red hexagons). Right: within each mineralized fibril, the stiff mineral platelets deform in tension and transfer the stress between adjacent platelets through shear in the interparticle collagen matrix (the red dashed lines indicate shear qualitatively, not implying homogenous deformation).*

Structural optimization of the individual bones requires that according to its mechanical function, each one will have a slightly different arrangement of the basic building blocks, the mineralized collagen fibrils. The consequence is that bending stiffness, fracture resistance and other mechanical properties will differ from site to site as a consequence of the different local architecture. (48) A common hypothesis is that the osteocytes sense the mechanical deformation of bone and thus, play a crucial role in the permanent adaptation process of bone. (4) The development of bone grafts based on the mineralization of self-assembled collagen fibrils in vivo and in vitro is an active area of research, showing great promise and success in clinical applications, on account of its compositional and structural similarity to autologous bone. (52)

2.6.2 Cartilage

Articular cartilage provides a resilient, low-friction bearing surface to bones where they articulate in diarthroidal joints. It is a remarkably smooth and tough material and protects the joint by distributing applied loads. (115) The mechanical properties of articular cartilage are determined by the content, arrangement and interactions of the tissue constituents, i.e., the three-dimensional collagen network, proteoglycans (PGs) and interstitial water. A schematic diagram illustrating typical articular cartilage structure is depicted in Fig. 2.21. Within articular cartilage, chondrocytes maintain the tissue structure by synthesizing and modulating collagen fibers and proteoglycan. (116)

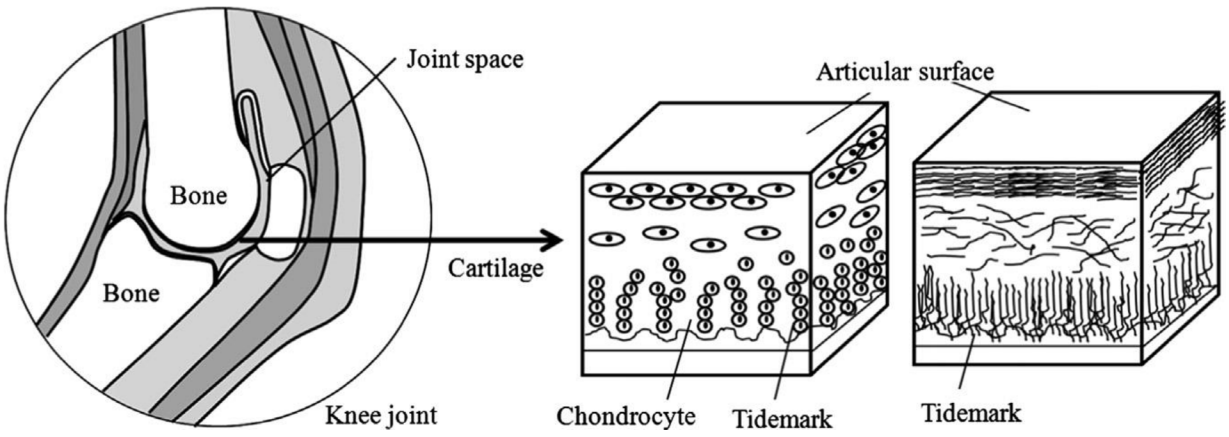

Fig.2.21. Schematic diagram of the knee joint and articular cartilage structure. Left and right schemes of the articular cartilage represent variable distribution and density (from high at the surface area to low at the bottom) of chondrocytes and fibrous structure, i.e., its gradient structure. (116)

The interstitial fluid pressure contributes strongly to the tissue stiffness under instant loads. However, under prolonged loads, fluid flows out of the tissue and PGs are mainly responsible for the tissue's compressive stiffness. Collagen fibers determine the tensile properties of articular cartilage. (117) The mechanical properties of articular cartilage are anisotropic and heterogeneous. Furthermore, due to its gradient structure, the mechanical properties also vary along a gradient. (116)

2.6.3 Tendons and ligaments

Another example of hierarchical collagenous tissues are tendons and ligaments, providing vital support to the musculoskeletal system, connecting bones with each other (ligaments) and with muscles (tendons). Tendon consists of a highly ordered hierarchy of successively larger structural

units, its structure is presented in Fig. 2.22. and is based on the same type of collagen fibrils as bone, with the difference that tendon is not normally mineralized.

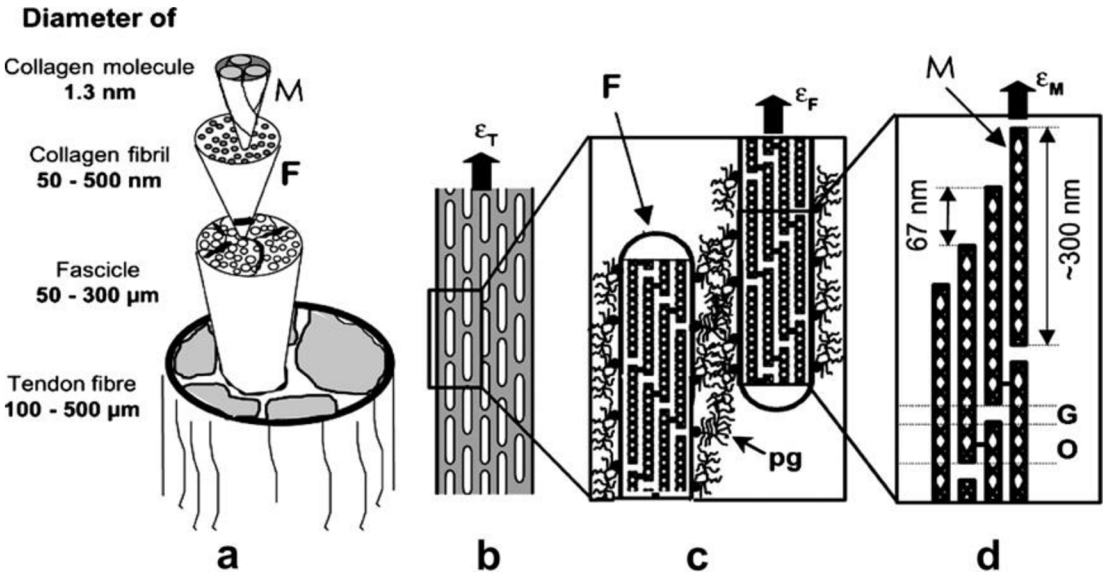

Fig. 2.22. a) Simplified tendon structure: tendon is made of a number of parallel fascicles containing collagen fibrils (marked F), which are assemblies of parallel molecules (marked M). b) The tendon fascicle can be viewed as a composite of collagen fibrils in a proteoglycan-rich matrix, subjected to a strain, ε_T. c) Some of the strain will be taken up by a deformation of the proteoglycan matrix. The remaining strain is transmitted to the fibrils. d) Triple-helical collagen molecules (M) are packed within fibrils in a staggered array with an axial spacing of D=67nm, when there is no load on the tendon. Since the length of the molecules (300nm) is not an integer multiple of the staggering period, there is a succession of gap (G) and overlap (O) zones. The lateral spacing of the molecules is around 1,5nm. The full 3D arrangement is not yet fully clarified, but seems to contain both regions of crystalline order and disorder. (118) (119) (120)

Collagen molecules aggregate into fibrils, and bundles of fibrils form fibres, many of which are aggregated into primary fiber bundles or subfascicles. Multiple subfascicles form secondary fiber bundles or fascicles, and several fascicles form tertiary fiber bundles. Most tendons consist of multiple fascicles, which is thought to be a fail-safe mechanism so that failure of one or more fiber bundles does not compromise the tendon strength. As illustrated in Fig. 2.23., fiber bundles are surrounded by a thin layer of connective tissue known as the endotenon, through which blood vessels, lymphatics and nerves pass. The whole tendon is bound by another thin layer (contiguous with the endotenon) known as the epitenon. A loose outer layer known as the paratenon surrounds most tendons (not shown), and some tendons are also surrounded by a specialized synovial sheath. (121)

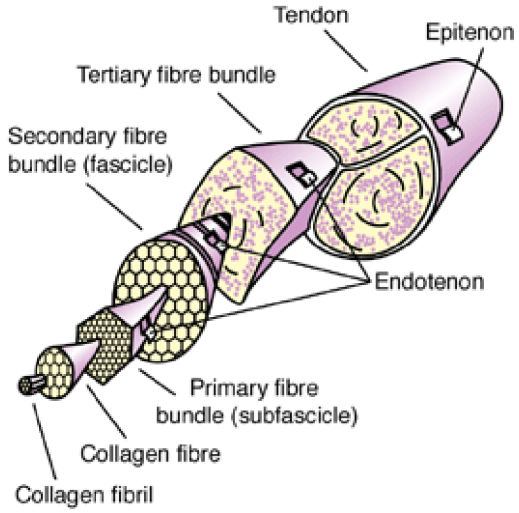

Fig. 2.23. Structure of the tendon. (121)

Tendons and ligaments enable musculoskeletal forces to be transmitted and redirected across skeletal joints within the body. Because of their high tensile strength (approx. 100-140MPa) and stiffness (approx. 1,0-1,5 GPa), tendons transmit muscle forces over long lengths with minimal „in series stretch“. By transmitting tensile stresses, as flexible structures tendons and ligaments also easily bend and change shape to accommodate changes in joint position and skeletal orientation. (122)

All collagen I-based tissues exhibit non-linear viscoelastic properties reflected in their stress-strain curves, where tendons and ligaments exhibit greater compliance at low stresses than at intermediate to higher stresses, enhancing their energy absorption capacity at low stress levels. This reduces their susceptibility to damage, which is important given the large number of loading cycles during an individual’s lifetime.

The low cell density of tendons and ligaments and the low metabolic activity of their fibroblast populations (123) (124) means that little energy is expended to transmit mechanical forces, compared to the much greater ATP consumption of muscle fibers that actively generate force and produce movement. Also due to their low hysteresis, a large fraction of the elastic strain energy stored in tendons during loading can be recovered upon unloading, making tendons highly resilient springs reducing muscle work and the energy cost of movement. (125)

2.6.4 Dentin

Dentin forms the bulk of mammalian teeth. It is covered by a thin, stiff and brittle layer of enamel protruding into the oral cavity. (126) Its basic constituents are a calcium-phosphate salt identified as dahllite, the organic component is mostly type I collagen (90%) in the form of a highly

crosslinked fibrous mesh. Other organic components include mostly non-collagenous proteins. The mineralization and hierarchical structure are illustrated in Fig. 2.24.

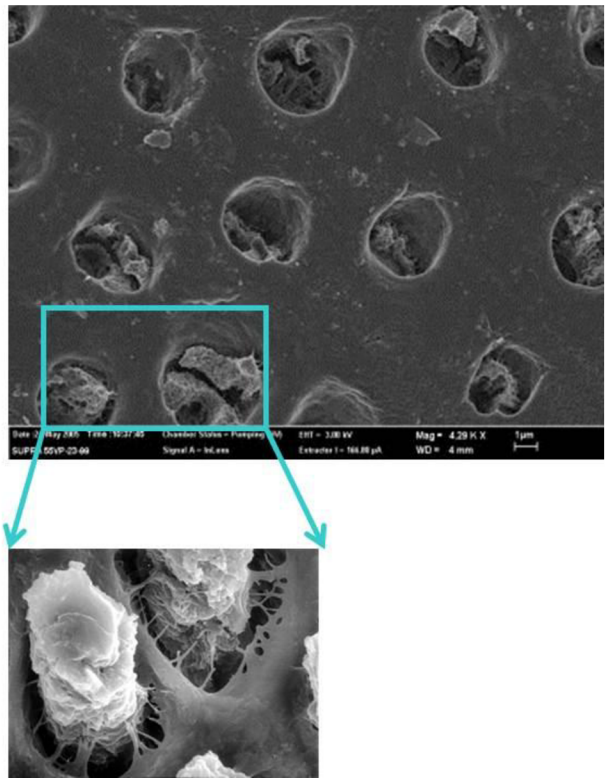

b)

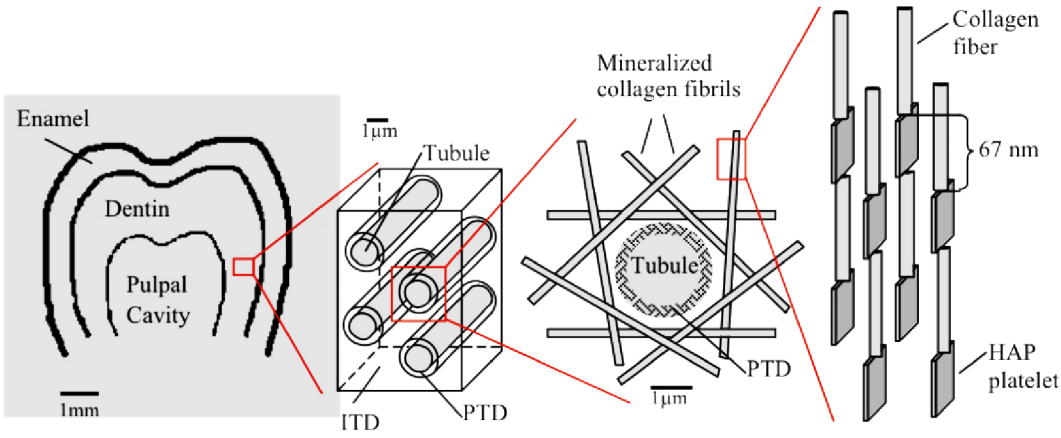

Fig. 2.24.(a) SEM of dentin cut perpendicularly to the tubuli showing the tubuli filled with HAP deposit. (b) Schematic of the hierarchical structure of teeth starting with the whole tooth molar (far left). Followed by the tubules surrounded by peritubular dentin (PTD) and intertubular dentin (ITD). This ITD is further composed of tangential mineralized collagen fibrils which are themselves hydroxyapatite and collagen composites (far right). (127)

In dentin, mineralized collagen fibrils are organized around long hollow cylinders called tubules. These tubules span the thickness of dentin, from the pulpal cavity to the surface of the dentin and are surrounded by a highly mineralized ring of hydroxyapatite called peritubular dentin (PTD). The mineralized collagen fibrils are then organized tangentially to the surface of the PTD creating the intertubular dentin (IDT). This complex structure allows dentin to be tough and strong, thus maintaining the structural integrity of teeth. (127)

Teeth are hard structures that need to be able to repeatedly withstand the application of sufficient load to perform their function (mastication). Their structure is formed only once and undergoes only minor biological changes over its lifetime. This is different compared to bones or tendons, which also function under load but undergo remodeling and restructuring in response to external mechanical stimulation. Consequently, tooth design, which to a large extent means dentin microstructure, represents an excellent solution to the overwhelming task of withstanding repeated tearing and compression load cycles during feeding. (126)

2.7 Polymer chain models

Ideal chains have no interactions between monomers that are far apart along the chain, even if they approach each other in space. Real chains interact with both their solvent and themselves. The relative strength of these interactions determines whether the monomers effectively attract or repel one another. At the so-called θ-temperature, chains are in nearly ideal conformations because the attractive and repulsive interactions between monomers cancel each other. The conformation of ideal chains is an essential starting point of most models in polymer physics. (59)

2.7.1 Conformation statistics

The fluctuations in bond length do not affect chain conformations, the angle between neighboring bonds called the tetrahedral angle $\theta = 68°$ is also almost constant. The main source of polymer flexibility is the variation of torsion angles. The zero value of the torsion angle φ_i corresponds to neighboring bond vectors being colinear and is called the trans state (t). The trans state of the torsion angle is the lowest energy conformation of the four consecutive CH_2 groups. The changes of the torsion angle φ_i lead to the energy variations illustrated in Fig. 2.25. These energy variations are due to changes in the distances and therefore interactions between carbon atoms and hydrogen atoms of this sequence of four CH_2 groups. The two secondary minima corresponding to the torsion angles $\varphi_i = \pm 120°$ are called gauche-plus (g+) and gauche-minus (g-). The energy difference between gauche and trans minima (Fig. 2.26.) determines the relative probability of a torsion angle being in a gauche state in thermal equilibrium. (59)

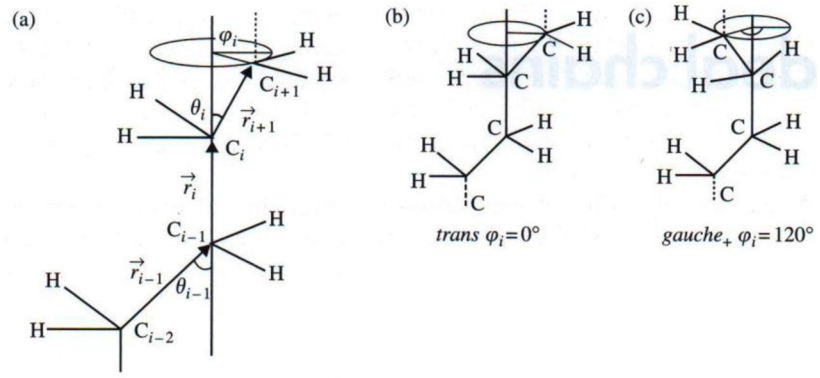

Fig. 2.25. a) Torsion angle φ_i for a sequence of three main-chain bonds. b) Trans state. c) Gauche-plus state.

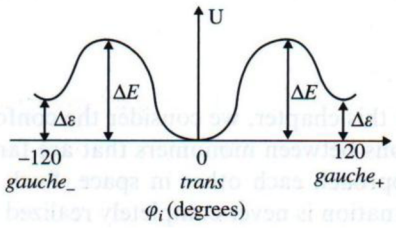

Fig.2.26. Torsion angle dependence of energy.

2.7.2 Ideal chain models

The various ideal chain models ignore interactions between monomers separated by large distances along the chain, however make assumptions about the allowed values of torsion and bond angles. Various models used to describe chain shape and conformation statistics are shown in the following Fig. 2.27. A single procollagen strand can be modelled as a shearable worm-like chain (WLC) and a collagen triple helix can be treated as either shearable WLC or WLC depending on the time scale of the excitations. Most synthetic polymers are treated as Gaussian chains.

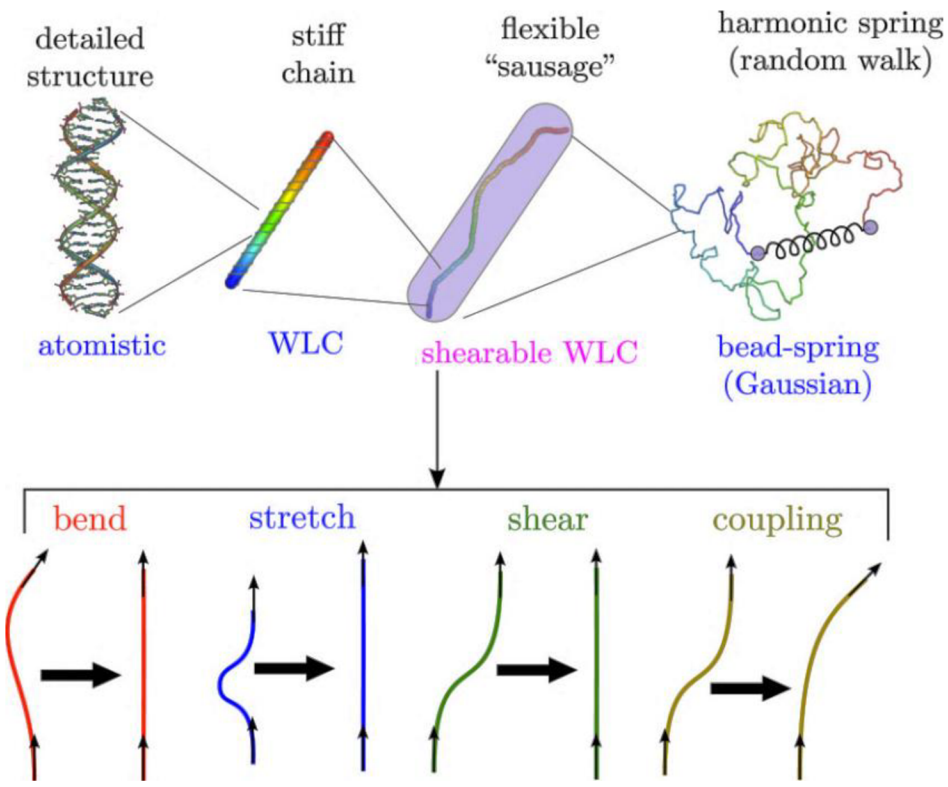

Fig. 2.27. Models used for conformation statistics description.

2.7.2.1 Freely rotating chain model

This model ignores differences between the probabilities of different torsion angles and assumes all torsion angles $-\pi < \varphi_i < \pi$ equally probable, ignoring the variations of the potential $U(\varphi_i)$. The freely rotating chain model assumes all bond angles are fixed and all torsion angles are equally likely and independent of each other.

2.7.2.2 Worm-like chain model

The worm-like chain (WLC) model (Fig. 2.28.) is a special case of the freely rotating chain model for very small values of the bond angle. It is an appropriate model for very stiff polymers such as double stranded DNA or fibrous proteins, for which the flexibility is due to fluctuations of the contour of the chain from a straight line rather than trans-gauche bond rotations.

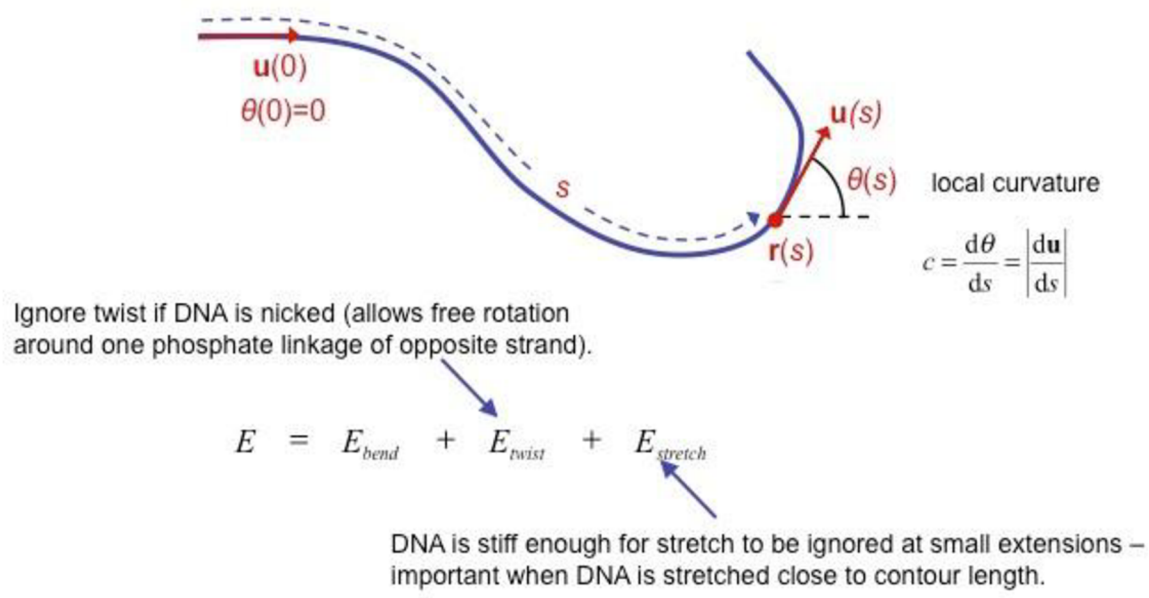

Fig. 2.28. The worm-like chain model does not account for local bond rotation and treats the molecule as a long flexible string. (9)

2.7.2.3 Hindered rotation model

The bond lengths and angles are assumed constant and torsion angles independent of each other. The torsion angle is taken to be hindered by a potential $U(\varphi_i)$ and the probability of any value of the torsion angle is taken to be proportional to the Boltzmann factor $exp[-U(\varphi_i)/kT]$. Most of the torsion angles are in low energy states, but also some higher energy states. The Boltzmann factor ensures that these higher energy states are less populated. The hindered rotation model assumes independent but hindered rotations of torsion angles with different potential profiles $U(\varphi_i)$ corresponding to different polymers.

2.7.2.4 Rotational isomeric state model

This most successful ideal chain model is used to calculate the details of conformations of different polymers. Bond lengths and bond angles are constant. Each molecule is assumed to exist only in discrete torsional states corresponding to the potential energy minima (see Fig. 2.26.)) The fluctuations about these minima are ignored. Each torsion angle can be in one of three states (t, g+, g-), in the rotational isomeric state model, these states are not equally probable, correlations between neighboring torsional states are included in the model.

2.8 Polymer chain dynamics

Polymer dynamics describes the motion of polymer chains in solution. In dilute solutions, the chains do not overlap. In the semi-dilute regime, the dynamics are strongly affected by the chain overlap and the possible formation of transient topological constraints. There are two types of inter-chain interactions: entangled and unentangled. Entanglements are topological constraints resulting from the fact that chains cannot cross through each other, in the case of unentangled interaction, the chains can move freely with respect to each other, both situations are illustrated below in Fig.2.29.

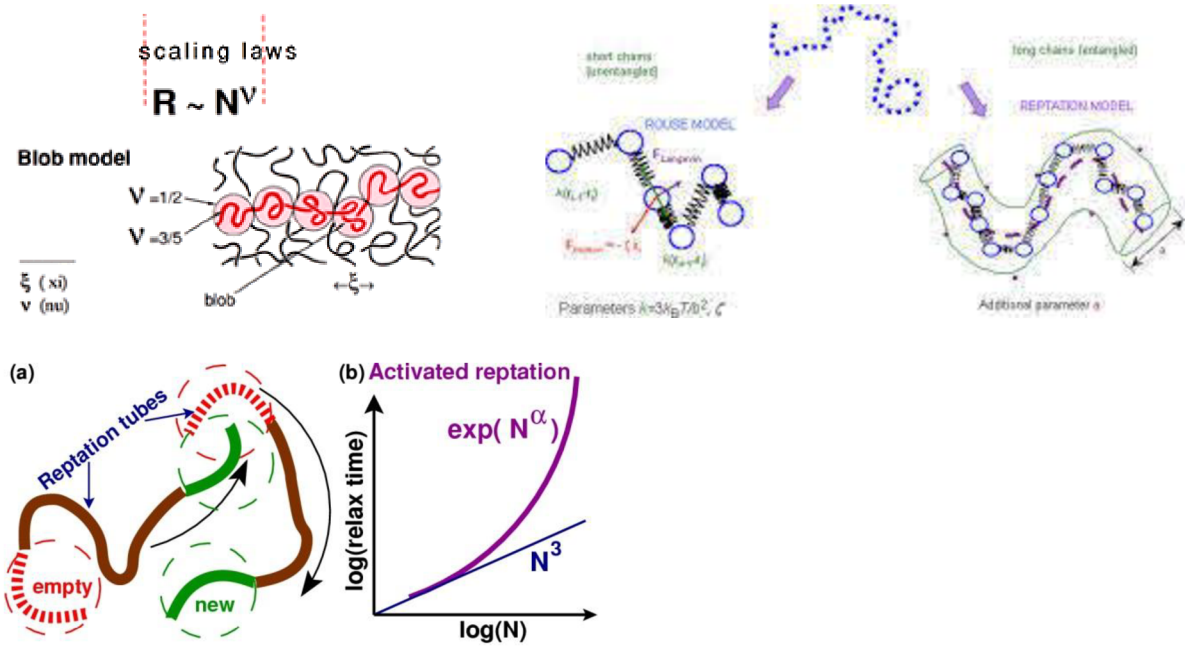

Fig. 2.29. (left) Reptation motion of a chain in concentrated polymer solution/melt showing the scaling (P-G DeGennes Nobel Price lecture). The red test chain can only move along the tube, whereas lateral displacements are prohibited by the entanglements with the black chains. The interactions with the black chains are non-entangled. (9)*(right) schematics of Rouse and reptation models, (bottom) Reptation movement of the tube within which the chain is obeying Rouse dynamics.*

2.8.1 Unentangled polymer dynamics

The three-dimensional mean-square displacement of a colloidal particle during time t is proportional to t, with the coefficient of proportionality related to the diffusion coefficient D:

$$\langle[\vec{r}(t) - \vec{r}(0)]^2\rangle = 6Dt \qquad (2.13)$$

When the motion obeys Eq. 2.13, it is called a simple diffusive motion (often referred to as Brownian). If a constant force $\vec{f}$ is applied to a small particle, pulling it through the liquid, the particle will achieve a constant velocity $\vec{v}$ in the same direction as the applied force. For a given particle and liquid, the coefficient relating force and velocity is the friction coefficient ς:

$$\vec{f} = \varsigma\vec{v} \tag{2.14}$$

There is an equal and opposite viscous drag force of the liquid acting on the particle. The diffusion coefficient D and the friction coefficient ς are related through the Einstein relation:

$$D = \frac{kT}{\varsigma} \tag{2.15}$$

2.8.1.1 Rouse model

The first successful molecular model of polymer dynamics was developed by Rouse. The chain in the Rouse model is represented as *N* beads connected by springs, see Fig. 2.30. Each bead is characterized by its own independent friction coefficient ς. Solvent is assumed to be freely draining through the chain as it moves.

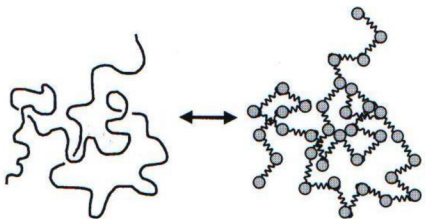

Fig. 2.30. In the Rouse model, a chain of N monomers is mapped onto a bead-spring chain of N beads connected by springs.

The total friction coefficient of the whole Rouse chain is the sum of contributions from each of the *N* beads $\varsigma_R = N\varsigma$. The diffusion coefficient of the Rouse chain is obtained from the Einstein relation:

$$D_R = \frac{kT}{\varsigma_R} = \frac{kT}{N\varsigma} \tag{2.16}$$

A polymer diffuses a distance of the order of its size during a characteristic time called the Rouse time, τ_R:

$$\tau_R \approx \frac{R^2}{D_R} \approx \frac{R^2}{kT/(N\zeta)} = \frac{\zeta}{kT} NR^2 \qquad (2.17)$$

The Rouse time has a special significance, on time scales shorter than the Rouse time, the chain exhibits viscoelastic modes, on time scales longer than the Rouse time, the motion of the chain is simply diffusive. (59)

2.8.1.2 Zimm model

The viscous resistance imparted by the solvent when a particle moves through it arises from the fact that the particle must drag some of the surrounding solvent with it. The force acting on a solvent molecule at distance *r* from the particle becomes smaller as *r* increases is called hydrodynamic interaction. In the case of a bead-spring model of a polymer chain, when one bead moves, there are hydrodynamic interaction forces acting on the other beads of the chain. The Rouse model ignores hydrodynamic interaction forces and assumes that the beads only interact through the springs that connect them, which is reasonable for polymer melts, but incorrect for a polymer in a dilute solution.

The hydrodynamic interactions between monomers and the solvent within the pervaded volume of the chain are strong, so when the polymer moves, it effectively drags the solvent within its pervaded volume with it. The Zimm model treats the pervaded volume of the chain as a solid object moving through the surrounding solvent.

The friction coefficient of the chain of size R being pulled through a solvent of viscosity η_S is given by Stokes' law:

$$\zeta_Z \approx \eta_S R \qquad (2.18)$$

From the Einstein relation, the diffusion coefficient of a chain in the Zimm model is reciprocally proportional to its size *R*:

$$D_Z = \frac{kT}{\zeta_Z} \approx \frac{kT}{\eta_S R} \qquad (2.19)$$

The Zimm model predicts that the chain diffuses as a particle with volume proportional to the chain's pervaded volume in solution. In the Zimm model, the chain diffuses a distance of order of its own size during the Zimm time τ_Z:

$$\tau_Z \approx \frac{R^2}{D_Z} \approx \frac{\eta_S}{kT} R^3 \qquad (2.20)$$

In dilute solution, the Zimm time is shorter than the Rouse time. In principle, a chain in a dilute solution could move a distance of order of its own size by Rouse motion, by Zimm motion, or some combination of the two.

In unentangled polymer dynamics, there are two limits: the Zimm limit applies to dilute solutions, where the polymer dynamics are described by the Zimm model; the Rouse limit applies to unentangled polymer melts, where hydrodynamic interactions are screened. In semi-dilute solutions there is a length scale called the hydrodynamic screening length ξ_h, separating these two types of dynamics. On length scales shorter than the hydrodynamic screening length, hydrodynamic interactions dominate and the dynamics are described by the Zimm model. On length scales larger than the screening length, the hydrodynamic interactions are screened by surrounding chains and the dynamics are described by the Rouse model. (59)

2.8.2 Entangled polymer dynamics – the reptation model

The topological constraints imposed by neighboring chains on a given chain restrict its motion to a tube-like region. As described by the Edwards tube model (Fig. 2.31.), the motion of the chain along the contour of the tube (the primitive path) is unhindered by topological interactions. Displacement of monomers in the direction perpendicular to the primitive path is restricted by surrounding chains to an average distance *a*, called the tube diameter.

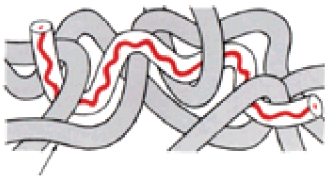

Fig. 2.31. The primitive path of an entangled polymer chain in the Edwards tube model. (128)

By utilizing the Edwards tube concept, deGennes reduced the many body problem of polymer motion in a melt to the motion of a single chain confined to a tube of surrounding chains and he proposed the simplest tube model for the motion of linear entangled polymers called the reptation model. In de Gennes' reptation model, an entangled chain diffuses along its confining tube in a way analogous to the motion of a snake or worm. This curvilinear motion is characterized by the

Rouse friction coefficient $N\zeta$. The curvilinear diffusion coefficient is simply the Rouse diffusion coefficient of the chain:

$$D_c = \frac{kT}{N\zeta}. \tag{2.19}$$

The time it takes for the chain to diffuse out of the original tube of a certain length is the reptation time, predicted to be a cube of the molar mass (though the experimentally measured scaling exponent is higher than 3). On length scales smaller than the tube diameter *a*, topological interactions are unimportant and the dynamics are similar to those in unentangled polymer melts as described by the Rouse model.

The stress-relaxation modulus in the reptation model is proportional to the fraction of the original tube remaining at time *t*. As time goes on, sections of the original tube are abandoned when the chain end first visits them. By solving this first-passage problem, the stress-relaxation modulus *G(t)* for the reptation model was calculated by Doi and Edwards:

$$G(t) = \frac{8}{\pi^2} G_e \sum_{odd\ p} \frac{1}{p^2} \exp\left(-\frac{p^2 t}{\tau_{rep}}\right). \tag{2.20}$$

This Doi-Edwards equation is the first attempt at a molecular model for viscoelasticity of entangled polymers. The reptation model prediction for the viscosity of an entangled polymer melt is determined by integrating the Doi-Edwards equation

$$\eta = \int_0^\infty G(t)dt = \frac{8}{\pi^2} G_e \sum_{odd\ p} \frac{1}{p^2} \int_0^\infty \exp\left(-\frac{p^2 t}{\tau_{rep}}\right) dt = \frac{\pi^2}{12} G_e \tau_{rep}, \tag{2.21}$$

where G_e is the plateau modulus and τ_{rep} is the reptation time required for the chain to escape from its tube. The viscosity of a polymer melt is predicted to be proportional to the molar mass for unentangled melts (the Rouse model) and proportional to the cube of molar mass for entangled melts (the reptation model). (59)

2.9 Viscoelasticity of collagen solutions and hydrogels, rheology

When materials are deformed, they display a small regime in which deformation is reversible or elastic. Once the forces on the material reach a certain level, deformation becomes irreversible and remains even after the load is removed. This is referred to as the plastic regime. Plastic deformation is typically followed by fracture, when the material breaks and fails. Many materials including biological tissues show this generic behavior. However, the details of the response to

mechanical load depend on the atomic and molecular makeup of the material; from nano- to macroscales. The overview of material scales and corresponding modes of deformation is depicted in Fig. 2.32. (7)

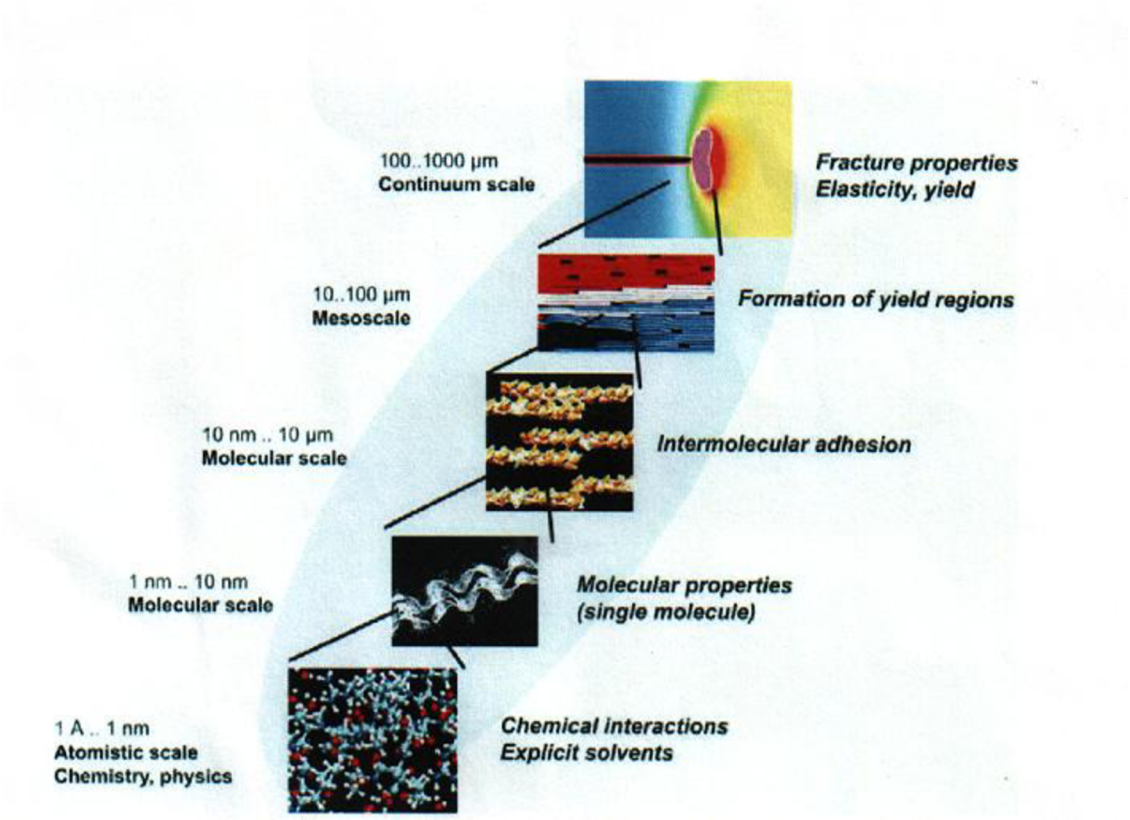

Fig. 2.32. Overview of different material scales, from nano to macro, here exemplified for collagenous tissue. (7)

2.9.1 Hydrogel viscoelasticity

Hydrogels have gained great attention in the last decades, mainly due to their biomedical applications. Hydrogels are three-dimensional, hydrophilic polymeric networks capable of retaining large amounts of water or biological fluids, characterized by a soft and rubbery consistence, thus bearing similarity to living tissues. Because of their hydrophilicity and other unique properties such as biocompatibility and biodegradability, hydrogels can be exploited as scaffolds for tissue engineering (129) (130), carriers for drug delivery (131) and other biomedical applications. Hydrogels may be chemically stable or “reversible” (physical gels) stabilized by molecular entanglements and/or secondary forces including ionic, H-bonding or hydrophobic interactions. (132) (133)

Most hydrogels suffer from a lack of mechanical strength, as a result, few hydrogels are used to bear significant mechanical load in current applications. (134) (135) (136) The poor mechanical properties of hydrogels originate from their low resistance to crack propagation due to the lack of an

efficient energy dissipation mechanism in the gel network (137) (138). To obtain hydrogels with a high degree of toughness, a number of techniques have been proposed such as topological gels (139), nanocomposite hydrogels (140) (see Fig. 2.33.), and the double network (DN) hydrogels (141). Typically DN hydrogels have a very special interpenetrating network (IPN) structure and are composed of a combination of a stiff, brittle first network and a soft, ductile second network, so when subjected to deformation, they can effectively relieve the stress concentration and increase the resistance against crack propagation. (142) This behavior is associated with the fracture of the rigid and brittle network, which serves as sacrifical bonds in the toughening of DN hydrogels. (143) (144) The load transfer between the two networks is via inter-network topological entanglement. (145)

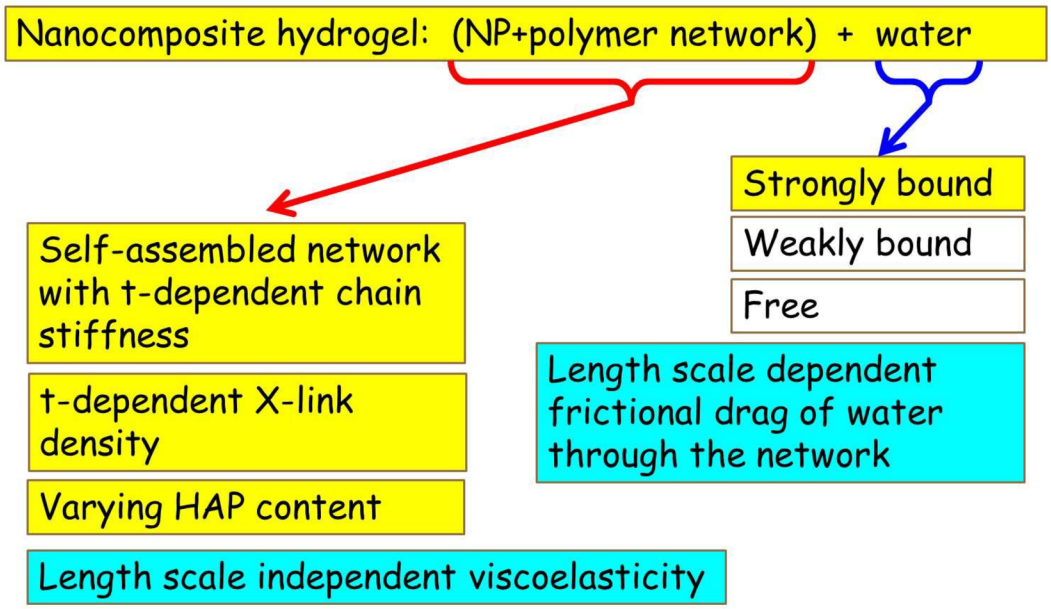

Fig. 2.33. Considerations of nanocomposite hydrogel viscoelasticity.

The deformation of hydrogels is time-dependent (see scheme 2.33. above), resulting from two concurrent molecular processes: the conformational change of the network and the migration of the solvent. The two processes result in viscoelasticity and poroelasticity as shown in Fig. 2.34. (146) (147)

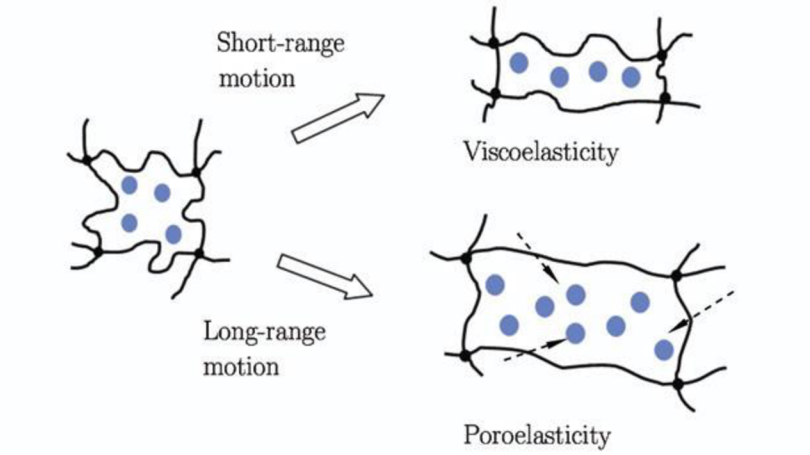

Fig. 2.34. A gel evolves by two molecular processes: the conformational change of the polymer network, and the migration of the solvent molecules. The two processes result in the macroscopic behavior of viscoelasticity and poroelasticity. In viscoelasticity, solvent molecules move relative to the polymer network over a short range. In poroelasticity, solvent molecules move relative to the polymer network over a long range. (146)

Physical gels can be disintegrated by changes in the environment conditions such as ionic strength, pH and temperature and have numerous biomedical applications in drug delivery, tissue engineering, etc. Covalently cross-linked networks form chemical gels. (132) (133) (148)

In an elastomeric gel, viscoelasticity results from the molecular processes such as sliding between the polymer chains and rotation of the joints between segments of an individual chain. (149) Dynamic viscoelastic properties of collagen solutions can be characterized by means of rheology, collagen solutions exhibit shear-thinning flow behavior. Lai et al. (2008) also found that both storage and loss modulus increased with the increase of frequency and concentration. (150)

2.9.2 Rheology

Rheology is the science of flow and deformation of matter. The relation between stress and deformation is a property of the material. Rheology can therefore be also defined as the study of stress-deformation relationships. (151) Uniaxial tension and simple shear are the two simplest types of deformation that can be applied to a material. The force *f*, causing the deformation can be normalized to the cross-section *A* of the sample results in shear stress, σ:

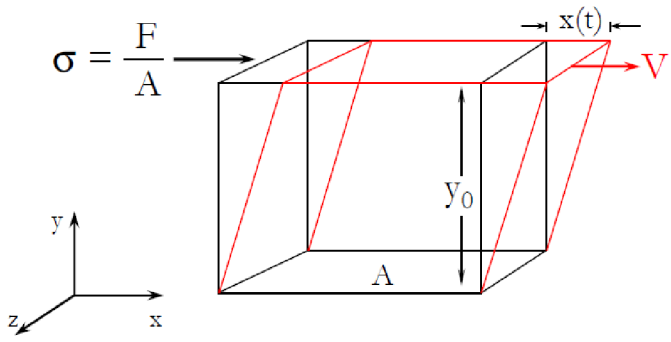

Fig. 2.35. Illustration of shear in a three-dimensional body.

The strain can be expressed as

$$\gamma = \frac{x(t)}{y_0}, \tag{2.22}$$

the strain rate as

$$\dot{\gamma} = \frac{V}{y_0}, \tag{2.23}$$

and the fluid viscosity as

$$\eta = \frac{\sigma}{\dot{\gamma}} \tag{2.24}$$

Materials behave in the linear matter as described by Hooke and Newton only on a limited small scale of stress or deformation. Polymers and many biological tissues, including collagen, are viscoelastic. (99) The viscous part of the response of such materials is due to the flow of polymeric chains (reptation – diffusive or forced) and represents mechanical energy dissipated during loading. Phenomenologically, such materials can be modelled as a set of mechanical springs and dashpots, such as the parallel Kelvin – Voigt model or the serial Maxwell model illustrated in Fig. 2.36. (152) (151)

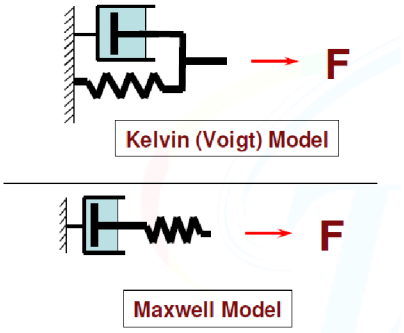

Fig. 2.36. The Kelvin – Voigt and Maxwell spring-dashpot models demonstrating viscoelastic behavior, where force depends on deformation and rate of deformation and vice versa. (151)

The spring corresponds to purely elastic behavior (Hookean solid); the tensile modulus, E, and the shear modulus, G, in a linearly elastic solid can be expressed as:

$$E = \sigma/\varepsilon \tag{2.25}$$

$$G = \frac{\tau}{\gamma} \tag{2.26}$$

The dashpot represents a purely viscous response (Newtonian fluid), where the stress is proportional to the strain rate:

$$\sigma = \eta.\dot{\gamma} \tag{2.27}$$

In the oscillatory mode, for a purely elastic material, the stress and strain are in phase, for a purely viscous material, they are out of phase. In a viscoelastic material, they are shifted by a phase lag, δ, as depicted below in Fig. 2.37.

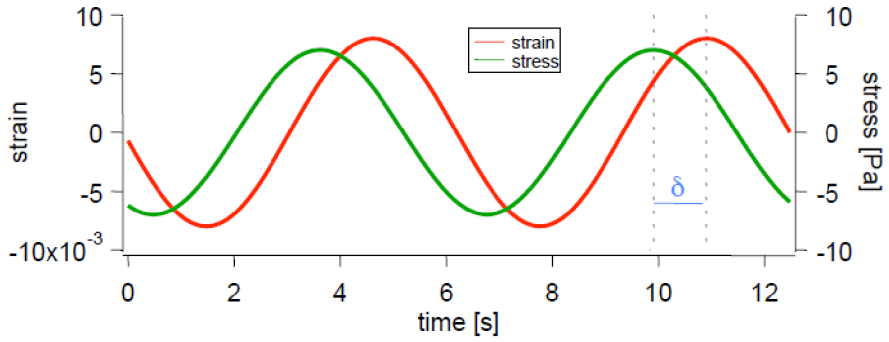

Fig. 2.37. The stress and strain are shifted for a viscoelastic material. (153)

In a viscoelastic material,

$$\gamma(\omega, t) = G'.\gamma_0.\sin(\omega t) + G''.\gamma_0.\cos(\omega t) \quad (2.28)$$

$$tan\delta = \frac{G''}{G'}, \quad (2.29)$$

where ω is the angular frequency, δ is the phase lag and γ_0 is strain amplitude, t is time. G' is the storage (in-phase, elastic) modulus and G'' is the loss (out-of-phase) modulus.

Rheology employs two basic approaches, the first applies force and measures deformation and/or deformation rate (controlled force, controlled stress), the second controls deformation and/or deformation rate and measures the force needed (controlled displacement, rotation, controlled strain or shear rate). The possible geometries appropriate for shear testing include concentric cylinders (low to medium viscosity), cone and plate (very low to high viscosity), parallel plates (very low viscosity to soft solids), and torsion (very soft to rigid solids). They are illustrated below in Fig. 2.38. For the collagen solutions that are the subject of our research, the cone and plate setup appears as the most advantageous, shear stress and shear rate are constant throughout the gap.

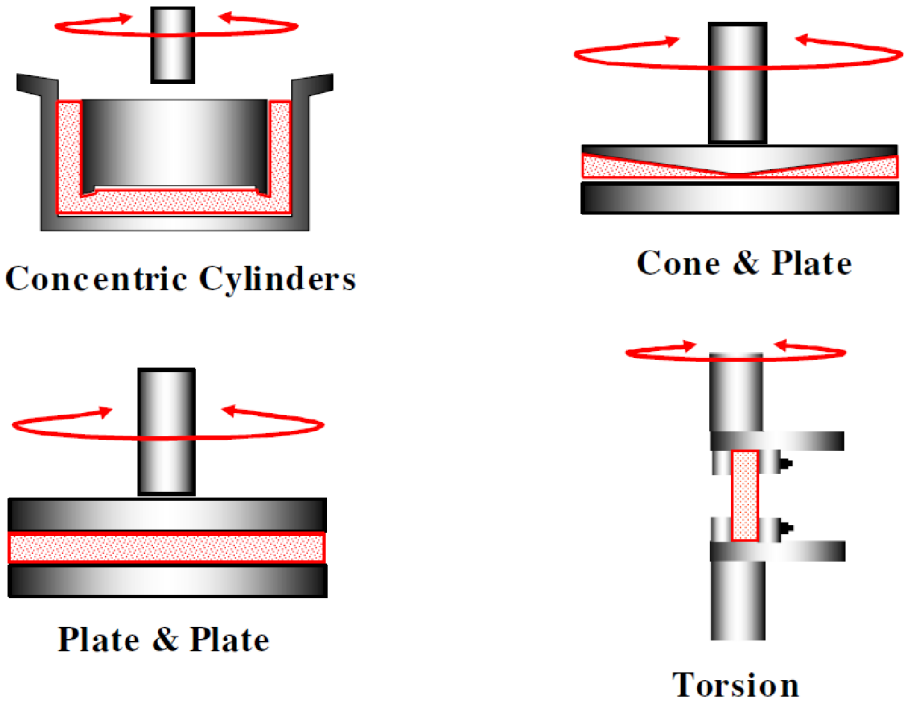

Fig.2.38. The possible rheometer geometries for shear testing. (153)

2.10 The deformation response of BPMs

Biological protein materials (BPMs) such as skin, bone or cytoskeletons feature complex, hierarchical structures. Their macroscopic mechanical behavior is controlled by the interplay between various properties throughout multiple length and time scales. In order to understand their deformation and fracture mechanisms, it is crucial to elucidate relevant molecular mechanisms decisive for response at each individual length scale. BPMs have a significantly different molecular structure than crystalline materials, which induces a variety of novel deformation mechanisms. Whereas crystalline materials show mechanisms such as movement of dislocations or crack extension and bridging, hierarchical BPMs feature molecular unfolding or sliding, where hydrogen bond rupture is of particular importance. (7) (154)

A major trait of BPMs is the occurrence of hierarchies and the abundance of weak interactions. Utilization of weak interactions makes it possible to produce strong materials at moderate temperatures and thus with limited energy use simply by multiplying the properties of molecular features characterized by these weak interactions. (155) The mechanical properties of biological protein materials have wide ranging implications in biology and medicine. Up to now, neither a systematic classification nor fundamental theories exist for different deformation and fracture mechanisms in biological protein materials. (7) Several attempts have been made to describe the deformation mechanics of collagen fibers and networks.

Large deformation is a critical physiological condition for collagen-rich tissue. The risk of catastrophic brittle-like failure needs to be minimized to sustain optimal biological function. The nanoscale ultrastructure of collagen may be designed to provide robust material behavior under large deformation by choosing long TC molecules. Robustness is achieved by the design for maximum strength and maximized energy dissipation by shear-like mechanisms. The requirement for maximum energy dissipation given by the following equation plays a crucial role in determining the optimal molecular length

$$E_{diss} = \int_{l=0}^{l=L_c} l\tau_{shear} dl = \frac{1}{2} L_c^2 \tau_{shear} \ , \qquad (2.30)$$

the expression for the dissipation energy is derived from the fact that the shear resistance between two TC molecules τ_{shear} leads to a contact-length L_c dependent force; and is equal to the work necessary to separate two fibers in contact along the length L_c under macroscopic tensile deformation. (48)

The key to comprehend the mechanical response of BPMs across the different time and length scales is to understand the rupture mechanics of hydrogen bonds (HBs) under laterally applied load. Typically, a variety of unfolding processes exist for a protein structure, each of which has a

specific reaction pathway and an associated energy barrier, mostly related to the bond-breaking mechanisms and rearrangements in the protein structure. Several theories exist that describe competing processes arising from mechanically induced instabilities of protein structures. These concepts stem primarily from a theory originally postulated by Bell.

Whereas continuum theories are suitable to describe the deformation of macroscopic structures, statistical concepts must be employed to accurately model the mechanical behavior of protein structures. Bell´s theory is one of the most widely used models to describe the statistical nature of bond breaking. (7)

In Bell´s theory, the off rate χ is the product of the natural bond vibration frequency ω_0 and the quasi-equilibrium likelihood of reaching the transition state with an energy barrier E_b that is reduced by mechanical energy $F.x_b.\cos(\theta)$, where F is the applied force, x_b is the distance between the equilibrated state (minimum of the well) and the transition state, and θ is the angle between the direction of the reaction pathway of bond breaking (x-direction) and the direction of applied load F (see Fig. 2.39.).

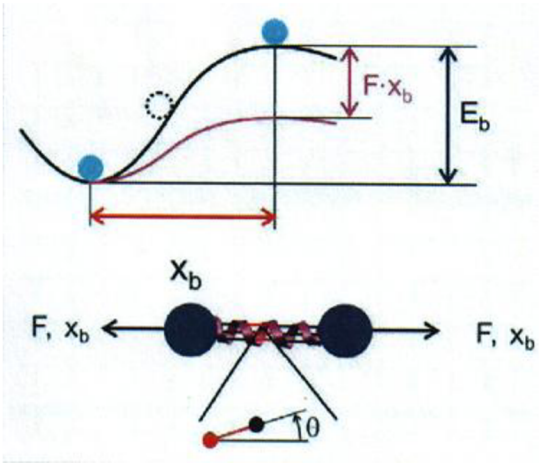

Fig. 2.39. Statistical theory to predict the bond rupture mechanics. The graph depicts the energy as a function of deformation. (7)

The angle can be determined by analyzing the molecular geometry. The off rate is given by:

$$\chi = \omega_0 . exp\left(-\frac{(E_b - F.x_b.\cos(\theta))}{k_b.T}\right) \qquad (2.31)$$

and describes how often a bond is broken per unit time (it equals the reciprocal of the lifetime of a bond). However, this equation does not describe the dependence of the pulling speed at which a bond breaks because of the applied pulling force. Instead, it only provides an estimate of the time scale at which the bond will be broken. In order to overcome this limitation, a modification needs to

be made based on the following idea: the speed *v* at which a bond is broken equals the distance that needs to be overcome in order to break the bond (x_b) divided by the time for bond breaking. Consequently, v is the product of $\chi.x_b$. This leads to the following equation for the bond breaking speed:

$$v = \omega_0 x_b . exp\left(-\frac{(E_b - F.x_b.\cos(\theta))}{k_b.T}\right), \tag{2.32}$$

which can be rewritten as:

$$v = v_0 . exp\left(\frac{F.x_b.\cos(\theta)}{k_b.T}\right) \tag{2.33}$$

with v_0 as the natural bond-breaking speed (when no load is applied), defined as:

$$v_0 = \omega_0 . x_b exp\left(-\frac{E_b}{k_b.T}\right). \tag{2.34}$$

This modified framework enables the dependence between the unfolding force and the bond breaking speed to be studied or the average force at which a bond breaks at a certain rate to be calculated. It is expressed as follows:

$$F(v) = \left(\frac{k_b T.}{x_b \cos(\theta)}\right). lnv - \left(\frac{k_b T}{x_b \cos(\theta)}\right) lnv_0 = a. lnv + b \tag{2.35}$$

This equation predicts that the unfolding force depends logarithmically on the pulling speed in a nonequilibrated system. It contains two parameters *a* and *b*, which can be calculated from the parameters x_b and E_b at a certain temperature and angle. (7)

Equation (2.35) provides an immediate link between the molecular geometry (via the angle θ), the pulling rate, and the pulling force *F* that is necessary to lower the energy barrier in such a way that HBs can be broken at the applied pulling velocity. A possible strategy to determine the dependence of the unfolding force *F* on pulling speed, associated mechanisms, and energy barriers is to carry out MD simulations at different pulling rates, measure the dependence of the unfolding force on the pulling rate, and fit the parameters *a* and *b* to this data. This information can then be used to calculate the parameters x_b and E_b and thereby reconstruct the free energy landcape. (7)

In order to apply the extended Bell theory to the slow pulling regime, the parameters x_b and E_b must be modified. E_b is multiplied by a factor of three to account for the fact that three HBs rupture simultaneously instead of one, and the value of 1,25Å (corresponding to the transition distance of HBs) is used a s a value for x_b. (7)

Libonati et al. (156) identified the deformation mechanisms by visualizing the molecular structures of collagen/HAP at different deformation stages, which can be summarized as follows:

- Breaking of atomic interactions (i.e. electrostatic and vdW interactions, which require the lowest energy to be broken), between the collagen chains and between collagen and hydroxyapatite,
- Chain uncoiling and unfolding, due to the breakage of intramolecular H-bonds, which initially stabilize the collagen triple helix, and
- Sliding of the collagen chains on the hydroxyapatite surface in a discontinuous way, owing to the progressive breakage of H-bonds.

Fig. 2.40. presents snapshots from a simulation capturing the aforementioned deformation mechanisms:

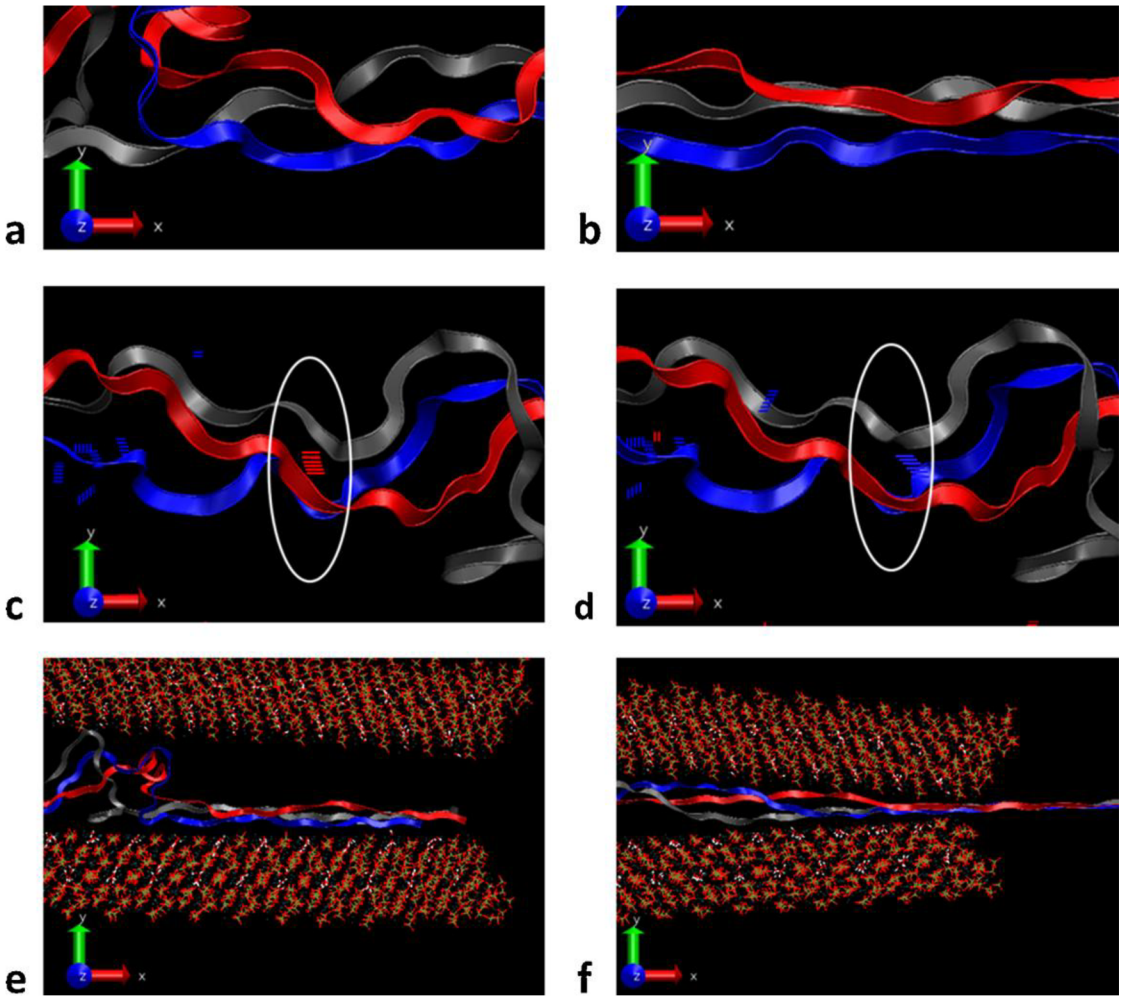

Fig. 2.40. Snapshots revealing the primary deformation mechanisms. (a and b) Chain uncoiling and unfolding in two consecutive steps, occuring due to breakage of intramolecular H-bonds, which initially stabilize the collagen triple helix. (c and d) Intra-molecular H-bonds formation and breakage (in c), an H-bond is highlighted in red lines, in d), this H-bond is broken and a new one represented by the blue line is formed. (e and f) Chain sliding and stretching: e) and f) show how the collagen chain slides on the mineral surfaces and how it is stretched as the force is applied. (156)

According to computational models, the intermolecular H-bonds play a major role in the interface strength of the studied nanocomposite system (a collagen/nHAP sandwich structure); the deformation mechanisms can be explained as follows. Initially, when the force-displacement trend is linear, chain unfolding and uncoiling via intramolecular H-bonds breakage occurs. Subsequently, continuous formation and breakage of inter-molecular H-bonds takes place, which facilitates protein sliding on the mineral surface in a discontinuous way, and hence increases the energy required for failure.

This trend is less clear in the solvated case due to the water-mediated effect (i.e. H-bonds form with water molecules also). Indeed, the presence of water, which interacts with both collagen and hydroxyapatite, reduces the direct coupling between the protein and the mineral. This concept has been shown in previous studies (114), where „sacrificial bonds“ such as H-bonds have been shown to play a crucial role. In fact, the progressive formation and breakage of such bonds act as a significant energy dissipation mechanism, leading to an increase in toughness. Final failure occurs by breakage of the tropocollagen molecule, being the weakest component, instead of the interface failure. (156)

2.11 Reinforcing mechanisms in polymer nanocomposites

Most of the existing mechanical models describing the effects of local nano-structure on the mechanical response of bone consider regular distribution of simple shaped rigid inclusions in a polymer continuum. Despite the fact that the discrete nature of the structure at the nano-scale is acknowledged in these models, the fundamental effects related to the molecular nature of the proteins forming the matrix are neglected and the fact that due to highly non-local response of polymers, the classical continuum mechanics is of limited validity is not taken into consideration. It has been suggested that the validity of continuum elasticity models can be extended to account for the nano-scale non-locality of deformation response of polymeric component by using higher order elasticity combined with molecular dynamics. The reinforcement in filled polymers consists of two main contributions. The first one independent of particle size is related to the volume of the rigid filler and it is dominating for particles larger than 1μm or with specific surface area smaller than $10m^2/g$. The second mechanism strongly related to the particle size and particle-chain interfacial interactions is due to the changes in molecular mobility and chain packing occuring above the matrix T_g. In nanocomposites above the matrix T_g, the second contribution becomes dominant. In addition, these effects can alter thermodynamic transitions in collagen, i.e., self-assembly.

To describe quantitatively the molecular mechanisms leading to significant increase of elastic modulus with nano-filler content above the T_g of neat matrix, Sternstein et al (157) (158) have

proposed the trapped entanglement model. This approach along with a simple reptation dynamics model allowed reasonably good prediction of the observed concentration dependence of viscoelastic moduli and the strain softening effect in PVAc/silica and PVAc/HAP nanocomposites as well as to estimate the change in terminal relaxation times caused by weakly interacting nanoparticles (159) (160) (161). The actual local discrete nano-scale structure has been homogenized, considering the polymer matrix consisting of a portion with significantly reduced mobility in a thin layer around the nanoparticles and a portion further away from the nanoparticle with mobility equal to that of the neat polymer. An alternative approach has been proposed by Douglas et al. (162) (163), attributing the observed steep increase in elastic modulus with adding nanoparticles to substantial alteration of the spatial distribution of chain relaxation times and, at the same time, changes in the chain packing near attractive or repulsive particles and consequent modification of the chain structural frustration.

To characterize mobility of a chain in a physically cross-linked polymer, one can use the longest relaxation time, τ_{rep}, expressing the time needed by the chain for a reptation motion along its length. The reptation relaxation time needed to move a chain through a tube, with diameter given by its surrounding chains, can be expressed (159):

$$\tau_{rep} = \frac{b^2 \zeta_0 N_K^2}{\pi^2 kT} \left(\frac{M}{M_e} \right) \left[1 - \left(\frac{M_e}{M} \right)^{1/2} \right] , \qquad (2.36)$$

where N_K is the number of statistical segments in a chain, ζ_0 is the segment friction coefficient, b is the length of statistical segment, k is the Boltzmann constant, T is the absolute temperature, M_e is the molecular weight of chain segments per entanglement. Note, that the term entanglement is used in the dynamic fragility sense (163).

In order to homogenize localized fluctuations in chain mobility (159), the nanocomposite was considered a two phase system, i.e., unperturbed or bulk chain and effective phase comprising nanoparticles and adsorbed chains in direct contact with filler surface. The addition of the nanoparticles into the polymer matrix can be taken as an analogy to sol-gel transition in colloids. In the percolation threshold, an infinite network of reduced mobility chains penetrates the whole sample and the longest relaxation time becomes infinite. In the case of physical filler-polymer "cross-links", the relaxation time increases to the finite value characteristic of the filler-polymer bond life-time. Thus, a basic scaling formula can be written in the form (159):

$$\tau_{composite}^{rec} = \tau_{rep}^{ads} v_{eff} \left(\frac{v_{eff} - v_{eff}^*}{1 - v_{eff}^*} \right)^{\nu} , \qquad (2.37)$$

where v_{eff}^{*} is critical effective filler volume fraction and v_{eff} is critical effective filler volume fraction and stem, i.e., unperturbed or bulk chain and effective phase comprising nanoparticles and adsorbed chains in direct contact with filler surface. The addition of the nanoparticles into the polymer matrix can be described by a percolation model, random clustering of effective hard spheres was considered only in the way similar as originally outlined by Jancar and Kucera (164).

3 Goals of the Thesis

The primary aim of this Thesis is to investigate the mechanisms and kinetics of the self-assembly of pure collagen I and the effects of hydroxyapatite nanoparticles on collagen morphogenesis. The structural variables investigated will be collagen I concentration and nanohydroxyapatite content. The solutions and hydrogels will be investigated for mechanical and rheological properties under varying external conditions such as amplitude, time and mode of excitations. Still another goal of the Thesis is to identify structural variables affecting the biomechanics of freeze-dried porous scaffolds made of these solutions and intended for bone and cartilage tissue engineering. Also the supramolecular structure of the collagen I/HAP nanocomposites will be studied, and the possible interaction modes of collagen-nanohydroxyapatite composites will be discussed. The effect of nanocomposite composition on the viscoelastic and rheological properties will be determined and an attempt to mathematically model the dependence of these properties on composition will be made. The emerging results will be discussed with possible motivation for future applications in tissue engineering and regenerative medicine.

4 Materials and Methods

4.1 Collagen solution preparation

The commercial collagen solution serving as the basis for all samples, PureCol, is a homogenous solution of 97% collagen type I and the remainder collagen type III, it is supplied at a concentration of 3mg/ml. The chemicals used in the production of collagen solutions are listed in Table 4.1. Although no special sterilization treatment was performed on the samples, care needed to be taken in order to avoid common bacteria contamination and also to maintain the temperature below 10°C to prevent any temperature history affecting the samples. The masses of the individual compounds were measured by SI-234 A analytical scale (Denver Instruments) and the pH monitoring was carried out by a digital pH-meter S2K712 (Isfetcom Japan).

Table 4.1. List of chemicals used for collagen solution sample preparation.

Chemical	Description	Source
PureCol	purified bovine collagen solution	Advanced Biomatrix, USA
Distilled water	H_2O	Laboratory
0,1M Sodium hydroxide	NaOH	Sigma Aldrich, Germany
Phosphate buffered saline	PBS	Sigma Aldrich, Germany
nHAP	hydroxyapatite nanoparticles	ÚCHM VUT Brno

4.1.1 Pure collagen I solutions

The pure collagen I solutions were prepared according to Table 4.2., first gradually adding the phosphate buffered saline (PBS) to the PureCol while gently stirring, then adjusting the pH by adding 0,1M NaOH to the optimal value of pH 7,2-7,6. The volume of the solution was further adjusted by adding distilled water to a total of 10ml per sample.

Table 4.2. Sample preparation table.

Sample Nr.	Volume PureCol	Volume PBS	Concentration	Abbreviation
1	8 ml	1 ml	2,4 mg/ml	2,4coll
2	6 ml	3 ml	1,8 mg/ml	1,8coll
3	4 ml	5 ml	1,2 mg/ml	1,2coll
4	2 ml	7 ml	0,6 mg/ml	0,6coll

4.1.2 Collagen I + nHAP solutions

The collagen I + nHAP solutions were prepared according to Table 4.3., first gradually adding the phosphate buffered saline (PBS) with 3mg/ml nHAP to the PureCol, then adjusting the pH by adding 0,1M NaOH to 7,2-7,6. The volume of the solution was further adjusted by adding distilled water to a total of 10ml per sample.

Table 4.3. Sample preparation table.

Nr.	V (PureCol)	V PBS with 3mg/ml nHAP	c (collagen I)	c (nHAP)	Abbreviation
1H	8 ml	1 ml	2,4 mg/ml	0,3 mg/ml	2,4coll0,3HAP
2H	6 ml	3 ml	1,8 mg/ml	0,9 mg/ml	1,8coll0,9HAP
3H	4 ml	5 ml	1,2 mg/ml	1,5 mg/ml	1,2coll1,5HAP
4H	2 ml	7 ml	0,6 mg/ml	2,1 mg/ml	0,6coll2,1HAP

The irregularly shaped hydroxyapatite nanoparticles (specific surface area of 190 m^2g^{-1}, BET, Quantachrome, USA) were kindly provided by the Institute of Materials and Mechanics Engineering. HAP was prepared by a precipitation reaction of calcium nitrate and ammonium phosphate in the presence of ammonium hydroxide and TRITON as a surfactant. The resulting particles were oval-shaped with a clean phase composition confirmed via X-Ray diffraction (XRD) analysis. The particles were treated hydrothermally at 150°C for up to 8 hours and ground on a planet mill for 4 hours. The most isometric and round of the produced hydroxyapatite nanoparticle lots was chosen. The nanoparticles form aggregates of around 100nm in diameter, as measured on Philips XL 30 microscope and depicted in Fig. 4.1.

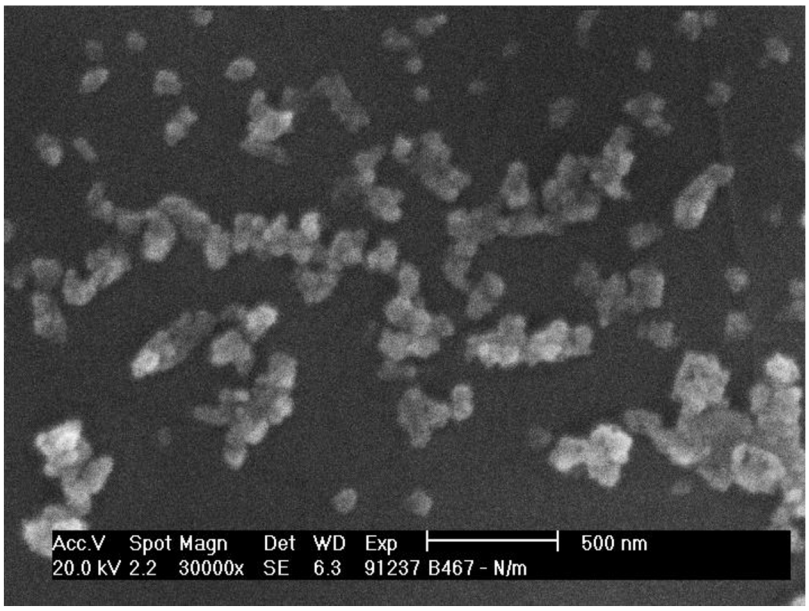

Fig. 4.1. SEM micrograph of the hydroxyapatite nanoparticles used in our experiments.

4.2 Rheology of collagen solutions

The mechanical properties of our collagen solutions, pure and nHAP modified, were investigated using an AR G2 Rheometer (TA Instruments, USA) in both dynamic oscillatory shear and continuous flow modes. Mechanical property data were collected through TA Rheology Advantage Data Analysis software (TA Instruments, USA). Every measurement was repeated three times and the results were determined as the mean values and the errors were calculated as standard deviations. The data was processed through OriginLab 8.1 software. Collagen solution samples were placed onto the Peltier plate serving as temperature control at 10°C and all measurements were carried out in a 2°cone and plate setup as depicted in Fig. 4.2. with the gap set as 60 µm. The solvent was prevented from evaporating by means of a solvent trap. In all experiments, the solutions had the same recent past thermal and mechanical protocol.

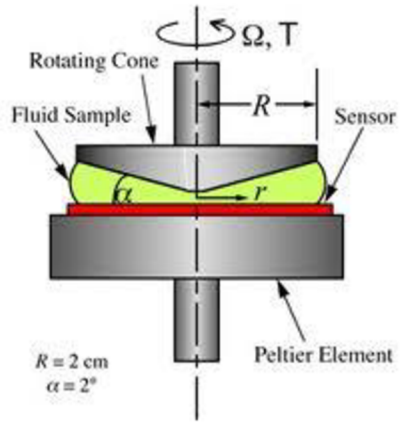

Fig. 4.2. The cone and plate setup on the rheometer

In the cone and plate geometry, shear stress and shear rate are constant throughout the gap. This technique is suitable for low to medium viscosity fluids. If there are particles in the fluid, they should be less than 10% of the truncation gap. The HAP nanoparticles used in our experiments meet this requirement.

4.2.1 Strain amplitude sweep

The most reliable range of strain which can be exploited for reproducible measurements lies within the linear region of the G‘ shear strain dependence (G‘ independent of strain), the linear viscoelastic region (LVR). The elastic modulus G‘ was measured for all samples in oscillatory mode with 1Hz frequency under shear strain ranging from 10^{-3} to 10^{3} %. First, the samples were equilibrated at 37°C for 40 min in order for self-assembly to take place, then during the strain amplitude sweep step, the moduli G‘ and G‘‘ were measured with the increasing shear strain.

4.2.2 Time sweep

The kinetics of collagen solution mechanical properties evolution was evaluated via time sweep oscillatory rheological measurements, enabling us to study the collagen self-assembly and gel formation manifesting itself through changes in the mechanical properties such as the elastic modulus G‘. Also the effect of adding nHAP to pure collagen solutions on these mechanical properties was investigated. The time period over which the measurements were performed was selected as one hour, which should be sufficient for self-assembly to occur based on the results of previous research efforts and the manufacturer’s directions.

First, the samples were conditioned at 10°C in the rheometer during a 2 minute equilibration, then the temperature was set to 37°C, mimicking physiological temperature, the time sweep measurement commenced at shear frequency 1Hz under a shear strain 1%.

4.2.3 Viscosity rate dependence

The dependence of collagen solution viscosity on the shear rate and the influence of the system composition was studied. Unlike the previous dynamic oscillatory mode, in this measurement, the flow was continuous. Pure collagen I and collagen I solutions with added nHAP were equilibrated at 10°C for 2 minutes in the first conditioning step. In the second conditioning step, the samples were equilibrated for 40min at physiological temperature 37°C, allowing self-assembly to take place. The dependence of the viscosity on the shear rate was investigated, the shear rate ranging from 1 rad/s to 100 rad/s.

5 Results, Discussion

5.1 Determining the linear viscoelastic strain interval

The storage and loss moduli G‘ and G‘‘, resp., were measured employing the 2° cone-plate geometry in dynamic oscillating mode using the AR G2 rheometer over a wide interval of shear strain amplitude (10^{-3} to 10^{3}). The aim of these large amplitude oscillatory shear (LAOS) measurements was to determine the maximum strain limiting the linear viscoelasticity region (LVR) to be utilized in all the following experiments and to characterize the nature of interactions in the investigated systems. The requirement was that the strain used must lie in a region where G‘ is independent of strain. For neat collagen I solution 2,4 mg/ml as a model situation, the resulting dependence is depicted in Fig. 5.1.:

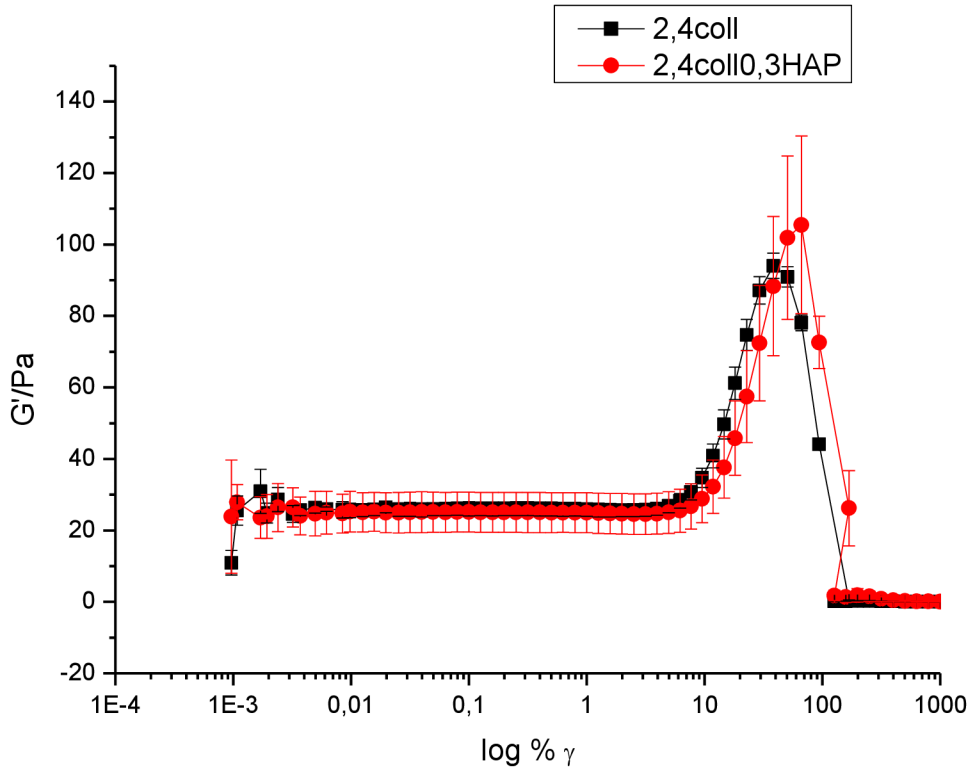

(a)

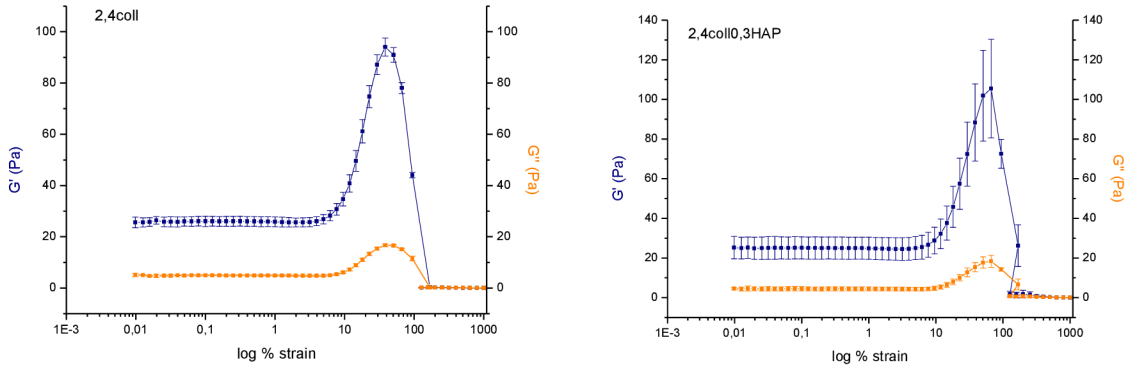

(b) (c)

Fig. 5.1. (a) The dependence of storage modulus G' on amplitude of shear strain γ for neat collagen solution (2,4coll) and collagen with added nHAP (2,4coll0,3HAP), presenting a linear viscoelasticity regime followed by strain stiffening and a breakdown of the self-assembled structure accompanied by a loss of the mechanical properties for shear strain amplitude between above 50%. The elastic modulus is zero for strains exceeding 100%.(b) G´and G´´ for the neat 2,4coll, (c) G´and G´´ for the 2,4coll,0.3HAP.

At low strains for $0{,}001\% \leq \gamma \leq 1\%$, the G' was relatively stable and constant (independent of shear strain amplitude) suggesting no structural transformation in the process. Above $\gamma \approx 10\%$, the G' increased significantly followed by a decrease to $G' \approx 0$ for $\gamma \geq 100\%$. This is a typical LAOS (large amplitude oscillatory shear) response of an associating system reflecting increasing rigidity of the existing 3D supramolecular structure followed by a collapse of the network due to mechanical disintegration. Since this behavior occured for both neat collagen and coll/HAP nanocomposites, one can conclude that for the given composition, the response is fully related to the supramolecular structure of collagen. The maximum G´ was slightly reduced by adding HAP as well as shifted towards lower shear strain amplitude. This may suggest that in the particular composition, HAP disrupts formation of the collagen supramolecular assembly as a result of the partial depletion of the amine termini available for assembly due to interactions with HAP hydroxyls, as already shown in our published paper (165).

For the remaining neat collagen I solutions, the linear viscoelasticity regime was also observed to lie reliably between 0,1 and 1% shear strain. We have, therefore, chosen 1% shear strain to be applied in all the following measurements used to determine G´. The location of the linear viscoelastic region we have found is in good agreement with other published data (166) and also the usual strains in a bone are below 0,3%. (4) The fact that for both neat collagen and collagen/HAP nanocomposites the G´´ is always lower than G´ leads to a conclusion that the viscoelastic behavior of

the systems investigated is controlled by the elasticity of the network with only a minor contribution from the viscous response. Collagen gels demonstrate elasticity derived predominantly from forming a hybrid cross-link network by crosslinking telopeptides and also from weak inter- and intra-molecular interactions. This means that the character of the viscoelastic response of the systems investigated resembles that of the bone matrix.

All the collagen solutions investigated exhibit a shear stiffening with increasing strain, characterized by a distinct peak formation, followed by a destruction of the system and the collapse of the storage modulus towards zero. The extent of this strain stiffening (increase of G') was determined by subtracting the baseline value at 1% strain from the peak height. The experimental data fit (the full lines connecting the individual points) for moduli in both pure and nHAP modified collagen solutions was best with an exponential function. The data analyzed are an average of three repetitions, the results are presented as mean values, the standard deviation was found to be lower or equal to 10% in all measurements.

The nHAP addition did not affect the observed collagen strain-stiffening phenomenon over a broad range of concentrations. However, the increase of collagen concentration in coll/HAP nanocomposite above 50 vol.% led to the exponential increase of ΔG' and ΔG'' shown in Fig. 5.3. HAP nanoparticles strongly affect the ordering and relaxation dynamics of the surrounding collagen chains on the segment scale level, producing extensive changes of mechanical and physical properties on much larger macro scale. The dispersion of NPs in a polymer matrix is known to play a critical role in nanocomposite mechanics as demonstrated in Figure 5.8. The observed uniform spatial distribution of spherical nanoparticles of hydroxyapatite resembles that observed in a natural bone tissue. It was found that for random packing, a significant portion of interparticle distances is shorter than the chain length necessary to form entanglements. Thus, in the framework of the Sternstein model, the random particle packing is essential for enhancing chain incremental stiffness due to strong chain confinement *via* interaction with filler surfaces at much smaller filler content than predicted using uniform particle spacing. We suggest that this is also the mechanism causing the substantial stiffening observed in our model systems.

Sternstein assumed that the average interparticle distance is comparable with the chain end-to-end distance even at low filler volume fractions, v_f. Adsorption of chains onto nanoparticle surface leads to the creation of surface-chain loops and interparticle bridges. These chain segments can be relatively short and their conformation statistics deviates from the Gaussian behavior significantly. Elasticity of non-Gaussian chains can be described using the Langevin function based theory of rubber elasticity. Moreover, these short chain segments are in a state that is more elongated than the chain-end-to-end distance referred to as the reference state bias. Under a given time scale of measurement, the average lifetime of filler-polymer bonds is long enough so that the non-Gaussian

chain segments can behave in a way similar to chains between junctions in a chemical network. Such a system exhibits substantially greater stiffness compared to a long Gaussian chain network. From the arguments put forward above, the importance of the interparticle spacing becomes obvious.

Sternstein's theory of nanocomposite reinforcement is based on the Langevin rubber elasticity of finite chain segments situated at the filler-polymer interface. This theory considers elasticity, which takes only changes of conformation entropy upon chain loading into account. As the chain extension approaches its limit, corresponding to *r/Nb*, the conformation entropy of a chain segment drops and the chain retractive force increases very rapidly. The retractive force can be than expressed as:

$$f = \frac{k_B T}{b} L^*(r/Nb), \tag{5.1}$$

where k_B is the Boltzmann constant, T is temperature and L^* is the inverse Langevin function, r is the chain end-to-end separation, N is number of monomer units and b is the monomer unit length. The elasticity of short chain segments has to take into account the bond angle, which is under given conditions almost undeformable. This leads to the correction that full elongation of flexible chains corresponds to maximum extension of 0.816*Nb* and not simply *Nb*.

Structural proteins such as collagen can undergo self-assembly process resembling first order thermodynamic transitions in forming micro-fibrils which control to a great extent the mineralization process, i.e., HAP NP deposition to form mineralized fibrils as basic building blocks of bones. The existence of thermodynamically phase separated states is ubiquitous in mixtures. NP clustering via phase separation is particularly common if there are unfavorable polymer-NP interactions, relative to the NP-NP interactions. Indeed, when polymer-NP interactions are highly unfavorable, there may be no thermodynamically stable NP dispersion. The self-assembled structure must have a higher order than the isolated components, be it a shape or a particular task that the self-assembled entity may perform. Another distinctive feature of SA is that the building blocks are not only atoms and molecules, but span a wide range of nano- and mesoscopic structures, with different chemical compositions, shapes and functionalities. For SA to take place without intervention of external forces, the process must lead to a lower Gibbs free energy, thus self-assembled structures are thermodynamically more stable than the single, unassembled components.

A direct consequence is the general tendency of self-assembled structures to be relatively free of defects. Weak interactions and thermodynamic stability rationalise the *adaptability* to perturbations exerted by the external environment often found in self-assembled systems. Small fluctuations that alter thermodynamic variables can lead to marked changes in the structure and even compromise it, either during or after SA. The weak nature of interactions is responsible for the flexibility of the architecture and allows for rearrangements of the structure in the direction

determined by thermodynamics. If fluctuations bring the thermodynamic variables back to the starting condition, the structure is likely to go back to its initial configuration.

A recurrent problem in the blending of collagen and nanoparticles is the propensity of HAP nanoparticles to self-assemble into clusters that can greatly affect the collagen ordering morphology and the very nature of the collagen order-disorder transition. Thermal fluctuations in collagen systems characteristically drive the ordering phase transition order from second to first order by the well known Brazovskii mechanism. An infinitesimal amount of disorder can destabilize the first order phase transition by transforming into some “glass-like” state where ordering is so frustrated that only a highly rounded remnant of the original phase transition then exists. It has been proposed that the self-assembly of nanoparticles into extended structures can serve as a template for the directed collagen assembly when the extended nanoparticle superstructures remain localized to the suitable microdomains, implying a synergistic interaction between the nanoparticle assembly and collagen ordering processes. This suggests that the capacity of the clustered nanoparticles to span different collagen domains is important for disrupting the collagen ordering process.

The extended nanoparticle structures can more easily form transient networks both through direct interaction between the nanoparticles or through chain bridging between the nanoparticles, where a “bridging” chain is a chain in contact with at least two different nanoparticles. These non-continuum mechanisms are believed to play a significant role in property enhancement in polymer nanocomposites compared to more "classically" behaving microcomposites. The fraction of bridging chains seems to be a useful “order parameter” for characterizing the polymer-nanoparticle interactions. If the polymer-nanoparticle interactions were sufficiently small, the bridging would not be expected to play significant role, however, we have shown that the chain stiffening can become enormous due to perturbation of entanglement mobility due to random nanoparticle packing resulting in "trapped" entanglements. One interpretation of the biomechanical function associated with the extensive nonlinear stiffening is a passive protection for soft tissues when shear deformations become large. It is the subject of further research to investigate the possible strain recovery behavior.

Our results indicate that a fully developed collagen gel was formed showing $G' > 10\ G''$ and exhibiting plateau G' at low strain rates. Such an elastic response reflects the presence of an underlying network that is capable of storing elastic energy over long timescales. Figure 5.2 depicts three possible scenarios forming local constraints to molecular movement of collagen nanofibrils/triplehelices which may result in gelation. They include attraction at junctions (a), spatial correlation between adjacent molecules (b) and jamming at junctions (c) (167). The second scenario is relevant for the portion of collagen triplehelices participating in formation of multiple nano- and micro fibrils. The third scenario applies to growing rigid microfibrils the ends of which can jam into

the bodies of adjacent fibrils. From the CLSM observations of large microfibril formation (Fig. 5.17), it seems that the spatial correlation (mechanism (b)) is the dominant one in our case. Fibrils at different length scales are formed by a thermodynamically controlled transition from an angularly uncorrelated to a helical state. (168) .

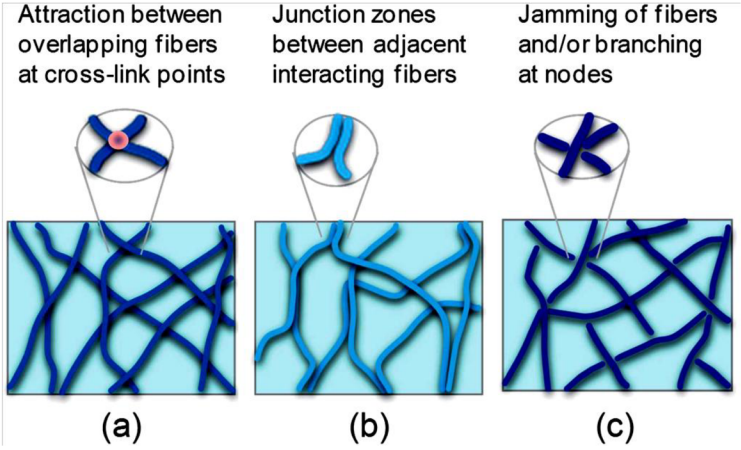

Fig. 5.2. Possible scenarios of local constraint formation. (167)

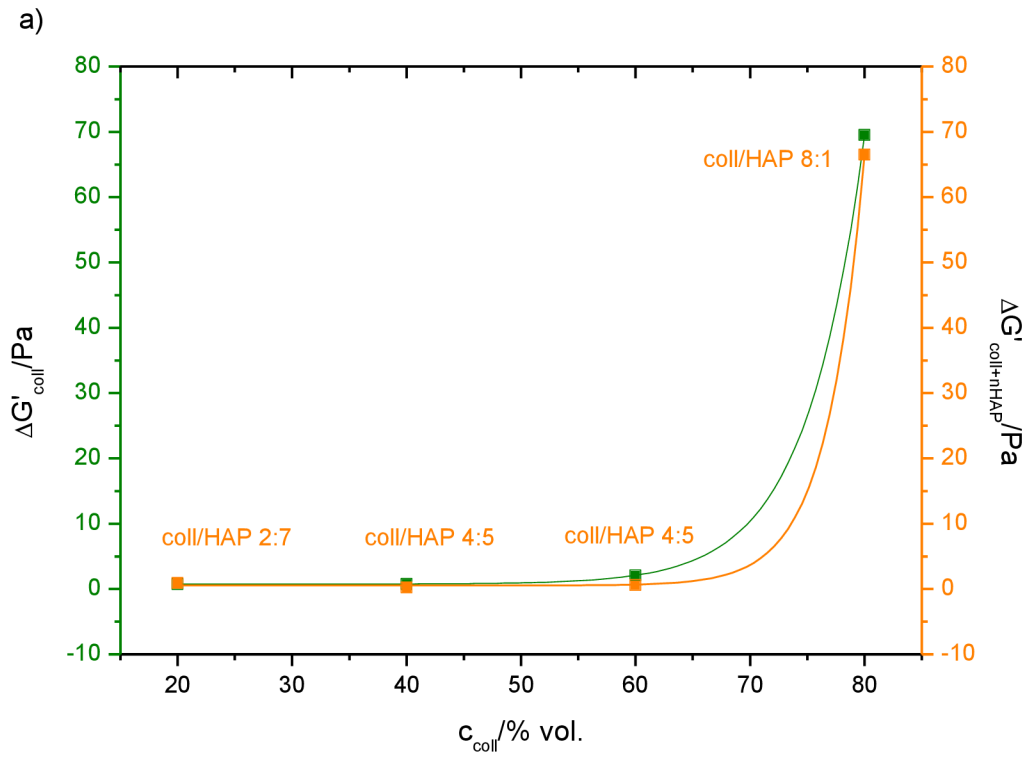

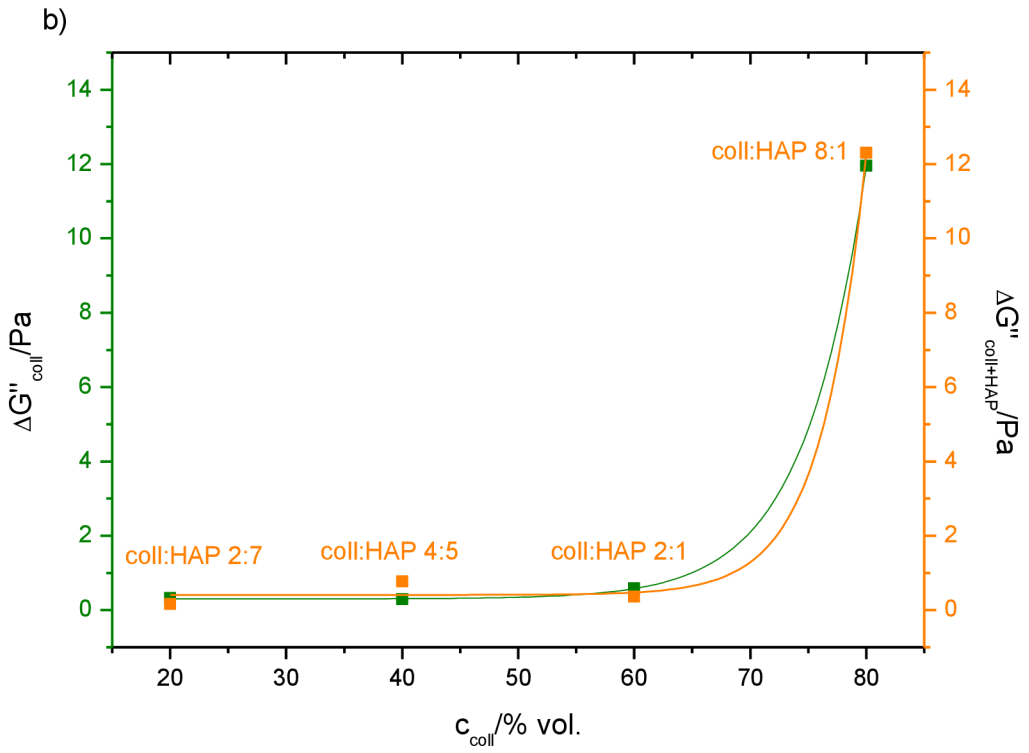

Fig.5.3. The composition dependence of the a)ΔG' and b)ΔG'' (calculated from a baseline formed by the LVR) for both neat collagen and collagen with nHAP.

The shear strain amplitude at which the failure of the structure has occured (termed yield strain for the purpose of this work) was determined as the position of the ΔG´ peak, beyond which mechanical stiffness decreases towards zero. For neat collagen, it was observed in the vicinity of the shear strain of 50 %. The effect of HAP addition resulted in a shift of this peak to greater strain amplitude, especially for 2,4coll0,3HAP, where the yield strain increased by 20%, thus a slight composition modification enhanced the mechanical properties of the resulting collagen-HAP nanocomposite, implicating an interaction at the molecular level that cannot be attributed to the individual components (the simple superposition of their mechanical properties). In the less concentrated collagen solutions this effect was not statistically significant, see Fig. 5.4. The results of the remaining collagen I solution compositions are listed in the Annex, Section 1.

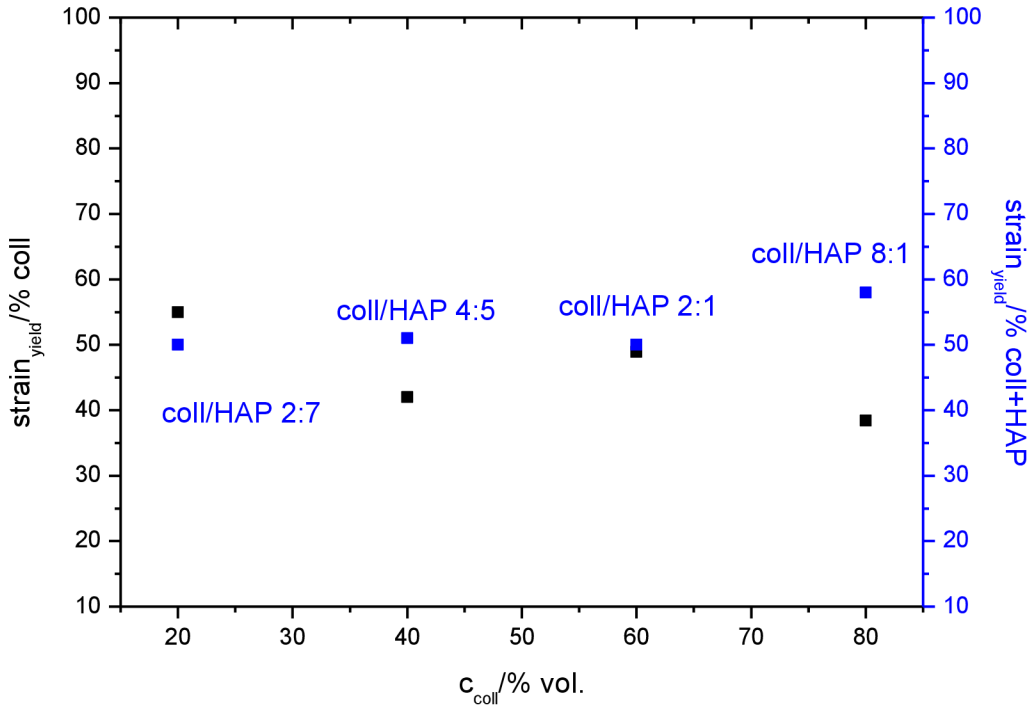

Fig.5.4. The effect of nHAP addition on the yield strain.

5.2 Reinforcing mechanisms in coll/HAP nanocomposite gels

Any of the existing micromechanics models (170) predict the relative increase of the composite modulus over that of the neat matrix by approximately only by factor of 1.35 (35%). For comparison, the simple Guth-Gold model (170):

$$\frac{G_c}{G_m} = G_r = 1 + 2.5v_f + 14.1v_f^2 \,, \qquad (5.2.)$$

where v_f is the filler volume fraction, is plotted in Fig. 5.5b). Even the Mooney model (170) predicted increase of the shear modulus, by adding v_f = 0.15, only 35% over the modulus of the neat matrix. Thus the observed several fold increase of storage modulus cannot be explained considering only the simple volume replacement reinforcement theory and molecular reinforcement mechanisms have to be taken into account.

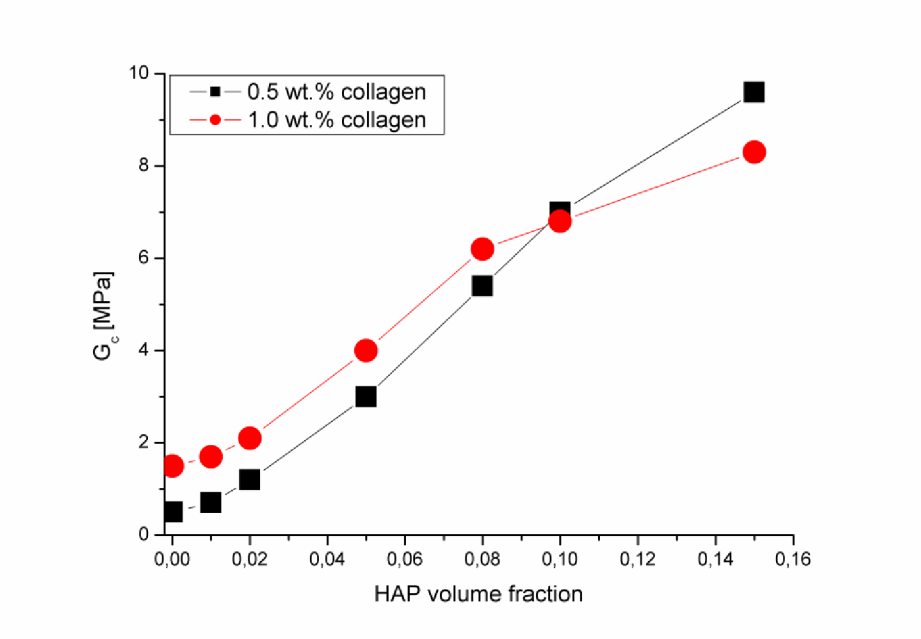

Figure 5.5.(a) Concentration dependence of the shear modulus of the nanocomposites, G_c.

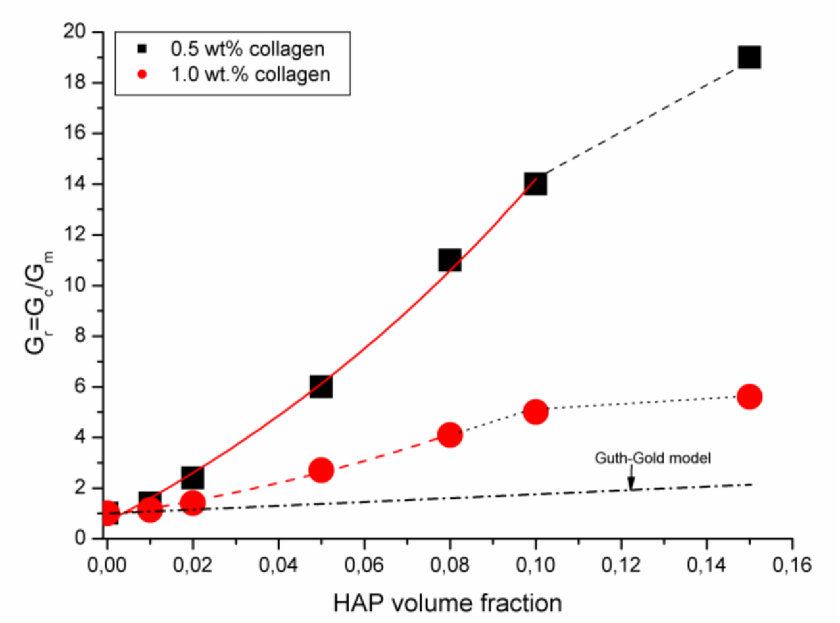

Figure 5.5.(b) Concentration dependence of the relative shear modulus of the nanocomposite, G_r. G_m is the modulus of a neat collagen matrix. Effect of the chain mobility on the reinforcing mechanism is evident from the difference between the 0.5 wt.% and 1.0 wt.% collagen. Comparison with simple volume replacement Guth-Gold (Eq. 5.2.) model is shown.

Considering the tropocollagen triple helix molecule a worm-like chain with *L/d*=200, we obtain the reptation time:

$$\tau_{rep} \cong \frac{2}{5}\frac{\kappa_b{}^2 \zeta_0 N_K^2}{(kT)^3}\left(\frac{M}{M_e}\right)\left[1-\left(\frac{M_e}{M}\right)^{1/2}\right], \qquad (5.3.)$$

where κ_b is the characteristic bending rigidity of the collagen chain estimated to be about 15 kcal/mol/rad^2. (171) If such a chain approaches an impermeable surface, the chain conformational entropy and internal energy under given conditions can alter very substantially depending on the particle-chain interaction energy and chain flexibility. For a weak interaction energy such as hydrogen bonds, the average number of adsorbed segments, N_a, is scaled simply as $N_a = N_k^n$, where the exponent n = 1/2, and the terminal relaxation time of a worm like chain near a particle can be expressed in the form:

$$\tau_{rep}^{ads} = 2\frac{\kappa_b{}^2 N_K{}^{5/2}}{(kT)^3 N_e}\left[\zeta_0 N_K{}^{1/2} + \zeta_a\right], \qquad (5.4)$$

where ζ_a is the friction coefficient of adsorbed chain and N_e is the number of statistical segments per entanglement.

The interactions between collagen C-termini and OH- bonds on the HAP nanoparticles with dimensions on the same scale as the thickness of tropocollagen triple helix have a tremendous effect on the retardation of their reptation dynamics (Fig. 5.8.). At the same time, the C-termini in the collagen phase become more depleted than the N-termini resulting in further reduction of collagen fibrillogenesis leading to a perturbance of the collagen network structure. In addition, the reduced mobility and chain confinement result in further disturbing the formation of collagen fibrils. As a result, the structure of the chemically cross-linked collagen network becomes more defective and dependent on the HAP content. On the other hand, the number of physical cross-links due to HAP-Co interaction increases rapidly resulting in much stiffer network (157) with rigidity strongly dependent on the strain level as described by the Mullins effect.

In order to obtain at least a qualitative comparison of experimentally observed behavior with theoretical prediction, the Co/HAP nanocomposite gel was considered a filled polymer network above its T_g. Since collagen resembles a worm like chain rather than a random Gaussian coil, Langevin rubber elasticity has been used. The Langevin rubber elasticity considers elasticity, which takes only changes of conformation entropy upon chain loading into account. As the chain extension approaches its limit, corresponding to $C(r/N_k l_k)$, the conformation entropy of a chain segment drops and the chain retractive force increases very rapidly; r is the worm like chain end-to-end distance, N_k is number of Kuhn segments and l_k is the segment length and C is the characteristic ratio. The retractive force of a worm like chain loaded in tension can be expressed as (172):

$$F(x)=\frac{kT}{L_p}\left[\frac{1}{4\left(1-\frac{x}{L_c}\right)^2}-\frac{1}{4}+\frac{x}{L_c}\right], \qquad (5.5.)$$

where L_p is the persistence length, L_c is the contour length and x is the pulling distance. Substituting (κ_b/kT) for L_p yields:

$$F(x)=\frac{(kT)^2}{\kappa_b}\left[\frac{1}{4\left(1-\frac{x}{L_c}\right)^2}-\frac{1}{4}+\frac{x}{L_c}\right]. \qquad (5.6.)$$

Considering Eq. 5.6., the retractive force of the collagen network can be expressed in the form:

$$f=\frac{(kT)^2}{2\kappa_b}L^{-1}\left(\frac{rkT}{2N_k\kappa_b}\right), \qquad (5.7.)$$

where k is the Boltzmann constant, T is temperature and L^{-1} is the inverse Langevin function.

In order to demonstrate the effect of chain immobilization on stiffening the Co/HAP nanocomposites, collagen network was modeled as a 3D tetrafunctional polymer network with affine cross-links. The model network was built to preserve the fundamental features corresponding to real collagen structure (Fig. 5.6.). At each node, three chains were considered flexible rubbery chains and the fourth one was marked as the collagen triple helix. During deformation of the neat network, the three flexible chains were deformed according to Langevin single chain elasticity:

$$\sigma=\frac{1}{3}E\sqrt{N_s}L^{-1}\left(\frac{\lambda_{chain}}{N_S}\right), \qquad (5.8.)$$

where λ_{chain} is the draw ratio of chain, L^{-1} is the inverse Langevin function and N_s is the number of statistical segments. Deformation of the fourth triple helix chain was calculated considering four possible types of its behavior, i.e., (i) undeformable rigid rod, (ii) Hookean spring, (iii) long rubbery chain and (iv) short rubbery chain. Length of the collagen triple helix chain was considered 280nm, and length of the flexible chain was calculated from the relation for a Kuhn chain model with 78 segments corresponding to 26 amino acids.

It has been shown that presence of nanoparticles effectively alters the distribution of the length of chain segments towards the shorter segment lengths. These segments exhibit greater stiffness than the longer chain segments (Fig. 5.7.). For filler content of 1 vol%, segments with incremental stiffness higher than one effective entanglement strand represent about 5 % of polymer matrix. In a nanocomposite filled with 10 vol% of nanoparticles, such portion is already about 65% from the entire amount of polymer matrix. Thus, in nano-particle filled polymers, chain entanglements become a second-order interaction, while the "trapped entanglements" induced by non-penetrable filler nanoparticles become a first-order interaction. At the same time, randomly distributed solid HAP nanoparticles confine tropocollagen molecules significantly (Fig. 5.8.). Assuming random particle packing, the average interparticle distance reaches particle diameter for v_f = 0.015. (173)

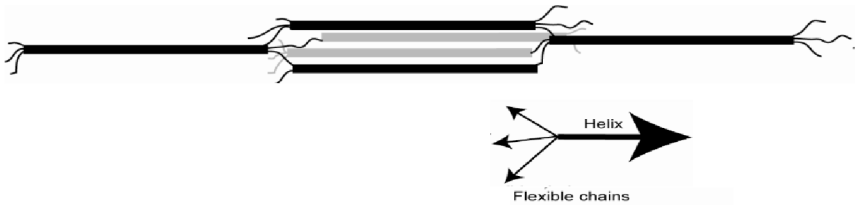

Figure 5.6. Schematic drawing of the simplified structure of the neat collagen network considered in the simple network model considering Langevin elasticity.

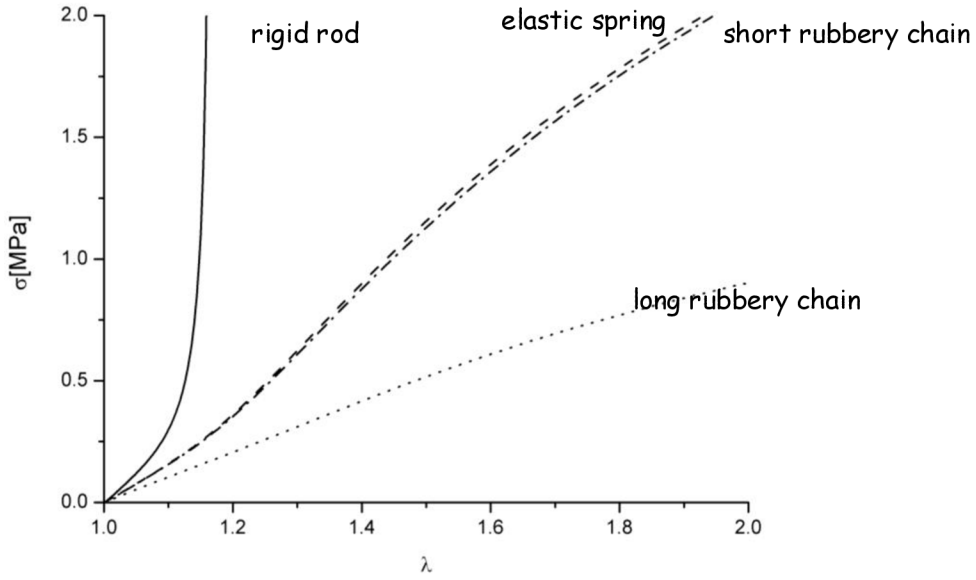

Fig. 5.7. Deformation response of a collagen network with varying the model used for deformation response of the collagen and assuming the Langevin rubber elasticity (Eq. 5.6.).

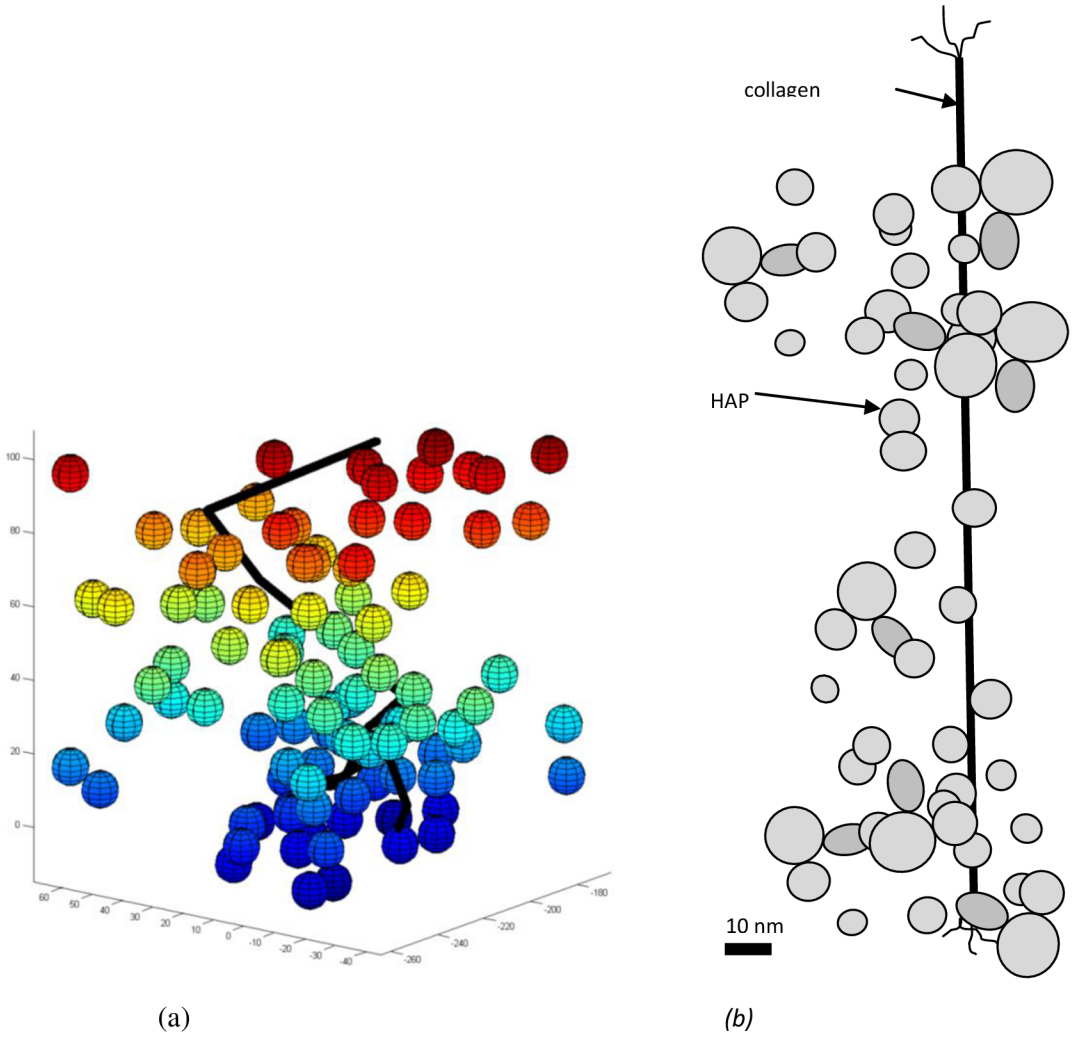

Fig. 5.8. a) Simulated random 3D distribution of monodisperse HAP nanoparticles and worm like collagen chain for 0.5 wt.% Co filled with 5 vol.% of HAP nanoparticles (d=10 nm). The distribution was generated using AGLOMER generator. Size of the simulated box is approximately 100nmx100nmx100nm. b) Schematic 2D drawing of the the ratio between volume occupied by collagen chain and HAP nanoparticles for 0.5 wt.% Co filled with 5 vol.% of HAP nanoparticles. For simplicity, the collagen triple helix is shown in extended conformation. The area fractions occupied by collagen and HAP correspond to the composition of the Co(0.5)/HAP nanocomposite.

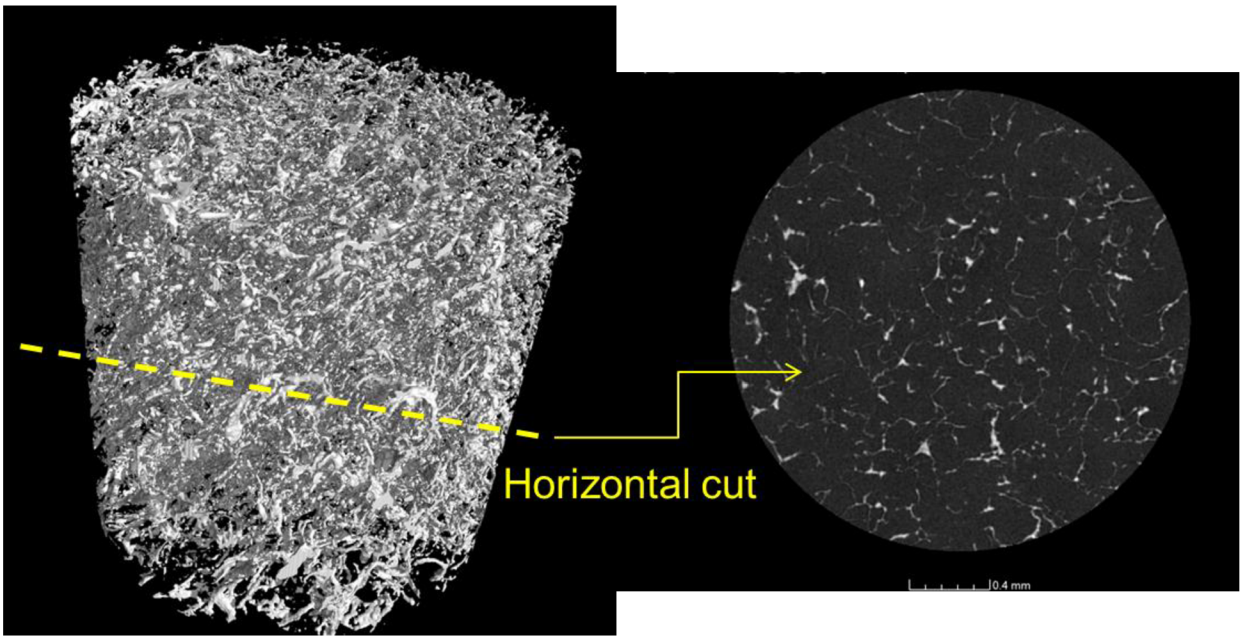

(a)

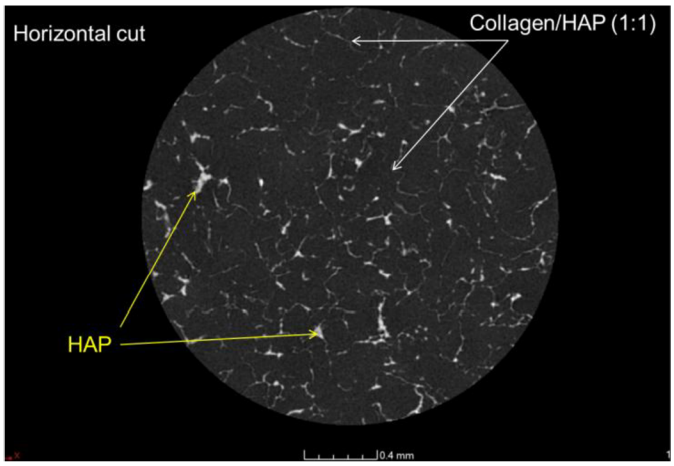

(b)

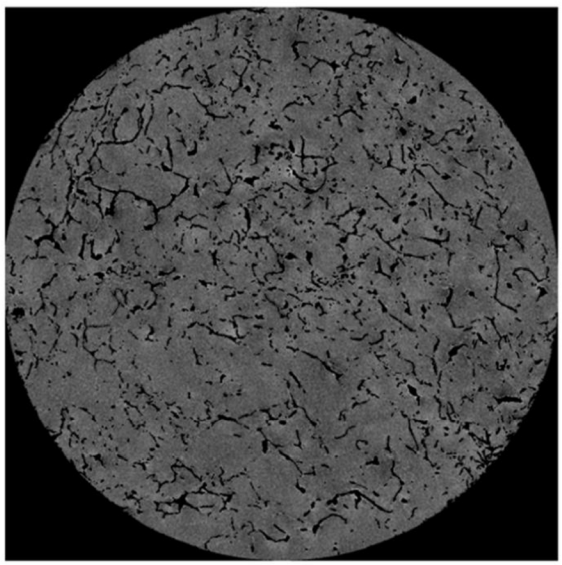

(c)

Fig. 5.9. a) 3D microCT image of the coll/HAP nanocomposite network from a freeze-dried nanocomposite hydrogel with 1:1 coll:HAP ratio (left) and a horizontal cut of the image (right) showing distribution of colagen fibrils and HAP particles. (b) the same as the panel (a) right with arrows indicating position of collagen and HAP. (c) computer processed image (b) with software removed collagen showing the 2D distribution of HAP particles.

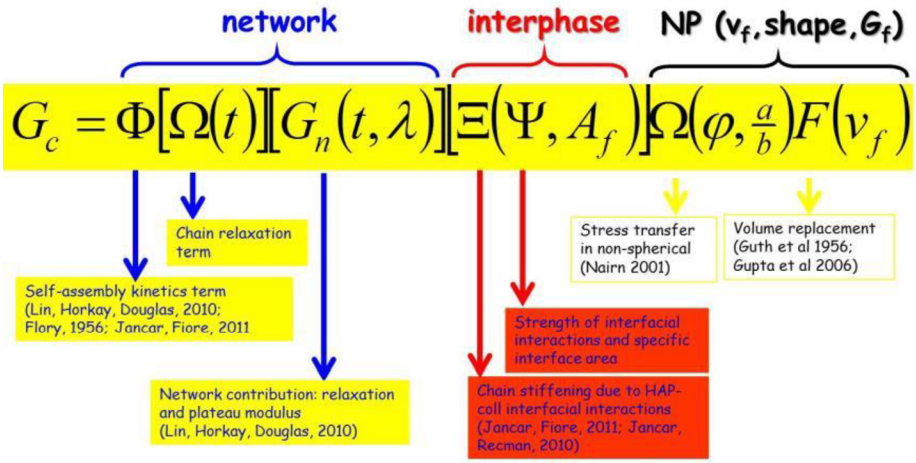

(a)

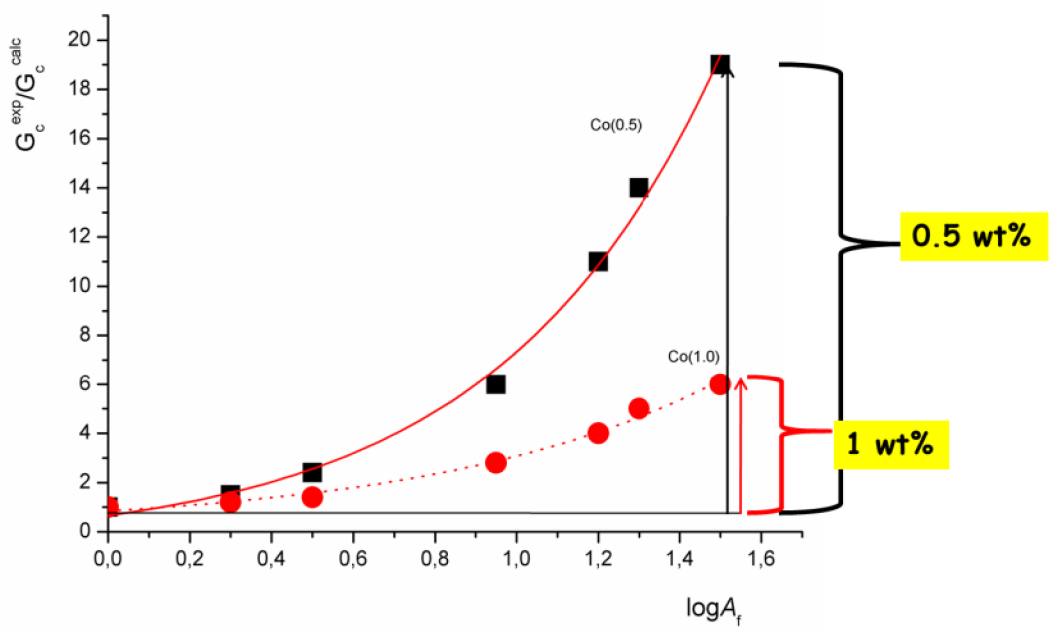

(b)

Fig. 5.10. (a) Model of the shear modulus of nanocomposite hydrogels proposed by Jancar et al (165) *based on the localized network viscoelasticity model of Lin-Douglas-Horkay* (173) *with self-assembly and chain relaxations term including chain stiffening at the interface.*

(b) Plot of the experimentally determined normalized shear storage modulus. Full and dotted lines represent contributions of molecular chain stiffening predicted using model of Lin-Douglas-Horkay modified by Jancar et al (Eq. shown in Fig 5.10. (a)) (165)

The effect of HAP nanoparticle content incorporated into collagen on the storage moduli (G') of model nanocomposite gels containing was investigated. A simple chain reptation dynamics approach was used to describe the molecular reinforcing mechanism at the nano-scale and the

controlling role of the area of contact between the matrix and the reinforcement. An "immobilized chain percolation network" with individual chains obeying Langevin rubber elasticity filled with randomly distributed HAP nanoparticles 20 nm in diameter was demonstrated to provide means for analyzing the meso-scale mechanical response of the Coll/HAP nanocomposite networks considering nano-scale structural information. In our analysis, the role of water in determining the G´ has not been included and the behavior of the hydrogels was ascribed solely to the length scale independent viscoelasticity of the solid network. This approach seems a reasonable approximation for low solid content hydrogels formed by networks with strongly bound water enhancing the effective diameter of the network chains where the contribution of the length scale dependent drag of water through the network does not influence the overall shear stress considerably.

5.3 Kinetics of network gelation

The kinetics of collagen self-assembly was investigated employing dynamic oscillatory rheology by measuring the time evolution of viscoelastic moduli utilizing dynamic oscillatory time sweep rheological measurements, as described by Yang et al. (79). Collagen solutions of varying collagen and nHAP content were subjected to oscillatory shear under 1Hz frequency and 1% strain over a period of 90 minutes at physiological temperature of 37 ^{o}C. Solutions were neutralized and kept before measurement at 4 ^{o}C and the self-assembly was initiated at the beginning of the measurement by raising T to 37 ^{o}C. The mean value from three measurements is presented along with the standard deviation, which in all cases does not exceed 25%.

The collagen self-assembly proceeded in three phases as illustrated in Fig. 5.11. The initial phase corresponding to the breakdown of a weakly connected structure formed in the solution during the time between the sample preparation and measurement and manifesting itself by a decrease in the viscoelastic moduli. The minimum G´ value is reached at 1,5.10^{3} s indicating complete loss of elastic properties. The breakdown of a weakly associated structure is supported by the G´´ being greater than G´ during this stage, suggesting rather viscous character of the response. In the second stage, the microfibril and fibril self-assembly occurs resulting in the change of the shear strain response from viscous liquid to viscoelastic gel manifested by G´ being larger than G´´. At 2 x 10^{3} s after reaching the minimum G´, a plateau G´is obtained signalizing the completion of the self-assembly under the conditions of the experiment.

The evolution of the viscoelastic moduli in time for the neat and HAP modified 2,4coll, respectively, is shown in Fig. 5.12 (a) and (b), respectively. The obtained results are in agreement with those published in literature for neat collagen (166) (69). Collagen triplehelices assemble first in aggregates of 5-17 molecules (nuclei) followed by assembly of these nuclei into microfibrils 30-300

nm in diameter with greatly variable length (79). Two or more of these microfibrils then assemble into bundles forming extended fibers that can branch and interconnect, thus forming a network. Formation of this structure is analogous to gelation observed in the course of thermoset cure. The development of collagen network was found to be consistent with the percolation theory of branched network formation (175). Interconnection between fibers are due to topological constraints formed by entanglements resulting in a complex physicochemical gel structure (176).

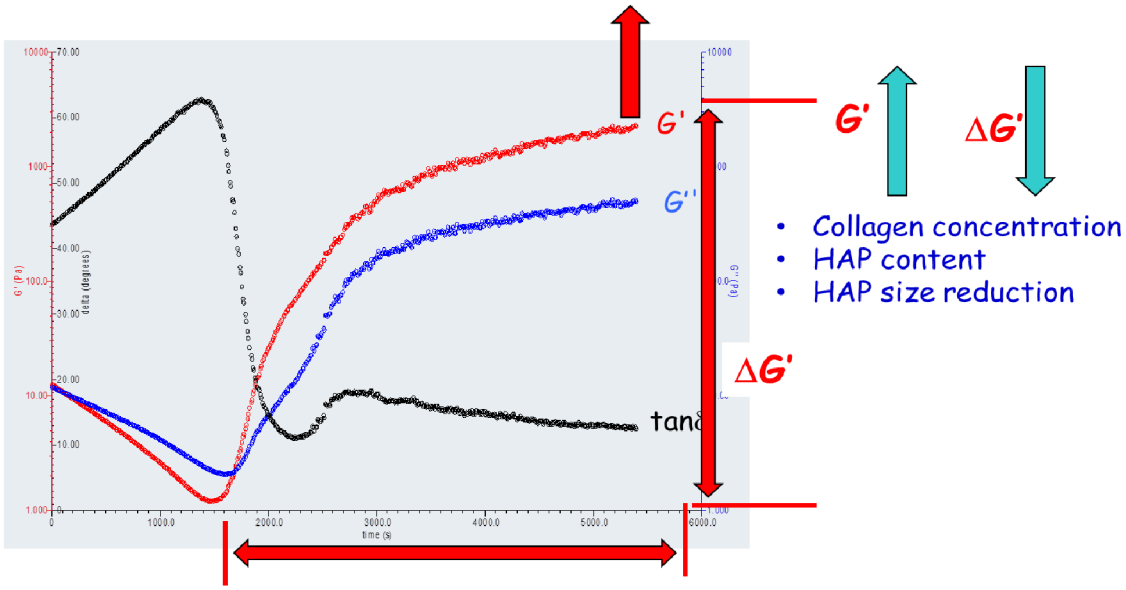

Fig. 5.11. Plot of the characteristic time dependence of the storage and loss shear modulus and tanδ for collagen/HAP solutions measured at 37 ^{o}C and frequency of 1Hz showing the initial period, in which the structure formed between sample preparation and measurement is disassembled followed by the submicron fibril formation and reaching the network plateau modulus after approximately 2 x 10^3 s.

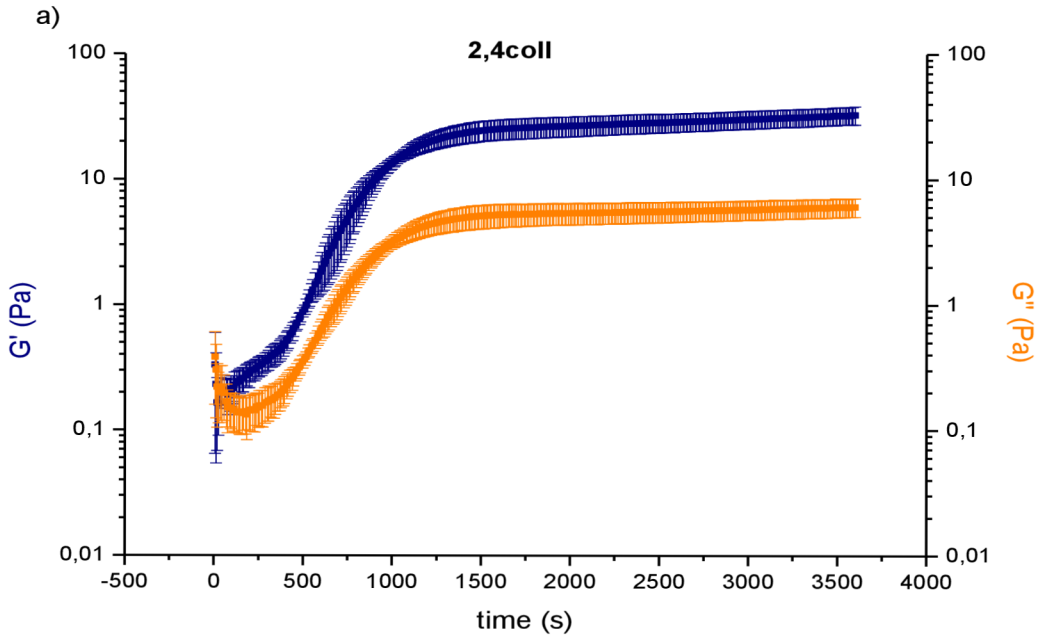

(a)

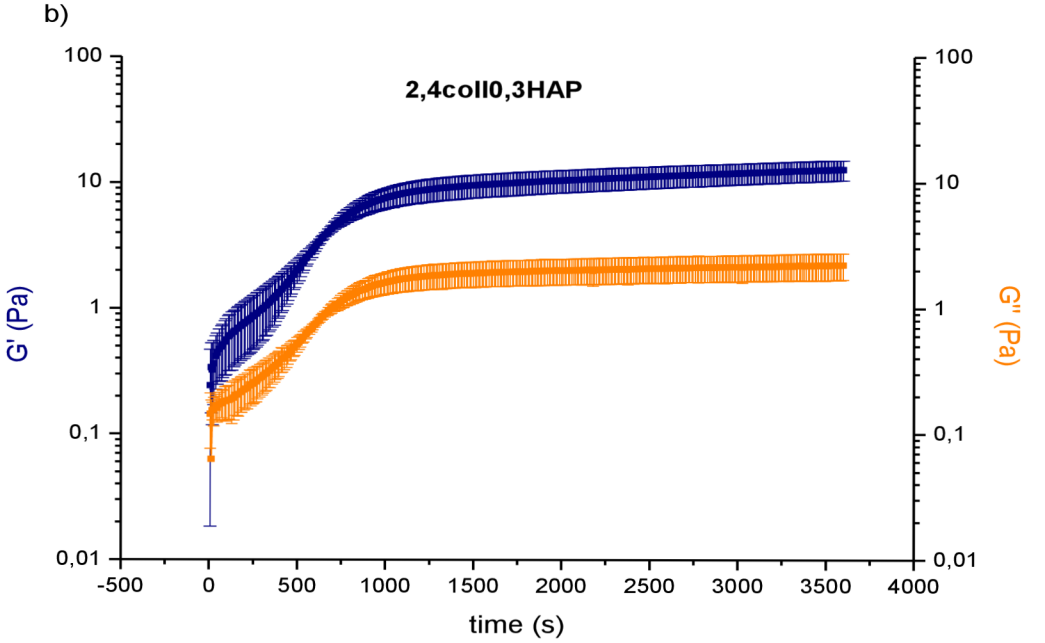

(b)

Fig. 5.12. a) The evolution of the viscoelastic moduli through time for neat collagen 2,4mg/ml. The self-assembled moduli plateaus are reached after 1,5.10^3 s.b) The evolution of the viscoelastic moduli through time for collagen 2,4mg/ml with 0,3mg/ml nHAP. The self-assembled moduli plateaus are reached after 1,0.10^3 s, suggesting the earlier onset of self-assembly compared to the neat solution facilitated by the presence of nHAP.

The addition of 0,3mg/ml nHAP did not change the character of the gelation kinetics significantly. Collagen and HAP concentrations control the plateau modulus obtained under given thermodynamic conditions. At this particular composition, however, the addition of nHAP results in a decrease of the viscoelastic plateau modulus, which contradicts the traditional wisdom of the volume replacement reinforcing mechanism. The plateau moduli are reached in 1,5 x 10^3 s for 2,4coll and at 1,0 x 10^3 s for 2,4coll0,3HAP. The earlier completion of collagen self-assembly can be explained by the bioactive nHAP facilitating acceleration of the self-assembly nuclei formation by weak interactions, but its low concentration results in a lower number of these nuclei. The time evolution of G´and G´´ seems to follow the same functional form. This can be attributed to the fact that the process of collagen gelation by self-assembly and stiffening due to presence of rigid HAP are additive in nature.

The effect of nHAP addition on the viscoelastic moduli characterizing the ongoing self-assembly is shown in Fig. 5.13. for neat and HAP modified 2,4coll matrix. The resulting moduli of neat self-assembled collagen are higher compared to the nHAP modified system. At the same time, plateau modulus is achieved at shorter time for the HAP modified collagen. Considering the slope of the growth portion of the G´(t) and G´´(t) as a measure of the rate of self-assembly, adding the HAP reduced the self-assembly rate significantly. This, along with the reduction of the absolute values of plateau G´and G´´, leads to a conclusion that HAP reduces the ability of collagen microfibrils to self assemble into larger fibers and hinders formation of the fibril network responsible for the gelation to occur. Our conclusions are in fair agreement with the rheological studies relating the size of the formed fibrils to the rheological behavior of collagen networks (166). Structurally, we propose that the amine termini of tropocollagen interact with the surface hydroxyls of HAP. This leads to a partial depletion of assembly controlling amine termini from the collagen sol causing the observed drop in the extent of gelation. This hypothesis is in agreement with the model of collagen fibrillogenesis proposed by Kadner et al. (174).

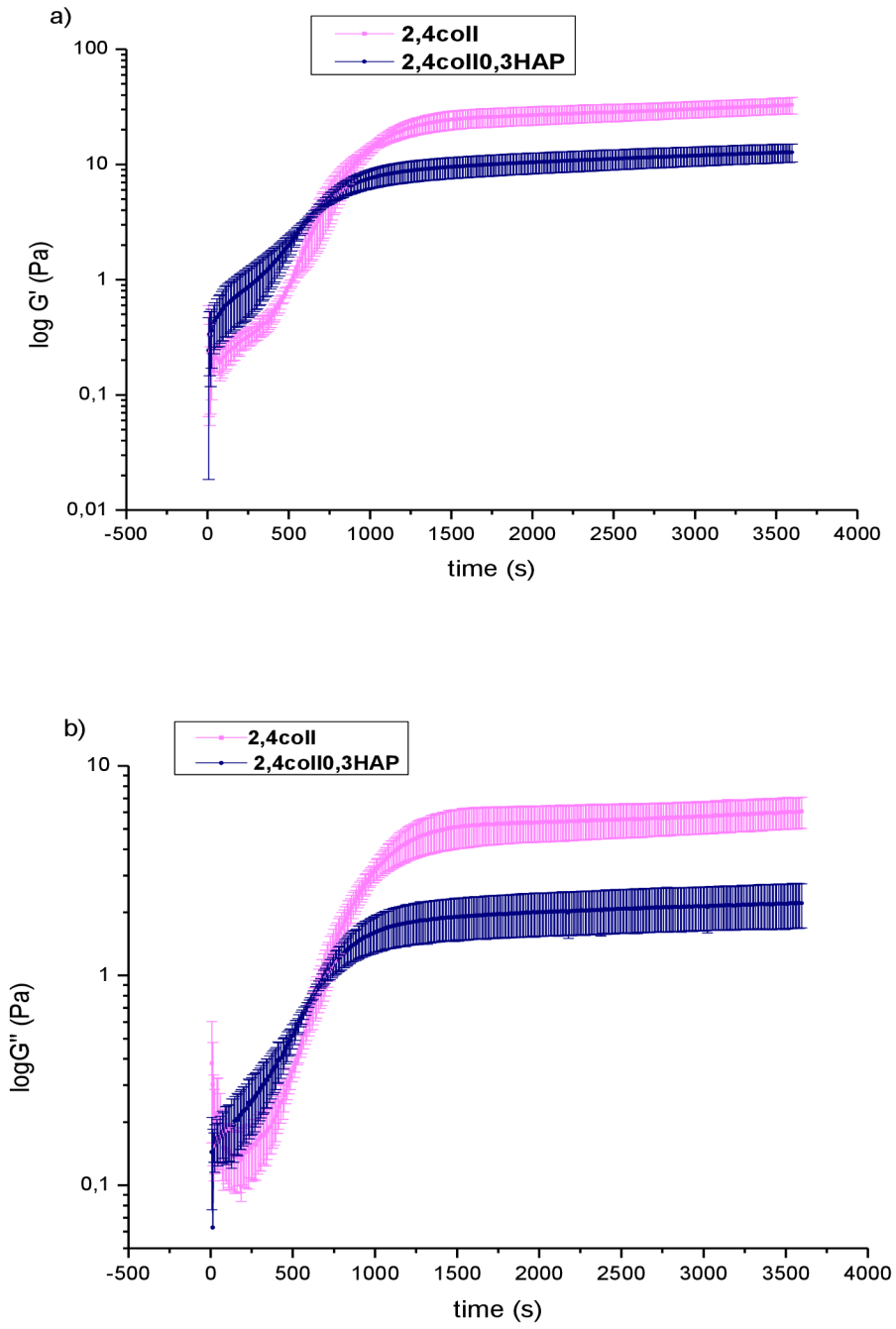

Fig. 5.13. a) The comparison of storage moduli time evolution for 2,4coll and its nHAP modified counterpart, 2,4coll0,3HAP. The onset of self-assembly takes place earlier in the nanocomposite, while the neat solution reaches a higher value of plateau storage modulus. b) A similar trend is observed for the loss moduli.

The results obtained in investigating the composition dependence of the kinetics of self-assembly are summarized in the following text and in Fig. 5.14. For the neat collagen I, both the storage and loss moduli increased exponentially with increasing collagen concentration. The increase was steeper for the neat collagen systems compared to HAP modified collagen. However, when the

coll/HAP ratio is lower than 1, a structure exhibiting large viscoelastic moduli (40-fold higher compared to the plateau values) is formed at the very beginning of the experiment. This structure is broken down during the first 500 s of the experiment leading to a significant drop in G´. For times longer than 500 s, the structure transformation proceeds toward the plateau moduli similarly to the nanocomposite networks with coll/HAP ratio greater than 1. In all cases, however, the plateau G´ obtained for systems with coll/HAP ratio smaller than 1 is lower compared to gels with coll/HAP ratio >1.

This phenomenon can be ascribed to the formation of large metastable HAP nanoparticle aggregates held together solely through weak short distance physical HAP-HAP interactions. Thermodynamically, the controlling parameter is the decrease of the system enthalpy upon aggregation. In agreement with the Einstein–Stokes model of hydrodynamics of dispersion of particles in a liquid, systems with larger particles exhibit greater resistance to flow, thus, the G´ and, especially, the G´´ reach their maximum. As expected from the Einstein-Stokes model, greater effect is observed on the viscous portion of the response, e.g., on the G´´. The weak attractive HAP-HAP forces are acting over very short distance and, thus, they are unable to withstand the dynamic oscillatory shear forces throughout the entire measurement period. As a result, the formed HAP agglomerates are progressively disintegrated resulting in a reduction of their size causing significant drop of the hydrodynamic resistance of the system sol. At the same time, the entropy of the system grows due to improved dispersion of HAP nanoparticles. Then, tropocollagen self-assembly starts similarly to the neat systems, however, for the reasons mentioned above, collagen network formation is partially hindered by the HAP agglomerates resulting in smaller G´ and G´´ at the plateau. The kinetic plots of collagen solution self-assembly for all the other compositions can be found in the Annex.

The comparison of G´(t) and G´´(t) dependences for various collagen solution compositions is illustrated in Fig. 5.15. The initial lag phase is shortened with increasing collagen concentration, which is consistent with the data and hypothesis established in literature (79). At the same time, adding the HAP nanoparticles extends the time needed to break down the structures formed between sample preparation and the measurement. It is also consistent with the hypothesis proposed in Section 5.3., that between the sample preparation and measurement, reversible structures are formed that are disrupted and broken down by the dynamic oscillatory shear forces that they are subjected to when the measurement commences. Therefore, the initial test period must be considered more of a conditioning phase unifying the starting gel structure. Also, the phenomenon described above (the formation of a temporary structure with high moduli caused by the abundance of nHAP) regarding samples with higher nHAP content, is observed.

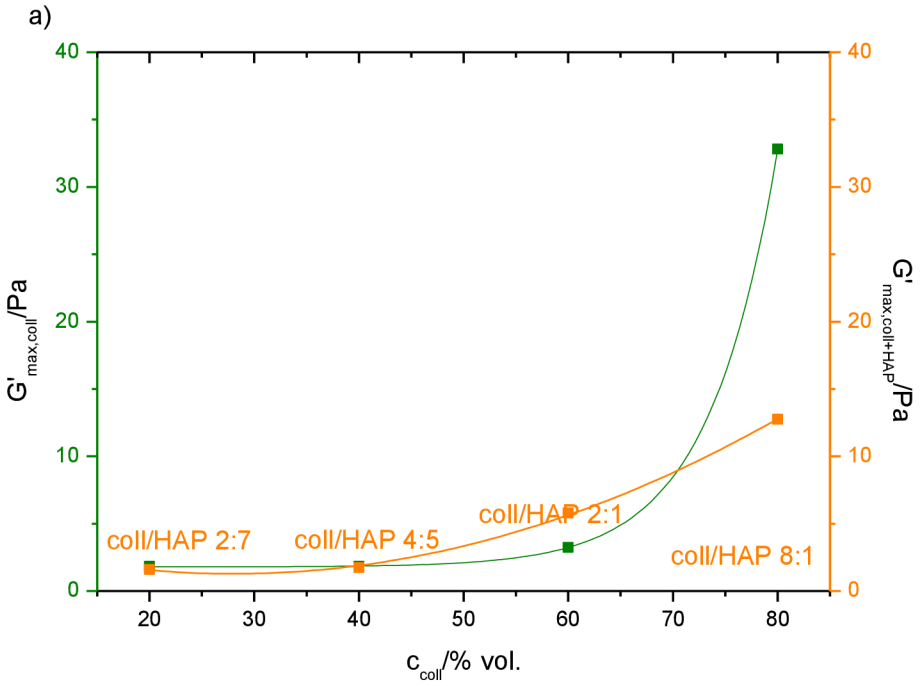

(a)

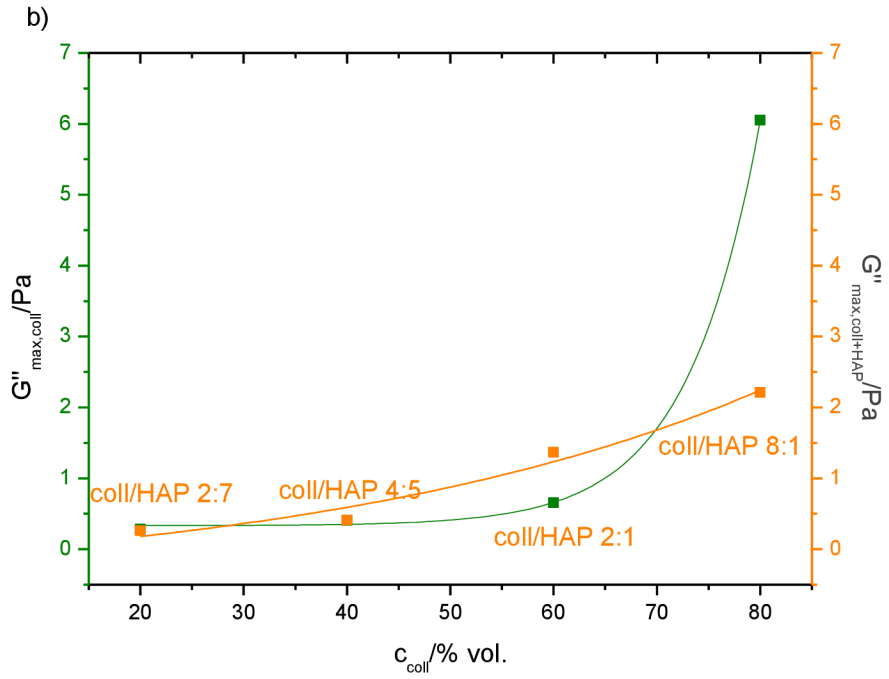

(b)

Fig.5.14. a) The composition dependence of maximum self-assembled (plateau) storage moduli for neat collagen I solutions and collagen solutions containing nHAP. The storage modulus increases exponentially with increasing collagen concentration.b) The composition dependence of maximum loss moduli for pure collagen I and collagen I with added nHAP. A weaker exponential collagen concentration dependence is observed along with an increase in G''.

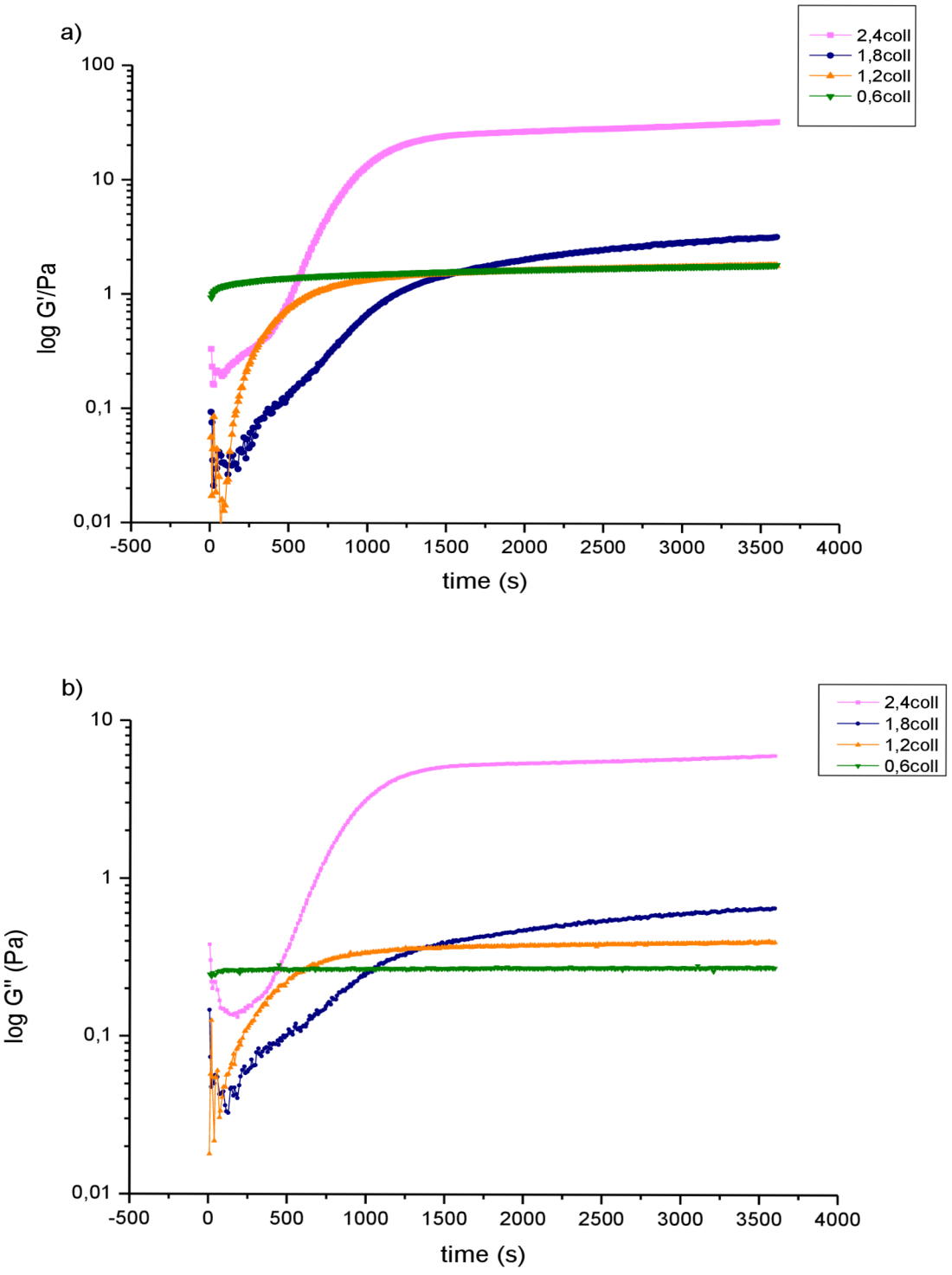

Fig.5.15 .a) The comparison of storage modulus time evolution for varying neat collagen I compositions. b) The comparison of loss modulus time evolution for varying neat collagen I compositions.

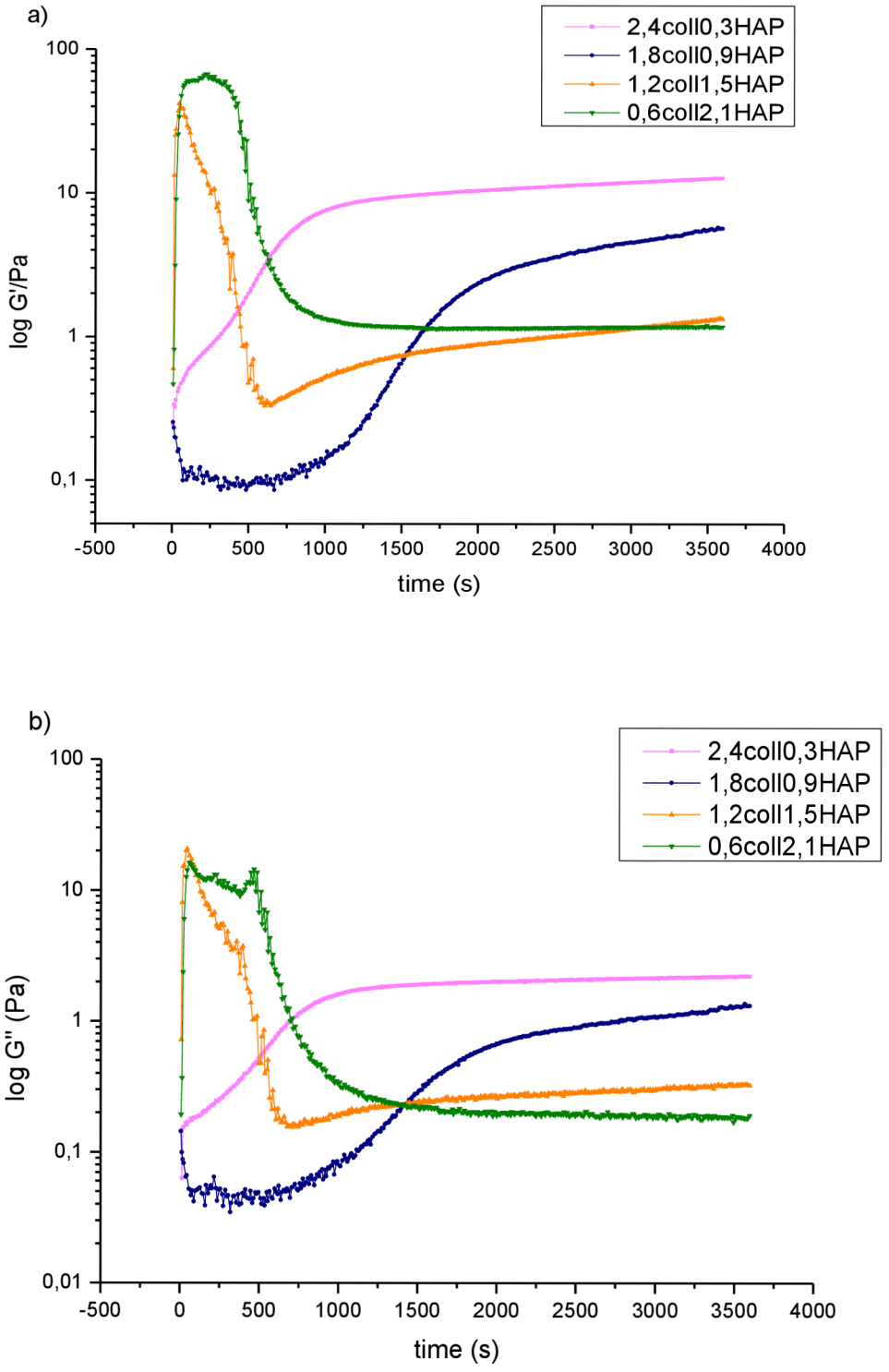

Fig.5.16. a) The comparison of storage modulus time evolution for varying coll+HAP compositions. b) The comparison of loss modulus time evolution for varying coll+HAP compositions.

The important results arising from these kinetic self-assembly experiments include that the viscoelastic plateau moduli increase exponentially with collagen concentration for neat collagen I solutions. This is in agreement with the model of worm like chain micelle self-assembly proposed in literature (168). For collagen I with added nHAP, the resulting dependence is also exponential, but flatter. The crossover of the exponential fits is 70% collagen vol. concentration. Above this concentration, the collagen content dictates the self-assembly. The effect of nHAP is marked toward higher HAP/coll ratios, causing the early onset of assembly (apparently already during the equilibration on the Peltier plate, while reaching the required physiological temperature). During the first 500s, a peak in the elastic modulus and the formation of a viscoelastic network is observed, but during the following 500s, the structure breaks down and only a small plateau modulus appears after self-assembly. This suggests the formation of a reversible physical network structure with the increase of temperature at the start of measurement caused by an abundance of nHAP. This structure is however unstable and the weak interactions holding it together are broken within minutes. After 30 mins, the values of the elastic moduli approx. reach plateaus in all samples.

The dependence of mechanical properties on the system composition can be summarized as follows: the absolute value of the elastic modulus increases with concentration of collagen, where more molecules are available for crosslink formation, also the more concentrated (less dilute) the solution, the more entangled the collagen chains become, also resulting in an increase in G'. The ΔG', however, decreases with the increase collagen concentration. This may be interpreted that in the first phase (which may be looked upon as a conditioning pre-shear step), only weak physical interactions are destroyed, however entanglement effects remain.

The nHAP addition results in a similar effect, although this cannot be attributed to entanglement, the sheer number of stiff nHAP particles contributes to an increases of G' during the entire experiment (the G' dependence is vertically shifted upwards and flatter, resulting in a ΔG' decrease). Also, the effect of the variation of nHAP particle size was studied, with decreasing nHAP particle size, an increase of G' was observed together with a decrease in ΔG'. The smaller particles stiffen the structure more effectively, enabling closer packing of the collagen molecules compared to the larger ones, which may in fact inhibit self-assembly by disabling the collagen molecules to move easily into close proximity necessary for higher-order structures to form.

In Fig 5.17 (a) and (b), the morphology of the freeze dried coll/HAP nanocomposite networks produced from the collagen solutions investigated previously is visualized using SEM micrographs at two magnifications. The sample depicted in the Fig. 5.17 (a) and (b) was frozen after reaching the plateau on the G´(t) to -50 ^{o}C and then freeze dried. Hence, it seems reasonable to assume that the structure formed and revealed by the SEM represents the characteristic dynamic equilibrium morphology of the coll/HAP nanocomposite network. The network consists of two main structural

features. These are the HAP coated fibrils and 3D structure formed by randomly spatially arranged thin collagen films with minimal HAP deposit. This structure is consistent with the observed reduction of the plateau G´ with HAP addition hindering the collagen gelation consisting of creating entangled collagen microfibril network (167). This network forms the observed thin film structure as a result of the low collagen concentration in the hydrogel. Most of the HAP nanoparticles are attached at the surface of the fibrillar structures forming an independent fibrilar network contributing to the hydrogel plateau moduli less than the entangled collagen film structure.

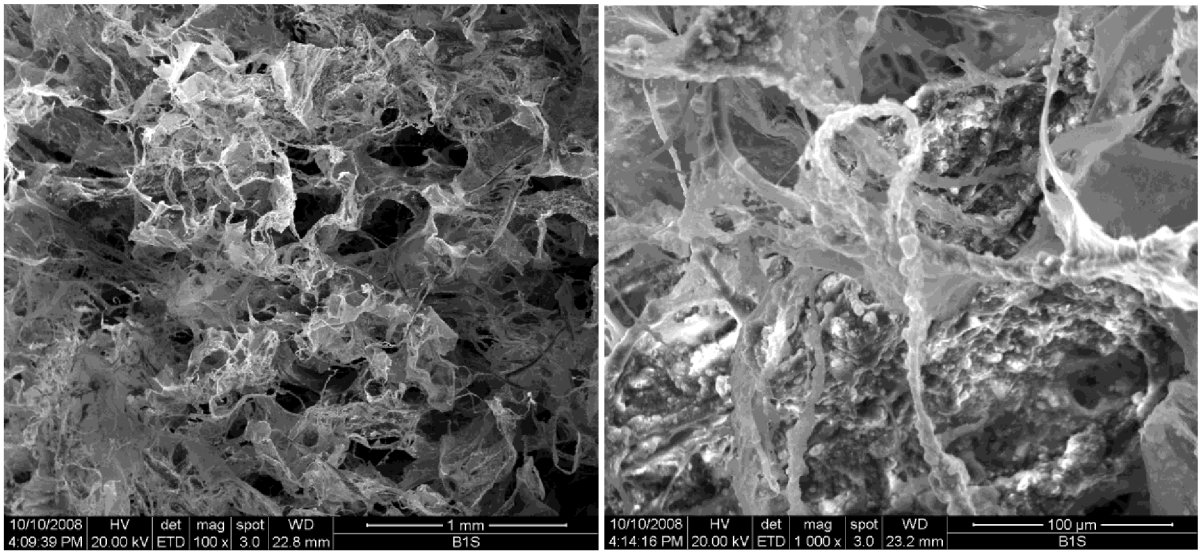

(a) (b)

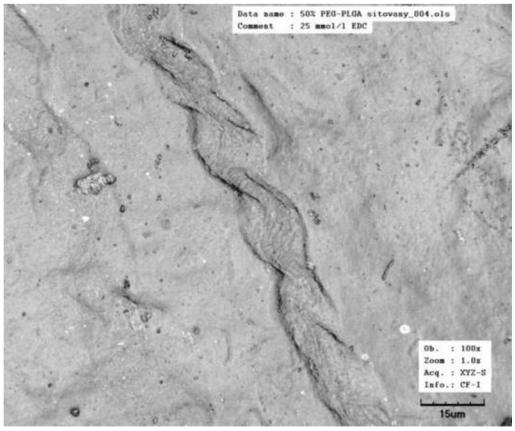

(c)

Fig. 5.17. (a) and (b) SEM micrographs of the fracture surface of a broken freeze-dried collagen/HAP nanocomposite network showing clearly deposition of HAP nanoparticles on the surface of fibrilar collagen.(c) Confocal Laser Scanning Microscope (CLSM) observation revealed the formation of left-hand twisted collagen fibril approximately 12 μm in diameter in samples left at 37 ^{o}C and pH 7 overnight.

In order to visualize the fibril formation, neat collagen solution was left overnight to self-assemble at 37 ^{o}C and the resulting left-handed twisted collagen fibril approximatelly 12 μm in diameter was observed by confocal laser scanning microscopy (CLSM) shown in Fig. 5.17 (c). Despite relatively small magnification, the aligned twisted microfibril structure of the collagen fibril is clearly visible.

Another result of this work which may be further exploited is the fact that although we are unable to avoid the formation of some sort of a self-assembled structure during laboratory manipulation with the sample (the period between sample preparation and measurement), we are able to erase any such history by subjecting the sample to approximately 5 x 10^2 s of oscillatory shear (1Hz, 1% strain) as a conditioning step.

5.4 The dependence of viscosity on the shear rate

The shear rate dependence of viscosity for neat collagen and nHAP modified collagen solutions was investigated using continuous shear flow measurements, unlike the experiments presented in the previous paragraph which were performed employing the oscillatory shear mode. The standard plots of viscosity as a function of the shear rate for all the systems investigated are shown in Figure 5.18 (a)-(d). For comparison, plots of viscosity as a function of the shear rate for systems with varying collagen concentration and/or HAP content, respectively, are shown in Figure 5.19. In Figure 5.20, the zero shear viscosity is plotted as a function of the collagen concentration and coll/HAP ratio.

All the systems investigated exhibited shear thinning behavior (see Fig. 5.19), which is in agreement with the published data of Lai et al. (150). Addition of HAP did not change the character of their rheological behavior significantly regardless of the system composition. Adding nHAP caused reduction of the dependence of the high shear rate viscosity on the collagen content compared to the neat collagen gels (Fig. 5. 20). The shear rate viscosity data were extrapolated towards zero shear rate, as demonstrated by Tominaga et al. (144) and the extrapolated zero shear rate viscosities were plotted as a function of collagen concentration and nHAP addition (Fig. 5.20.). It was shown that the zero shear rate viscosity exhibits composition dependence similar to G´ and, thus, similar models can be used for its structural interpretation.

There is a significant difference in the effect of collagen concentration on the zero shear viscosity between neat and HAP modified systems (Fig. 5.20). While for neat collagen systems the dependence exhibits a high concentration viscosity limit (monotonous increasing asymptotic behavior), adding HAP results in a significant drop in viscosity of at coll/HAP ratios below 1 followed by its steep increase. This is consistent with the systems´ structure proposed in the previous paragraph. In the case of HAP modified collagen, the composition dependence of the zero shear

viscosity seems to fit the Boltzmann S-shaped function with the inflection point near the 50 vol.% collagen. Such a behavior has been observed for systems exhibiting phase inversion. In other words, at low collagen content, the HAP forms the majority phase in the network. Since the HAP aggregates are disrupted by the shear flow, the zero shear viscosity remains almost constant or slightly decreases. In this region, the collagen self-assembly is effectively prohibited. Near the 50 vol% collagen, phase transition occurs resulting a collagen becoming the majority phase of the network capable of self-assemble to a small extent. As a result, the zero shear viscosity starts to increase with further decrease of the HAP content, eventually asymptotically approaching the neat collagen viscosity.

Also, the difference Δη between the zero and maximum shear rate viscosity for neat and HAP modified collagen is plotted as a function of collagen content (Fig. 5.21.). The Δη can be considered a measure of the extent of shear thinning. While there is consistent trend for the neat collagen exhibiting a monotonous stepwise increase of Δη with collagen content, the Δη dependence on collagent content for HAP modified systems exhibits two types of behavior. At low collagen content below 50 vol. %, adding HAP did not have any effect on Δη compared to the neat collagen systems. In other words, HAP did not change the extent of collagen shear thinning. Above the 50 vol.% collagen, HAP decreases the extent of collagen shear thinning significantly. Again, this rheological behavior is consistent with the hypothesis of phase inversion put forward above.

These results may be interpreted that a small amount of added nHAP facilitates the formation of a reversible physical mineralized collagen network, where the intermolecular interactions maintain a more viscous character of the self-assembled gel. It seems that an over-abundance of nHAP may result in the formation of nHAP aggregates that do not promote self-assembly through sterical hindrance in the hypothetical gap regions. This can also explain the difference between properties of the coll/HAP gels prepared by mixing collagen with pre-synthetized nHAP particles and those prepared by in-situ precipitation of nHAP in the collagen gel as observed during formation of mineralized fibrils in healthy bone. Our results are, thus, strongly supportive of novel direction in preparing 3D scaffolds for bone tissue engineering utilizing sol-gel nHAP or β-tri-calcium phosphate (β-TCP) precipitation at a certain stage of collagen fibril self-assembly.

a)

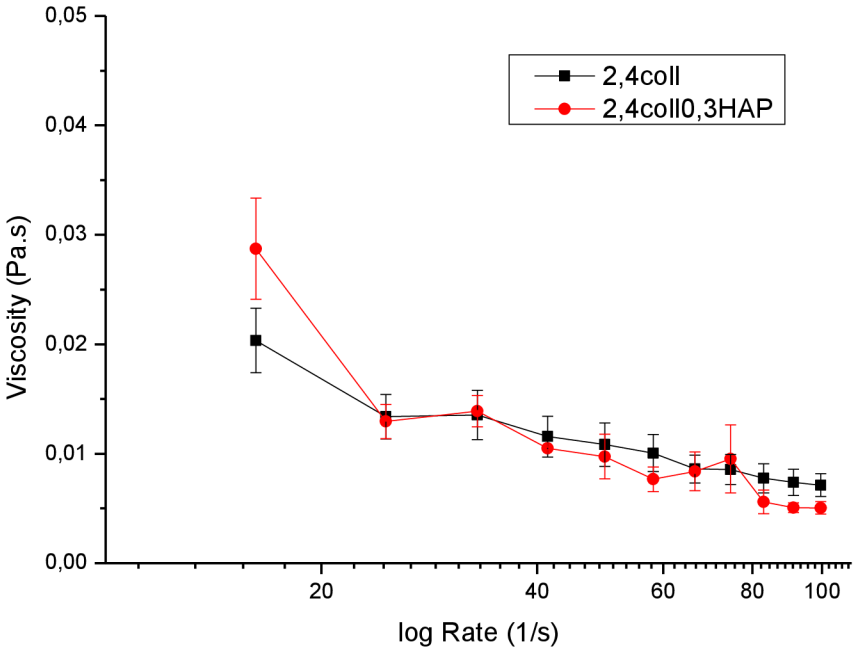
0,05
0,04
0,03
0,02
0,01
0,00
Viscosity (Pa.s)
2,4colI
2,4colI0,3HAP
20
40
60
80
100
log Rate (1/s)

b)

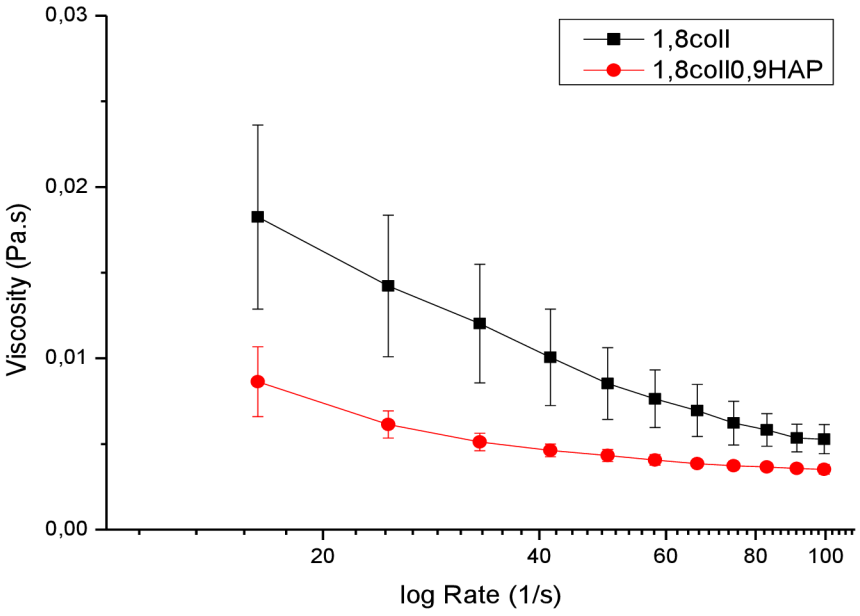
0,03
0,02
0,01
0,00
Viscosity (Pa.s)
1,8colI
1,8colI0,9HAP
20
40
60
80
100
log Rate (1/s)

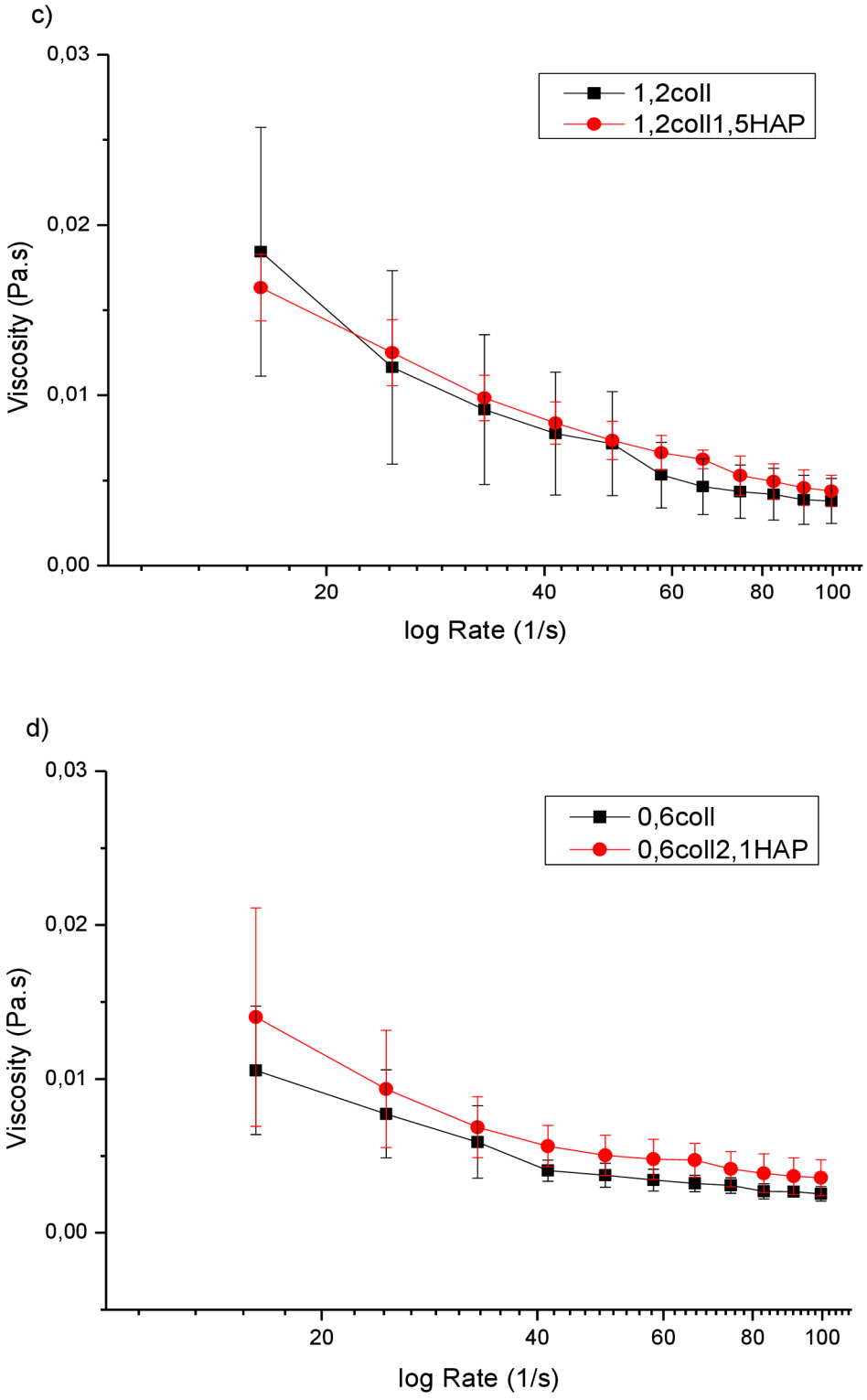

Fig. 5.18. The dependence of the viscosity on the shear rate for a) 2,4coll and 2,4coll0,3HAP, b) 1,8coll and 1,8coll0,9HAP, c) 1,2coll and 1,2coll1,5HAP, d) 0,6coll2,1HAP

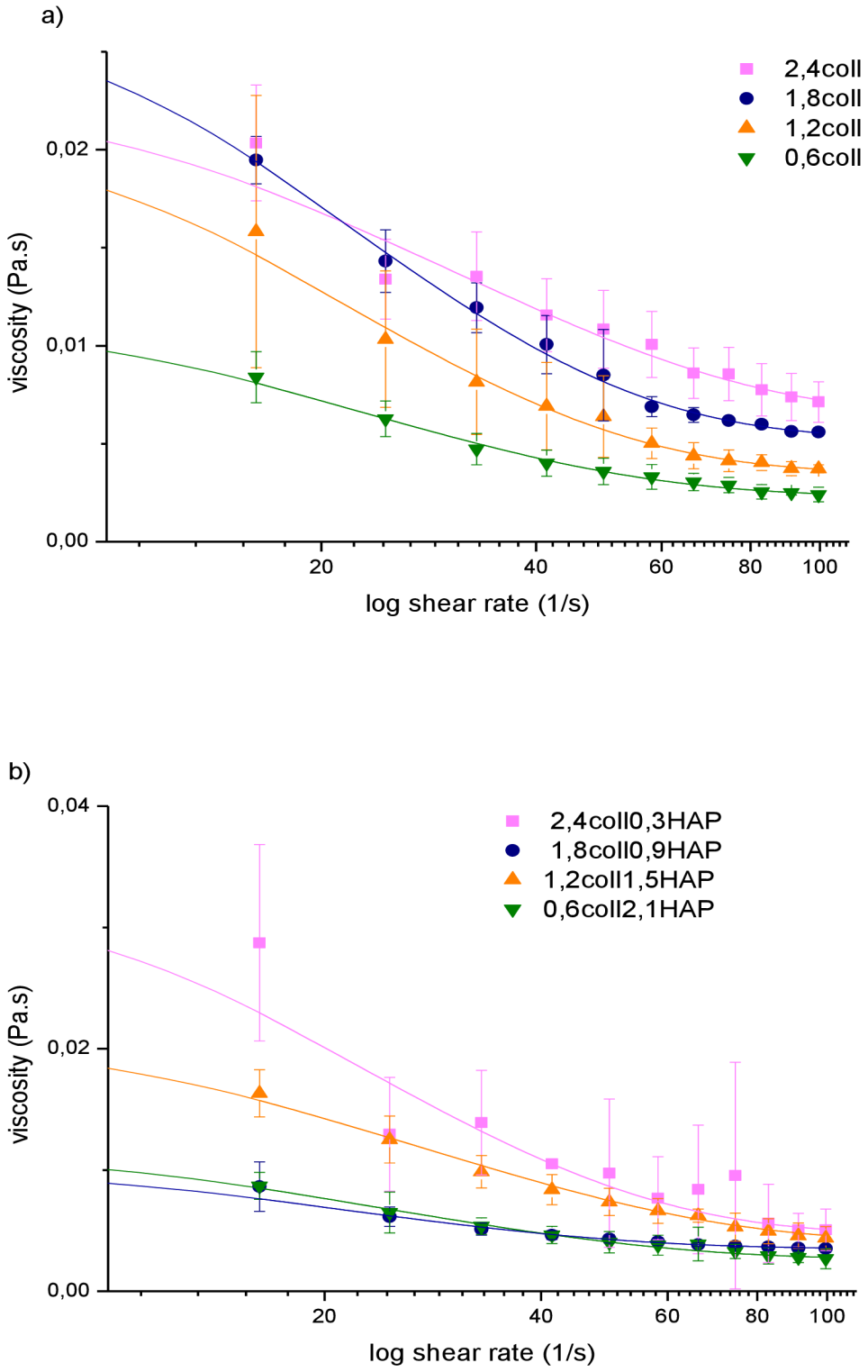

Fig 5.19. a) The dependence of viscosity on the shear rate for neat collagen solutions is similar for all measured concentrations with only a slight vertical shift downwards with decreasing concentration. The extrapolated data from the exponential fit are illustrated as full lines b) The dependence of viscosity on the shear rate for collagen solutions with the addition of nHAP is also a flat exponential, however the values converge towards a small interval with increasing shear rate. The extrapolated data from the exponential fit are illustrated as full lines.

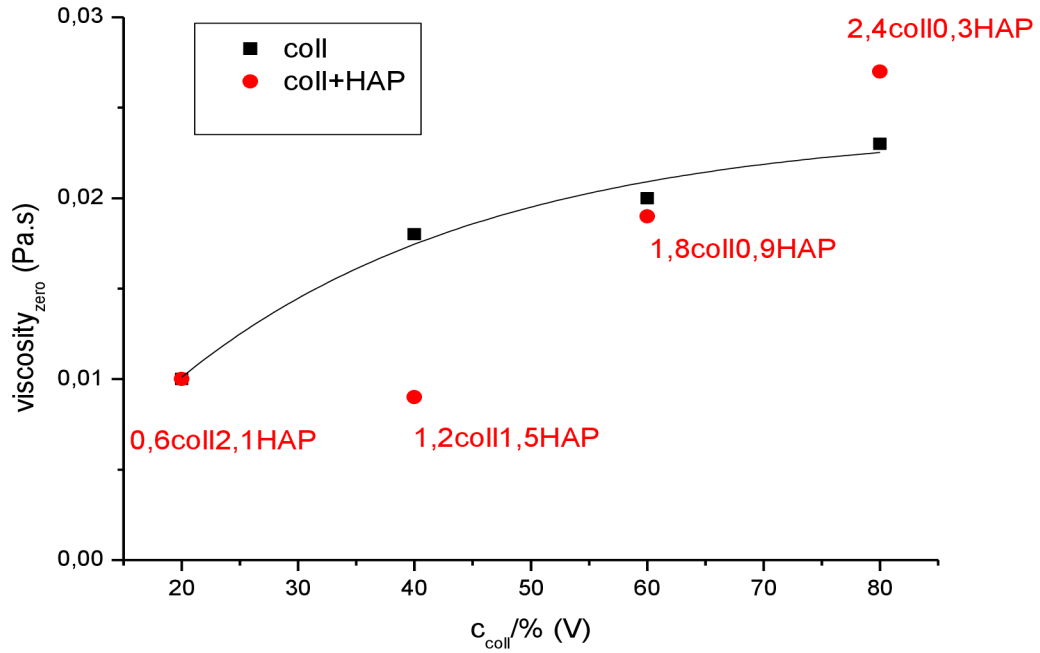

Fig. 5.20. The extrapolated zero shear rate viscosities for all measured collagen solution compositions. The addition of nHAP increases the viscosity only in 2,4coll0,3HAP. The fitted full line connecting the zero shear rate viscosity concentration dependence serves as a guide for the eye.

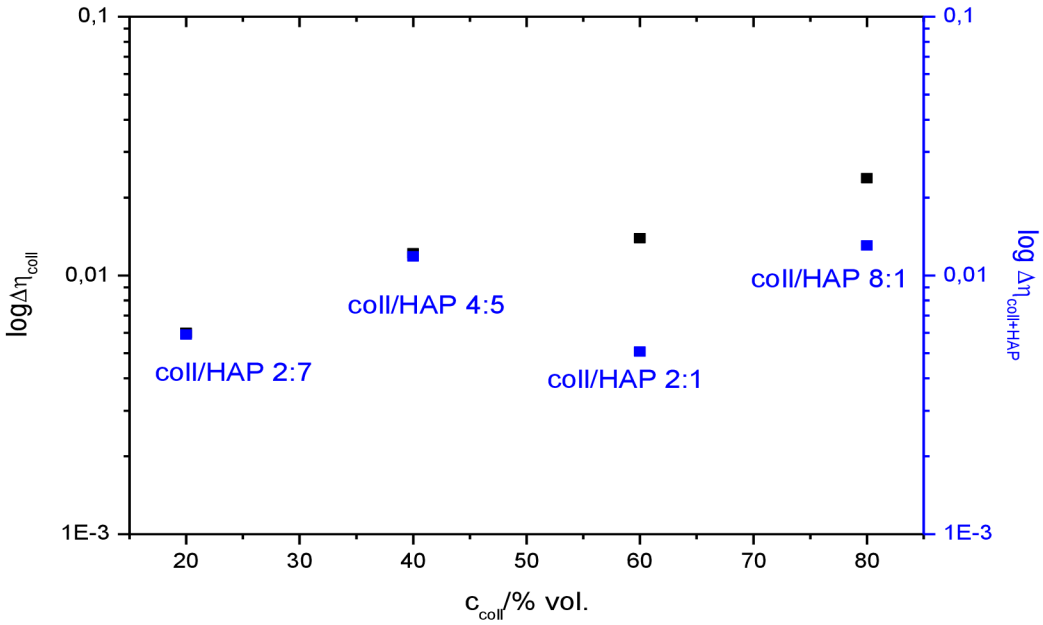

Fig.5.21. Plot of the composition dependence of the viscosity decrease during shear thinning of collagen I solutions, both neat and nHAP modified. It follows from the results that the addition of small amounts of nHAP such as in 2,4coll0,3HAP decrease the extent of shear thinning.

5.5 Morphology of the freeze dried collagen/HAP networks

For engineering bone tissues, a suitable scaffold, exhibiting optimal physical properties and biocompatibility, provides initial mechanical stability for surgical implantation and supports even cell distribution and differentiation. In the previous paragraphs, we have shown that collagen/nHAP nanocomposite gels exhibit reasonable balance of physical and biological properties desired for preparing scaffolds for bone tissue engineering. These nanocomposites exhibit their properties and perform their functions at the meso-scale, however, their hierarchical structure is formed at multiple length scales with the main focus of this work on the nano- and micro- scales. An attempt was made to analyze formation of the microscale structure of self-assembled collagen and collagen/HAP nanocomposite microfibrils to ascertain the role of individual components in morphogenesis of the networks controlling the performace of their hydrogels.

The Coll/HAP nanocomposites investigated can be considered filled polymer gels with hybrid chemical and physical cross-links. In time, acid desolved heterotrimer tropocollagen I tends to form fibrillar assemblies via self-assembly by burying the hydrophobic residues within the fibril. (174) This process has the character of a true thermodynamic transition of first order similarly to polymer crystallization as proposed by Flory more than 50 years ago (168). The formed fibrils have relatively sharp N-terminal tips and blunt C-terminal tips. (169) This process is accelerated with increasing concentration of procollagen molecules in the solution. Similarly to crystallization, however, fibrils formed from more concentrated solutions can be assumed to be less well developed and the formed highly branched network gel structure may attain a time dependent quasi-equilibrium state.

Fig. 5.22. Photo of the 3D porous freeze-dried neat collagen network.

The freeze-dried porous collagen network was photographed at the macroscale (Fig. 5.22.) and at the micro-scale employing SEM. The network was modified by adding HAP, or crosslinked by using carbodiimide chemistry prior to experiments and/or clinical trials using animal models to ensure the desired stability of the network. Differences in the pore size and distribution and also the wall structure were observed in SEM micrographs of porous freeze-dried collagen networks both neat and with nHAP and are shown in Figs. 5.25 and 5.29.

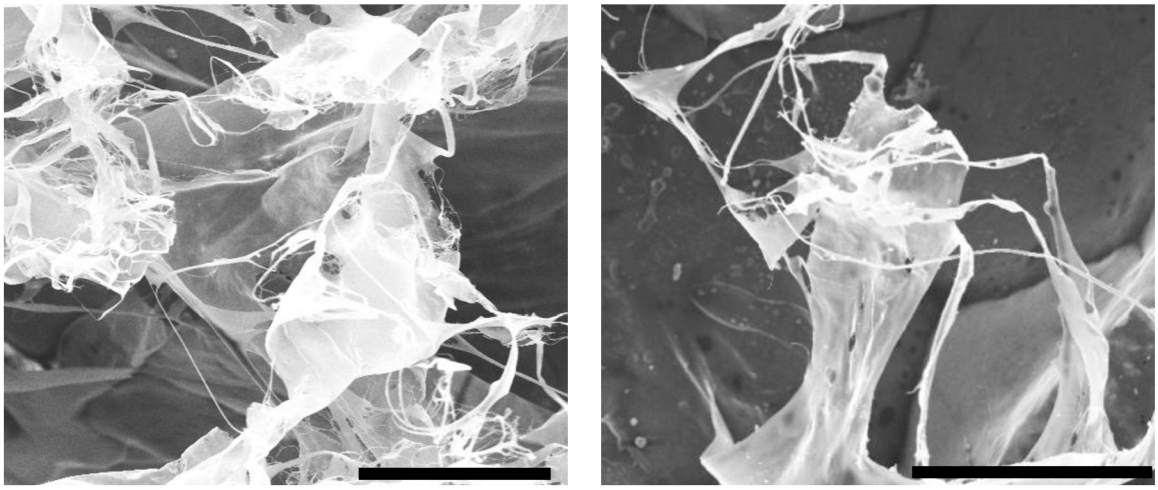

Fig. 5.23. SEM micrographs of freeze-dried porous uncrosslinked (left) and crosslinked (right) neat collagen network. Bar in the right lower corner represents 2 μm.

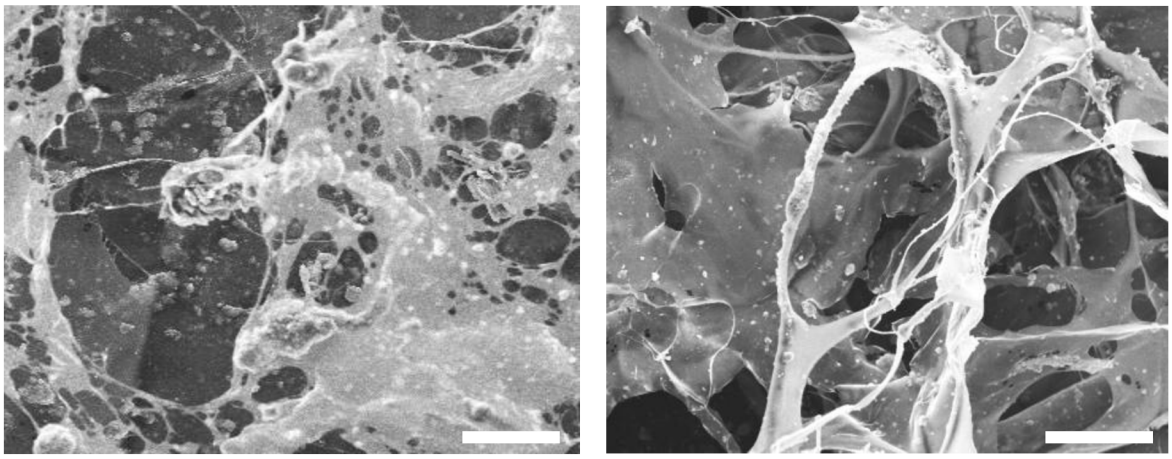

Figure 5.24. SEM micrographs of freeze-dried porous uncrosslinked (left) and crosslinked (right) collagen/HAP networks containing 20 wt.% hydroxyapatite nanoparticles. Bar in the right lower corner represents 20 μm.

The micrographs shown in Figs. 5.23 and 5.24 reveal several important differences between the overall morphology of the uncross-linked and cross-linked neat and HAP modified collagen I networks. In all the cases investigated, morphology (supramolecular structure) of the 3D network consists of two basic structural elements. These are the elongated collagen fibrils and thin randomly

oriented films forming walls between individual pores originated from removal of water during freeze-drying. Adding HAP and/or cross-linking did not change the nature of the basic structural elements, however, affected the size of the fibrils and the compactness of the films.

At first, the cross-linking of neat collagen (Fig. 5.24) resulted in formation of larger diameter fibrils and thicker walls separating the pores in the freeze-dried self-assembled collagen network. This is in agreement with the classical model of gelation mechanism proposed by Flory by adding attractive interaction between the overlapping fibrils at cross-link points to the junction zones and fibril jamming gelation mechanisms existing in un-cross-linked collagen (167).

At second, adding the nHAP resulted in two main structural differences (Fig. 5.25) compared to the neat collagen systems. First, addition of nHAP, hindering the collagen self-assembly, to the un-cross-linked collagen resulted in the disruption of some of the thin films separating the pores and a significant portion of nHAP deposited itself onto these films. Second, thin collagen fibrils formed in un-cross-linked collagen remained nHAP free most probably because of their small diameter providing insufficient attractive interaction for the nHAP particles of substantially greater diameter. Cross-linking greatly reduced the detrimental effect of nHAP on the pore wall structure and the larger fibrils were able to retain nHAP particles to a great extent, resulting in the formation of truly “mineralized” collagen fibrils.

The following series of SEM micrographs in Fig. 5.25. illustrates the effect of the 10%, 20% and 30% nHAP addition to uncrosslinked neat collagen at the 500 µm scale. A closer look at the same scaffolds is presented in Fig. 5.26. at the 100µm scale. Carbodiimide crosslinked versions of these networks were also produced and SEM micrographs are shown in Fig. 5.27. and Fig. 5.28.

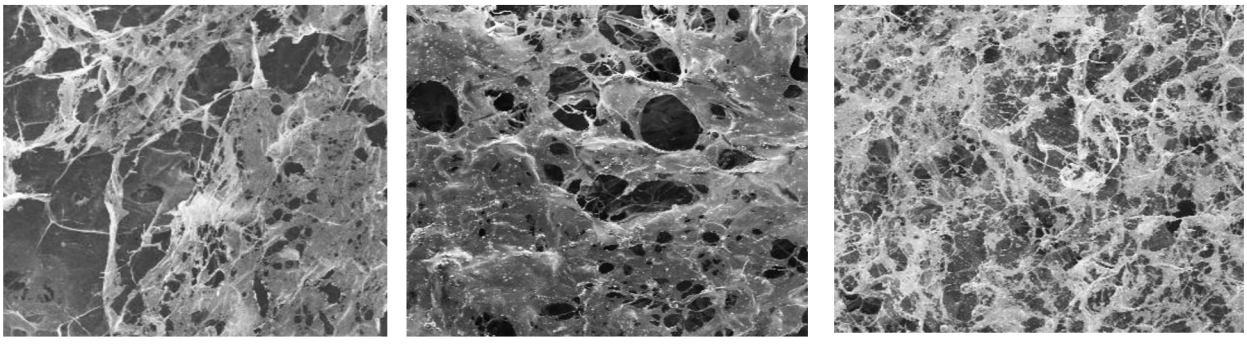

a) b) c)

Fig. 5.25. SEM micrographs of un-cross-linked collagen I freeze-dried network at the 500 µm scale with a) 10% nHAP, b) 20% nHAP, c) 30% nHAP

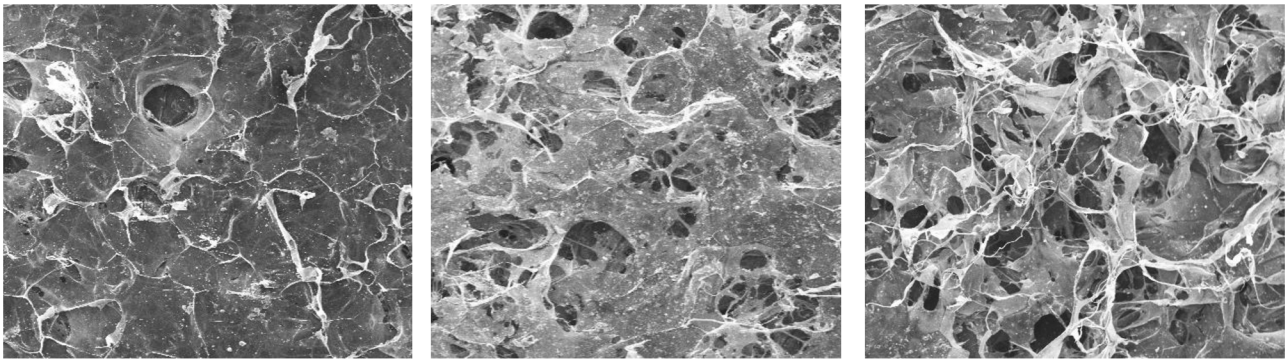

a) *b)* *c)*

Fig. 5.26. SEM micrographs of freeze-dried collagen I carbodiimide crosslinked network at the 500 µm scale with a) 10% nHAP, b) 20% nHAP, c) 30% nHAP

The extent of the changes in morphology was proportional to the HAP content which is shown in Figs. 5.25 and 5.27 for un-cross-linked and in Figs. 5.26 and 5.28 for carbodiimide cross-linked collagen. As expected, the disruption of the original morphology of the neat freeze-dried collagen network is greater for un-cross-linked compared to cross-linked networks.

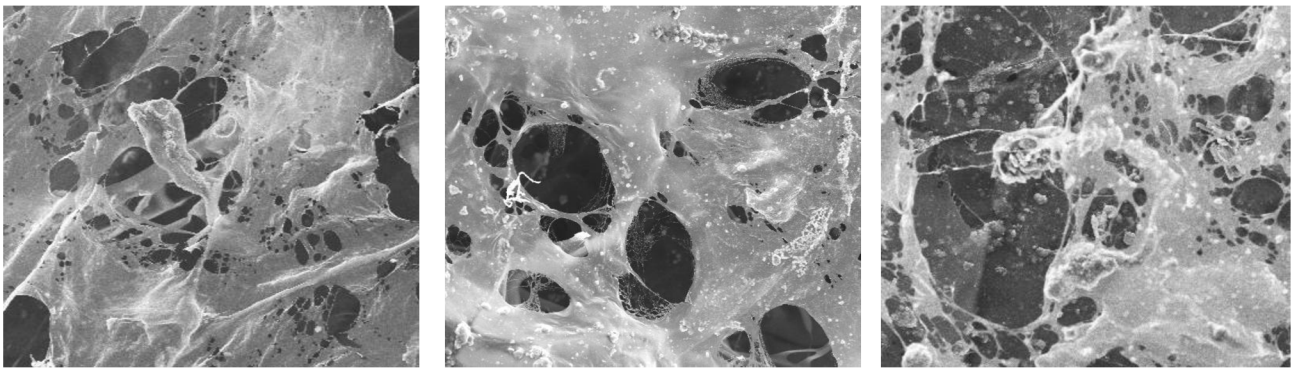

a) *b)* *c)*

Fig. 5.27. SEM micrographs of freeze-dried un-cross-linked collagen I network at the 100 µm scale with a) 10% nHAP, b) 20% nHAP, c) 30% nHAP

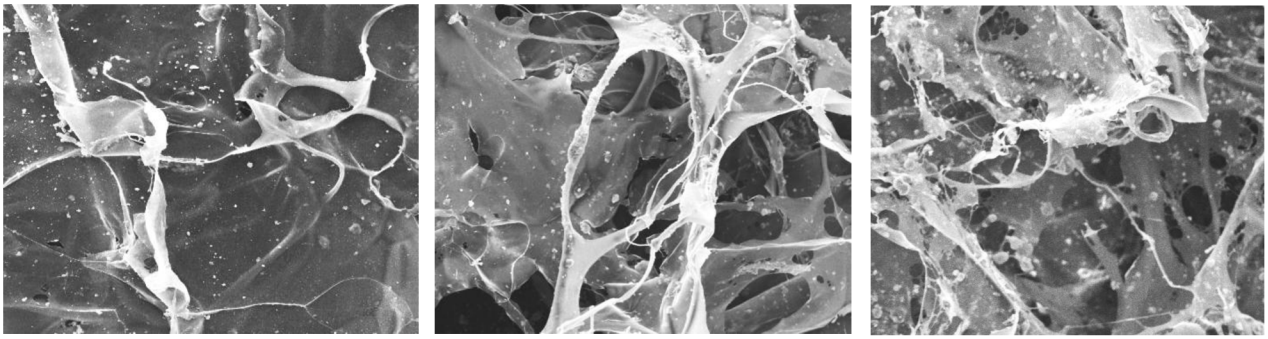

a) *b)* *c)*

Fig. 5.28. SEM micrographs of freeze-dried collagen I carbodiimide cross-linked network at the 100 µm scale with a) 10% nHAP, b) 20% nHAP, c) 30% nHAP

5.6 Use of freeze dried collagen/HAP networks in bone tissue engineering

3D porous scaffolds were prepared by freeze-drying the coll/HAP nanocomposite hydrogels of different composition. These scaffolds were exploited in cell assays at the Institute of Experimental Medicine, CAS Prague, Faculty of Medicine, MU Brno and in clinical research of bone diseases and segmental defects at the Faculty of Veterinary Medicine, VFU Brno employing animal models. Scaffolds were either used in a native form, seeded with mesenchymal stem cells (MSCs) or containing various blood derivatives. Results of this Thesis were utilized in determining the best coll/HAP network composition providing the desired balance of biomechanical properties, biological properties to host MSMs and surgical handling characteristics.

Neat collagen networks (Fig. 5.29 left) both native and cross-linked were used in treating defects in large joint cartilage in miniature pigs (Fig 5. 30) and the coll/HAP based networks (Fig. 5.29 right) were used to prepare scaffolds for the regeneration of large bone segmental defects in rabbits (Fig. 5. 33). The MSCs attached to the scaffold are shown in Fig. 5.31. in the SEM micrograph as well as in an immunofluorescence snapshot (Fig. 5.32 right), clearly documenting the biocompatible character of our scaffolds, which are currently successfully utilized in animal testing and being prepared for human clinical trials (Fig. 5.33.)

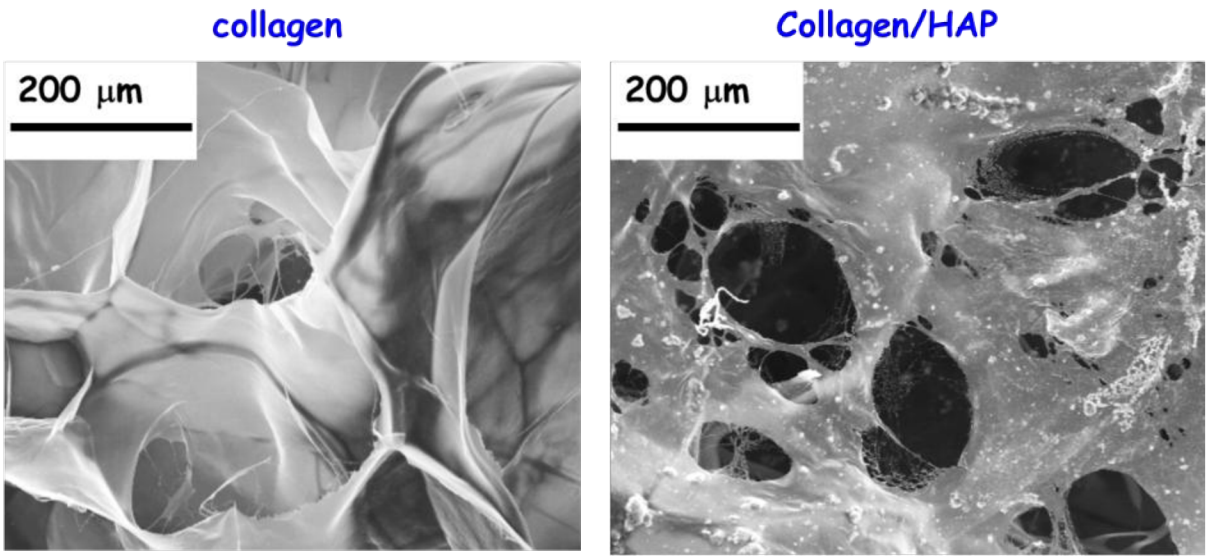

Fig. 5.29. SEM micrographs of freeze-dried neat collagen (left) and coll/HAP (right) networks. SEM revealed significant differences in both the size and size distribution of pores and wall structure.

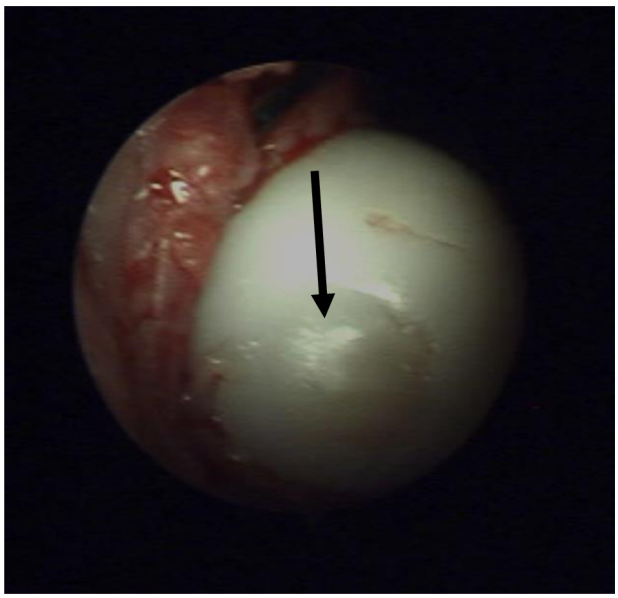

Fig. 5.30. Photograph of the newly formed hyaline cartilage in a condyle defect in miniature pig after 16 weeks healing period (arrow). The defect was treated with porous neat collagen scaffold seeded with 2 x 10^6 MSCs (courtesy of Professor A. Nečas, VFU Brno).

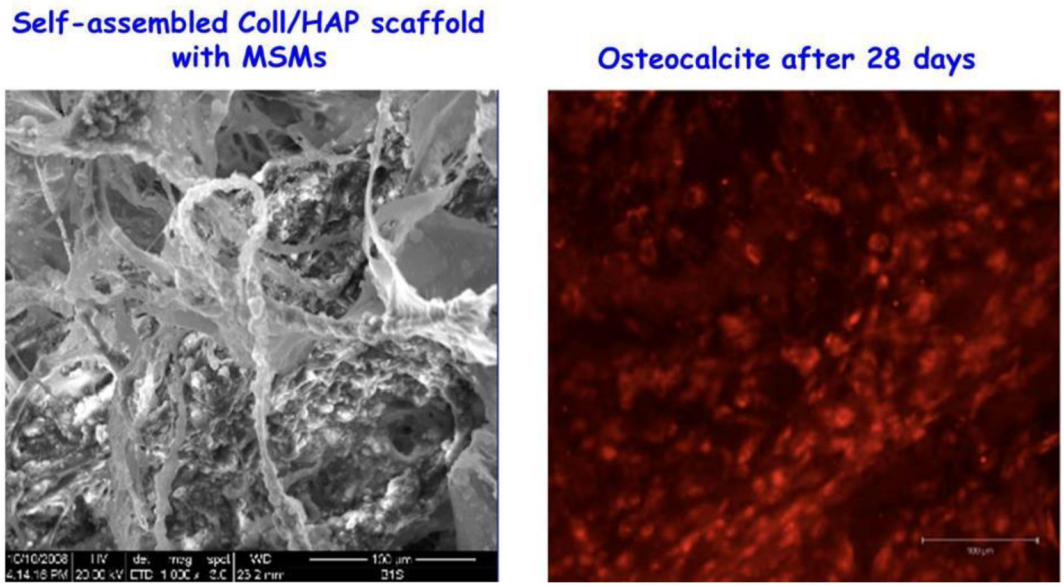

(a) (b)

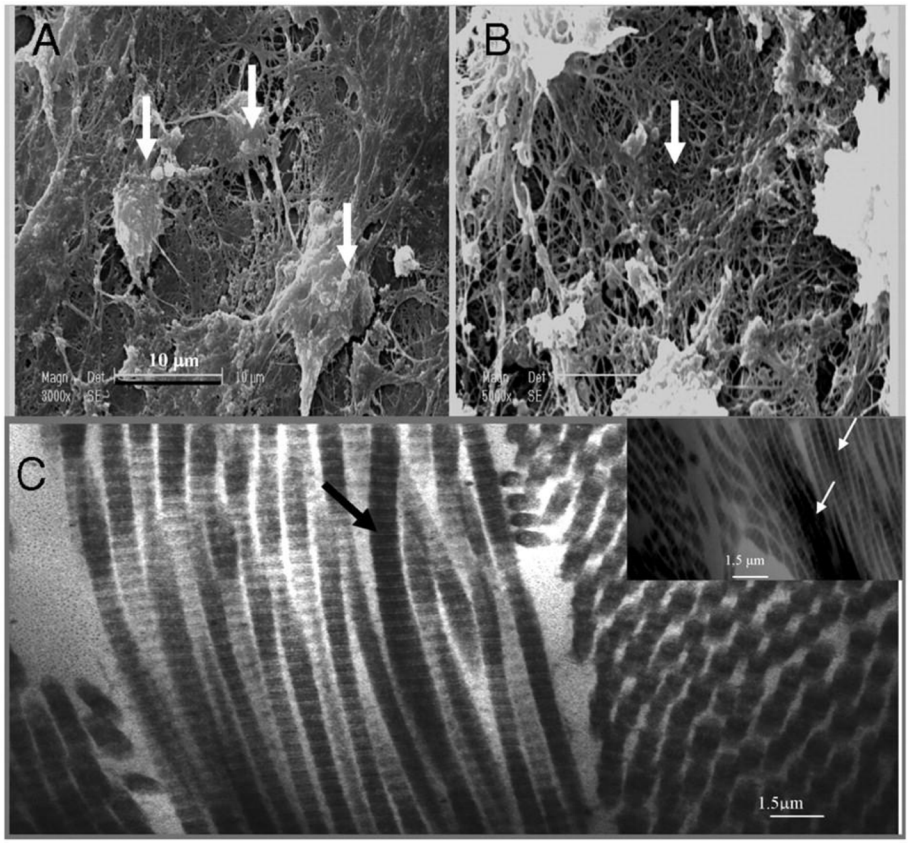

(c)

Fig.5.31. (a) SEM micrograph of the freeze-dried self assembled coll/HAP network scaffold seeded with MSCs clearly showing MSC attachment in the direction of collagen fibril orientation. (b) Ex vivo osteocyte secreted calcite after 28 days at 37 °C at pH 7. (right, courtesy of doc. A. Hampl, MU Brno). (c) ESEM micrographs of a natural bone tissue near the growth plate of a femur bone (courtesy of Prof. P. Hansma, University of California Santa Barbara, USA).

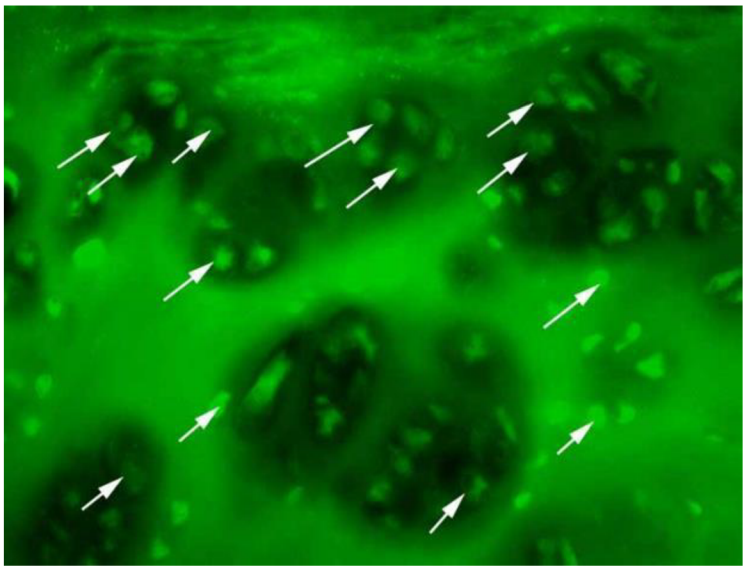

Fig. 5.32. Imunofluorescence of DiI marker on membrane chondrocytes differentiated from seeded MSCs on collagen/HAP scaffolds seeded with allogenous MSCs (arrows, magnification 400x) (courtesy of Professor A. Nečas, VFU Brno).

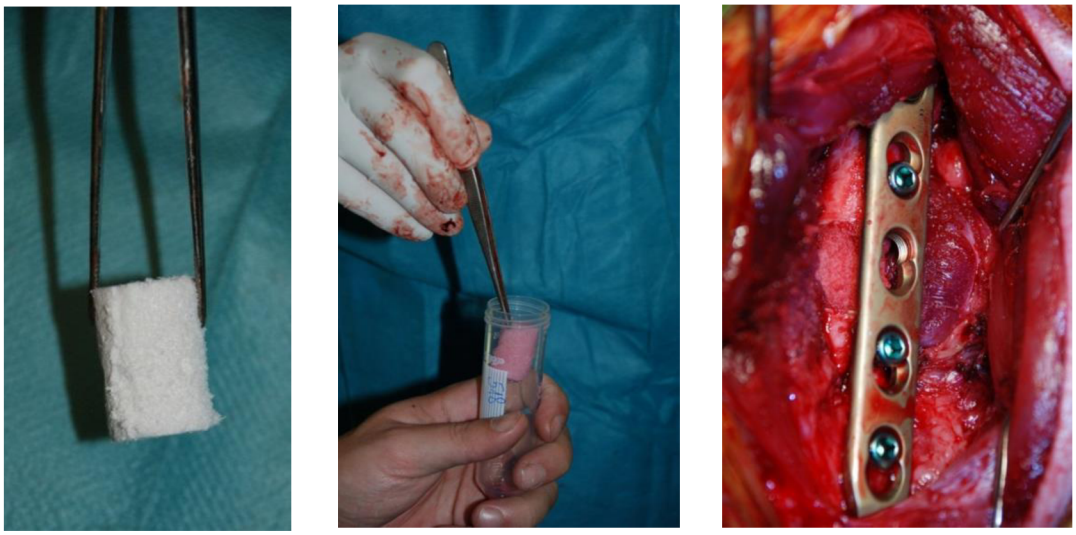

Fig. 5.33. Photograph of freeze-dried porous Coll/HAP scaffold (left) prior to MSC seeding. The Coll/HAP scaffold seeded with 2.6 x 10^6 MSCs prior to insertion during surgery to repair segmental defect in a rabbit (middle) and the scaffold after placement in tibia defect fixed with titanium plate (right) (courtesy of Professor A. Nečas, VFU Brno).

6 Conclusion

Tailored biomaterials with tunable functional properties are desirable for many applications ranging from drug delivery to regenerative medicine. To improve the ability to predict and "tailor" custom patient properties and functions of biopolymer materials, multiple design parameters need to be considered, along with appropriate models.

Rheological experiments were conducted employing an AR-G2 rheometer with a 2° cone and solvent trap in several modes. First, the linear viscoelastic region (LVR) was determined by establishing a strain interval, where G' was independent of strain. The strain 1% was selected, which is in good agreement with other published data. Also, the usual daily strains of bone are approx. 0.3%.

The effect of matrix composition and HAP content on the shear storage modulus of the Co/HAP nanocomposites considered for manufacturing of porous scaffolds for bone tissue engineering has been investigated at 37 ^{o}C. The results showed that adding the HAP nanoparticles in both Co(0.5) and Co(1) resulted in several fold increase in the storage modulus greatly above the predictions based on simple volume replacement micromechanics models. Hence, the proposed molecular reinforcement mechanisms are based on stiffening the worm like collagen chains *via* interactions with HAP nanoparticles resulting in retarded reptation in the vicinity of nanoparticles causing effective shortening of the rubbery network chains and percolation of HAP nanoparticle confined chains. This model provides reasonable framework for qualitative explanation of the observed concentration dependences of the storage modulus. Above v_f=0.1, the experimentally measured modulus negatively deviated from the predicted trend which has been attributed to the preferential interaction between the collagen C-termini and OH- groups of HAP resulting in their depletion. This caused deterioration of the network structure and, thus, reduction of its modulus. This fundamental finding can have implications in understanding the observed optimal HAP content in natural bone tissue.

The kinetics of self-assembly was studied using dynamic oscillatory shear time sweep rheology, following the time evolution of the viscoelastic moduli. The self-assembly proceeded as described in literature, initiated by a lag phase (nucleus formation), followed by a growth phase accompanied by a steep increase in the storage modulus, suggesting the formation of an elastic collagen network. The nHAP did not enhance the value of this elastic modulus significantly, but facilitated the earlier onset of self-assembly through weak physical interactions. Also, in samples with nHAP/coll ratio higher than 1, a structure resulting from the presence of an abundance of nHAP with a high modulus was formed and broken down during the first 500 s. Lower plateau self-assembled moduli were reached as self-assembly progressed.

All collagen solutions showed shear-thinning behavior fitted well by flat exponentials, which is in agreement with published research. The viscosity dependences were extrapolated towards zero shear rate in order to determine the effect of composition. Also the decrease in viscosity (extent of shear thinning) was calculated and related to the nHAP content. The zero shear rate viscosity increased exponentially with increasing collagen concentration. In 2,4coll0,3HAP, the viscosity was increased substantially by the nHAP addition, however in larger quantities, the nHAP did not contribute to larger viscosity values. Also in 2,4coll0,3HAP, the extent of shear thinning was decreased, whereas in samples with higher nHAP content, this was not observed.

3D porous scaffolds were prepared by freeze-drying the coll/HAP nanocomposite hydrogels of different composition. Scaffolds with structure optimized based on results of this Thesis were utilized in treating defects in large joint cartilage in miniature pigs and for the regeneration of large bone segmental defects in rabbits.

7 List of abbreviations

AFM	atomic force microscopy
ATP	adenosine triphosphate
BPM	biological protein material
CLSM	confocal laser scanning microscopy
coll	collagen
ECM	extracellular matrix
FE	finite element
FTIR	Fourier-transform infrared (spectroscopy)
HAP	hydroxyapatite
HB	hydrogen bond
IPN	interpenetrating network
ITD	intertubular dentin
LAOS	large amplitude oscillatory shear
MD	molecular dynamics
nHAP	nanohydroxyapatite
NMR	nuclear magnetic resonance
NP	nanoparticle
PBS	phosphate buffered saline
PG	proteoglycan
PTD	peritubular dentin
SA	self-assembly
SEM	scanning electron microscopy
TC	tropocollagen
TE	tissue engineering
TEM	transmission electron microscopy
XRD	X-Ray diffraction

8 References

1. **Meyers, M.A., Chen, P., Lin, A.Y. and Seki, Y.** Biological materials: Structure and mechanical properties. *Prog.Mater.Sci.* 53, 2008, Vols. 1-206.

2. **Gronau, G., et al.** A review of combined experimental and computational procedures for assessing biopolymer structure-process-property relationships. *Biomaterials.* 33, 2012, Vols. 8240-8255.

3. **Gautieri, A., et al.** Viscoelastic properties of model segments of collagen molecules. *Matrix Biology.* 31, 2012, Vols. 141-149.

4. **Fratzl, P. and Weinkamer, R.** Nature's hierarchical materials. *Prog. Mater. Sci.* 52, 2007, Vols. 1263-1334.

5. **Espinosa, H.D., et al.** Merger of strcture and material in bone and nacre - Perspectives on de novo biomimetic materials. *Prog.Mater.Sci.* 54, 2009, Vols. 1059-1100.

6. **Gautieri, A., Vesentini, S., Redaelli, A., Buehler, M.J.** *Hierarchical structure and nanomechanics of collagen microfibrils from the atomistic scale up.* Milano : ACS Publications, NanoLetters, 2010.

7. **Buehler, M.J., Ackbarow, T.** Fracture mechanics of protein materials. *Materials Today.* September 2007, Vol. 10, 46-58.

8. **Meyers, M.A., et al.** Biological materials: Structure and mechanical properties. *Progress in Materials Science.* 53, 2008, Vols. 1-206.

9. **Maarel, J.R.C. van der.** *Introduction to Biopolymer Physics.* Singapore : World Scientific Publishing Co., 2008.

10. **Yao, H.-B., et al.** Hierarchical assembly of micro/nano-building blocks: bio-inspired rigid structural functional materials. *Chem. Soc. Rev.* 40, 2011, Vols. 3764-3785.

11. **Weertman, J. and Weertman, J.R.** *Physical Metallurgy.* North Holland : Cahn RW, 1970.

12. **Wegst, U.G.K. and Ashby, M.F.** *Philos.Mag.* 84, 2004, Vols. 2167-2186.

13. **O'Brien, F.J.** *Materials Today.* 14, 2011, Vols. 88-95.

14. **Liu, X. and Ma, P.X.** *Annals of Biomedical Engineering.* 32, 2004, Vols. 477-486.

15. **Sionkowska, A. and Kozlowska, J.** Properties and modification of porous 3-D collagen/hydroxyapatite composites. *International Journal of Biological Macromolecules.* 52, 2013, Vols. 250-259.

16. **Bondar, B., Fuchs, S., Motta, A., Migliaresi, C., Kirkpatrick, C.J.** Funcionality of endothelial cells on silk fibroin nets: Comparative study of micro- and nanometric fibre size. *Biomaterials.* 2008, Sv. 29, 561-572.

17. **Oreffo, R.O., Triffitt, J.T.** Future potentials for using osteogenic stem cells and biomaterials in orthopedics. *Bone.* 1999, Vol. 2, 5S-9S.

18. **Hollister, S.J., Lin, C.Y.** Computational design of tissue engineering scaffolds. *Comput. Methods Appl. Mech. Engrg.* 2007, Vol. 169, 2991-2998.

19. **Trojani, Ch., Boukhecba, F., Scimeca, J.-C., Vandenbos, F., Michiels, J.-F., Daculsi, G., Boileau, P., Weiss, P., Carle, G.F., Rochet, N.** Ectopic bone formation using an injectable biphasic calcium phosphate/Si-HPMC hydrogel composite loaded with undifferentiated bone marrow stromal cells. *Biomaterials.* 2006, Vol. 27, 3256-3264.

20. **Puppi, D, et al.** Polymeric materials for bone and cartilage repair. *Progress in Polymer Science.* 35, 2010, Vols. 403-440.

21. **Klapperich, C.M., Bertozzi, C.R.** Global gene expression of cells attached to a tissue engineering scaffold. *Biomaterials.* 2004, Vol. 25, 5631-5641.

22. **Zhang, Y., Wang, Y., Shi, B., Cheng, X.** A platelet-derived growth factor releasing chitosan/coral composite scaffold for periodontal tissue engineering. *Biomaterials.* 2007, Vol. 28, 1515-1522.

23. **Badylak, S.F.** The extracellular matrix as a biologic scaffold material. *Biomaterials.* 2007, Vol. 28, 3587-3593.

24. **Jansen, E.J.P, Sladek, R., Bahar, H., Yaffe, A., Gijbels, M.J., Kuijer, R., Bulstra, S., Guldemond, N.A., Binderman, I., Koole, L.H.** Hydrophobicity as a design criterion for polymer scaffolds in bone tissue engineering. *Biomaterials.* 2005, Vol. 26, 4423-4431.

25. **Mayorga, M.** Biomaterials based tissue engineering. *biomed.brown.edu.* [Online] 2011.

26. **Wiedemann, A.L., Ahmad, M., Gutwald, R., Lauer, G., Hubner, U., Schmelzeisen, R.** How to optimize seeding and culturing of human osteoblast-like cells on various biomaterials. *Biomaterials.* 2003, Vol. 23, 3319-3328.

27. **Rice, W.L., Firdous, S., Gupta, S., Hunter, M., Foo, Ch.W.P., Wang, Y., Kim, H.J., Kaplan, D.L., Georgakoudi, I.** Non-invasive characterization of structure and morphology of silk fibroin materials using non-linear microscopy. *Biomaterials.* 2008, Vol. 29, 2015-2024.

28. **Shin, H.** Fabrication methods of an engineered microenvironment for analysis of cell-bioamterial interactions. *Biomaterials .* 2007, Vol. 28, 126-133.

29. **Weiner, S., Wagner, H.D.** *Annu. Rev. Mater. Sci.* 28, 1998, Vol. 271.

30. **Weiner, S., Traub, W., Wagner, H.D.** *J. Struct. Biol.* 126, 1999, Vol. 241.

31. **Fratzl, P., et al.** *J.Mater.Chem.* 14, 2004, Vols. 2115-2123.

32. **Svensson, A., Nicklasson, E., Harrah, T., Panilaitis, B., Kaplan, D.L., Brittberg, M., Gatenholm, P.** Bacterial cellulose as a potential scaffold for tissue engineering of cartilage. *Biomaterials.* 2005, Vol. 26, 419-431.

33. **Thomson, R.C., Yaszemski, M.J., Powers, J.M., Mikos, A.G.** Hydroxyapatite fiber reinforced poly(hydroxyester) foams for bone regeneration. *Biomaterials.* 1998, Vol. 19, 1935-1943.

34. **Mastrogiacomo, M., Papadimitropoulos, A., Cedola, A., Peyrin, F., Giannoni, P., Pearce, S.G., Alini, M., Giannini, C., Guagliardi, A., Cancedda, R.** Engineering of bone using bone marrow stromal cells and a silicon-stabilized tricalcium phosphate biceramic: Evidence for a coupling between bone formation and scaffold resorption. *Biomaterials.* 2007, Vol. 28, 1376-1384.

35. **Lisignoli, G., Cristino, S., Piacentini, A., Toneguzzi, S., Grassi, F., Cavallo, C., Zini, N., Solimando, L., Maraldi, N.M., Facchini, A.** Cellular and molecular events during chondrogenesis of human mesenchymal stromal cells grown in a three-dimensional hyaluronan-based scaffold. *Biomaterials.* 2005, Vol. 26, 5677-5686.

36. **Freyria, A.M., Cortial, D., Ronziére, M.C., Guerret, S., Herbage, D.** Influence of medium composition, static and stirred conditions on the proliferation of and matrix expression of bovine articular chondrocytes cultured in a 3D collagen scaffold. *Biomaterials.* 2004, Vol. 25, 687-697.

37. **Roche, S., Ronziere, M., Herbage, D., Freyria, A.** Native and DPPA cross-linked collagen sponges seeded with bovine epiphyseal chondrocytes used for cartilage tissue engineering. *Biomaterials.* 2001, Vol. 22, 9-18.

38. **Saldanha, V, Grande, D.A.** Extracellular matrix protein gene expression of bovine chondrocytes cultured on resorbable scaffolds. *Biomaterials.* 2000, Vol. 21, 2427-2431.

39. **Christmann, K., Lee, R.J.** Biomaterials for the treatment of myocardial infection. *Journal of the American Coll. of Cardiol.* 2006, Vol. 48, 5.

40. **Grayson, W.L., Chao, P. G., Marolt, D., Kaplan, D., Novakovic, G.** *Engineering custon-designed osteochondral tissue grafts.* New York : Elsevier, 2008.

41. **Hench, L.L.** Biomaterials: a forecast for the future. *Biomaterials.* 1998, Vol. 19, 1419-1423.

42. **Buehler, M.J., Keten, S.** PhysOrg. *PhysOrg.com.* [Online] PhysOrg.com, 2008.

43. **Břížďala, J.** Bílkoviny. *E-Chembook.eu.* [Online] 2013.

44. **Cummings, B.** Notes for Pakistan. *notesforpakistan.com.* [Online] Pearson Education, Inc., 2010.

45. **Buehler, M.J., Keten, S., Ackbarow, T.** Theoretical and computational hierarchical nanomechanics of protein materials: Deformation and fracture. *Progress in Mat. Science.* 2008, Vol. 53, 1101-1241.

46. **NDTResourceCenter.** NDT Resource Center. *ndt-ed.org.* [Online] Iowa State University, 2011.

47. **IndianaUniversity.** Purdue University Fort Wayne. *ipfw.edu.* [Online] 2010.

48. **Buehler, M.J.** Nature designs tough collagen: Explaining the nanostructure of collagen fibrils. *PNAS.* 2006, Vol. 103, 12285-12290.

49. **Fu, S.L., Dean, R.** Structural characterization of the products of hydroxyl-radical damage to leucine and their detection on proteins. *Biochemical Journal.* 1997, Vol. 324, 41-48.

50. **Hulmes, D.J.S.** Collagen Diversity, Synthesis and Assembly. [book auth.] P. Fratzl. *Collagen Structure and Mechanics.* New York : Springer Science and Business Media, 2008.

51. **Fratzl, P.** Collagen - Strucuture and Mechanics. *Collagen: Structure and Mechanics, an Introduction.* New York : Springer Science+Business Media, 2008.

52. **Cui, F.-Z., Li,Y., Ge,J.** Self-assembly of mineralized collagen composites. *Materials Science and Engineering.* 57, 2007, Vols. 1-27.

53. **Myllyharju, J.** Intracellular post-translational modifications of collagens. *Top Curr Chem.* 247, 2005, Vols. 115-247.

54. **Niyibizi, C., Wnag, S. and Robbins, P.D.** Gene Therapy. *Nature.com.* [Online] Nature publishing group, 2014.

55. **Whitesides, G.M. and Mathias, J.P.** Molecular self-assembly and nanochemistry. *Science.* 254, 1991, Vols. 1312-1319.

56. **Whitesides, G.M. and Boncheva, M.** Beyond molecules: Self-assembly of mesoscopic and macroscopic components. *Proceedings of the National Academy of Sciences of the USA.* 99, 2002, Vols. 4769-4774.

57. **Min, Y., et al.** The role of interparticle and external forces in nanoparticle assembly . *Natur.Mater.* 7, 2008, Vols. 527-538.

58. **Prigogine, I.** *Non-equilibrium statistical mechanics.* New York : Wiley-Interscience, 1962.

59. **Rubinstein, M., Colby, R.** *Polymer Physics.* New York : Oxford University Press, 2003.

60. **de Carvalho, W., Djabourov, M.** Physical gelation under shear for gelatin gels. *Rheol Acta.* 1997, Vol. 36, 591 - 609.

61. **Jancar, J. and Balkova, R.** Effect of interfacial interactions on the crystal growth rate in model Pe/Si(Osub2) nanocomposites: comparing experiments with Lauritzen-Hoffman model and MD simulation. *Polymer Engineering and Science.* 2013.

62. **Giraud-Guille, M.-M.** Liquid crystalline phases of sonicated type I collagen. *Biol.Cell.* 67, 1989, Vols. 97-101.

63. **Besseau, L. and Giraud-Guille, M.-M.** Stabilization of fluid cholesteric phases of collagen to ordered gelated matrices. *J.Mol.Biol.* 251, 1995, Vols. 197-202.

64. **Giraud-Guille, M.-M., et al.** Liquid crystalline properties of type I collagen: Perspectives in tissue morphogenesis. *C.R.Chimie.* 11, 2008, Vols. 245-252.

65. **Giraud-Guille, M.-M.** Liquid crystallinity in condensed type I collagen solutions. *J.Mol.Biol.* 224, 1992, Vols. 861-873.

66. **Fertala, A., Sieron,A.L., Adachi, E. and Jimenez, S.A.** Collagen II containing a Cys substitution for arg-alpha1-519. *Biochemistry .* 40, 2001, Vols. 14422-14428.

67. **Steplewski, A., Hintze, V. and Fertala, A.** Molecular basis of organization in collagen fibrils. *J.Struct.Biol.* 157, 2007, Vols. 297-307.

68. **Kadler, K.E., Lightfoot, S.J. and Watson, R.B.** Biochemistry of the procollagen N-peptidase. *Methods Enzymol.* 1995.

69. **Parry, D.A. and Craig, A.S.** Growth and development of collagen fibrils in connective tissue. *Ultrastructure of the Connective Tissue Matrix.* 1984, Vols. 34-64.

70. **Gobeaux, F., Mosser, A., Anglo, A., Panine, P., Davidson, P., Giraud-Guille, M.M.** Fibrillogenesis in dense collagen solutions: A physicochemical study. *Journal of Molecular Biology.* 376, 2008, Vol. 1509.

71. **Hulmes, D.J.S., Miller, A., Parry, D.A.D., Piez, K.A., Woodhead-Galloway, J.** Analysis of the primary structure of collagen for the origins of molecular packing. *J. Mol. Biol.* 1973, Vol. 79, 137.

72. **Trus, B.L., Piez, K.A.** Molecular packing of collagen: three-dimensional analysis of electrostatic interactions. *J. Mol. Biol.* 1976, Vol. 108, 705-732.

73. **Holmes, D.F., Capaldi, M.J., Chapman, J.A.** Reconstitution of collagen fibrils in vitro; the assembly process depends on the initiating procedure. *Int.J.Biol.Macromol.* 1986, Vol. 8, 161-166.

74. **Holmes, D.F., et al.** STEM/TEM studies of collagen fibril assembly. *Micron.* 32, 2001, Vols. 273-285.

75. **Christiansen, D.L., Huang, E.K., Silver, F.H.** Assembly of type I collagen: Fusion of fibril subunits and the influence of fibril diameter on mechanical properties. *Matrix Biol.* 2000, Vol. 19, 409-420.

76. **Silver, F.H., Freeman, J.W., Seehra, G.P.** Collagen self-assembly and the development of tendon mechanical properties. *J. Biomech.* 2003, Vol. 36, 1529-1553.

77. **Forgacs, G., Newman, S.A., Hinner, B., Maier, C.W., Sackmann, E.** Assembly of collagen matrices as a phase transition revealed by structural and rheologic studies. *Biophys.J.* 2003, Vol. 84, 1272-1280.

78. **Ward, N.P., Hulmes, D.J.S., Chapman, J.A.** Collagen self-assembly in vitro: electron microscopy of initial aggregates formed during the lag phase. *J. Mol. Biol.* 190, 1986, Vols. 107-112.

79. **Yan, M., et al.** Effect of concentration, pH and ionic strength on the kinetic self-assembly of acid-soluble collagen from walleye pollock skin. *Food Hydrocolloids.* 29, 2012, Vols. 199-204.

80. **Yang, Y., Kaufman, L.J.** Rheology and confocal reflectance microscopy as probes of mechanical properties and structure during collagen and collagen/hyaluronan self-assembly. *Biophysical Journal.* 2009, Vol. 96, 1566-1585.

81. **Wess, T.J.** Collagen fibrillar structure and hierarchies. [book auth.] P.Fratzl. *Collagen Structure and Mechanics.* New York : Springer Science+Business Media, 2008.

82. **Lu, S., Sacks, M.S., Chung, S.Y., Gloeckner, D.C., Pruchnic, R., Huard, J., de Groat, W.C., Chancellor, M.B.** Biaxial mechanical properties of muscle-derived cell seeded small intestinal submucosa for bladder wall reconstitution. *Biomaterials.* 2005, Vol. 26, 443-449.

83. **Baker, S.C., Atkin, N., Gunning, P.A., Granville, N., Wilson, K., Wilson, D., Southgate, J.** Characterisation of electrospun polystyrene scaffolds for three dimensional in vitro biological studies. *Biomaterials.* 2006, Vol. 27, 3136-3146.

84. **Douglas, J.F.** *Theoretical issues relating to thermally reversible gelation by supermolecular fiber formation.* Gaithersburg : Langmuir, 2009.

85. **Avery, N.C., Bailey, A.J.** Restraining cross-links responsible for the mechanical properties of collagen fibers: natural and artificial. [book auth.] P.Fratzl. *Collagen Structure and Mechanics.* New York : Springer Science+Business Media, 2008.

86. **Parkinson, J., Kadler, K.E. and Brass, A.** Simple physical model of collagen fibrillogenesis based on diffusion limited aggregation. *J Mol Biol.* 247, 1994, Vols. 823-831.

87. **Prockop, D.J. and Fertala, A.** Inhibition of the self-assembly of collagen I into fibrils with synthetic peptides. Demonstration that self-assembly is driven by site-specific binding sites on the monomers. *J Biol Chem.* 273, 1998, Vols. 15598-15604.

88. **Cisneros, D.A., et al.** Observing growth steps of collagen self-assembly by time-lapse high-resolution atomic force microscopy. *Journal of Structural Biology.* 154, 2006, Vols. 232-245.

89. **Weiner, S. and Addadi, L.** At the cutting edge . *Science.* 298, 2002, Vols. 375-376.

90. **Sukhodub, L.F., et al.** Collagen-hydroxyapatite-water interactions investigated by XRD, piezogravimetry, infrared and Raman spectroscopy. *Journal of Molecular Structure.* 704, 2004, Vols. 53-58.

91. **Wozney, J.M., Rosen, V.** Bone morphogenetic protein and bone morphogenetic protein family in bone formation and repair. *Clin. Orthop. Rel. Res.* 1998, Vol. 346, 26-37.

92. **Suchanek, W., Yoshimura, M.** Processing and properties of hydroxyapatite-based biomaterials for use as hard tissue replacement implants. *J. Mater. Res.* 1998, Vol. 13, 94-117.

93. **Ducheyne, P., Qiu, Q.** Bioactive ceramics: the effect of surface reactivity on bone formation and bone cell function. *Biomaterials .* 20, 1999, Vol. 2287.

94. **LeGeros, R.Z., LeGeros, J.P., Daculsi, G., Kijkowska, R.** *Calcium phosphate biomaterials: preparation, properties and biodegradation.* New York : Marcel Dekker, 1995.

95. **Burg, K.J.L., Porter, S., Kellam, J.F.** Biomaterial developments for bone tissue engineering. *Biomaterials.* 2000, Vol. 21, 2347-2359.

96. **Salimi, M.N. and Anuar, A.** Characterizations of biocompatible and bioactive hydroxyapatite particles. *Procedia Engineering.* 53, 2013, Vols. 192-196.

97. **Rivera-Munoz, E.** Hydroxyapatite-based materials: Synthesis and Characterization. [book auth.] R. Fazel-Rezai. *Biomedical Engineering: Frontiers and Challenge.* 2011.

98. **Ficai, A., et al.** Self-assembled collagen/hydroxyapatite composite materials. *Chemical Engineering Journal.* 160, 2010, Vols. 794-800.

99. **Kumar, S.K. and Krishnamoorti, R.** Nanocomposites: Structure, Phase Behavior and Properties. *Annu.Rev.Chem.Biomol.Eng.* 1, 2010, Vols. 37-58.

100. **Fratzl, P.** Cellulose and collagen: from fibres to tissues. *Curr.Opin.Colloid Interface Sci.* 2003, Vol. 8, 32-39.

101. **Schaefer, D.W. and Justice, R.S.** How nano are nanocomposites? *Macromolecules.* 40, 2007, Vols. 8501-8517.

102. **Katti, D.R., Pradhan, S.M. and Katti, K.S.** Directional dependence of hydroxyapatite-collagen interactions on mechanics of collagen. *Journal of Biomechanics.* 43, 2010, Vols. 1723-1730.

103. **Ji, J., Bar-on, B. and Wagner, D.** Mechanics of electrospun collagen and hydroxyapatite/collagen nanofibers. *Journal of the Mechanical Behavior of Biomedical Materials.* 13, 2012, Vols. 185-193.

104. **Tien, W.-B., Chen, M.-T. and Yao, P.C.** Effects of pH and temperature on microstructure and morphology of hydroxyapatite/collagen composites synthesized in vitro. *Materials Science and Engineering.* 32, 2012, Vols. 2096-2102.

105. **Alberts, B., et al.** *Molecular Biology of the Cell.* New York : 4th ed. Garland Science, 2002.

106. **Rho, J.Y., Kuhn-Spearing, L. and Zioupos, P.** Mechanical properties and the structure of bone. *Med. Eng. Phys.* 20, 1998, Vols. 90-102.

107. **Gelinsky, M., Welzel, P.B., Simon, P., Bernhardt, A., König, U.** Porous three-dimensional scaffolds made of mineralised collagen: Preparation and properties of biomimetic nanocomposite material for tissue engineering of bone. *Chemical Engineering Journal.* 2008, Vol. 137, 84-96.

108. **Bandyopadhayy-Ghosh, S.** Bone as a collagen-hydroxyapatite composite and its repair. *Trends in Biomaterials and Artificial Organs.* 22, 2008, Vols. 112-120.

109. **Deymier-Black, A.C., et al.** Evolution of load transfer between hydroxyapatite and collagen during creep deformation of bone. *Acta Biomaterialia.* 8, 2012, Vols. 253-261.

110. **Gao, H., et al.** Materials become insensitive to flaws at the nanoscale. *Proceedings of the National Academy of Sciences.* 100, 2003, Vols. 5597-5600.

111. **Launey, M.E., Buehler, M.J. and Rithcie, R.O.** On the mechanistic origins of toughness in bone. *Annual Review of Materials Research.* 40, 2010, Vols. 25-53.

112. **Buehler, M.J.** Atomistic and continuum modeling of mechanical properties of collagen: elasticity, fracture and self-assembly. *Journal of Materials Research.* 21, 2006, Vols. 1947-1691.

113. —. Molecular nanomechanics of nascent bone: fibrillar toughening by mineralization. *Nanotechnology.* 18, 2007.

114. —. Nanomechanics of collagen fibrils under varying cross-link densities: atomistic and continuum studies of flaw tolerant nanostructures. *Journal of the Mechanical Behavior of Biomedical Materials.* 1, 2008, Vols. 59-67.

115. **Gupta, H.S., et al.** Cooperative deformation of mineral and collagen in bone at the nanoscale. *Proceedings of the National Academy of Sciences.* 103, 2006.

116. **Burgin, L.V., Edelsten, L. and Aspden, R.M.** The mechnical and material properties of elderly human articular cartilage subject to impact and slow loading. *Medical Engineering and Physics.* 36, 2014, Vols. 226-232.

117. **Ahn, H., et al.** 3D braid scaffolds for regeneration of articular cartilage. *Journal of the Mechanical Behavior of Biomedical Materials.* 34, 2014, Vols. 37-46.

118. **Mäkelä, J.T.A., Huttu, M.R.J. and Korhonen, R.K.** Structure-function relationships in osteoarthritic human hip joint articular cartilage. *Ostheoarthritis and Cartilage.* 20, 2012, Vols. 1268-1277.

119. **Hulmes, D.J.S.** Building collagen molecules, fibrils and suprafibrillar structures. *J Struct Biol.* 137, 2002, Vols. 2-10.

120. **Hulmes, D.J.S., Wess, T.J., Prockop,D.J. and Fratzl, P.** Radial packing, order and disorder in collagen fibrils. *Biophys J.* 68, 1995, Vols. 1661-1670.

121. **Orgel, J., et al.** The in situ supermolecular structure of type I collagen. *Structure.* 9, 2001, Vols. 1061-1069.

122. **Riley, G.** Structure of tendon. *Expert reviews in Molecular Medicine.* 7, 2005, Vol. 5.

123. **Biewener, A.A.** Tendons and Ligaments: Structure, Mechanical Behavior and Biological Function. [book auth.] P. Fratzl. *Collagen Structure and Mechanics.* New York : Springer Science+Business Media, 2008.

124. **Benjamin, M. and Ralphs, J.R.** Tendons and ligaments: An overview. *Histol. Histopathol.* 12, 1997, Vols. 1135-1144.

125. **Rumian, A.P., Wallace, A.L. and Birch, H.L.** Tendons and ligaments are anatomically distinct but overlap in molecular and morphological features. *J Orthop Res.* 25, 2007, Vols. 458-464.

126. **Biewener, A.A.** *Animal Locomotion.* Oxford : Oxford University Press, 2003.

127. **Zaslansky, P.** Dentin. [book auth.] P. Fratzl. *Collagen Structure and Mechanics.* NY : Springer Science+Business Media, 2008.

128. **Black-Deymier, A.** Collagen-based structural biocomposites. *Dunand Research Group.* [Online] Northwestern University, 2014.

129. **Stump, P.** Novel Separation of Polymer Systems with High Throughput and Separation Performance Characteristics. *Hessian Intellectual Property Organization.* [Online] Hessen Agentur , EU, 2014.

130. **Drury, J.L. and Mooney, D.J.** Hydrogels for tissue engineering: scaffold design variables and applications. *Biomaterials.* 24, 2003, Vols. 4337-4351.

131. **Palumbo, F.S., et al.** Chemical hydrogels based on a hyaluronic acid-graft-a-elastin derivative as potential scaffolds for tissue engineering. *Mater.Sci.Eng.* 2013.

132. **Qiu, Y. a Park, K.** Environment-sensitive hydrogels for drug delivery. *Adv. Drug Delivery Rev.* 64, 2012, Sv. 49-60.

133. **Hoffman, A.S.** Hydrogels for biomedical applications. *Adv. Drug Deliv. Rev.* 43, 2002, Vols. 3-12.

134. **Peppas, N.A., et al.** Hydrogels in pharmaceutical formulations. *Eur. J. Pharm. Biopharm.* 50, 2000, Vols. 27-46.

135. **Gong, J.P., et al.** Double-network hydrogels with extremely high mechanical strength. *Adv.Mater.* 15, 2003, Vols. 1155-1158.

136. **Stevens, L., et al.** Ionic covalent entanglement hydrogels from gellan gum, carrageenan and an epoxy-amine. *Soft Matter.* 9, 2013, Vols. 3009-3012.

137. **Johnson, J.A., et al.** Some hydrogels having novel molecular structures. *Progress in Polymer Science.* 35, 2010, Vols. 332-337.

138. **Ahagon, A. and Gent, A.** Threshold fracture energies for elastomers. *Polym.Phys.Ed.* 13, 2003, Vols. 1903-1911.

139. **Brown, H.R.** A model of the fracture of double network hydrogels. *Macromolecules.* 40, 2007, Vols. 3815-3818.

140. **Okumura, Y. and Ito, K.** The polyrotaxane gel: a topological gel by figure-of-eight crosslinks. *Adv.Mater.* 13, 2001, Vols. 485-487.

141. **Sharifi, S., et al.** Biodegradable nanocomposite hydrogel structures with enhanced mechanical properties prepared by photo-crosslinking solutions of poly (trimethylene carbonate)-poly(ethylene-glycol)-poly(trimethylene carbonate) macromonomers and nanoclay particles. *Acta Biomaterialia.* 8, 2012, Vols. 4233-4243.

142. **Fei, R., et al.** Ultra-strong thermoresponsive double network hydrogels. *Soft Matter.* 9, 2013, Vols. 2912-2919.

143. **Yu, Q.M., et al.** Direct observation of damage zone around the crack tips in double-network gels. *Macromolecules .* 42, 2009, Vols. 3852-3855.

144. **Gong, J.P.** Why are double network hydrogels so tough? *Sof Matter.* 6, 2010, Vols. 2583-2590.

145. **Tominaga, T., et al.** The molecular origin of enhanced toughness in double-network hydrogels: A neutron scattering study. *Polymer.* 48, 2007, Vols. 7449-7454.

146. **Ahmed, S., et al.** Brittle-ductile transition of double netowork hydrogels: Mechanical balance of two networks as the key factor. *Poylmer.* 55, 2014, Vols. 914-923.

147. **Hu, Y. and Suo, Z.** Viscoelasticity and poroelasticity in elastomeric gels. *Acta Mechanica Solida Sinica.* 25, 2012, Vol. 5.

148. **Xu, X., et al.** One-pot facile synthesis of silica reinforced double network hydrogels. *Chemical Engineering Journal.* 240, 2014, Vols. 331-337.

149. **Dragan, E.S.** Design and applicatios of interpenetrating polymer network hydrogels. *Chemical Engineering Journal.* 243, 2014, Vols. 572-590.

150. **Schapery, R.A.** Nonlinear viscoelastic and viscoplastic constitutive equations based on thermodynamics. *Mechanics of Time-dependent Materials.* 1, 1997, Vols. 209-240.

151. **Lai, G., Li, Y. and Li, G.** Effect of concentration and temperature on the rheological behavior of collagen solution. *International Journal of Biological Macromolecules .* 42, 2008, Vols. 285-291.

152. **Baiardo, M.** *Mechanical characterization of liquids (Rheology) and solids (Dynamic Mechanical Analysis).* Brno : TA Instruments, 2008.

153. **Ward, I.M.** *Mechanical properties of solid polymers.* New York : Wiley Interscience, 1971.

154. **Vader, D. and Wyss, H.** Harvard University. *Introduction to Rheology.* [Online] 2014.

155. **Gupta, H.S.** Nanoscale deformation mechanisms in collagen. [book auth.] P. Fratzl. *Collagen Structure and Mechanics.* New York : Springer Science+Business Media, 2008.

156. **Buehler, M.J.** Hierarchical nanomechanics of collagen fibrils. [book auth.] P. Fratzl. *Collagen Strucutre and mechanics.* New York : Springer Science+Business Media, 2008.

157. **Libonati, F., Nair, A.K., Vergani,L. and Buehler, M.J.** Mechanics of collagen-hydroxyapatite model nanocomposites. *Mechanics Research Communications.* 2013.

158. **Sternstein, S.S. and Zhu, A.J.** *Macromolecules.* 35, 2002, Vols. 7262-7273.

159. **Zhu, A. and Sternstein, S.S.** *Compos.Sci.Technol.* 63, 2003, Vol. 1113.

160. **Kalfus, J. and Jancar, J.** *J.Polym.Sci.* 45, 2007, Vol. 1380.

161. —. *Polym.Compos.* 28, 2007, Vol. 365.

162. —. *Polym.Compos.* 743, 2007.

163. **Douglas, J.F. and McKenna, G.** *Macromolecules.* 26, 1993, Vol. 3282.

164. **Riggleman, R.A., Douglas, J.F. and de Pablo, J.J.** *J.Chem.Phys.* 126, 2007, Vol. 234903.

165. **Jancar, J. and Kucera, J.** *Polymer Composites.* 1991.

166. **Jančář, J., Jančářová, E. and Žídek, J.** Combining reptation dynamics and percolation in modeling viscoelastic response of collagen based nanocomposites. *Journal of Computational and Theoretical Nanoscience.* 7, 2010, Vols. 1257-1264.

167. **Arevalo, R.C, Urbach, J.S. and Blair, D.L.** Size-dependent rheology of type I collagen networks. *Biophysical Journal.* 99, 2010, Vols. L65-L67.

168. **Raghavan, S.R. and Douglas, J.F.** *Soft Matter.* 8, 2012, Vol. 8539.

169. **Douglas, J.F.** *Langmuir.* 25, 2009, Vol. 8386.

170. **Ahmed, S. and Jones, F.R.** *J.Mater.Sci.* 25, 1991, Vols. 4933-4942.

171. **Buehler.** *Progress in Materials Science.* 53, 2008, Vols. 1101-1241.

172. **Fantner, G.E., et al.** *Biophysical J.* 90, 2006, Vols. 1411-1418.

173. **Zidek, J., Kucera, J. and Jancar, J.** *CMC.* 2010.

174. **Lin, D.C., Douglas, J.F. and Horkay, F.** Development of minimal models of the elastic properties of flexible and stiff polymer networks with permanent and thermo-reversible crosslinks. *Soft Matter.* 8, 2010, Vols. 3548-3561.

175. **Kadler, K.E., Hojima, Y. and Prockop, D.K.** Assembly of collagen fibrils de novo by cleavage of the type I pC-collagen with procollagen C-proteinase. *J.Biol.Chem.* 260, 1987, Vols. 15696-15701.

176. **Durand, D., et al.** *Europhys. Lett.* 3, 1987, Vol. 297.

177. **Forgacz, G., et al.** *Biophysical J.* 84, 2003, Vol. 1272.

178. **Kadner, K.E., Hill, A. and Canty-Laird, E.G.** *Current Opinion in Cell Biology.* 20, 2008, Vols. 495-501.

179. **Flory, P.** *Science.* 124, 1956, Vols. 53-60.

180. **Landis, W.J. and Silver, F.H.** *Comparative Biochemistry and Physiology.* 133, 2002, Vols. 1135-1137.

181. **Hing, K.A., Best, S.M. and Bonfield, W.** Characterization of porous hydroxyapatite. *J. Mater. Sci. Mater. Med.* 10, 1999, Vols. 135-145.

182. **Black, J. and Mattson, R.U.** Relationship between porosity and mineralization in the Haversian osteon. *Calcif. Tissue Int. .* 34, 1982, Vols. 332-336.

183. **Chung, E.J., Jakus, A.E. and Shah, R.N.** In situ forming collagen-hyaluronic acid membrane structures: Mechanism of self-assembly and applications in regenerative medicine. *Acta Biomaterialia.* 2012.

184. **Mosser, G., et al.** *Matrix Biol.* 25, 2006, Vol. 3.

185. **Zhang, M., et al.** The rheological and structural properties of fish collagen cross-linked by N-hydroxysuccinimide activated adipic acid. *Food hydrocolloids.* 30, 2013, Vols. 504-511.

186. **Zhang, M., et al.** Rheological properties of fish skin collagen solutions: effects of temperature and concentration. *Korea-Australia Rheology Journal.* 22, 2010, Vols. 119-127.

187. *On the multiscale hierarchy in materials systems.* **Pan, N.** Liberec, Czech Republic : 7th International Conference TEXSCI 2010, 2010.

9 Annex

9.1 Determining the linear viscoelastic region

9.1.1 Individual neat collagen solutions

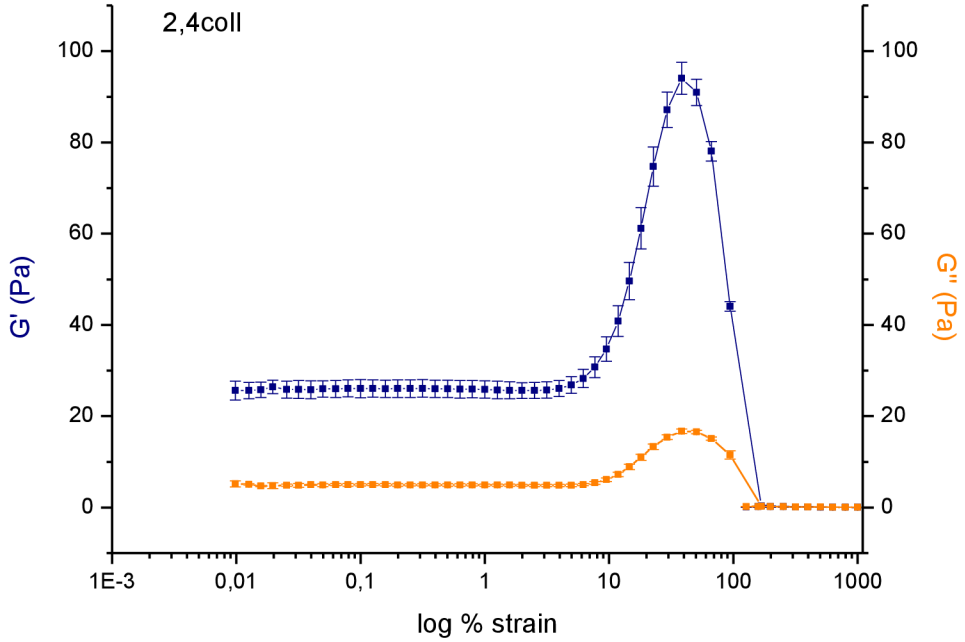

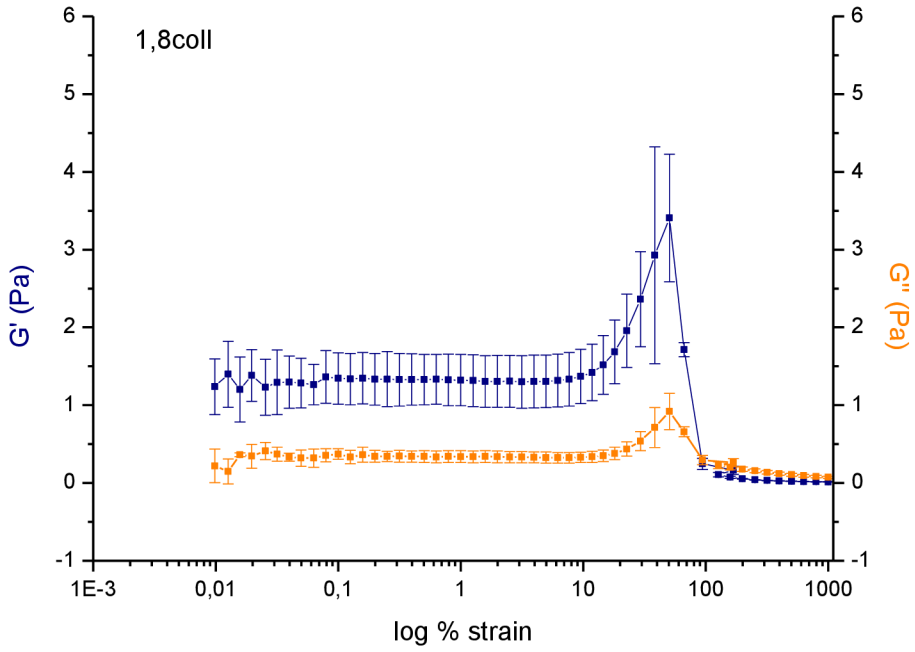

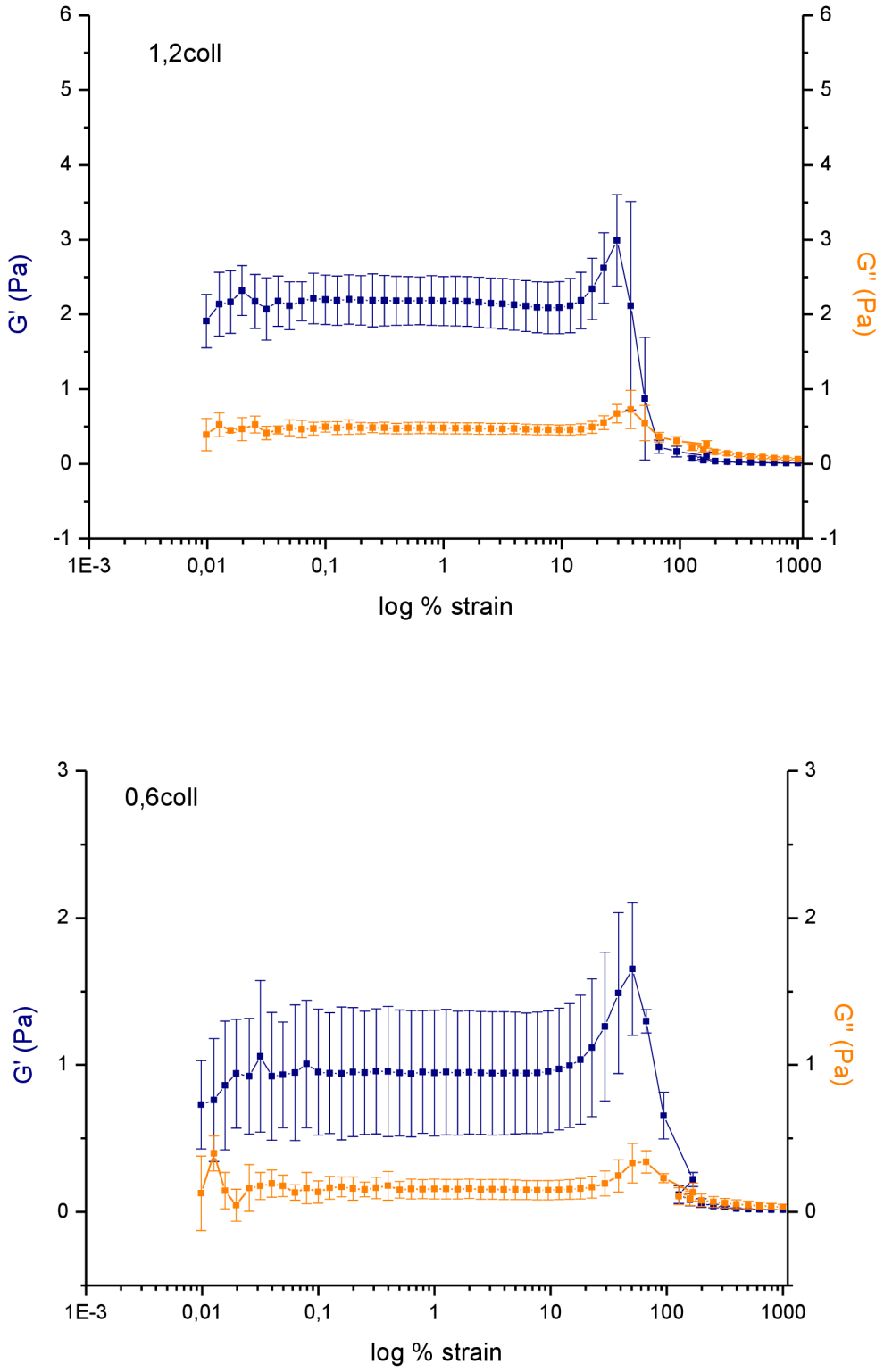

Fig. 9.1. The LVR was found to be reliably in the interval between 0,1% and 10% strain. Above 10% strain, shear stiffening behavior was observed, followed by a destruction of the self-assembled structure accompanied by a loss of mechanical properties

9.1.2 Individual collagen + nHAP solutions

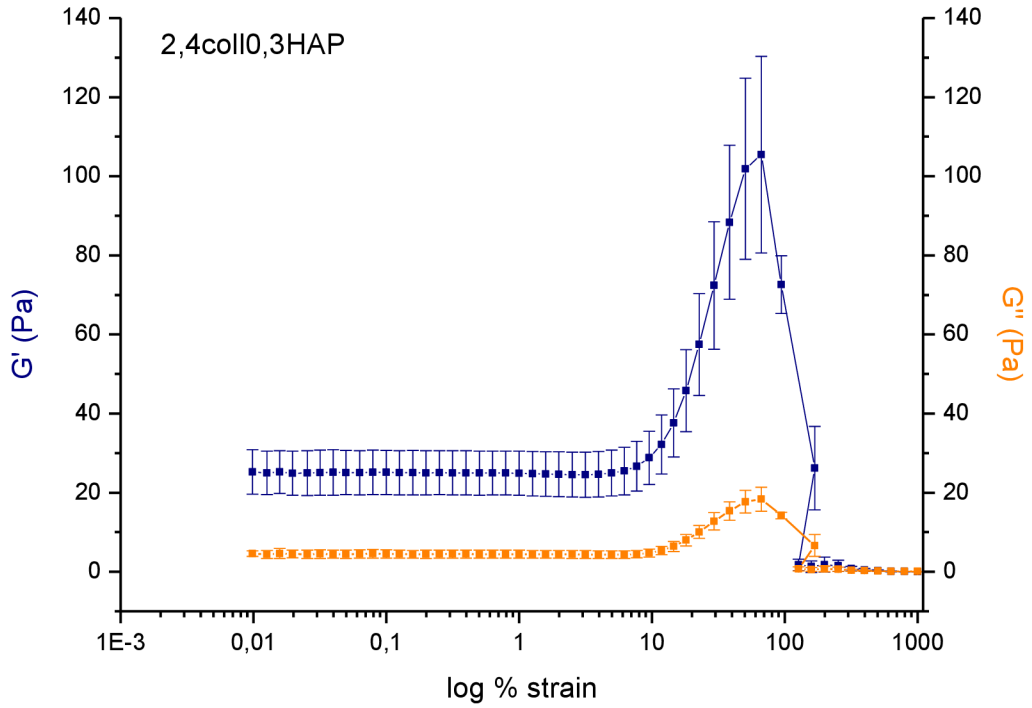

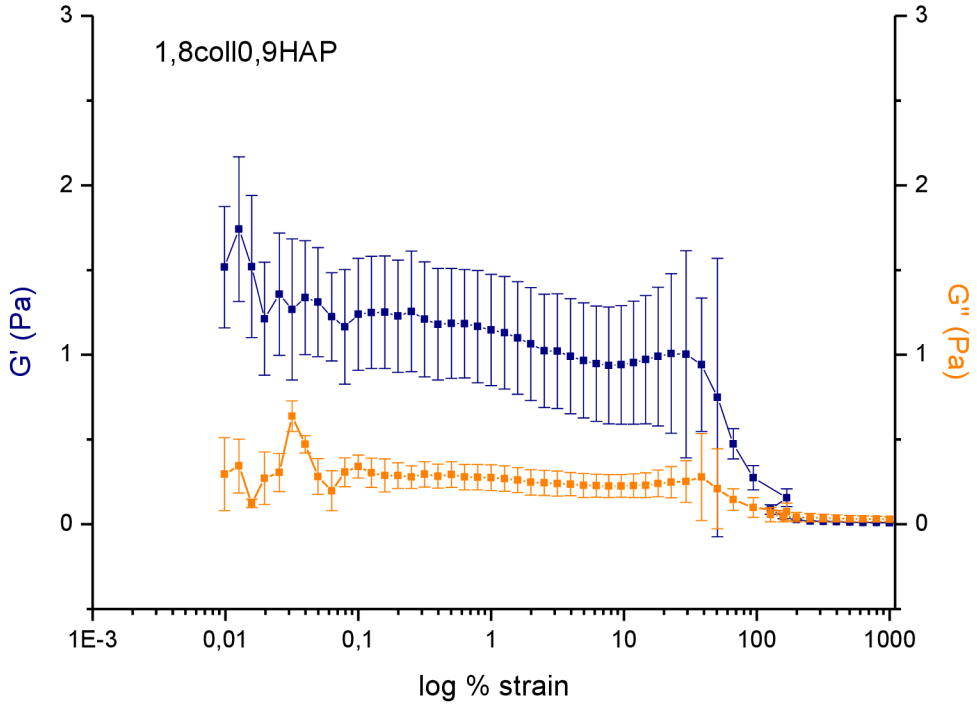

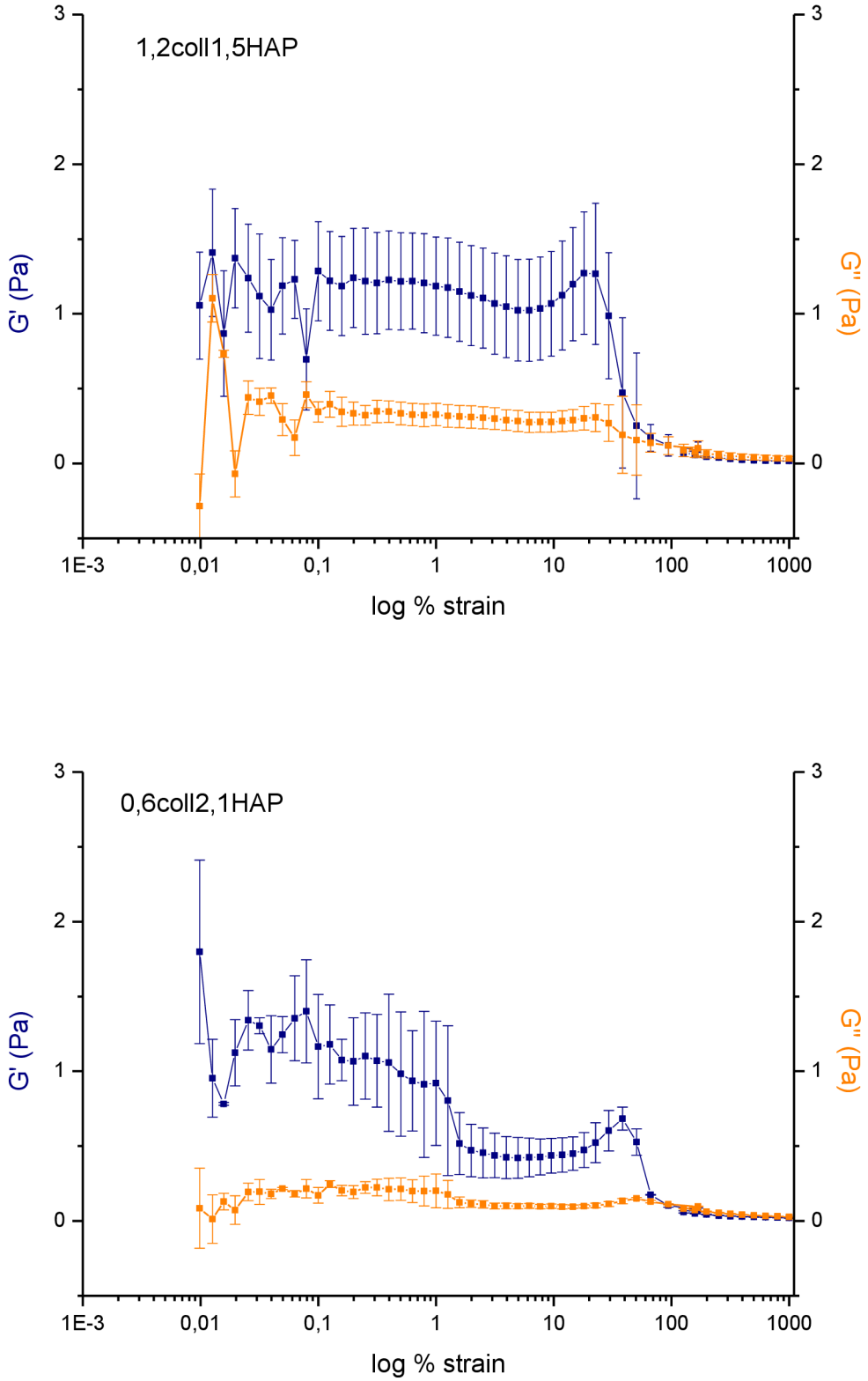

Fig. 9.2. The LVR determined for the solutions containing HAP was similar to the neat collagen solutions, however the strain stiffening was observed to a smaller degree.

9.1.3 The effect of nHAP content on G' and G''

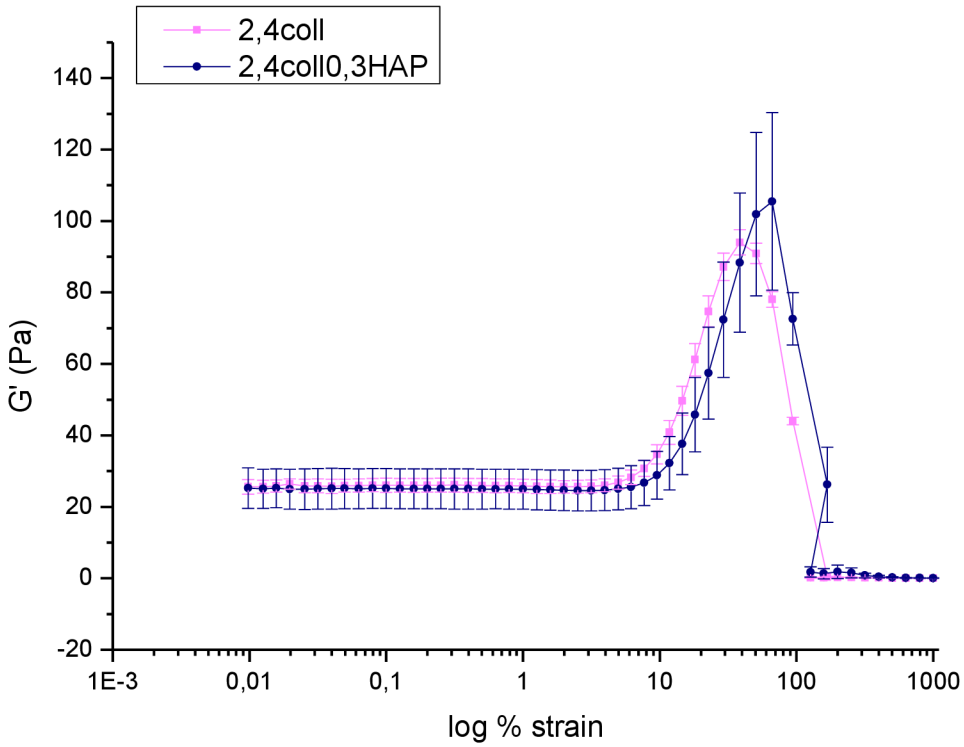

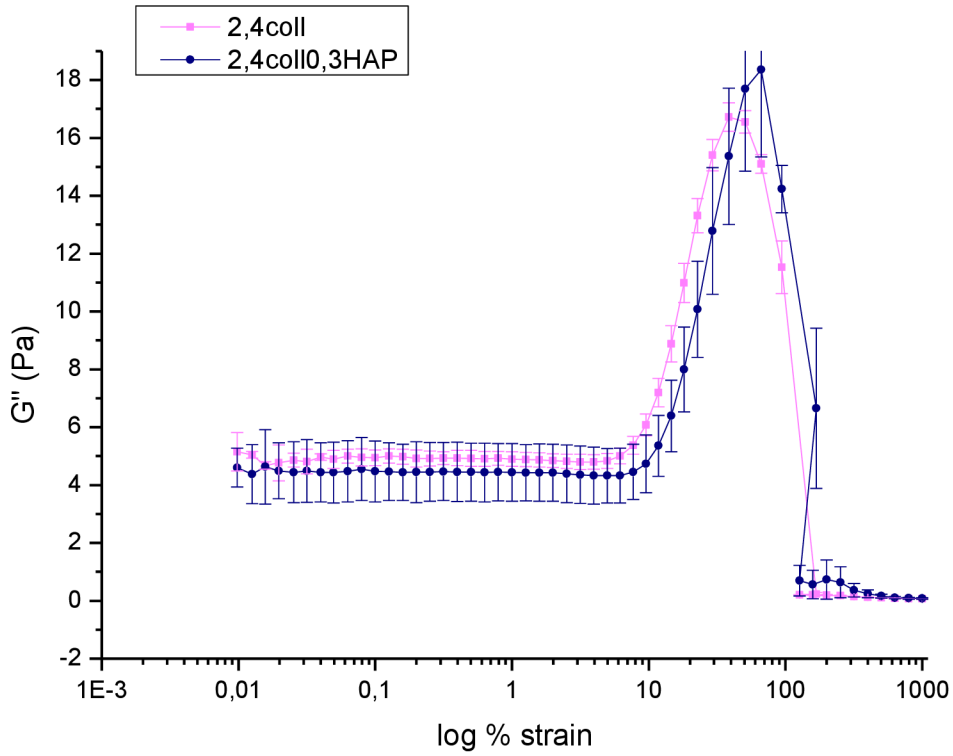

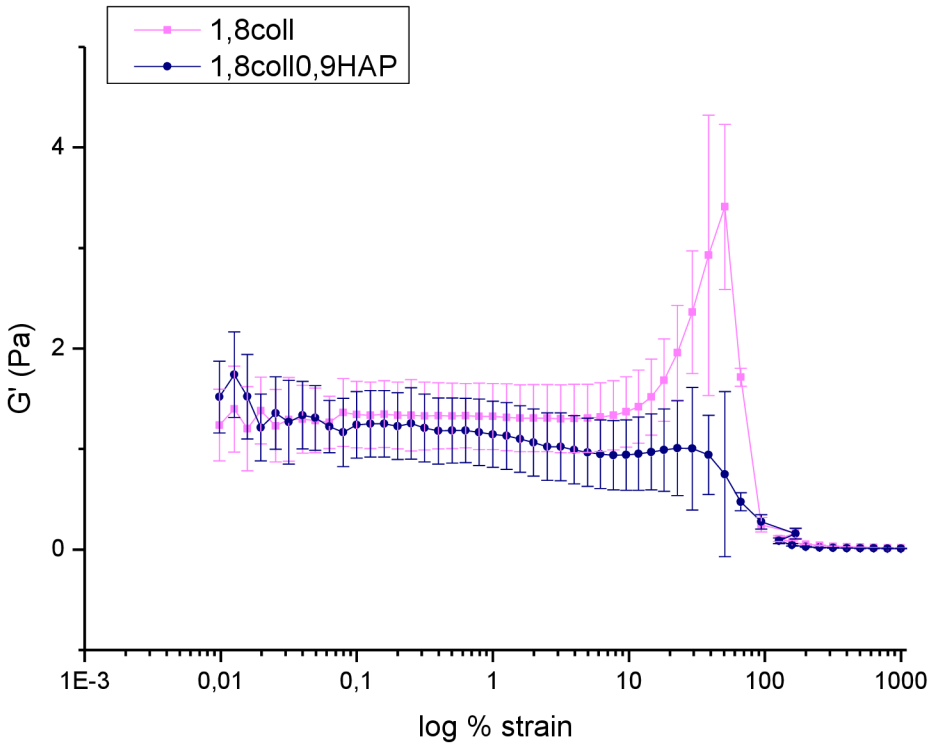
1,8coll
1,8coll0,9HAP
G' (Pa)
4
2
0
1E-3
0,01
0,1
1
10
100
1000
log % strain

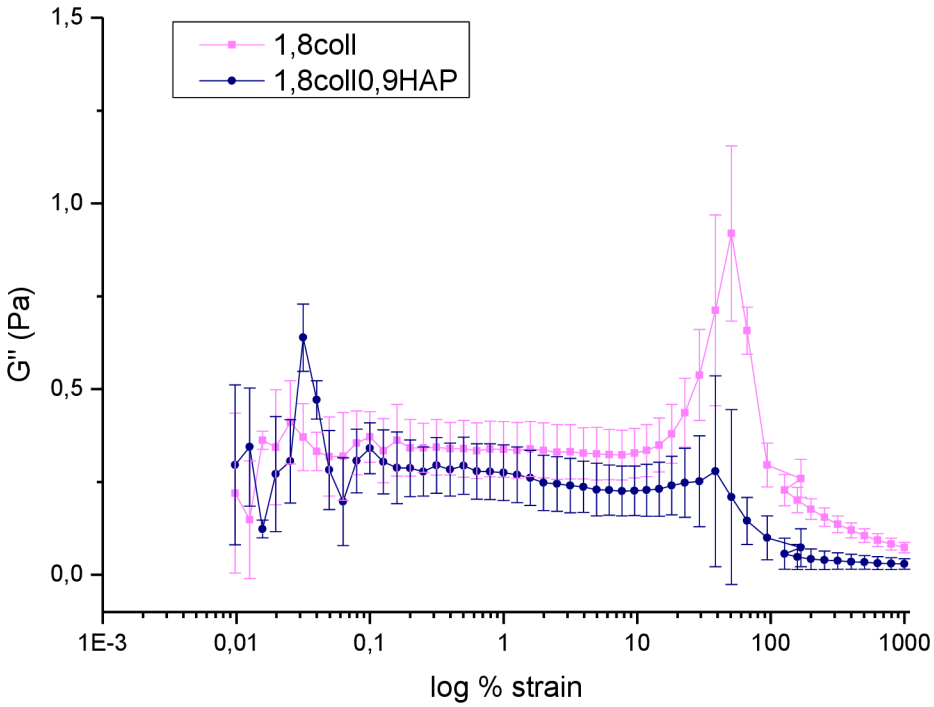
1,8coll
1,8coll0,9HAP
G'' (Pa)
1,5
1,0
0,5
0,0
1E-3
0,01
0,1
1
10
100
1000
log % strain

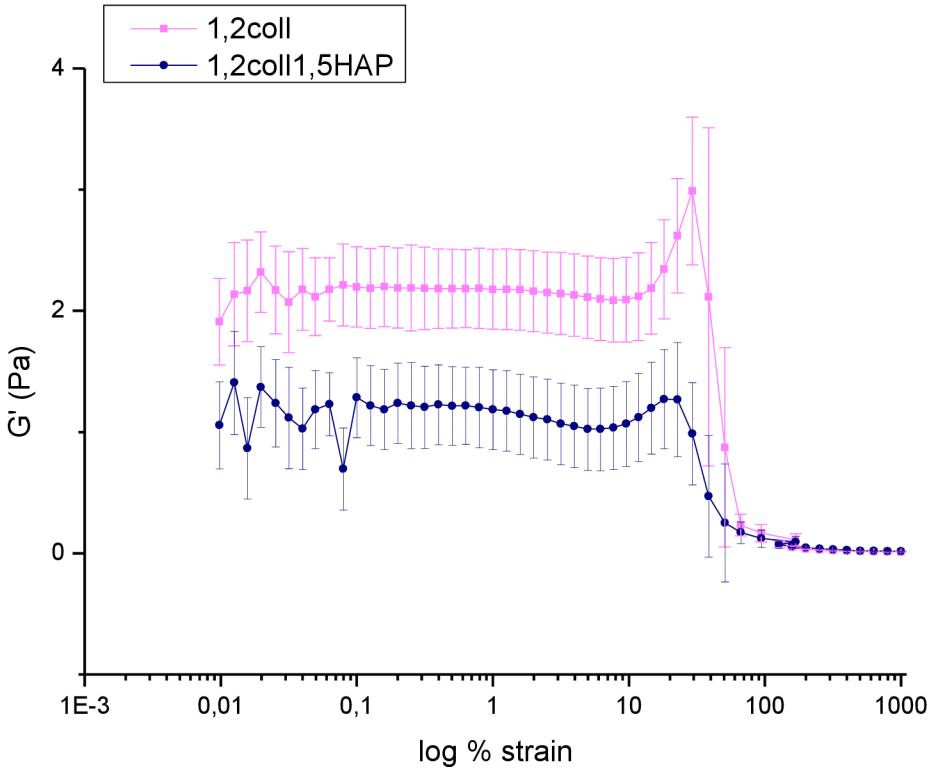
1,2coll
1,2coll1,5HAP
G' (Pa)
4
2
0
1E-3
0,01
0,1
1
10
100
1000
log % strain

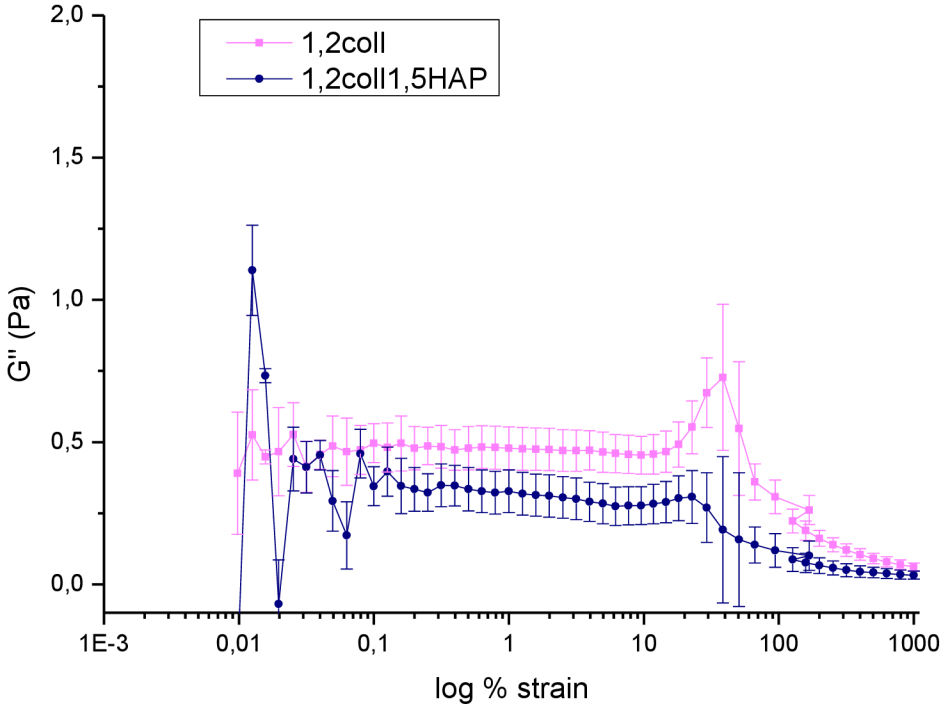
1,2coll
1,2coll1,5HAP
G'' (Pa)
2,0
1,5
1,0
0,5
0,0
1E-3
0,01
0,1
1
10
100
1000
log % strain

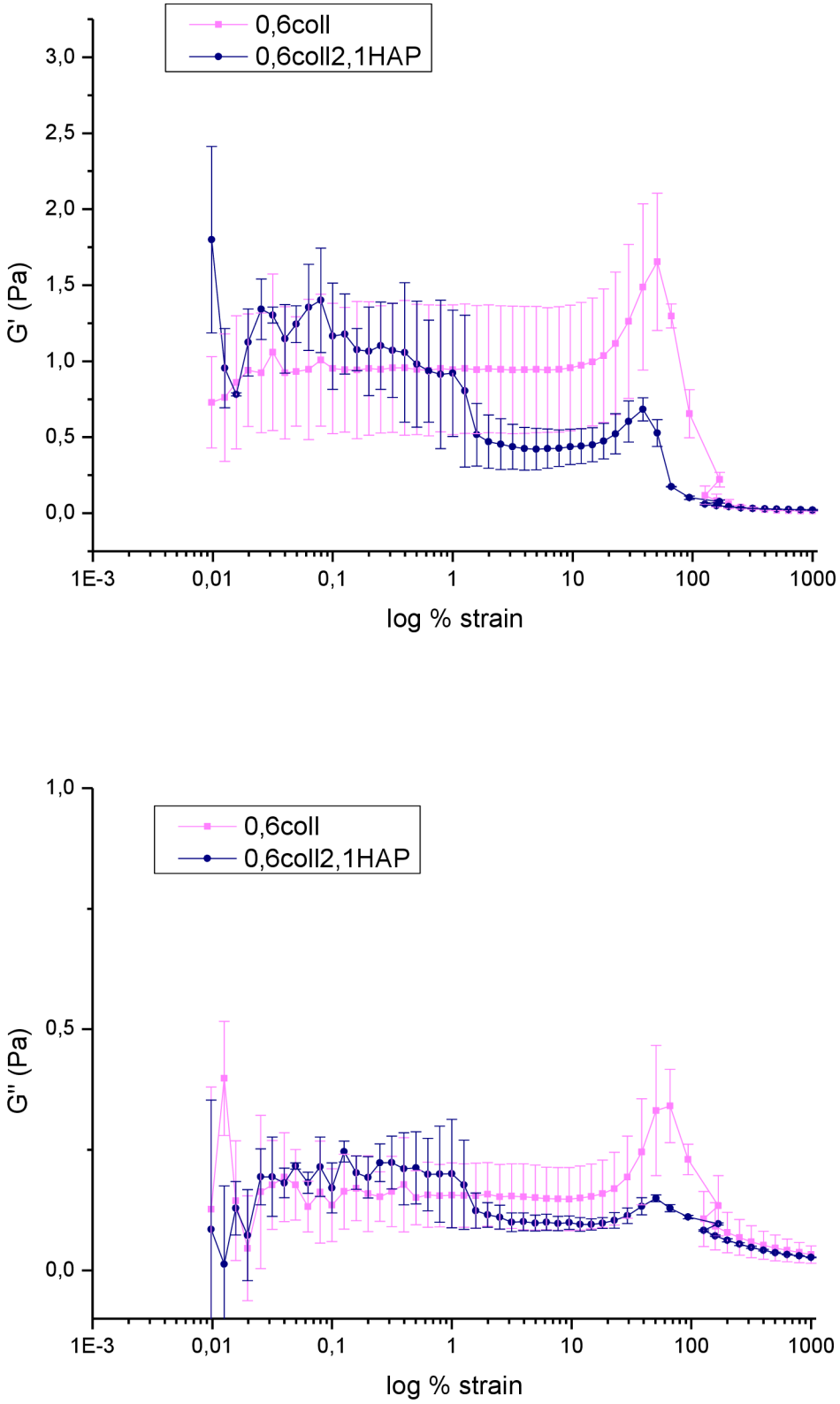

Fig. 9.3. The effect of nHAP content on the strain dependences of the viscoelastic moduli for all the investigated coll/HAP system compositions.

9.1.4 Summarization

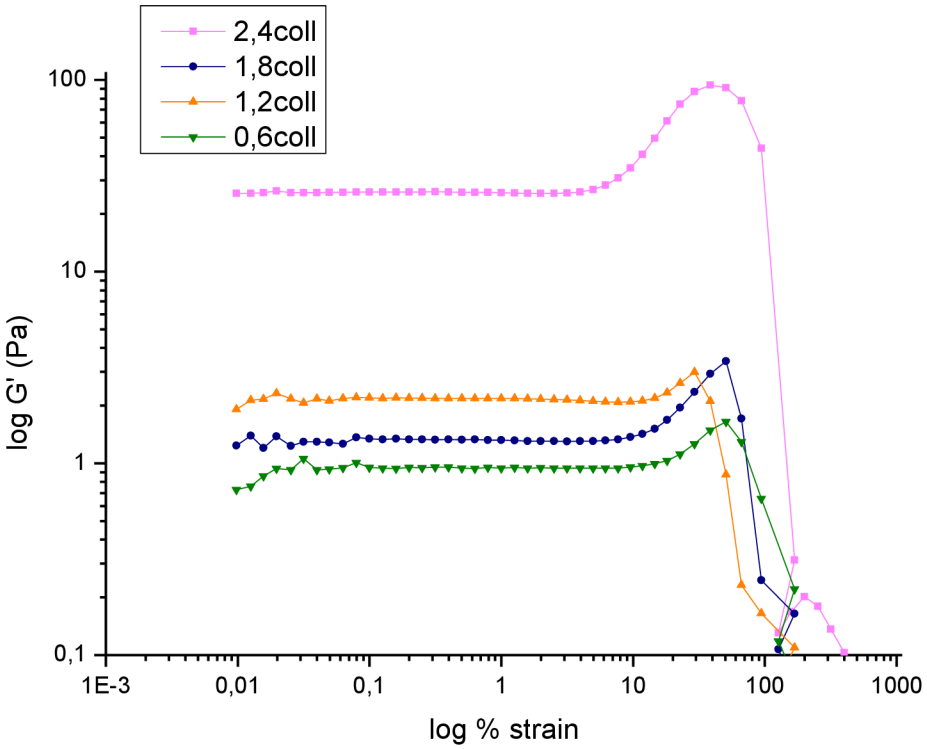

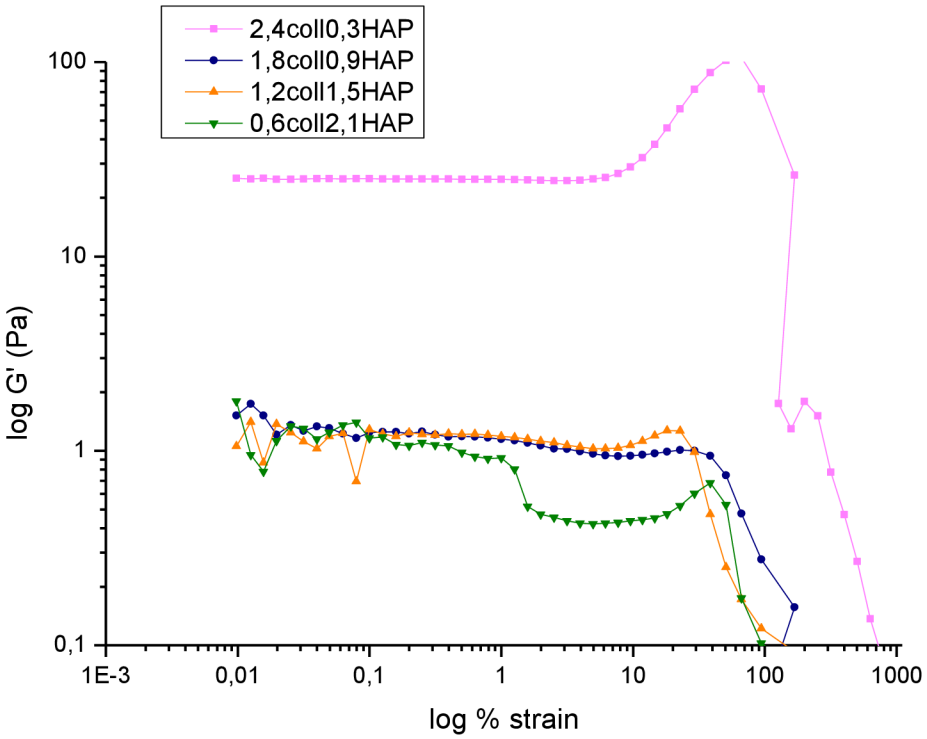

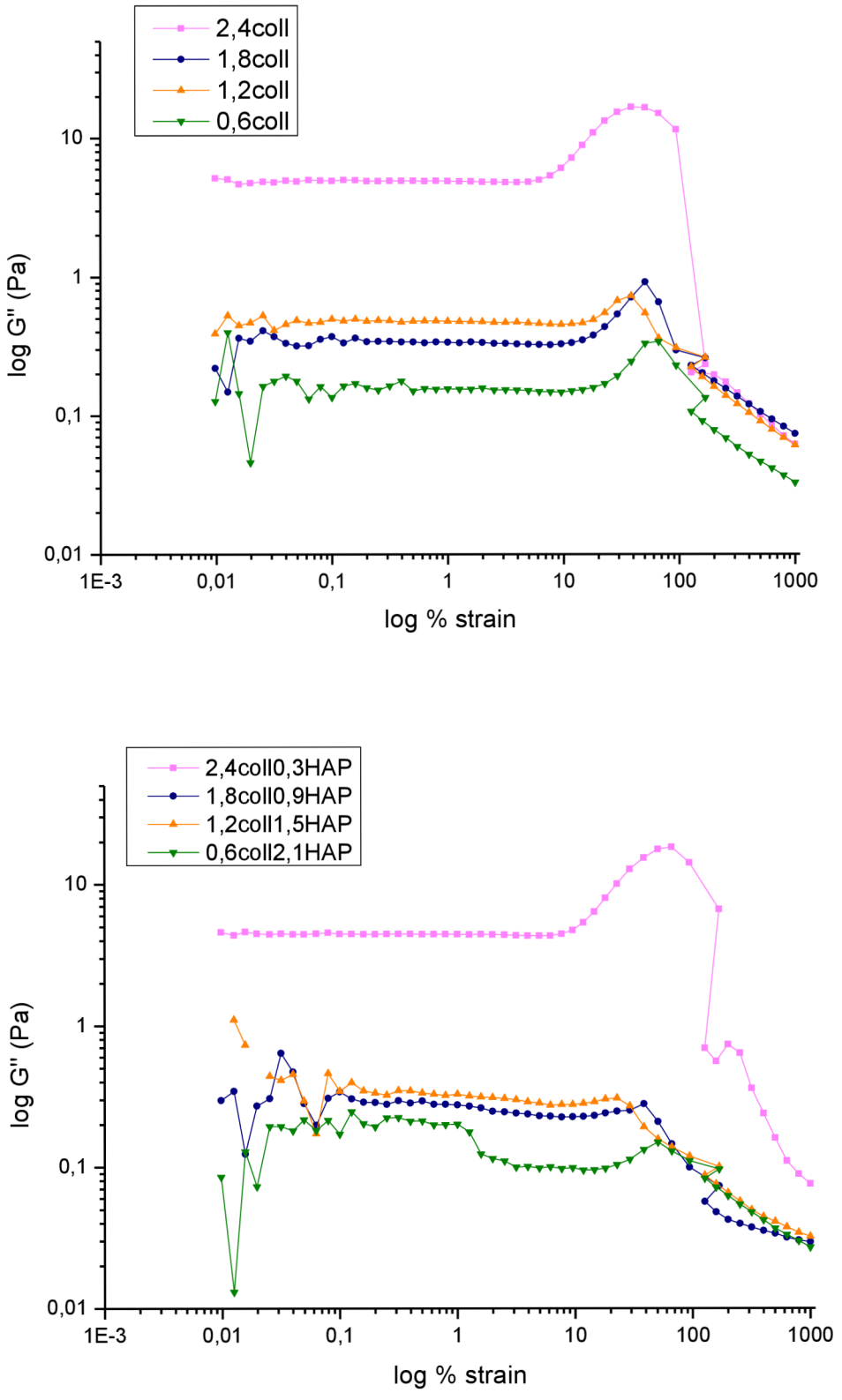

Fig. 9.4. The data demonstrate that regardless of the composition, the LVR is maintained approximately the same in all cases, the only slight deviation was the sample 0,6coll2,1HAP, where the behavior was less regular.

9.2 Kinetics of network gelation

9.2.1 Individual neat collagen solutions

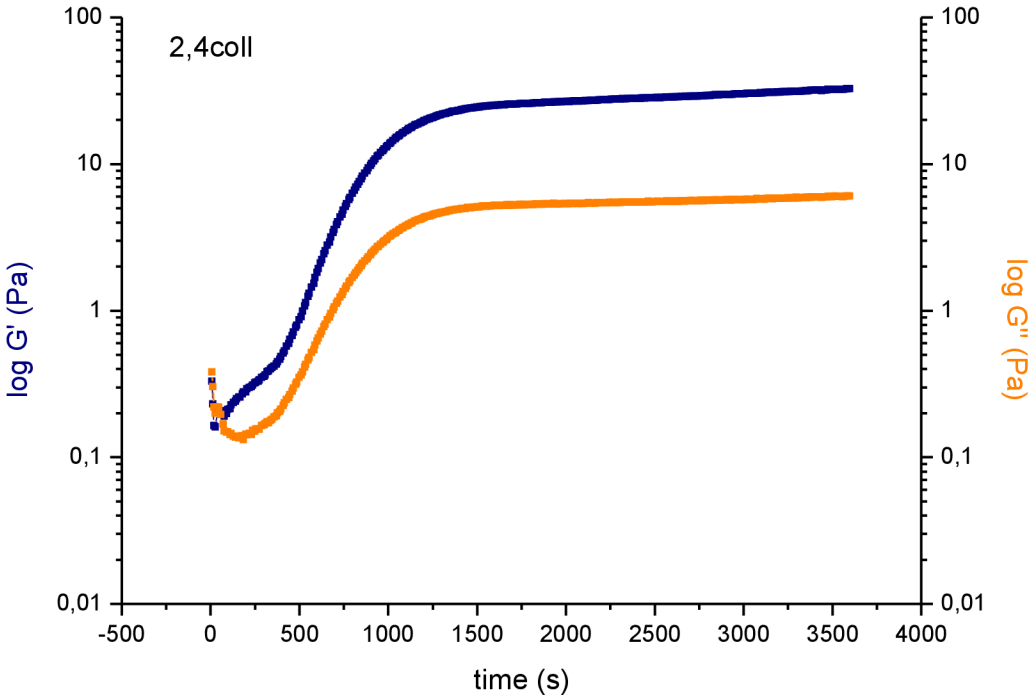

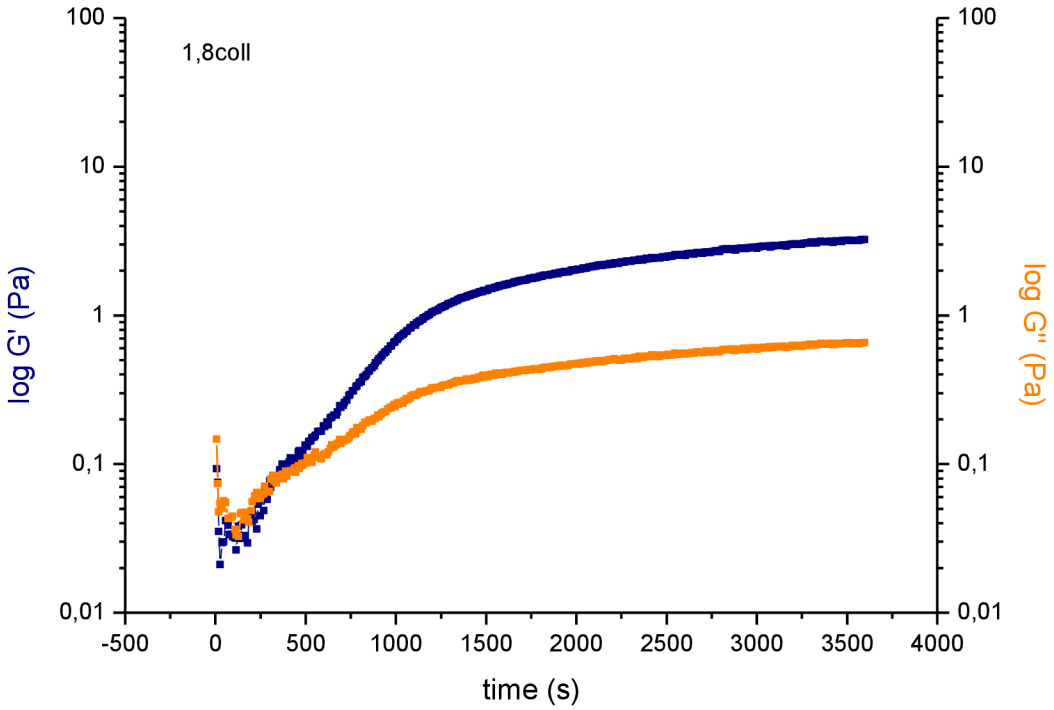

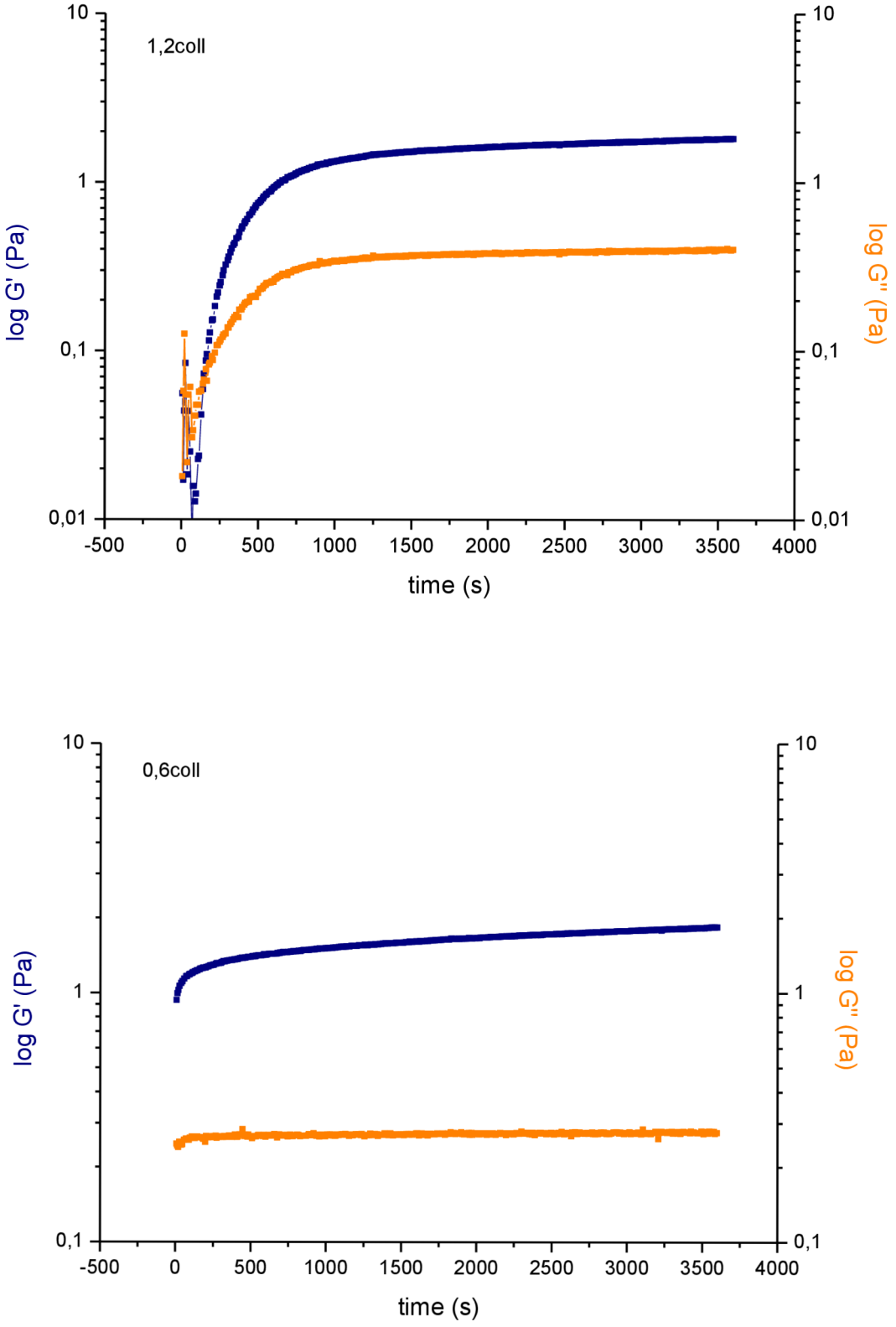

Fig. 9.5. The evolution of the viscoelastic moduli through time. It appears that with decreasing concentration, the initial lag phase is shortened and the growth phase steeper. The viscoelastic moduli values increase with increasing concentration, as expected and in agreement with published results.

9.2.2 Individual collagen + nHAP solutions

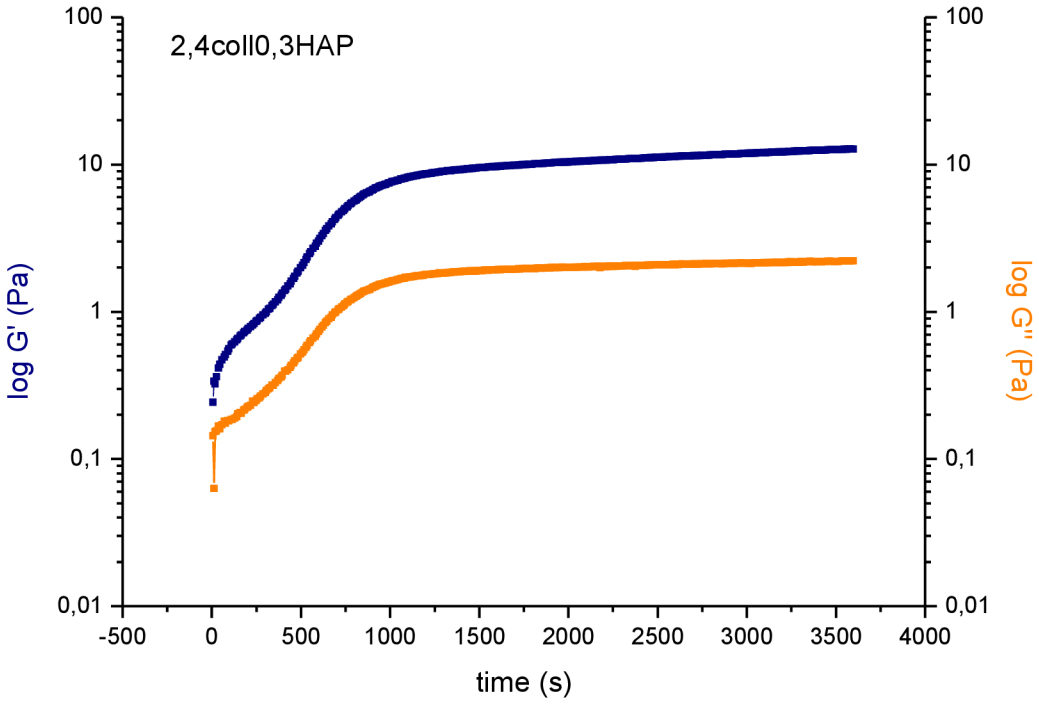

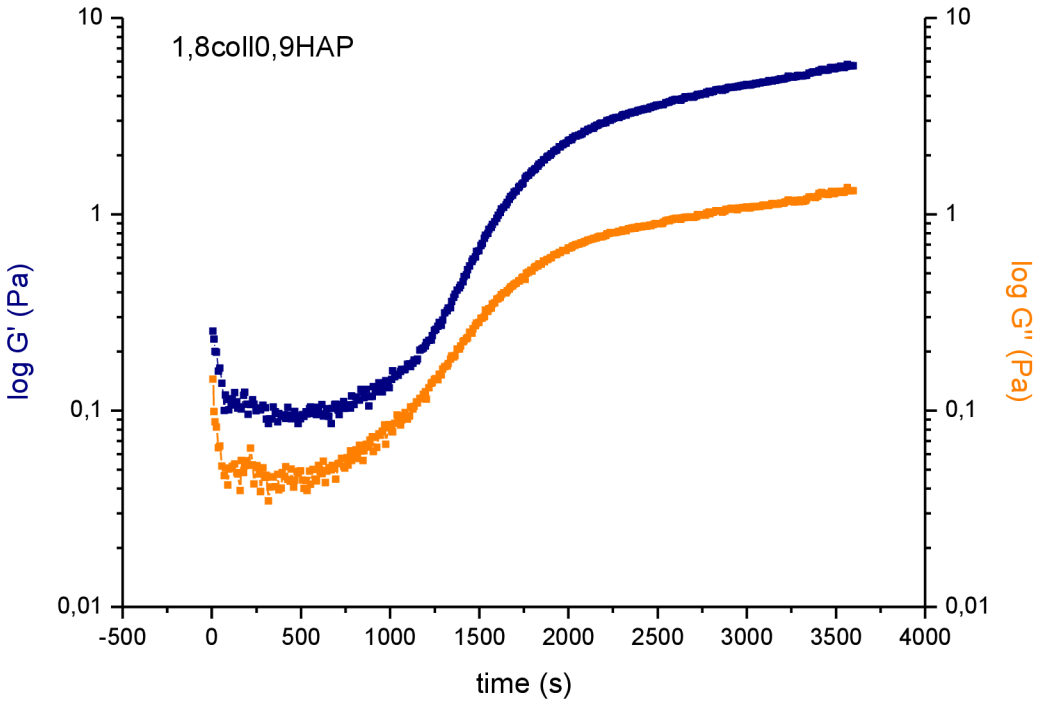

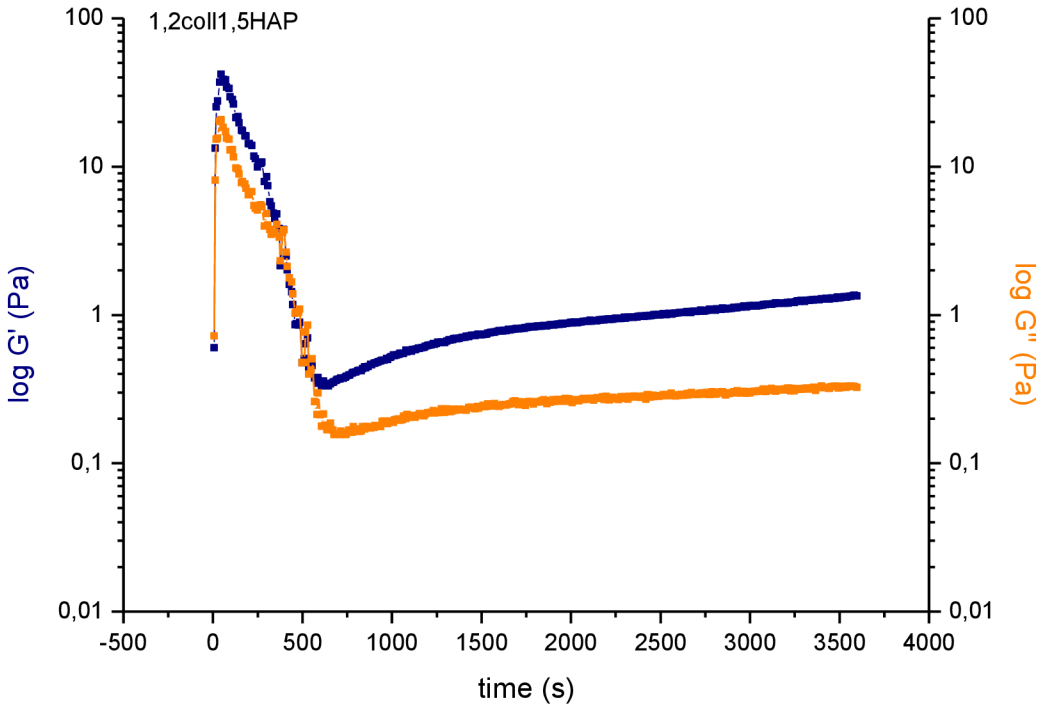

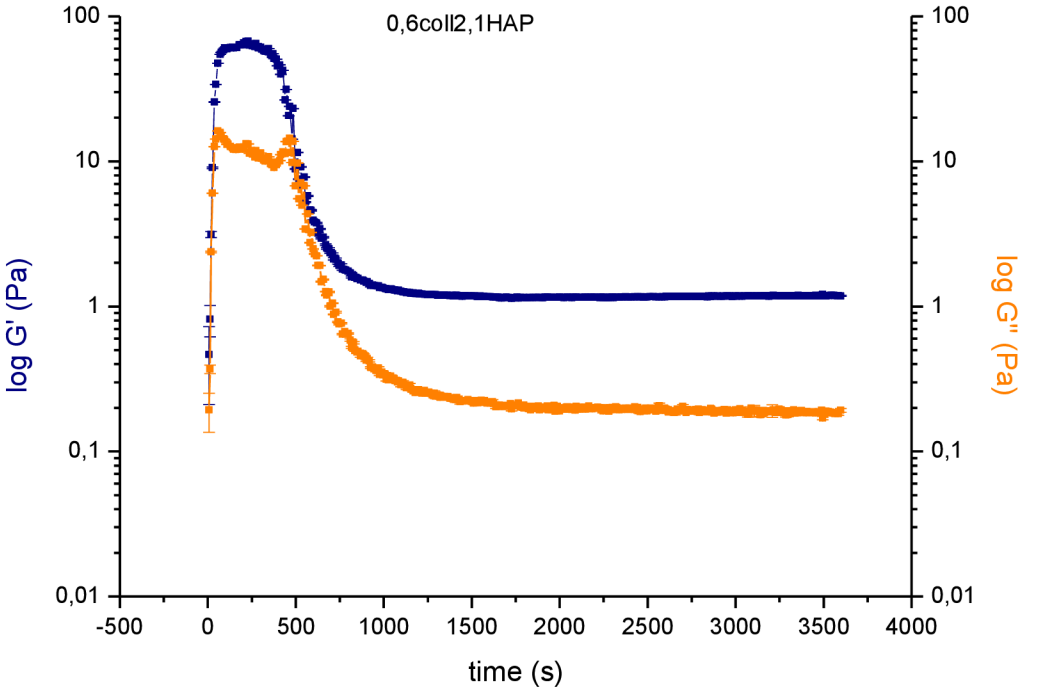

Fig. 9.6. The evolution of viscoelastic moduli in collagen I solutions containing nHAP. In the presence of a large amount of nHAP such as in 1,2coll1,5HAP or 0,6coll2,1HAP, the formation of a weak physical temporary structure with large moduli and its breakdown due to the dynamic oscillatory shear forces within the first 500s is observed.

9.2.3 The effect of nHAP content on G' and G''

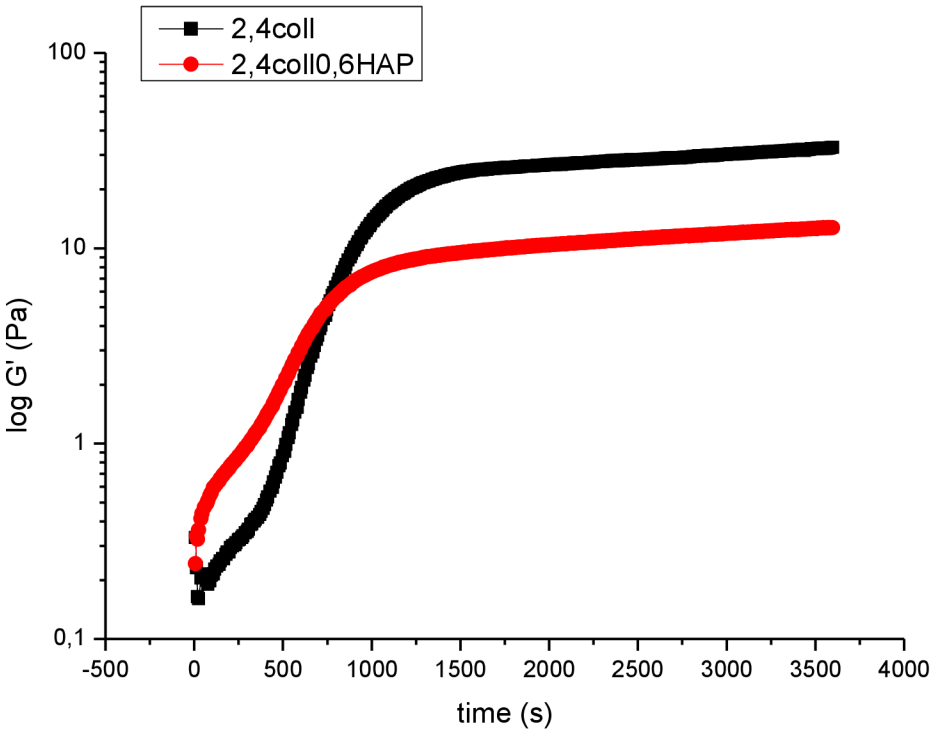

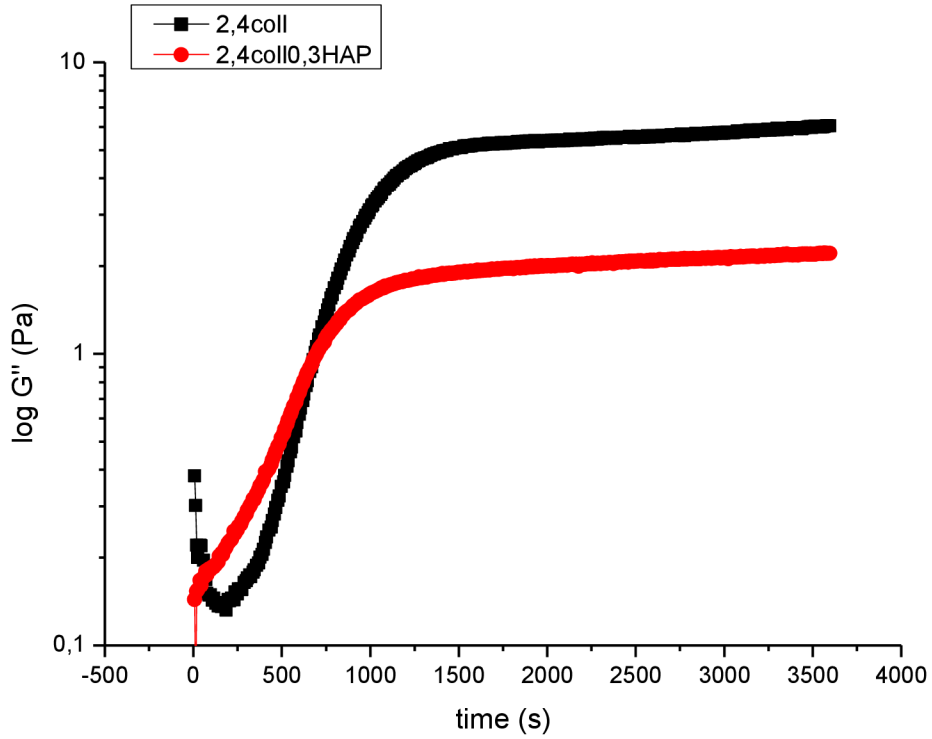

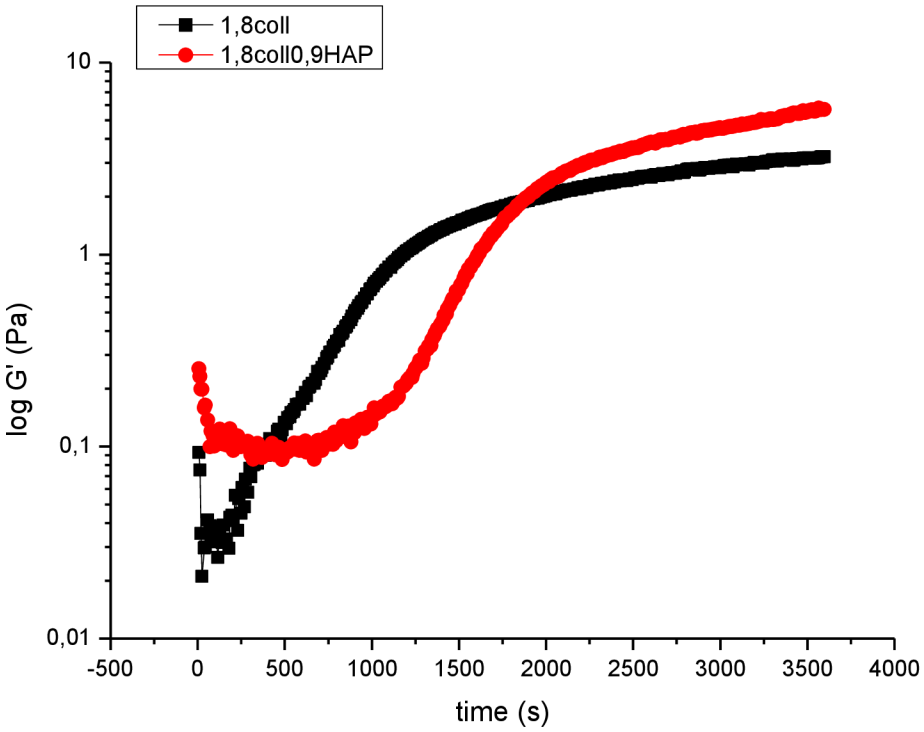
1,8coll
1,8coll0,9HAP
10
1
0,1
0,01
log G' (Pa)
-500
0
500
1000
1500
2000
2500
3000
3500
4000
time (s)

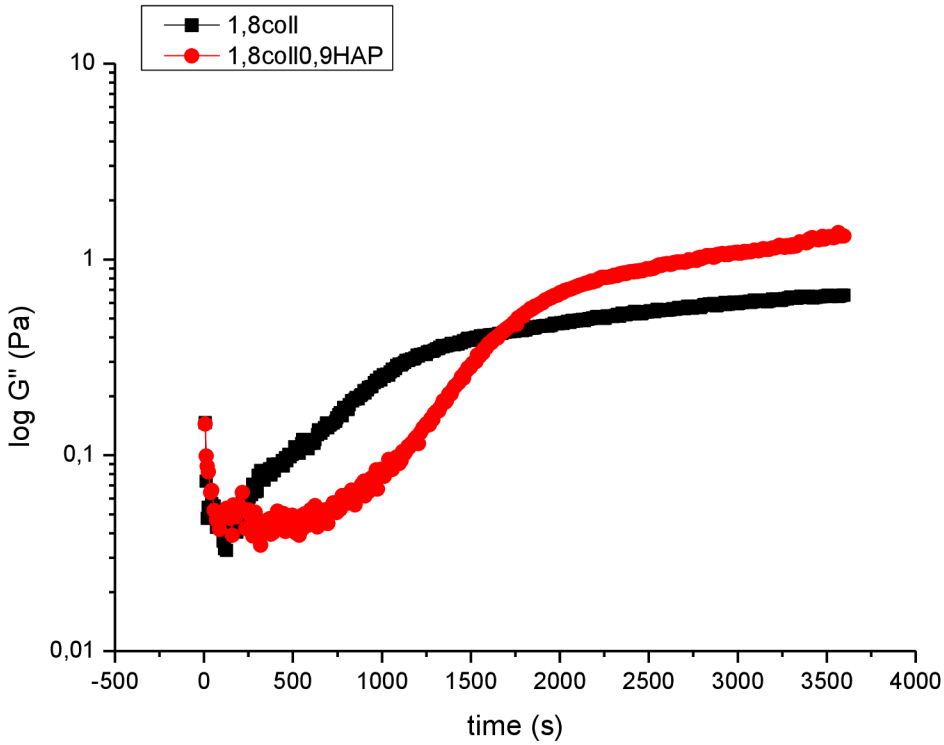
1,8coll
1,8coll0,9HAP
10
1
0,1
0,01
log G'' (Pa)
-500
0
500
1000
1500
2000
2500
3000
3500
4000
time (s)

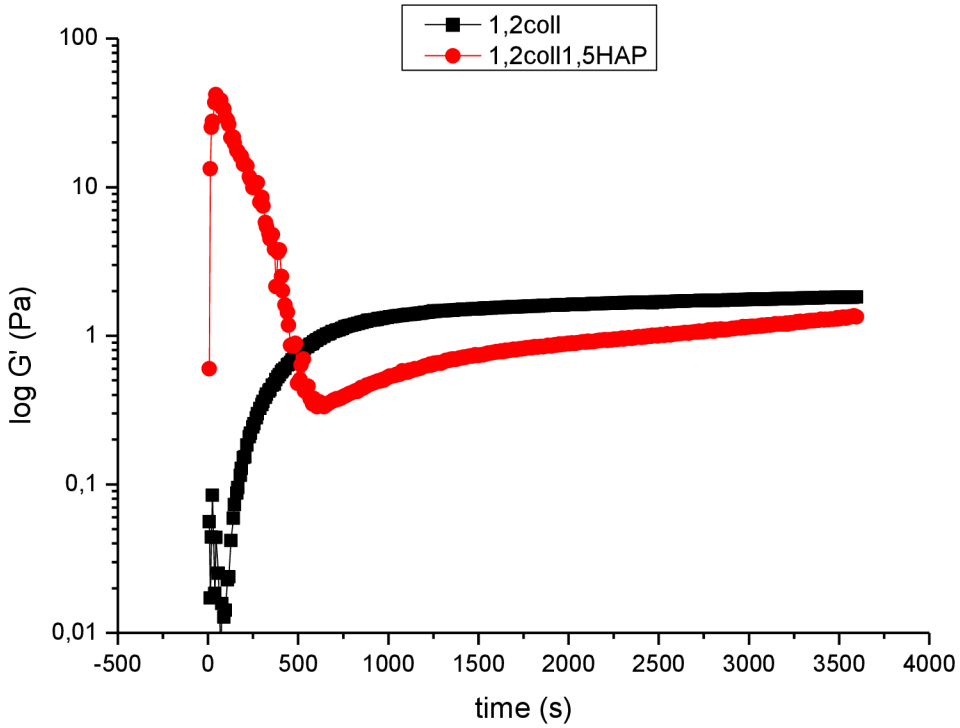
1,2coll
1,2coll1,5HAP
log G' (Pa)
time (s)
100
10
1
0,1
0,01
-500
0
500
1000
1500
2000
2500
3000
3500
4000

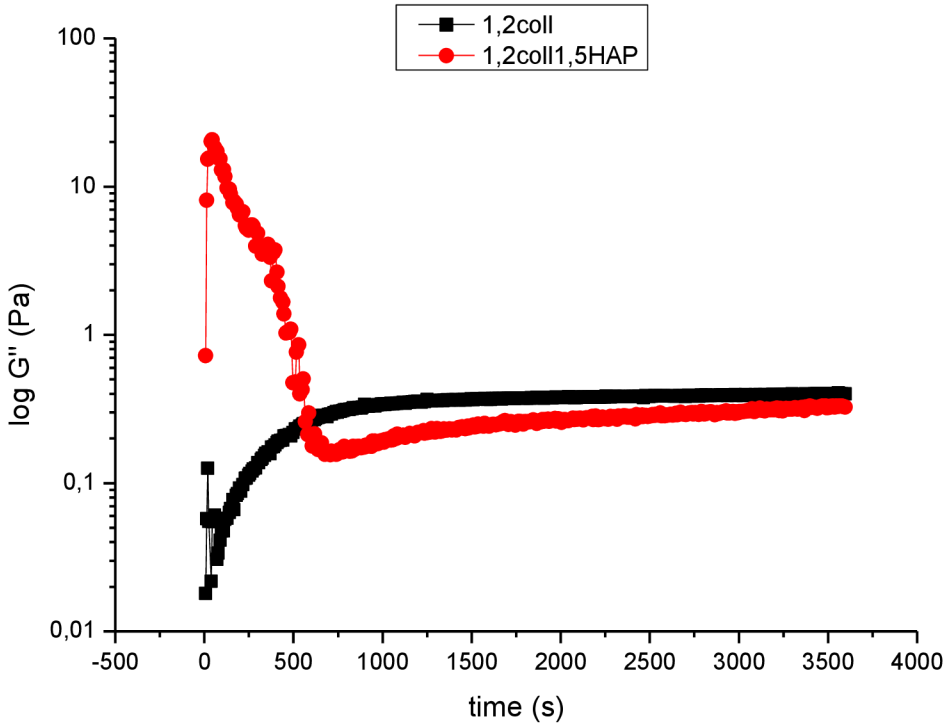
1,2coll
1,2coll1,5HAP
log G'' (Pa)
time (s)
100
10
1
0,1
0,01
-500
0
500
1000
1500
2000
2500
3000
3500
4000

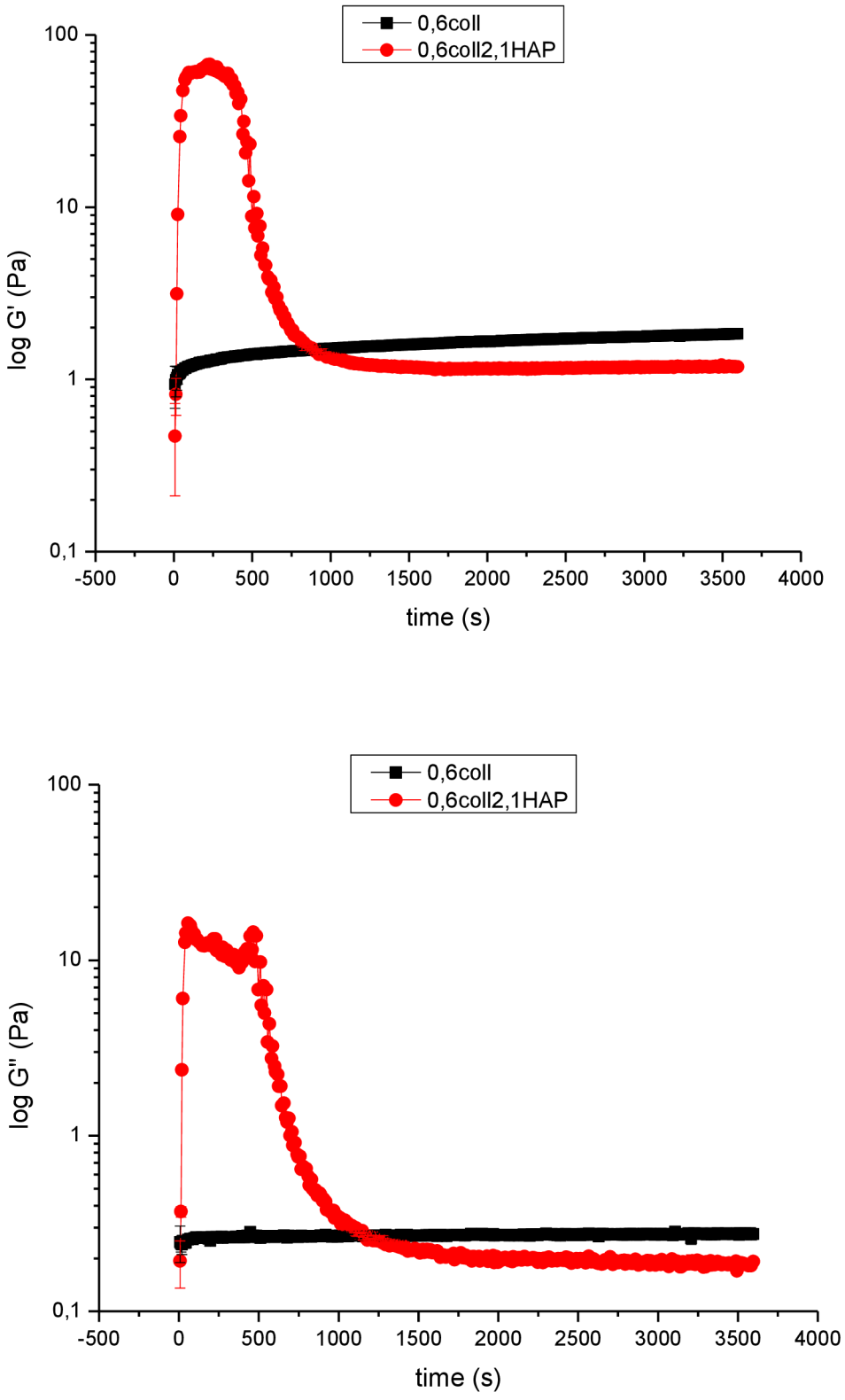

Fig. 9.7.The effect of nHAP addition on the time evolution of viscoelastic moduli for all studied coll/HAP system compositions.